NATURAL PRODUCTS AS A POWERFUL SOURCE OF ANTIOXIDANTS

Ganna Petruk

Dottorato in Biotecnologie - XXX ciclo

Università di Napoli Federico II

Dottorato in Biotecnologie – XXX ciclo

Università di Napoli Federico II

NATURAL PRODUCTS AS A POWERFUL SOURCE OF ANTIOXIDANTS

Ganna Petruk

Dottorando: Ganna Petruk

Relatore: Dr. Daria Maria Monti

Coordinatore: Prof. Giovanni Sannia

A coloro che mi
hanno sempre sostenuto
e continuano a farlo

*"A person who **never** made a **mistake***
***never** tried anything **new**"*

-Albert Einstein

INDEX:

RIASSUNTO

I radicali liberi rappresentano un'importante minaccia all'omeostasi degli organismi aerobici; tali specie sono caratterizzate dalla presenza di uno o più elettroni spaiati nell'orbitale più esterno, ciò li rende specie instabili e reattive.

La produzione di radicali liberi può essere innescata nelle cellule da numerosi processi, come l'assorbimento di luce ultravioletta o raggi X, l'esposizione ai pesticidi, al fumo di sigaretta, ad idrocarburi aromatici e altre sostanze. Essi, però, si formano anche come sottoprodotto di normali processi metabolici, come ad esempio nella catena di trasporto degli elettroni nei mitocondri.

Le specie reattive dell'ossigeno (ROS) possono svolgere un duplice ruolo all'interno del sistema biologico: da una parte sono mediatori citotossici e delle vie di segnalazione cellulare, mentre dall'altra, ad elevate concentrazioni, possono danneggiare le strutture cellulari, inclusi i lipidi, le membrane, le proteine e gli acidi nucleici. In quest'ultimo caso si parla di stress ossidativo. Il danno ossidativo, se cronico, può portare all'insorgenza di malattie a sviluppo tardivo, come il cancro, l'aterosclerosi, l'artrite e le malattie neurodegenerative.

Gli organismi aerobici hanno sviluppato un sofisticato meccanismo di protezione contro i danni indotti dai radicali liberi, attraverso l'uso di antiossidanti enzimatici (superossido dismutasi, catalasi, glutatione perossidasi) e non- (albumina, transferrina, glutatione), endogeni ed esogeni.

Negli ultimi anni sta crescendo l'interesse, da parte dei consumatori, verso l'uso di antiossidanti di origine naturale. Quindi, la ricerca si sta focalizzando sempre di più sulla caratterizzazione e l'applicazione di antiossidanti naturali, dati anche gli elevati costi di produzione degli antiossidanti sintetici. Inoltre, tali molecole naturali mostrano un'ampia gamma di applicazioni, dall'impiego nei prodotti farmaceutici e alimentari, all'uso come integratori dietetici, alimenti per animali, cosmetici ed altri.

Naturalmente, nel caso degli antiossidanti sintetici, è relativamente facile trovare il tipo ed il dosaggio dell'antiossidante che possa essere considerato sicuro, mentre nel caso di antiossidanti estratti da fonti naturali, la presenza di diverse sostanze attive nella miscela rende più difficile l'identificazione e la quantificazione del contributo delle singole molecole, senza considerare che, oltre alle sostanze attive, i prodotti naturali contengono altri componenti.

L'obiettivo del presente progetto di dottorato è stato quello di analizzare l'attività antiossidante degli estratti ottenuti da diverse fonti naturali o microorganismi per studiare i loro effetti benefici contro lo stress ossidativo e per caratterizzare la loro composizione chimica. Lo scopo ultimo è quello di ottenere molecole da utilizzare nell'industria alimentare e/o cosmetica.

È risaputo che il consumo regolare di frutta e verdura è in grado di prevenire diverse malattie, come il cancro, le malattie cardiovascolari e altre. Uno dei prodotti continuamente assunti nella cosiddetta dieta mediterranea ed asiatica, considerate come le più sane, è il pomodoro. Questo ortaggio, ricco di diverse molecole attive,

viene consumato sia fresco che in seguito a lavorazione. Pertanto, come prima fonte di antiossidanti sono stati analizzati due diversi tipi di pomodoro:

- Zebrino (ZBR), una varietà attualmente presente in commercio;
- DHO, un nuovo ibrido ottenuto in seguito all'incrocio di due varietà di pomodoro.

ZBR è noto per avere alti livelli di antiossidanti, tra cui carotenoidi, composti fenolici e vitamina C. In letteratura è riportato che alcuni antiossidanti perdono la loro attività in seguito alla cottura, mentre il licopene viene assorbito in modo più efficiente in seguito al processamento termico. Ciò è dovuto al fatto che le temperature elevate comportano la trasformazione delle forme *trans*- in forme *cis*-, la cui biodisponibilità è molto più efficiente. Pertanto è stata analizzata l'attività antiossidante dell'estratto lipofilico ottenuto da questo pomodoro, prima e dopo il processamento termico. I risultati ottenuti hanno dimostrato che gli estratti erano completamente biocompatibili con le linee cellulari analizzate. Inoltre, essi erano in grado di proteggere le cellule dallo stress ossidativo indotto dall'arsenito di sodio. Si è anche scoperto che il composto attivo era il licopene, e che l'azione antiossidante del solo licopene era inferiore rispetto all'estratto totale, sostenendo così l'idea del sinergismo tra le molecole antiossidanti presenti nel pomodoro.

Successivamente, l'attenzione si è rivolta ad un nuovo ibrido di pomodoro, detto doppio omozigote (DHO). Questo è stato ottenuto tramite la tecnica del "*quantitative trait loci pyramiding"*, che ha permesso l'introduzione di regioni genomiche specifiche della specie *Solanum pennellii* nel genoma della varietà coltivata *Solanum lycopersicum* M82. Questi loci codificano l'espressione proteine/enzimi responsabili della produzione di acido ascorbico e diversi fenoli. L'estratto idrofilico ottenuto dal DHO è stato testato su cheratinociti umani non tumorali (immortalizzati). È stato dimostrato che l'estratto aveva un'attività anti-proliferativa sulle cellule tumorali umane mentre non era tossico sulle cellule normali. Inoltre, l'estratto era in grado di proteggere le cellule dallo stress ossidativo e dall'infiammazione indotti dalle radiazioni UVA e che tale effetto benefico era dovuto all'elevata quantità di acido ascorbico.

La bacca di açai è stata classificata come il frutto più nutriente di tutta la foresta amazzonica. Questa bacca risulta essere ricchissima di antocianine (antiossidanti normalmente presenti nella frutta viola e rosso scuro), proteine, acidi grassi, fibre, vitamine e minerali. Questo frutto cresce su una palma (*Euterpe oleracea* Martius) che si trova nella pianura dell'Amazonia. Si dice che la longevità degli aborigeni amazzoniani sia dovuta proprio ad un elevato consumo di questa bacca. Inoltre, è stato dimostrato che la quantità di antocianine (molecole responsabili del "paradosso francese") presenti in açai é di gran lunga superiore a quella presente nel vino rosso. Quindi, l'estratto idrofilico ottenuto da queste bacche è stato utilizzato per studiarne gli effetti su fibroblasti immortalizzati. Le cellule venivano prima incubate con l'estratto e poi esposte alle radiazioni UVA. Gli estratti hanno mostrato un'eccellente attività antiossidante, e, mediante frazionamento ed analisi di spettrometria di massa, sono stati identificati i derivati della cianidina e malvidina. Tali molecole presentano numerosi anelli aromatici con diversi gruppi -OH, riconosciuti come i responsabili dell'azione antiossidante. Successivamente, si è valutata anche la capacità dell'estratto di agire su cellule già stressate. I risultati hanno chiaramente dimostrato che sia l'estratto totale, sia le frazioni contenenti i derivati di cianidina e malvidina erano

in grado di ripristinare i livelli intracellulari di ROS e GSH e inibire l'attivazione della cascata delle MAP chinasi. Questo risultato ha permesso di ipotizzare nuovi possibili utilizzi dell'estratto di açai, come ad esempio nei prodotti alimentari o in creme doposole.

È importante sottolineare che in tutti e tre i casi sopraelencati, sono stati adoperati solventi organici per estrarre gli antiossidanti, in quanto essi presentano un'elevata efficienza di estrazione e applicabilità nei campi più svariati. È' generalmente noto che la resa dell'estrazione chimica dipende dalla polarità del solvente, dalla quantità di tempo, dalla temperatura, dal rapporto campione-solvente, nonché dalla composizione chimica e caratteristica fisica del campione. Pertanto, non esiste una procedura universale di estrazione, idonea all'estrazione di tutte le molecole attive di una pianta. Tuttavia, ci sono diversi inconvenienti nell'uso di solventi organici:

1. essi possono estrarre anche alcuni componenti indesiderati, come gli zuccheri, gli acidi organici e i grassi, richiedendo, di conseguenza, ulteriori passaggi di purificazione;
2. i solventi organici sono molto costosi e per rimuoverli serve energia, con conseguente aumento dei costi di estrazione;
3. alcuni di essi sono tossici per la salute umana, anche se presenti solo in tracce.

Quindi, al fine di minimizzare tali problemi, è stato messo a punto un nuovo protocollo di estrazione delle molecole attive da frutto di açai con solventi non tossici (legge 2009/32/CE), come l'etanolo e l'isopropanolo. Successivamente, l'attività antiossidante degli estratti di açai è stata confermata mediante saggi su cellule esposte allo stress ossidativo.

Inoltre, recentemente, è stato ottenuto un estratto acquoso, per semplice spremitura, dai cladodi (parte non commestibile) del fico d'india (*Opuntia ficus-indica*). È stato dimostrato che l'estratto era ricco in carboidrati e in tre derivati fenolici, cioè acido piscidico, eucomico e 2-idrossi-4- (4'-idrossifenil)-butanoico. La presenza dei tre derivati fenolici ci ha incoraggiati a studiare tale estratto come antiossidante. I cheratinociti umani sono stati trattati con l'estratto e poi sottoposti a stress ossidativo mediante raggi UVA. I risultati ottenuti hanno mostrato una chiara attività antiossidante dell'estratto sulle cellule. Inoltre, la presenza dei carboidrati permette di formare una rete molecolare e di mantenere un'enorme quantità d'acqua, costituendo una barriera protettiva sulla superfice della pelle accelerando anche la rimarginazione delle ferite.

Le piante e i loro frutti non sono le uniche fonti di antiossidanti, infatti essi possono essere prodotti, sotto forma di metaboliti secondari, anche da diversi microorganismi. Per questo motivo è stata valutata l'attività antiossidante di due batteri: un membro degli *Sphingomonadales* ed un *Bacillus subtilis*. Mentre nel primo caso sono stati estratti gli antiossidanti dal batterio, nel secondo caso l'intera spora del batterio è stata usata come agente anti-stress.

Nel 2011, dallo strato superficiale del mare di Pozzuoli (Napoli) è stato isolato un nuovo ceppo batterico, *Novosphingobium sp.* PP1Y (denominato PP1Y). Le acque in cui è stato trovato questo microorganismo sono inquinate da diversi tipi di idrocarburi aromatici, i quali vengono usati da PP1Y come fonte primaria di carbonio. Dalla parziale caratterizzazione di PP1Y è emerso che tale ceppo batterico fa parte di un

gruppo di proteobatteri Gram-negativi, i cui genomi sono ricchi in sequenze che codificano idrolasi glicosiliche, glicosiltransferasi e carotenoidi. La capacità antiossidante dell'estratto lipofilico di PP1Y è stata analizzata conducendo esperimenti sia *in vitro* (sulle cellule del carcinoma del colon umano) che *in vivo* (su *C. elegans*[i]). In entrambi i casi, l'estratto di PP1Y ha dato eccellenti risultati. Infatti, sia le cellule che i vermi erano in grado di resistere allo stress ossidativo. In seguito l'estratto è stato frazionato e le frazioni sono state sottoposte ad analisi di spettrometria di massa. Dai risultati è emerso che la frazione attiva aveva uno spettro UV-visibile paragonabile a quello della nostoxantina, antiossidante prodotto dai batteri della famiglia degli *Sphingomonadales*, di cui PP1Y fa parte. Attualmente sono in corso analisi volte a confermare l'identità di tale molecola. Dal punto di vista biotecnologico ed economico la produzione di carotenoidi a partire da un ceppo batterico risulta molto conveniente e fornisce un'alternativa valida alla sintesi chimica, i cui prodotti vengono spesso considerati pericolosi sia per l'uomo che per l'ambiente.

Successivamente, l'attenzione è stata rivolta all'uso di *Bacillus subtilis* come batterio antiossidante. L'idea è nata dall'osservazione che tale batterio è in grado di produrre un gran numero di molecole attive che gli permettono di sopravvivere in diversi habitat naturali: il corpo umano, il bestiame ed il suolo. Per questo motivo il ceppo di *B. subtilis* è stato ampiamente studiato ed ora è commercializzato in vari ambiti industriali, da quello alimentare e farmaceutico (come probiotico) a quello cosmetico (come prodotti per la cura della pelle). Considerando che le spore presentano alta resistenza alle condizioni avverse, è stato ipotizzato l'utilizzo di questo microorganismo come antiossidante. L'attività antiossidante delle spore di *B. subtilis* è stata testata sui cheratinociti umani normali esposti all'arsenito di sodio. I risultati ottenuti hanno dimostrato che le cellule pre-incubate con le spore erano in grado di resistere ai danni indotti dall'agente pro-ossidante, non perché le spore riducessero la produzione di ROS, ma perché le spore inducevano l'attivazione del fattore di trascrizione Nrf-2, il quale, una volta attivato, trasloca nel nucleo attivando la trascrizione di enzimi antiossidanti e di proteine detossificanti.

Una delle sfide più ambiziose di questo secolo prevede la riduzione al minimo della dipendenza dalle risorse fossili e della produzione di rifiuti solidi e liquidi. Infatti, l'Unione europea è impegnata a promuovere un modello rigenerativo che utilizza risorse in modo intelligente ed efficiente, sviluppando un'economia circolare. In questo contesto, le microalghe hanno acquisito una notevole importanza, avendo un potenziale uso che va dalla semplice produzione di biomasse per alimenti e mangimi ad applicazioni che prevedono un ricavo di molecole ad alto valore aggiuntivo.

In questo contesto si è cercato di unire gli scopi di due progetti di dottorato: ricavare l'amido (progetto seguito dalla Dott.ssa Imma Gifuni) e gli antiossidanti (progetto in questione) dalle microalghe. Durante il processo di estrazione dell'amido dalla *Chlorella sorokiniana* Shihiraet Krauss si ottiene una frazione di scarto molto ricca in antiossidanti. Dunque, nell'ottica della bio-economia circolare, è stata analizzata l'attività antiossidante di questa frazione sul sistema *in vivo* di *C. elegans*[i]. I risultati hanno dimostrato che il trattamento dei vermi con l'estratto favoriva la loro resistenza allo stress ossidativo. In particolare, tale resistenza era dovuta all'attivazione del fattore di trascrizione DAF-16/FOXO, che svolge un ruolo simile a Nrf-2 nei mammiferi. In seguito al frazionamento dell'estratto mediante HPLC a fase inversa ed alla successiva analisi mediante spettrometria di massa è risultato che le frazioni attive

erano ricche in acidi grassi polinsaturi a catena lunga (PUFA), carotenoidi, porfirine, un derivato della quercetina ed alcuni triacilgliceroli. Tali componenti, miscelati tra di loro, sono responsabili dell'attività antiossidante delle microalghe.

In conclusione, durante il presente progetto di dottorato, sono stati isolati e testati molti antiossidanti provenienti da varie fonti naturali. In generale è stato dimostrato che gli estratti grezzi hanno un'attività antiossidante simile o migliore rispetto alla molecola isolata. Ciò suggerisce la possibilità di utilizzare l'estratto intero nell'industria alimentare o cosmetica, evitando così elevati costi di purificazione di singole molecole e soddisfacendo la crescente domanda del mercato di additivi naturali, che vengono percepiti dal consumatore come più sicuri.

In futuro sarebbe interessante combinare tra loro questi estratti con lo scopo di ottenere effetti additivi o sinergici. Ovviamente, si tratterebbe di un approccio complicato, dato che la maggior parte degli antiossidanti agiscono in reazioni di ossido-riduzione che sono reversibili. Inoltre, alcuni di essi (ad esempio l'ascorbato) possono agire sia come antiossidanti che come pro-ossidanti, a seconda delle concentrazioni e dello stato di salute della cellula. Infine, dato il ruolo importante dei ROS come mediatori dei normali processi di segnali intracellulari, la determinazione del dosaggio ottimale richiederebbe una regolazione fine, per evitare effetti collaterali dovuti alla perturbazione del bilancio redox necessario per il normale funzionamento cellulare.

[i]Gli esperimenti su *C. elegans* sono stati effettuati nel laboratorio del Prof. Michael Wink, Istituto di Farmacia e Biotecnologia Molecolare, Heidelberg, Germania.

SUMMARY

Synthetic antioxidants could be replaced by the valid bio-based alternatives. These renewable and low cost resources are available and offers a market opportunity for a green supply of raw materials for different industrial and health products.

The aim of the present PhD project was to analyse the antioxidant activity of extracts obtained from different natural sources or microorganisms, in order to study their beneficial effects against oxidative stress injury and to characterize their chemical composition to obtain molecules to be used in food or cosmetic industry.

Therefore, fruits and vegetables were considered a good starting point, as it is widely known that they are rich in molecules with antioxidant activity.

As a first goal, the methanol extracts from two tomato varieties and from açai berries were analysed. These products are among the most consumed in Mediterranean and Brazilian diet, respectively. The beneficial effects of the extracts were demonstrated on a cell-based model in which oxidative stress was induced and the molecules responsible for the antioxidant activity were determined.

Thereafter, to avoid the toxicity and high costs of solvent extractions, the attention was focused on extracts obtained without the need of solvents. In particular, the antioxidant activity of a water extract from the cladodes of *Opuntia ficus-indica* was analysed. The whole extract, as well as its active molecules, showed a good ability to protect human keratinocytes from UVA induced oxidative stress.

Plants and their fruits are not the only source of antioxidants, as these are metabolites produced by microbes. From a biotechnological and economical point of view, the production of antioxidants by microorganisms is very convenient and provides an alternative to chemical synthesis. For this reason, two bacterial strains were used in different ways. In the first case, a lipophilic extract from *Novosphingobium sp.* PP1Y was obtained and tested, as the characterization of this recently isolated microorganism showed the presence of a great abundance of genes encoding for carotenoids. PP1Y extract was able to counteract oxidative stress in an *in vitro* system on cells as well as in an *in vivo* system on *C. elegans*. In the second case, the whole spore from the bacterium *Bacillus subtilis* was used as antioxidant. The results showed that incubation with spores induced the activation in the treated cells of Nrf-2 pathway, which induced the transcription of anti-stress response genes.

Finally, a waste fraction from microalgae *Chlorella sorokiniana* Shihiraet Krauss was tested for its antioxidant activity. This fraction was discarded after starch purification (PhD project of Dr. Imma Gifuni). Therefore, in order to minimize the generation of waste, the recovery of high-value products was attempted. It was demonstrated that the cascade approach was a good strategy to produce starch and active antioxidants.

In conclusion, in the present PhD thesis, different antioxidants from natural sources have been isolated and tested, and extracts from these sources showed an antioxidant power similar or higher than the isolated molecules. This opens the way to the use of the whole extract in food or cosmetic industries, avoiding the high costs for the purification of single compounds, in accordance with the increasing demand of natural products endowed with pro-healthy effects.

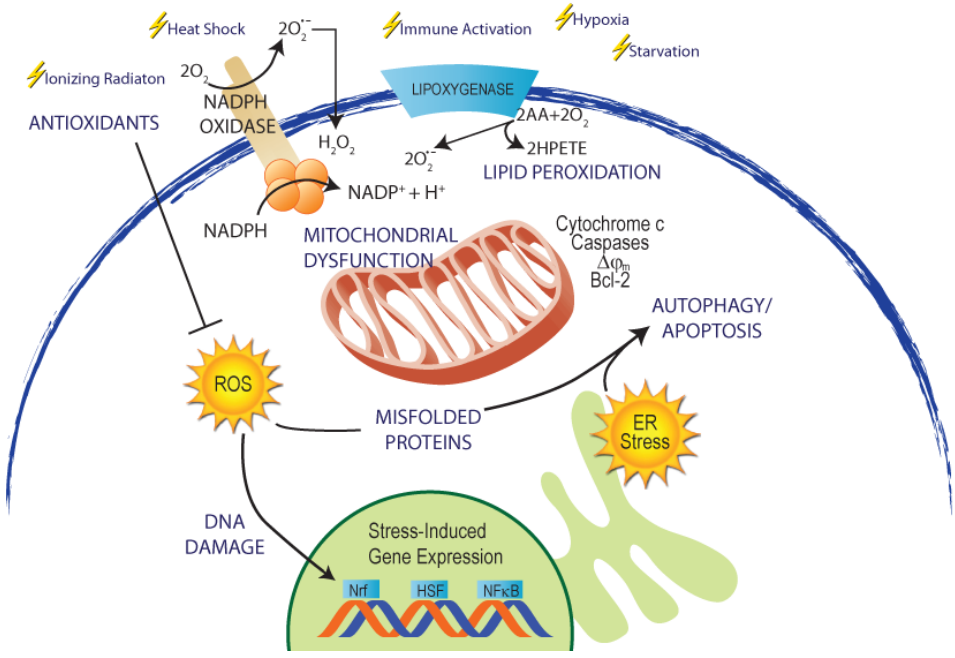

Image taken from http://www.enzolifesciences.com/platforms/cellular-analysis/oxidative-stress/

1.1 Free radical formation and oxidative stress

In eukaryotic cells, oxidative stress is considered as an unequal condition between intracellular reactive oxygen species (ROS) and antioxidants levels. This imbalance leads to DNA damage, lipid peroxidation, as well as to the activation of signalling pathways that induce an unlimited growth of cells, their inability to differentiate, and the insurgence of a malignant phenotype[1–6]. It is noteworthy that ROS are recognized for playing a dual role: they prevent the insurgence of diseases by assisting the immune system, mediating cell signaling and playing an essential role in apoptosis but, on the other hand, they can damage important macromolecules in cells and may have a role in carcinogenesis and cardiovascular disease[7]. In fact, it is well documented that oxidative stress is involved in many pathologies, such as cardiovascular diseases, neurodegenerative disorders, and cancers[8,9].

From a metabolic point of view, oxygen is necessary for all aerobic organisms and acts as terminal oxidant in the mitochondrial respiratory chain, which is the main source of energy for the cell. However, the univalent reduction of oxygen leads to ROS formation[10]. Examples of oxygen-centred free radicals include superoxide ($O_2^{\bullet-}$), peroxyl ($ROO^{\bullet}$), alkoxyl ($RO^{\bullet}$) and hydroxyl ($HO^{\bullet}$). These by-products are highly unstable and active towards chemical reactions with other molecules, as nitric oxide ($NO^{\bullet}$) form reactive nitrogen species (RNS) and constitute the basis for the formation of a multitude of additional oxidative signalling elements, including the highly reactive and potentially damaging peroxynitrite ($ONOO^-$)[11,12]. Both ROS and RNS may target cysteine thiols, leading to oxidative modifications and giving life to reactive sulphur species (RSS)[13]. In the cell, however, free radical formation continuously occurs due to enzymatic and non-enzymatic reactions. Enzymatic reactions, which serve as source of free radicals, include those involved in the respiratory chain, phagocytosis, prostaglandin synthesis, and in the cytochrome P-450 system[14], whereas non-enzymatic reactions include those between oxygen and organic compounds, as well as reactions initiated by ionizing process. Furthermore, free radicals are derived either from normal essential metabolic processes in the cells or from external sources. Endogenous free radicals are generated from immune cells activation, inflammation, mental stress, excessive exercise, ischemia, infection, cancer and aging.

As for the latter, over the past four decades, a number of studies have shown, from invertebrates to humans, an age-related increase damage in a variety of molecules (lipid, protein, sugars and DNA) due to chronic exposure to oxidative stress[15–17].

Instead, exogenous ROS results from air and water pollution, cigarette smoke, alcohol, heavy or transition metals (Cd, Hg, Pb, Fe, As), certain drugs (cyclosporine, tacrolimus, gentamycin, bleomycin), industrial solvents, cooking (smoked meat, used oil, fat) and UV radiations[18]. In particular, UV radiations are considered one of the most harmful exogenous factors for the human skin, as, in addition to the development of erythema, ROS are produced. Damages induced by UV radiations strongly depend on the wavelength of the incident photons that hit the cell[19]. In particular, in the UVB range (280-295 nm), direct light absorption by DNA results mainly in dimerization reactions between adjacent pyrimidine bases. UVA radiations (320-400nm), considered more dangerous than UVB (280-320nm), are extremely weakly absorbed by DNA, but rather excite endogenous chromophores, leading to DNA damage. This occurs through the production of reactive singlet oxygen that could react with all DNA bases. However, when the single oxygen reacts with guanine, the process generates 8-oxo-7,8-dihydro-

2'-deoxyguanosine (8-oxo-dG)[20]. While normally guanine pairs with cytosine, 8-oxo-dG pairs with adenine. The resulting point mutation will be translated in a mutated proteinThis is one of the reasons why ROS are assumed to be involved in cancer formation and aging[21].

UVA radiations may also promote the formation of hydroxyl radicals *via* the photosensitized production of superoxide anions, which are highly reactive and with low specificity, so that they can induce a wide range of DNA damage.

Many studies have focused on metals-induced toxicity and carcinogenicity, emphasising their role in the generation of ROS and RNS in biological systems. Metal-mediated formation of free radicals may cause different modifications to DNA bases, may increase lipid peroxidation, and may change calcium and sulfhydryl homeostasis[22]. Arsenic, a natural element widely present in food, water, air and soil is able to induce oxidative stress[23]. Its inorganic form exists predominantly in trivalent (As^{3+}, such as sodium arsenite and arsenic trioxide) or pentavalent (As^{5+}) form and is generally considered more harmful than its organic form[24,25]. Many studies confirmed the generation of free radicals during arsenic metabolism in cells. Indeed, it has been reported that the exposure of human cell lines to sodium arsenite increases the production of ROS[26–28], which induce intracellular oxidative stress and result in oxidative DNA damage and finally end into apoptosis[29,30].

1.3 Role of ROS and their targets

When the stress is severe, survival is dependent on the ability of the cell to adapt or resist to the stress, and to repair or replace damaged molecules. Alternatively, cells may respond to the insult by undergoing apoptosis, a process aimed at preserving the organism by removing damaged cells. Among the main stress signaling pathways and/or central mediators activated in response to oxidant injury, the extracellular signal-regulated kinase (ERK), c-Jun amino-terminal kinase (JNK) and p38 mitogen-activated protein kinase (MAPK) signaling cascades, the phosphoinositide 3-kinase (PI(3)K)/Akt pathway, the nuclear factor (NF)-kB signaling system, p53 activation, and the heat shock response have to be considered. In general, the heat shock response, ERK, PI(3)K/Akt and NF-kB signaling pathways exert a pro-survival influence during oxidant injury, whereas activation of p53, JNK and p38 are more commonly linked to apoptosis. However, numerous exceptions to these generalities can be found[31].

The main targets of ROS are proteins, DNA and RNA molecules, as well as sugars and lipids. In particular, proteins can be modified in three distinct ways: (i) a specific amino acid can be oxidized, (ii) the peptide can be cleaved after a reaction with the free radical, or (iii) protein cross-linking can be formed due to reactions with lipid peroxidation products. In the case of nucleic acids, the damage induced by free radicals can be both chemical and structural. Examples of these are the production of base-free sites, deletions, modification of all bases, frame shifts, strand breaks, nucleic acid-protein cross-links and chromosomal arrangements. As for sugar modifications, the formation of oxygen free radicals during early glycation could contribute to glycoxidative damage[32]. Lipid peroxidation is initiated by an attack towards a fatty acid's side chain by a radical in order to abstract a hydrogen atom from a methylene carbon. After the removal, the carbon centered lipid radical can undergo molecular rearrangement and react with oxygen forming a peroxyl radical. These highly reactive molecules can obtain hydrogen atoms from the surrounding molecules and propagate a chain reaction of lipid peroxidation. Finally, another way to generate lipid peroxides

is through the attack on polyunsaturated fatty acids or their side chain by the singlet oxygen which is a very reactive form of oxygen[33].

1.4 Antioxidants and health maintenance

Organisms have evolved antioxidant systems to protect themselves against toxic oxygen by-products. Khlebnikov defined antioxidants as ‘‘any substance that directly scavenges ROS or indirectly acts to up-regulate antioxidant defences or inhibit ROS production’’[34]. Another antioxidant property is the ability, after scavenging the radical, to form a new, more stable, radical, through intramolecular hydrogen bonding on further oxidation[35]. Different antioxidants can help the body in counteracting the negative effects induced by ROS, endogenous, i.e. produced by the body, and exogenous, i.e. obtained from the diet. The first class can be divided in enzymatic- and non-defences, such as:

- Superoxide dismutase (SOD), an enzyme that alternately catalyses the dismutation of the superoxide (O_2^-) radical into either ordinary molecular oxygen (O_2) or hydrogen peroxide (H_2O_2). The enzyme exists in 3 forms: a) Cu/Zn SOD present mainly in the cytosolic matrix, b) MnSOD localized preferentially in mitochondria and c) extracellular SOD[22];
- Catalase, which works almost in the same way, since H_2O_2 can be a weak reductant as well as a fairly strong oxidant. This enzyme is present in the peroxisome of aerobic cells and it is very efficient in promoting the conversion of H_2O_2 to water and molecular oxygen[22];
- Glutathione peroxidase, which acts in association with the tripeptide glutathione (GSH), present in high concentration in cells. The enzyme catalyses the conversion of H_2O_2 or organic peroxide to water or alcohol while simultaneously oxidizing GSH. Glutathione peroxidase can reduce lipid peroxides as well as H_2O_2 and this enzyme is important in the prevention of lipid peroxidation to maintain the structure and function of biologic membranes[22].

Non-enzymatic defenders include:

- iron and copper-binding extracellular proteins (e.g., albumin, transferrin, lactoferrin, haptoglobin, and ceruloplasmin)[36];
- other cellular compounds (e.g., quinones, glutathione, uric acid, and bilirubin)[36].

Enzymatic and non-enzymatic defences are complementary to each other, since they act against different species in different cellular compartments. However, despite these defence systems (able either to suppress free radical formation and chain initiation or to scavenge free radical and chain propagation), some ROS can still “escape” and cause damage. In this case, the third level of defence intervenes. This level of antioxidant defence includes lipolytic (lipases), proteolytic (peptidases or proteases) and other enzymes (DNA repair enzymes, methionine sulphoxide reductase, ligases, nucleases, polymerases, proteinases, phospholipases and various transferases) as well as chaperones, including HSPs.

Moreover, exogenous antioxidants, introduced by the diet, may help the endogenous antioxidant system. This class of active molecules can be divided into synthetic and natural antioxidants. Examples of synthetic antioxidants include: nitroxides, spin traps[37], Mn-porphyrin superoxide dismutase mimics[38], salens, able not only to dismutate superoxide but also decompose products of this reaction, hydrogen peroxide[39], GPX mimetics, coenzyme Q analogues[40], aminosterols[41], etc. Unfortunately, high dosage of synthetic antioxidants can be carcinogenic thus, the attention to natural antioxidants is heightened by gradually phase out synthetic additives which have been traditionally used in the food chain and cosmetic industry[42]. Natural phytonutrients/phytochemicals with antioxidant activity can be classified in:

- Flavonoids (e.g. quercetin, rutin, isoflavins, anthocyanins and catechins);
- Polyphenols (e.g. phenolic acids, resveratrol, gallic acid, cannabinods, salicylic acid)
- Carotenoids (e.g. α- and β- carotene, lutein, lycopene, zeaxanthin and crocetin);
- Minerals (e.g. copper, manganese, iodide and zinc).

Ascorbic acid is absorbed through the gastrointestinal tract and is effective in scavenging the superoxide radical anion, hydrogen peroxide, hydroxyl radical, singlet oxygen and reactive nitrogen oxide[22]. Vitamin E halts lipid peroxidation by donating its phenolic hydrogen to the peroxyl radicals forming tocopheroxyl radicals that, despite also being radicals, are unreactive and unable to continue the oxidative chain reaction. Vitamin E is the only major lipid-soluble, chain breaking antioxidant found in plasma, red cells and tissues, allowing it to protect the integrity of lipid structures, mainly membranes[32]. Flavonoids are an antioxidant group of compounds composed of flavonols, flavanols, anthocyanins, isoflavonoids, flavanones and flavones. All these sub-groups of compounds share the same diphenylpropane skeleton. Some of the most important flavonoids are represented by catechin, catechin-gallate, quercetin and kaempferol[32]. Phenolic acids, a major class of polyphenols, are ubiquitous in plants. They have antioxidant activity as chelators and free radical scavengers with special impact over hydroxyl and peroxyl radicals, superoxide anions and peroxynitrites[43].

Carotenoids are pigments found in plants and microorganisms. There are over 600 carotenoids occurring in nature. The antioxidant activity of carotenoids arises primarily as a consequence of the ability of the conjugated double-bonded structure to delocalise unpaired electrons[44].

1.5 Antioxidants mechanism of action

Antioxidants can counteract free radicals by accepting or donating electron(s) to eliminate the unpaired condition of the radical. Antioxidant molecules may either directly react with the reactive radicals and neutralize them, or they may become new free radicals, less active and less dangerous than those neutralized. Then, they may be neutralized by other antioxidants or other mechanisms to terminate their radical status[45].

To explain antioxidant's mechanism of action, the process of lipid peroxidation can be used as an example (**Figure 1**)[46]. In the initiation stage, free radicals are formed through thermolysis, where the break of covalent bonds is induced by heat. Compounds that homolyze at relative low temperature (<100 ˚C) are important initiators of radical-based chain reactions, such as unsaturated fatty acids (UFA). The

UFA homolytic products are hydroxyl radical (HO•), alkyl radical (RO•) and hydroperoxyl radical (HOO•), which further react with triplet oxygen to form peroxyl radicals. These radical products have high energy and can bind to a hydrogen molecule of the lipid structure, forming hydroperoxides (primary oxidation products). The formation of hydroperoxides can be repeated several times, propagating the oxidation reaction.

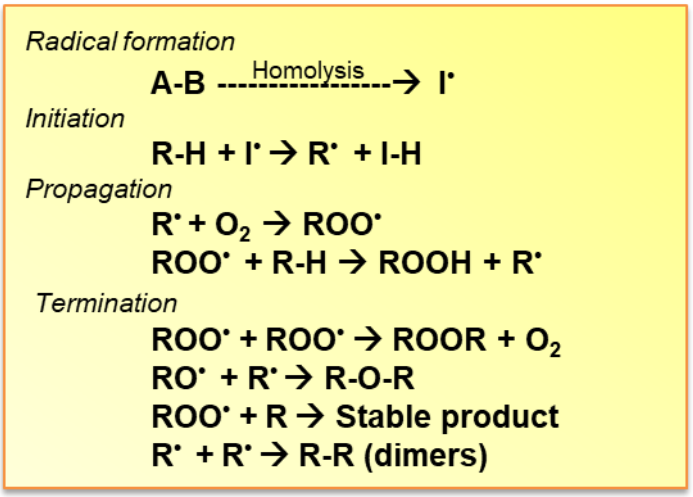

Figure 1*:* Steps in lipid peroxidation process. Once radicals are formed (generally indicated by •), they can react with different molecules in the cell, thus causing the formation of stable products which can be toxic.
Image taken from paper of Saldata et al.[46].

In the next oxidation step, hydroperoxides (or any other primary oxidation product) can interact with double bonds to form monomeric degradation products, such as ketones[47]. Alternatively, they can be cleaved to form low molecular weight products, such as aldehydes, ketones, alcohols and hydrocarbons. Finally, hydroperoxides can homolyze to form peroxyl or alkoxy radicals that further reacts to form stable dimer-like products. Antioxidants can interfere in any of these steps, thus blocking the propagation of radicals.

Therefore, antioxidants can be divided in:

- ✓ **Preventive**, as this class of antioxidants prevent the formation of free radicals. As an example, SOD and CAT enzymes decompose O_2^- and H_2O_2 in O_2 and H_2O[22];
- ✓ **Chain-breaking**, when the antioxidants interrupt free radical chain reactions. For example, α-tocopherol acts by giving the H from phenol group to the peroxyl radicals[48];
- ✓ **Physical quenching**, in which antioxidants neutralize the singlet oxygen by restoring its ground state with no oxygen consumption or product formation (β-carotene[49] and lycopene[50]);
- ✓ **Synergists of proper antioxidants**, i.e. substances able to increase the activity of chain-breaking antioxidants when applied in a mixture (citric acid);
- ✓ **Reducing agents**, such as thiols of sulfides (thioethers), which convert hydroperoxides into stable components in a non-radical way;
- ✓ **Metal chelators**, which convert metal pro-oxidants, especially iron or copper derivatives, into stable products. If not chelated, heavy metals

promote the decomposition of lipid hydroperoxides into free radicals. The importance of metal chelating is often neglected, but trace metals significantly contribute to the free-radical formation by decomposing lipid hydroperoxides into free radicals. Quercetin, tannins, and phytates are good examples of efficient metal chelators[51];

- ✓ **Inhibitor of pro-oxidative enzymes** (especially lipoxygenases).

1.6 Sources of natural antioxidants

Fruits and vegetables contain a range of different phytochemicals, which have been recognized for their potential health benefits. Several epidemiological studies have revealed that high fruits and vegetables intake appears to be positively correlated with reduced mortality induced by some types of "civilizational diseases", including cancer. One possible mechanism responsible for the positive effect has been attributed to the antioxidant activity of fruits and vegetables constituents[52].

To date, a large number of different natural products with high phenol/polyphenol content, and consequently with high antioxidant power, has been identified. Green tea, extra virgin olive oil, red wine, tomatoes, spices, berries, and aromatic herbs are among the most studied natural products; these natural products are very frequently and continuously assumed in the so-called Mediterranean and Asian diet, considered as healthy feeding diets[53,54].

Tomatoes are one of the most widely used and versatile fruit crops[55]. Epidemiological studies suggest that consumption of tomato and tomato-based products reduces the risk of chronic diseases, such as cardiovascular disease and cancer[56]. Typically, this protective action is attributed to antioxidant components, such as carotenoids (in particular, lycopene and β-carotene), ascorbic acid, flavonoids and tocopherols, and synergistic interactions among them[57–59].

Red grapes (*Vitis vinifera*) contain high levels of resveratrol (trans-3,5,4′-trihydroxystilbene, RV), a particularly abundant polyphenol (6.5 mg/L) which is also present in highly pigmented vegetables and fruits[60]. RV is considered a potent antioxidant[61], anticancer[62] and anti-inflammatory agent[63]. Grape seeds, rich in polyphenols, are a by-product derived from grape juice and wine processing[64]. Grape seeds have been shown to possess antioxidant properties both *in vivo* and *in vitro* due to flavonoids that can perform scavenging action on free radicals[65]. The native South American palm açaí berry (*Euterpe oleraceae* Mart.) has high polyphenolic and antioxidant levels[66–68]. Açaí has been shown to prevent hydrogen peroxide-induced cell damage[69], lower oxidative stress in neutrophils[68] and reduce inflammatory signaling in microglial cells[70]. Olives and olive oil contain high levels of oleuropein (OLE), a phenol compound with antioxidant activity[71,72]. Green tea is very high in polyphenols with potent antioxidant and anti-cancer properties. The major polyphenols in green tea are flavonoids (e.g., catechin, epicatechin, epicatechin gallate, epigallocatechin gallate (EGCG) and proanthocyanidins). EGCG is considered as the most significant active component, since it is able to inhibit lipid peroxidation[73].

Therefore, dietary antioxidants are considered beneficial for their potential protective role in the insurgence of several pathologies[74]. In the last few years, a worldwide interest in finding new and safe antioxidants from alternative sources has increased. Among these, microalgae have gained considerable importance, as they are capable, under stress conditions, of producing significant amounts of substances with high added value, e.g. carotenoids, phenolic compounds and polyunsaturated

fatty acids[75]. Recently, a strain of *Streptomyces* bacteria, producing antioxidant molecules, has been isolated from mangrove environments[76–78], thus supporting the importance of research of new bacterial strains with antioxidant activity[79].

1.7 Aim of the thesis

The general aim of this PhD project is to obtain antioxidants from different natural sources to be used in food or cosmetic industry (as food additive or as skin-care lotion, respectively). In particular, the following sources have been used:

- Vegetables/fruits: (i) the effects of heating on the antioxidant activity of a commercial tomato variety (**Chapter 2**); characterization of the antioxidant activity of a hydrophilic extract (ii) of a new tomato hybrid (**Chapter 2**) and (iii) of açai berry (**Chapter 3**); (iiii) the antioxidant activity of a water extract from *Opuntia ficus-indica* L. cladodes (**Chapter 4)**.
- Bacteria: (i) alternative use of spores from *Bacillus subtilis* as new antioxidants (**Chapter 5**); (ii) antioxidant activity of a lipophilic extract from *Novosphingobium sp.* PP1Y bacterial strain (**Chapter 6**).
- Waste products: antioxidant activity of a lipophilic extract from the microalga *Chlorella sorokiniana*, after starch-extraction (**Chapter 7**).

In each case, the *in vitro* antioxidant activity, the protective effects against oxidative stress injury on a cell-based model, the identification of the main class of active molecules was evaluated. In the case of lipophilic antioxidants from *Novosphingobium* sp. PP1Y bacterial strain and microalga *Chlorella sorokiniana*, the antioxidant activity was evaluated *in vivo* on a *C. elegans* model.

1.8 Bibliography

1. Claxton, L. & Woodall, G. A review of the mutagenicity and rodent carcinogenicity of ambient air. *Mutat. Res. Mutat.* **636,** 36–94 (2007).
2. Dhalla, N. S., Temsah, R. M. & Netticadan, T. Role of oxidative stress in cardiovascular diseases. *J. Hypertens.* **18,** 655–73 (2000).
3. Dalle-Donne, I., Rossi, R. & Colombo, R. Biomarkers of oxidative damage in human disease. *Chemistry (Easton).* **52,** 601–623 (2006).
4. Valko, M. … Telser, J. Free radicals and antioxidants in normal physiological functions and human disease. *Int. J. Biochem. Cell Biol.* **39,** 44–84 (2007).
5. Sayre, L. M., Smith, M. a & Perry, G. Chemistry and biochemistry of oxidative stress in neurodegenerative disease. *Curr. Med. Chem.* **8,** 721–738 (2001).
6. Gholamian-Dehkordi, N., Luther, T., Asadi-Samani, M. & Mahmoudian-Sani, M. R. An overview on natural antioxidants for oxidative stress reduction in cancers; a systematic review. *Immunopathol. Persa* **3,** (2017).
7. Seifried, H. E., Anderson, D. E., Fisher, E. I. & Milner, J. A. A review of the interaction among dietary antioxidants and reactive oxygen species. *J. Nutr. Biochem.* **18,** 567–579 (2007).
8. Sjöblom, T. The consensus coding sequences of human breast and colorectal cancers. *Science (80-.).* **314,** 268–274 (2006).
9. Somers, C. M. Reduction of particulate air pollution lowers the risk of heritable mutations in mice. *Science (80-.).* **304,** 1008–1010 (2004).

10. Chance, B., Sies, H. & Boveris, A. Hydroperoxide metabolism in mammalian organs. *Physiol. Rev.* **59,** 527–605 (1979).

11. Fukuto, J. M. … Wink, D. A. Small molecule signaling agents: The integrated chemistry and biochemistry of nitrogen oxides, oxides of carbon, dioxygen, hydrogen sulfide and their derived species. *Chem. Res. Toxicol.* **25,** 769–793 (2012).

12. Cortese-Krott, M. M. … Feelisch, M. The reactive species interactome: Evolutionary emergence, biological significance and opportunities for redox metabolomics and personalized medicine. *Antioxid. Redox Signal.* (2017). doi:10.1089/ars.2017.7083

13. Giles, G. I. & Jacob, C. Reactive sulfur species: An emerging concept in oxidative stress. *Biol. Chem.* **383,** 375–388 (2002).

14. Liu, T., Stern, A., Roberts, L. J. & Morrow, J. D. The isoprostanes: novel prostaglandin-like products of the free radical-catalyzed peroxidation of arachidonic acid. *J. Biomed. Sci.* **6,** 226–35 (1999).

15. Warner, H. R. Superoxide dismutase, aging, and degenerative disease. *Free Radic. Biol. Med.* **17,** 249–258 (1994).

16. Bohr, V. A. & Anson, R. M. DNA damage, mutation and fine structure DNA repair in aging. *Mutat Res* **338,** 25–34 (1995).

17. Sohal, R. S. & Weindruch, R. Oxidative stress, caloric restriction and aging. *Science (80-.).* **273,** 59–63 (1996).

18. Pham-Huy, L. A., He, H. & Pham-Huy, C. Free radicals, antioxidants in disease and health. *Int. J. Biomed. Sci.* **4,** 89–96 (2008).

19. Ravanat, J.-L., Douki, T. & Cadet, J. Direct and indirect effects of UV radiation on DNA and its components. *J. Photochem. Photobiol. B Biol.* **63,** 88–102 (2001).

20. Ravanat, J. L. … Cadet, J. Damage to isolated DNA mediated by singlet oxygen. *Helv. Chim. Acta* **84,** 3702–3709 (2001).

21. Aust, A. E. & Eveleigh, J. F. Mechanisms of DNA oxidation. *Proc. Soc. Exp. Biol. Med.* **222,** 246–252 (1999).

22. Valko M, Rhodes CJ, Moncol J, Izakovic M, M. M. Free radicals, metals and antioxidants in oxidative stress-induced cancer. *Chem. Biol. Interact.* **160,** 1–40 (2006).

23. Chen, C., Jiang, X., Zhao, W. & Zhang, Z. Z. Dual role of resveratrol in modulation of genotoxicity induced by sodium arsenite *via* oxidative stress and apoptosis. *Food Chem. Toxicol.* **59,** 8–17 (2013).

24. Rossman, T. G. Mechanism of arsenic carcinogenesis: An integrated approach. *Mutation Research - Fundamental and Molecular Mechanisms of Mutagenesis* **533,** 37–65 (2003).

25. Hughes, M. F. … Thomas, D. J. Arsenic exposure and toxicology : A historical perspective arsenic. *Toxicological* **123,** 305–332 (2011).

26. Ruiz-Ramos, R., Lopez-Carrillo, L., Rios-Perez, A. D., De Vizcaya-Ruiz, A. & Cebrian, M. E. Sodium arsenite induces ROS generation, DNA oxidative damage, HO-1 and c-Myc proteins, NF-kappaB activation and cell proliferation in human breast cancer MCF-7 cells. *Mutat. Res.* **674,** 109–115 (2009).

27. Zhang, Z. … Shi, X. Reactive oxygen species mediate arsenic induced cell transformation and tumorigenesis through Wnt/beta-catenin pathway in human colorectal adenocarcinoma DLD1 cells. *Toxicol Appl Pharmacol* **256,** 114–121 (2011).

28. Imlay, J. a. Pathways of oxidative damage. *Annu. Rev. Microbiol.* **57,** 395–418 (2003).

29. Hei, T. K. & Filipic, M. Role of oxidative damage in the genotoxicity of arsenic. *Free Radic. Biol. Med.* **37,** 574–581 (2004).

30. Wang, T. S., Kuo, C. F., Jan, K. Y. & Huang, H. Arsenite induces apoptosis in Chinese hamster ovary cells by generation of reactive oxygen species. *J. Cell. Physiol.* **169,** 256–268 (1996).

31. Finkel, T. & Holbrook, N. J. Oxidants, oxidative stress and the biology of ageing. *Nature* **408,**

239–247 (2000).

32. Carocho, M. & Ferreira, I. C. F. R. A review on antioxidants, prooxidants and related controversy: Natural and synthetic compounds, screening and analysis methodologies and future perspectives. *Food Chem. Toxicol.* **51,** 15–25 (2013).

33. Halliwell, B. & Chirico, S. Lipid peroxidation: Its mechanism, measurement and significance. *Am. J. Clin. Nutr.* **57,** 715S–724S (1993).

34. Khlebnikov, A. I., Schepetkin, I. A., Domina, N. G., Kirpotina, L. N. & Quinn, M. T. Improved quantitative structure-activity relationship models to predict antioxidant activity of flavonoids in chemical, enzymatic and cellular systems. *Bioorg. Med. Chem.* **15,** 1749–70 (2007).

35. Halliwell, B. Antioxidants : The basics-what they are and how to evaluate them. *Adv. Pharmacol.* **38,** 3–20 (1991).

36. Krinsky, N. I. Mechanism of action of biological antioxidants. *Proc. Soc. Exp. Biol. Med.* **200,** 248–254 (1992).

37. Day, B. J. Antioxidants as potential therapeutics for lung fibrosis. *Antioxid. Redox Signal.* **10,** 355–370 (2008).

38. Esposito, E. & Cuzzocrea, S. Role of nitroso radicals as drug targets in circulatory shock. *British Journal of Pharmacology* **157,** 494–508 (2009).

39. Chatterjee, P. K. … Thiemermann, C. EUK-134 reduces renal dysfunction and injury caused by oxidative and nitrosative stress of the kidney. *Am. J. Nephrol.* **24,** 165–177 (2004).

40. Pandolfo, M. Drug Insight: antioxidant therapy in inherited ataxias. *Nat. Clin. Pract. Neurol.* **4,** 86–96 (2008).

41. Kavanagh, R. J. & Kam, P. C. A. Lazaroids : efficacy and mechanism of action of the 21-aminosteroids in neuroprotection. *Br. J. Anaesth.* **86,** 110–119 (2001).

42. Jiang, J. & Xiong, Y. L. Natural antioxidants as food and feed additives to promote health benefits and quality of meat products: A review. *Meat Sci.* **120,** 107–117 (2016).

43. Piazzon, A. … Nardini, M. Antioxidant activity of phenolic acids and their metabolites: Synthesis and antioxidant properties of the sulfate derivatives of ferulic and caffeic acids and of the acyl glucuronide of ferulic acid. *J. Agric. Food Chem.* **60,** 12312–12323 (2012).

44. Mortensen, A., Skibsted, L. & Truscott, T. The interaction of dietary carotenoids with radical species. *Arch. Biochem. Biophys.* **385,** 13–19 (2001).

45. Lü, J.-M., Lin, P. H., Yao, Q. & Chen, C. Chemical and molecular mechanisms of antioxidants: experimental approaches and model systems. *J. Cell. Mol. Med.* **14,** 840–860 (2010).

46. Saldana, M. D. A. & Martinez-Monteagudo, S. I. Oxidative stability of fats and oils measured by differential scanning calorimetry for food and industrial applications. in *Applications of calorimetry in a wide context - Differential scanning calorimetry, isothermal titration calorimetry and microcalorimetry* (InTech, 2013). doi:10.5772/54486

47. Kamal-Eldin, A. & Pokorný, J. *Analysis of lipid oxidation*. (2005).

48. Azzi, A. Molecular mechanism of α-tocopherol action. *Free Radic. Biol. Med.* **43,** 16–21 (2007).

49. Stahl, W. & Sies, H. Lycopene: a biologically important carotenoid for humans? *Arch. Biochem. Biophys.* **336,** 1–9 (1996).

50. Di Mascio, P., Kaiser, S. & Sies, H. Lycopene as the most efficient biological carotenoid singlet oxygen quencher. *Arch. Biochem. Biophys.* **274,** 532–538 (1989).

51. Leopoldini, M., Russo, N., Chiodo, S. & Toscano, M. Iron chelation by the powerful antioxidant flavonoid quercetin. *J. Agric. Food Chem.* **54,** 6343–6351 (2006).

52. Svobodová, A., Rambousková, J., Walterová, D. & Vostálová, J. Protective effects of phenolic fraction of blue honeysuckle fruits against UVA-induced damage to human keratinocytes. *Arch. Dermatol. Res.* **300,** 225–233 (2008).

53. Stefani, M. & Rigacci, S. Beneficial properties of natural phenols: Highlight on protection against

pathological conditions associated with amyloid aggregation. *BioFactors* **40,** 482–493 (2014).

54. Algamdi, N., Mullen, W. & Crozier, A. Tea prepared from *Anastatica hirerochuntica* seeds contains a diversity of antioxidant flavonoids, chlorogenic acids and phenolic compounds. *Phytochemistry* **72,** 248–254 (2011).

55. De Sousa, A. S., Borges, S. V., Magalhães, N. F., Ricardo, H. V. & Azevedo, A. D. Spray-dried tomato powder: Reconstitution properties and colour. *Brazilian Arch. Biol. Technol.* **51,** 807–814 (2008).

56. Giovannucci, E. Tomatoes, tomato-based products, lycopene, and cancer: Review of the epidemiologic literature. *JNCI J. Natl. Cancer Inst.* **91,** 317–331 (1999).

57. Raffo, A., La Malfa, G., Fogliano, V., Maiani, G. & Quaglia, G. Seasonal variations in antioxidant components of cherry tomatoes (*Lycopersicon esculentum* cv. Naomi F1). *J. Food Compos. Anal.* **19,** 11–19 (2006).

58. Podsędek, A., Sosnowska, D. & Anders, B. Antioxidative capacity of tomato products. *Eur. Food Res. Technol.* **217,** 296–300 (2003).

59. Martinez-Valverde, I., Periago, M. J., Provan, G. & Chesson, A. Phenolic compounds, lycopene and antioxidant activity in commerical varieties of tomato (*Lycopersicum esculentum*). *J. Sci. Food Agric.* **82,** 323–330 (2002).

60. Milardi, G. L., Stringaro, A., Colone, M., Bonincontro, A. & Risuleo, G. The cell membrane is the main target of resveratrol as shown by interdisciplinary biomolecular/cellular and biophysical approaches. *J. Membr. Biol.* **247,** 1–8 (2014).

61. Gülçin, İ. Antioxidant properties of resveratrol: a structure–activity insight. *Innov. Food Sci. Emerg. Technol.* **11,** 210–218 (2010).

62. Bai, Y. … Xie, L. P. Resveratrol induces apoptosis and cell cycle arrest of human T24 bladder cancer cells in vitro and inhibits tumor growth *in vivo*. *Cancer Sci.* **101,** 488–493 (2010).

63. Frémont, L. Biological effects of resveratrol. *Antioxid. Redox Signal.* **3,** 1041–1064 (2001).

64. Lau, D. W. & King, A. J. Pre- and post-mortem use of grape seed extract in dark poultry meat to inhibit development of thiobarbituric acid reactive substances. *J. Agric. Food Chem.* **51,** 1602–1607 (2003).

65. Yilmaz, Y. & Toledo, R. T. Major flavonoids in grape seeds and skins : Antioxidant capacity of catechin , epicatechin and gallic acid. *J. Agric. Food Chem.* **52,** 255–260 (2004).

66. Hogan, S. … Zhou, K. Antiproliferative and antioxidant properties of anthocyanin-rich extract from açai. *Food Chem.* **118,** 208–214 (2010).

67. Schauss, A. G. … Shanbrom, E. Antioxidant capacity and other bioactivities of the freeze-dried Amazonian palm berry, Euterpe oleraceae Mart. (Açai). *J. Agric. Food Chem.* **54,** 8604–8610 (2006).

68. Lichtenthaler, R. … Marx, F. Total oxidant scavenging capacities of *Euterpe oleracea* Mart. (Açai) fruits. *Int. J. Food Sci. Nutr.* **56,** 53–64 (2005).

69. Spada, P. D. S. … Salvador, M. Frozen fruit pulp of *Euterpe oleraceae* Mart. (Acai) prevents hydrogen peroxide-induced damage in the cerebral cortex, cerebellum, and hippocampus of rats. *J. Med. Food* **12,** 1084–8 (2009).

70. Poulose, S. M. … Shukitt-Hale, B. Anthocyanin-rich açai (*Euterpe oleracea* Mart.) fruit pulp fractions attenuate inflammatory stress signaling in mouse brain BV-2 microglial cells. *J. Agric. Food Chem.* **60,** 1084–1093 (2012).

71. Montedoro, G., Servili, M., Baldioli, M. & Miniati, E. Simple and hydrolyzable phenolic compounds in virgin olive oil. 1. Their extraction, separation, and quantitative and semiquantitative evaluation by HPLC. *J. Agric. Food Chem.* **40,** 1571–1576 (1992).

72. Montedoro, G. … Macchioni, A. Simple and hydrolyzable compounds in virgin olive oil. 3. Spectroscopic characterizations of the secoiridoid derivatives. *J. Agric. Food Chem.* **41,** 2228–2234 (1993).

73. Tyrrell, R. M. The molecular and cellular pathology of solar ultraviolet radiation. *Mol. Aspects Med.* **15,** 1–77 (1994).

74. Alia, M. … Goya, L. Quercetin protects human hepatoma HepG2 against oxidative stress induced by tert-butyl hydroperoxide. *Toxicol. Appl. Pharmacol.* **212,** (2006).

75. Priyadarshani, I. & Rath, B. Commercial and industrial applications of micro algae – A review. *J. Algal Biomass Util.* **3,** 89–100 (2012).

76. Raghava Rao, K. V. & Raghava Rao, T. Molecular characterization and its antioxidant activity of a newly isolated *Streptomyces coelicoflavus* BC 01 from mangrove soil. *J. Young Pharm.* **5,** 121–126 (2013).

77. Ser, H. L. … Lee, L. H. Presence of antioxidative agent, Pyrrolo[1,2-a]pyrazine-1,4-dione, hexahydro- in newly isolated Streptomyces mangrovisoli sp. nov. *Front. Microbiol.* **6,** 854 (2015).

78. Tan, L. T.-H. … Goh, B.-H. Investigation of antioxidative and anticancer potentials of Streptomyces sp. MUM256 isolated from malaysia mangrove soil. *Front. Microbiol.* **6,** 1316 (2015).

79. Tan, L. T. H. … Goh, B. H. Streptomyces sp. MUM212 as a source of antioxidants with radical scavenging and metal chelating properties. *Front. Pharmacol.* **8,** 276 (2017).

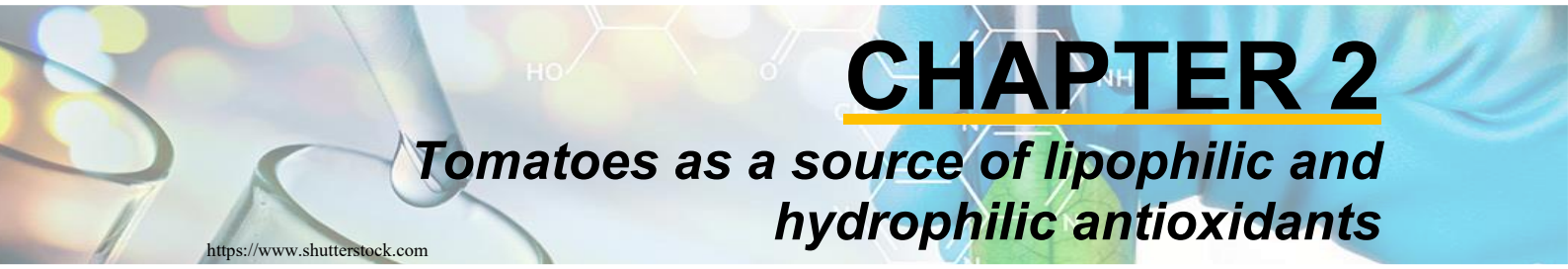

CHAPTER 2

Tomatoes as a source of lipophilic and hydrophilic antioxidants

Epidemiological studies demonstrated that regular consumption of fruits and vegetables, including tomatoes, can play an important role in preventing cancer and cardiovascular problems.
The healthy effect of tomato is due to the high content of different antioxidant molecules, such as lycopene, phenols, flavonoids and vitamins C and E.[1]

[1]Cheng, H. M., Koutsidis, G., Lodge, J. K., Ashor, A. W., Siervo, M., & Lara, J. (2017). Lycopene and Tomato and risk of cardiovascular diseases: A systematic review and meta-analysis of epidemiological evidence. *Critical Reviews in Food Science and Nutrition*, 1-18.

Research Article

SCI

Received: 21 March 2016 Revised: 21 June 2016 Accepted article published: 19 July 2016 Published online in Wiley Online Library: 18 August 2016

(wileyonlinelibrary.com) DOI 10.1002/jsfa.7910

Carotenoids in fresh and processed tomato (*Solanum lycopersicum*) fruits protect cells from oxidative stress injury

Rita Del Giudice,[a,†] Ganna Petruk,[a,†] Assunta Raiola,[b] Amalia Barone,[b] Daria Maria Monti[a*] and Maria Manuela Rigano[b*]

Abstract

BACKGROUND: Lipophilic antioxidants in tomato (*Solanum lycopersicum*) fruits exert important functions in reducing the risk of human diseases. Here the effect of thermal processing on the antioxidant activity of lipophilic extracts from the commercial tomato hybrid 'Zebrino' was analysed. Carotenoid content and lipophilic antioxidant activity were determined and the ability of tomato extracts in rescuing cells from oxidative stress was assessed.

RESULTS: Lipophilic antioxidant activity was completely retained after heat treatment and extracts were able to mitigate the detrimental effect induced by oxidative stress on different cell lines. Lycopene alone was able to rescue cells from oxidative stress, even if to a lower extent compared with tomato extracts. These results were probably due to the synergistic effect of tomato compounds in protecting cells from oxidative stress injury.

CONCLUSION: The current study provides valuable insights into the health effect of the dietary carotenoids present in fresh and processed tomato fruits.

Keywords: antioxidant power; carotenoids; cytotoxicity; lycopene; oxidative stress; *Solanum lycopersicum*

INTRODUCTION

Tomato (*Solanum lycopersicum*) is one of the most consumed vegetables worldwide and nowadays its consumption has further increased owing to the development of many processing products such as soups, juices, purees and sauces. It has been estimated that about 75% of tomatoes are consumed in processed form.[1] Among these processed tomatoes, 35% are consumed as sauces, 18% as tomato paste, 17% as canned tomatoes, 15% as juices and 15% as catsup.[1] Epidemiological studies suggest that consumption of tomato and tomato-based products reduces the risk of chronic diseases such as cardiovascular disease and cancer.[2] In particular, intake of tomato and tomato-based products has been consistently associated with lower risk of prostate, lung and stomach cancers.[3] Typically, this protective action is attributed to antioxidant components such as carotenoids, phenols and polyphenols as well as synergistic interactions among them.[4–7] Tomato fruits are considered one of the main sources of dietary antioxidants such as carotenoids, in particular α-carotene, β-carotene, lycopene, lutein and cryptoxanthin.[8] Indeed, tomato fruits contain 8–40 mg lycopene kg^{-1} fresh weight (FW), which corresponds to about 80% of the total dietary intake of this carotenoid.[9,10] Carotenoids are lipophilic pigmented molecules responsible for the different colours of fruits and vegetables and are synthesized by plants and microorganisms but not by animals. In plants, carotenoids protect against photo-damage and contribute to the photosynthetic machinery.[11,12] Carotenoids are important dietary sources of vitamin A, after β-carotene retinol bioconversion into pro-vitamin A.[13]

Oxidative stress, induced by the imbalance between the generation of reactive oxygen species (ROS) and the cellular capacity to detoxify these species with antioxidant molecules, has been implicated in the causation and development of several chronic diseases.[7] ROS can be generated by normal metabolic activity as well as by lifestyle factors such as smoking and diet. Many recent studies have investigated the role of dietary antioxidants that can mitigate the damaging effects of ROS,[8,14] and carotenoids have been proposed as good antioxidants able to act as free radical scavengers owing to their chemical structure.[15] Indeed, recently, it has been demonstrated that tomato lipophilic extracts were able to prevent hydrogen peroxide (H_2O_2)-induced cell death in a cell-based model system using rat cardiac H9c2 cells.[7] Generally, the carotenoid content of foods is not significantly modified by common household cooking methods such

* *Correspondence to: DM Monti, Department of Chemical Sciences, University of Naples Federico II, Complesso Universitario Monte Sant'Angelo, Via Cinthia 4, I-80126 Naples, Italy, E-mail: mdmonti@unina.it; or MM Rigano, Department of Agricultural Sciences, University of Naples Federico II, Via Università 100, I-80055 Portici (Naples), Italy, E-mail: mrigano@unina.it*

† *These authors contributed equally to the paper*

a *Department of Chemical Sciences, University of Naples Federico II, Complesso Universitario Monte Sant'Angelo, Via Cinthia 4, I-80126, Naples, Italy*

b *Department of Agricultural Sciences, University of Naples Federico II, Via Università 100, I-80055, Portici, Naples, Italy*

as microwave cooking, steaming and boiling, although extreme and extended heat treatments could cause oxidative degradation of carotenoids.[16,17] Moreover, the carotenoid lycopene has been demonstrated to be absorbed more efficiently from processed tomato products than from raw tomatoes.[18] However, only a few works have focused on the impact of processing on the general nutritional quality and antioxidant activities of tomato fruits.

In this study, the carotenoid content, lipophilic antioxidant activity and protective effects of tomato lipophilic extracts from the commercial tomato hybrid 'Zebrino' were examined. This cultivar has been selected since, during an on-going breeding program carried out at the Department of Agricultural Sciences, it was demonstrated that the fruits of this hybrid have a high content of bioactive compounds (carotenoids, phenolic compounds, vitamin C) endowed with antioxidant activity.[19] The protective effects of lycopene alone have also been evaluated in this study.

The current work seeks to evaluate the health-promoting properties of tomato fruits by evaluating both the antioxidant and protective effects of lipophilic extracts obtained from unprocessed and processed fruits. Consumers could benefit from the results reported in this paper by increasing their awareness of the health benefits of fresh and processed tomato fruits; moreover, these results could be used by fresh and industrial tomato producers for the development of tomato-based functional foods.

MATERIALS AND METHODS

Chemical reagents

Standards and reagents were purchased from Sigma (St Louis, MO, USA), while solvents were from Fluka (Buchs, Switzerland).

Plant material

Plant material consisted of the tomato genotype Zebrino (ZBR) (De Ruiters, Monsanto, St Louis, MO, USA). Plants were cultivated according to a randomized design with three replicates (ten plants per replicate) in an experimental field located in Acerra (Naples, Italy) in the year 2014. Each sample consisted of 20 pooled fruits per plot. The samples were harvested at the full ripe stage as used in the industry. Fruits were chopped, ground to a fine powder in liquid nitrogen using a Fimar FRI150 blender (Rimini, Italy) and kept at −80 °C until analyses. The studied genotype was processed according to a classical thermal treatment. Briefly, after washing for 5 min in water, tomatoes were treated for 10 min at 92 °C. An aliquot of treated tomatoes was passed through a pulper in order to obtain a puree. Glass cans were filled with 60% of treated whole tomatoes and 40% of puree and successively vacuum sealed. Then the filled jars were pasteurized at 100 °C for 30 min and cooled by water. The processed samples were homogenized using a Fimar FRI150 blender and kept at −80 °C until analyses. Three cans for each sample were collected and analysed.

Before chemical extraction, the dry matter content of all samples was determined by vacuum drying the samples for at least 12 h at 60 °C to constant weight. The moisture content of both processed and unprocessed samples was found to be around 900 g kg^{-1}. In particular, the mean dry matter content of fresh tomato was 100 g kg^{-1}, while that of processed tomato was 96 g kg^{-1}.

Extraction of lipophilic compounds

To obtain the lipophilic extract, 1 g of sample was extracted with 16 mL of acetone/hexane (40:60 v/v) using an IKA T 25 Ultra-Turrax High-Speed Homogenizer 115VAC (Cole-Parmer, Vernon Hills, IL, USA).[20] The mixture was centrifuged at 3500 × *g* for 5 min at 4 °C according to a modified procedure reported by Rigano *et al.*[21] Supernatants were collected and stored at −20 °C until analyses.

Carotenoid determination

For carotenoid determination, the absorbance of lipophilic extracts was read at 663, 645, 505 and 453 nm. *β*-Carotene and *cis*- and *trans*-lycopene isomer levels were calculated according to the equations reported by Zouari *et al.*[20] Total carotenoids were calculated by reading the absorbance at 480, 648 and 666 nm according to the formula reported by Wellburn.[22] Results were then converted into g kg^{-1} FW.

Antioxidant activity determination

Lipophilic antioxidant activity (LAA) was evaluated using the 2,2′-azinobis-(3-ethylbenzothiazoline-6-sulfonic acid) (ABTS) test.[23] The ABTS assay was performed as described by Rigano *et al.*[21] Briefly, 100 µL of supernatant, obtained from the extraction reported above, was added to 1 mL of $ABTS^{\bullet+}$, the mixture was incubated for 2.5 min and the absorbance was read at 734 nm. The standard curve was linear between 0 and 20 µmol L^{-1} Trolox and results were expressed as mmol Trolox equivalent (TE) kg^{-1} FW.

MTT test

Human HeLa adenocarcinoma cells, human hepatic carcinoma HepG2 cells, human breast adenocarcinoma MCF-7 cells and murine BALB/c 3T3 and SV-T2 fibroblasts (ATCC) were cultured in Dulbecco's modified Eagle's medium (DMEM) (Sigma-Aldrich, St Louis, MO, USA) supplemented with 100 mL L^{-1} foetal bovine serum (HyClone, Logan, UT, USA), 2 mmol L^{-1} L-glutamine and antibiotics. Cells were grown in a 5% CO_2 humidified atmosphere at 37 °C and seeded in 96-well plates at a density of 2×10^3 cells per well. Lipophilic tomato extracts, obtained as reported above, were dried by rotovapor (R-210, Buchi), re-dissolved in dimethyl sulfoxide (DMSO) and then added to the cells 24 h after seeding for dose-dependent cytotoxicity assays. After 48 h incubation, cell viability was assessed by the MTT assay as described in Galano *et al.*[24] Briefly, 3-(4,5-dimethylthiazol-2-yl)-2,5-diphenyltetrazolium bromide (MTT) reagent dissolved in DMEM in the absence of phenol red (Sigma-Aldrich) was added to the cells (0.5 mg mL^{-1} final concentration). Following 4 h incubation at 37 °C, the culture medium was removed and the resulting formazan salts were dissolved by adding isopropanol containing 0.01 mol L^{-1} HCl (100 µL per well). Absorbance values were determined at 570 nm using an automatic plate reader (Microbeta Wallac 1420, PerkinElmer, Waltham, MA, USA). Cell survival was expressed as percentage of viable cells in the presence of the tomato extract under test compared with control cells grown in the absence of the extract. Three separate analyses were carried out with each sample. Control experiments were performed either by growing cells in the absence of the extract or by adding to the cell cultures identical volumes of DMSO. The method used avoids any possibility of a DMSO effect on the final results.

Oxidative stress analyses

To evaluate the protective effect of lipophilic extracts against oxidative stress, cells were plated at a density of 4×10^4 cells cm^{-2}, incubated in the presence of 0.6 mg mL^{-1} lipophilic extracts or 0.4 µg mL^{-1} commercial *trans*-lycopene (Sigma) for 48 h and then treated with 300 µmol L^{-1} sodium arsenite (SA) for 2 h. At the end of incubation, cell viability was assessed by the MTT assay

as reported above, ROS production was measured by the DCFDA assay, glutathione (GSH) level was measured by the DTNB assay and lipid peroxidation was assessed by the TBARS method.

DCFDA assay

To determine ROS levels within the cytosol, cells were incubated with the cell-permeable redox-sensitive fluorophore 2′,7′-dichlorodihydrofluorescein diacetate (H_2-DCFDA) (Sigma-Aldrich) at a concentration of 25 µmol L^{-1} for 30 min at 37 °C. Cells were then washed twice with warm phosphate-buffered saline (PBS) supplemented with 1 mmol L^{-1} $CaCl_2$, 0.5 mmol L^{-1} $MgCl_2$ and 30 mmol L^{-1} glucose (PBS plus), detached by trypsin, centrifuged at 1000 × *g* for 10 min and re-suspended in PBS plus at a density of 1×10^5 cells mL^{-1}. H_2-DCFDA is non-fluorescent until, in the presence of ROS, it is hydrolysed by intracellular esterases and readily oxidized to the highly fluorescent 2′,7′-dichlorofluorescein (DCF). DCF fluorescence intensity was measured at an emission wavelength of 525 nm and an excitation wavelength of 488 nm using a PerkinElmer LS50 spectrofluorimeter. Emission spectra were acquired at a scanning speed of 300 nm min^{-1}, with five slit widths for excitation and emission. ROS production was expressed as percentage of DCF fluorescence intensity of the sample under test compared with the untreated sample. Three separate analyses were carried out with each extract. Control experiments were performed by supplementing cell cultures with identical volumes of DMSO.

DTNB assay

The interaction of the sulfhydryl group of GSH with 5,5′-dithiobis-2-nitrobenzoic acid (DTNB) produces a yellow-coloured compound, 5-thio-2-nitrobenzoic acid (TNB), whose intensity can be measured at 412 nm. Thus the rate of TNB production is directly proportional to the concentration of GSH in the sample. To estimate intracellular GSH levels, cells were detached by trypsin, centrifuged at 1000 × *g* for 10 min and re-suspendend in lysis buffer (300 mmol L^{-1} NaCl and 5 mL L^{-1} NP-40 in 100 mM Tris–HCl, pH7.4) containing protease inhibitors. After 30 min incubation on ice, lysates were centrifuged at 14 000 × *g* for 30 min at 4 °C. Supernatant protein concentration was determined by the Bradford assay. Then 50 µg of proteins were incubated with 3 mmol L^{-1} ethylenediaminetetraacetic acid (EDTA) and 144 µmol L^{-1} DTNB in 30 mmol L^{-1} Tris HCl (pH 8.2) and centrifuged at 14 000 × *g* for 5 min at room temperature. Finally, the absorbance of the supernatant was measured at 412 nm using a multiplate reader (BioRad, Hercules, CA, USA). GSH levels were expressed as percentage of TNB absorbance of the sample under test compared with the untreated sample. Three separate analyses were carried out with each extract. Control experiments were performed by supplementing cell cultures with identical volumes of DMSO.

Measurement of lipid peroxidation

Levels of lipid peroxidation were determined using the thiobarbituric acid (TBA)-reactive substance (TBARS) assay.[25] Cells were detached by trypsin and centrifuged at 1000 × *g* for 10 min, then 5×10^5 cells were re-suspendend in ice-cold PBS and mixed with 6.7 mL L^{-1} TBA and an equal volume of 200 mL L^{-1} trichloroacetic acid (TCA). Samples were then heated at 95 °C for 30 min, incubated on ice for 10 min and centrifuged at 3000 × *g* for 5 min at 4 °C. TBA reacts with oxidative degradation products of lipids, and complexes absorb at 532 nm. Lipid peroxidation levels were expressed as percentage of absorbance at 532 nm of the sample under test compared with the untreated sample. Three separate analyses were carried out with each extract. Control experiments were performed by supplementing cell cultures with identical volumes of DMSO.

Statistical analyses

Biological replicates of samples were analysed in triplicate. Quantitative parameters were expressed as mean ± standard deviation (SD). Differences among unprocessed and processed samples were determined using SPSS 6, Version 15.0 (SPSS Inc., Chicago, IL, USA). Significance was assessed by Student's *t* test at a significance level of 0.05.

RESULTS AND DISCUSSION

In this study, the antioxidant and protective activities of lipophilic extracts obtained from unprocessed and processed commercial tomato hybrid 'Zebrino' (ZBR) were analysed. This cultivar is characterized by a skin colour changing from dark green to dark brown/red, with green tiger stripes when fully ripe. Carotenoid content and LAA were examined and the ability of tomato lipophilic extracts and lycopene alone in rescuing cells from oxidative stress was assessed.

Carotenoid content and antioxidant activity

Figure 1A shows the change in the carotenoid content of ZBR extracts before and after heat treatment. The mean amount of total carotenoids in ZBR was 0.095 g kg^{-1} FW, and this value did not change significantly after thermal processing. Lycopene and

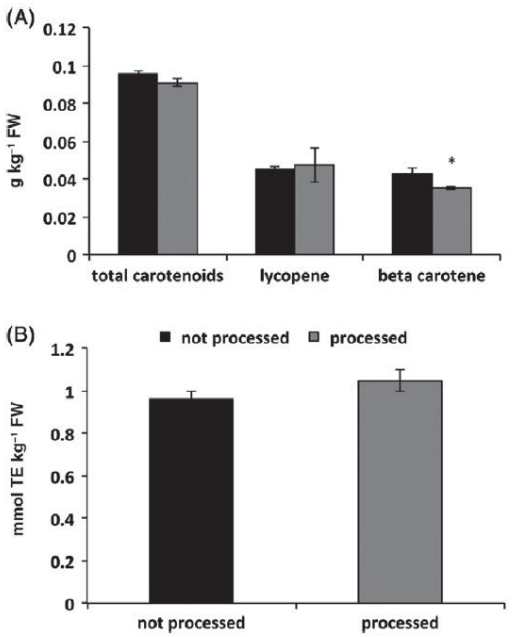

Figure 1. *In vitro* characterization of carotenoid tomato extracts. (A) Carotenoid content (g kg^{-1} FW) and (B) lipophilic antioxidant activity (mmol TE kg^{-1} FW) of ZBR lipophilic extracts before (unprocessed, black bars) and after thermal processing (processed, grey bars).

β-carotene represented about 47 and 45% of total carotenoids in unprocessed samples respectively. Frusciante *et al.*[26] and Rigano *et al.*[21] found that lycopene constituted about 90% of total carotenoids in different varieties of red tomatoes. On the contrary, the ZBR genotype shows a different lycopene/total carotenoid ratio and a higher content of β-carotene compared with common red tomatoes. These values correlate well with the presence of green tiger stripes on the skin and the deep green/brown flesh of the fully ripe fruit. After processing, the amount of lycopene did not change significantly, whereas a significant ($P < 0.05$) decrease of 17% in β-carotene level was recorded. In the literature, controversial data on carotenoid stability during thermal processing are reported. In accordance with our data, it has been reported that carotenoid content was stable in processed tomatoes.[16] Capanoglu *et al.*[27] reported a significant decrease in both lycopene (32%) and β-carotene (36%) levels, whereas Re *et al.*[28] reported an increase in lycopene levels in several tomato products. These contrasting results may depend on the different genotypes evaluated and on the temperature and time adopted in the processing methods.

Figure 1B shows the LAA in ZBR extracts before and after thermal processing. The mean LAA was 0.96 mmol TE kg^{-1} FW before processing and did not change after heat treatment. The lipophilic tomato extract may contain other antioxidant phytochemicals such as vitamin E. Our results, together with results from Li *et al.*,[7] demonstrated that carotenoids constitute the major fraction of lipophilic compounds in tomato fruits and contribute significantly to their overall antioxidant activity. The LAA reported in this study for the ZBR cultivar was higher than those reported for other tomato cultivars. Indeed, Cano *et al.*[29] measured an antioxidant activity of 0.81 mmol TE kg − 1 FW in tomato mature red fruit, whereas Toor and Savage[30] found mean levels of LAA equal to 0.18, 0.07 and 0.09 mmol TE kg^{-1} FW in the skin, pulp and seeds respectively of several tomato commercial cultivars.

Free radical scavenger activity of lipophilic tomato extracts

Afterwards, the maximum concentration of lipophilic extracts at which no significant cytotoxic effect is observed was evaluated. For this purpose, one normal cell line (immortalized murine fibroblast cell line BALB/c 3 T3) and four cancer cell lines were selected: BALB/c 3 T3 murine fibroblasts transformed with SV40 virus (SVT2), human adenocarcinoma cells (HeLa), human hepatic carcinoma cells (HepG2) and human breast adenocarcinoma cells (MCF-7). The viability of cells treated for 48 h with increasing amounts of tomato extracts was tested by the MTT reduction assay as an indicator of metabolically active cells.

The results of dose–response experiments are shown in Fig. 2. The values are the average of three independent experiments, each carried out with triplicate determinations. It was observed that 0.24 and 0.6 mg mL^{-1} lipophilic tomato extracts did not affect cell viability significantly, whereas at 1.2 mg mL^{-1} a cytotoxic effect was observed on all cell lines analysed. The concentration at which a cytotoxic effect was observed (1.2 mg mL − 1) was lower than that reported on rat cardiomyoblasts,[7] but in that study a different cell viability assay and incubation time (24 h) were used. Interestingly, both the extracts from unprocessed and processed fruits showed a similar effect on cell survival; however, on MCF-7 cells, a cytotoxic effect of the lipophilic extract obtained from fresh fruits was observed even at the lowest extract concentration. Based on these experiments, 0.6 mg mL^{-1} lipophilic tomato extract was selected as the optimal concentration to analyse the free radical scavenger activity against oxidative stress induced by

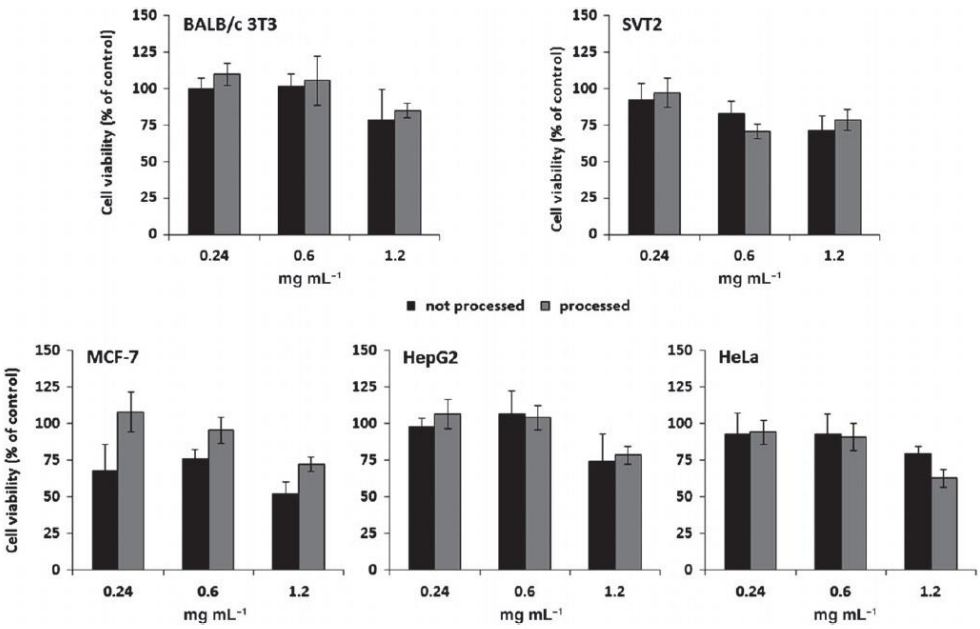

Figure 2. Effects of lipophilic tomato extracts on normal and cancer cells. BALB/c 3 T3, SVT2, MCF-7, HepG2 and HeLa cells were treated with increasing concentrations of lipophilic tomato extracts from unprocessed (black bars) and processed (grey bars) samples for 48 h. Cell viability was assessed by the MTT assay and expressed as described in the 'Materials and Methods' section. All values are given as mean ± SD ($n \geq 3$).

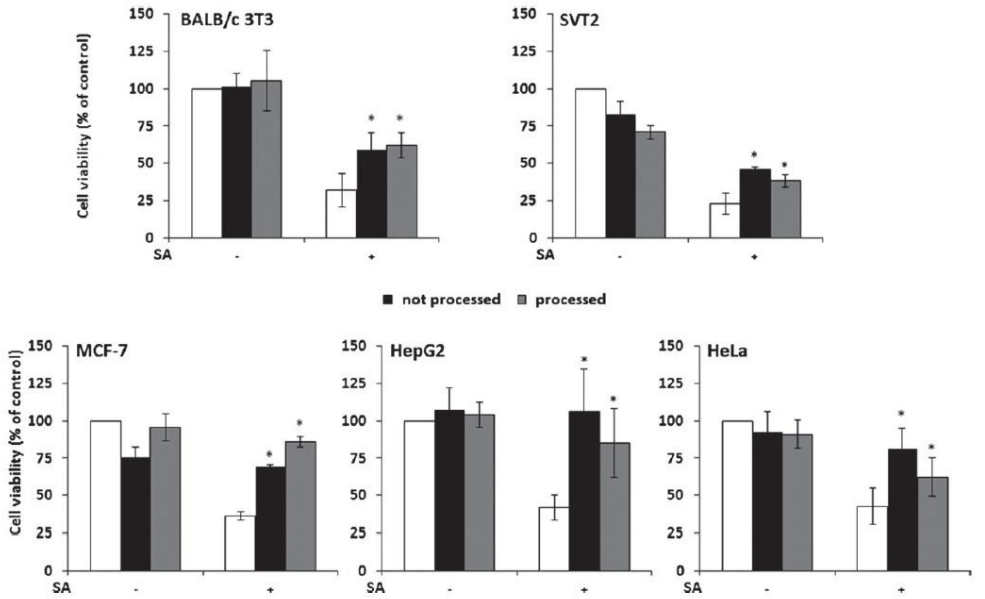

Figure 3. Effects of lipophilic tomato extracts on normal and cancer cells. BALB/c 3 T3, SVT2, MCF-7, HepG2 and HeLa cells were pre-incubated with 0.6 mg mL^{-1} lipophilic tomato extracts from unprocessed (black bars) and processed (grey bars) samples for 48 h and then treated with 300 µmol L^{-1} SA for 2 h. White bars refer to control cells, untreated (–) or treated with SA (+). Cell viability was assessed by the MTT assay and expressed as described in the 'Materials and Methods' section. All values are given as mean ± SD ($n \geq 3$). Asterisks (*) indicate values that are significantly different from SA-treated cells ($P < 0.01$) as determined by Student's *t* test.

sodium arsenite (SA). Among health hazards, inorganic arsenic, present in drinking water, is a major threat to human health, particularly in Asian countries (Bangladesh, Taiwan, Vietnam and India), Argentina, Chile and several states of the USA (Arizona, California and Nevada).[31,32] To inspect the ability of lipophilic tomato extracts to contrast SA-induced oxidative stress, cells were pre-incubated in the presence of lipophilic tomato extracts obtained from fruits processed by thermal treatment or from fresh fruits. Cells were then treated with SA as described in the 'Materials and Methods' section.

Cytoprotective activity of lipophilic tomato extracts

Cell viability was assessed by the MTT assay. As shown in Fig. 3, after SA treatment, cell viability was dramatically reduced compared with control cells in all cell lines analysed (white bars). Noteworthy, when cells were pre-incubated in the presence of lipophilic tomato extracts from either processed (grey bars) or unprocessed (black bars) samples, a strong protective effect was recorded. No significant differences were observed in the protective effect of extracts from unprocessed or processed fruits, thus suggesting that heat treatment does not affect the antioxidant power of tomato extracts. The recovery observed was about 50% in all cell lines analysed (Fig. 3, black and grey bars *versus* white bars). It is interesting to note that the unprocessed lipophilic tomato extract was able to significantly protect MCF-7 cells against oxidative stress even though, when tested in the absence of stress, it exerted a slight cytotoxic effect. The protective effect of the lipophilic extract observed in this study is in line with that reported on rat cardiomyoblasts in the presence of H_2O_2.[7]

Lipophilic tomato extracts mitigate SA-induced ROS production

We chose SVT2 cells as cancer cell line and BALB/c 3 T3 cells as normal cells to deeply inspect the effects of SA on cell redox homeostasis. Since perturbation in the cellular redox status is related to ROS production, we measured ROS levels in cells pre-treated with lipophilic tomato extracts, exposed to SA and treated with H_2-DCFDA. This cell-permeable oxidation-sensitive dye is converted to its fluorescent form in the presence of ROS. As shown in Fig. 4A, in normal cells, no significant ROS production was observed upon exposure to the lipophilic extracts, whereas SA induced an increase of 50% in ROS levels compared with control cells (white bars). Noteworthy, SA-induced ROS production was strongly decreased when cells were pre-treated with both unprocessed (58% decrease) and processed (48% decrease) lipophilic ZBR extracts. No significant difference was observed between unprocessed and processed tomato lipophilic extracts in protecting cells from ROS production. In cancer cells (Fig. 4B), instead, a slight increase in ROS levels was observed when cells were incubated with lipophilic extracts compared with untreated cells (20 and 40% increase for unprocessed and processed extracts, respectively). SA treatment resulted in a high increase in ROS levels (70%) compared with control cells, and pre-treatment with lipophilic extracts induced a significant reduction in ROS production (about 41 and 74% decrease for unprocessed and processed ZBR extracts, respectively). The unprocessed and processed extracts were able to protect cells from ROS production to the same extent. These results suggest that pre-treatment with lipophilic extracts is able to abolish ROS production induced by oxidative stress and that heat treatment does not affect the antioxidant activity of lipophilic extracts. This is particularly interesting considering that

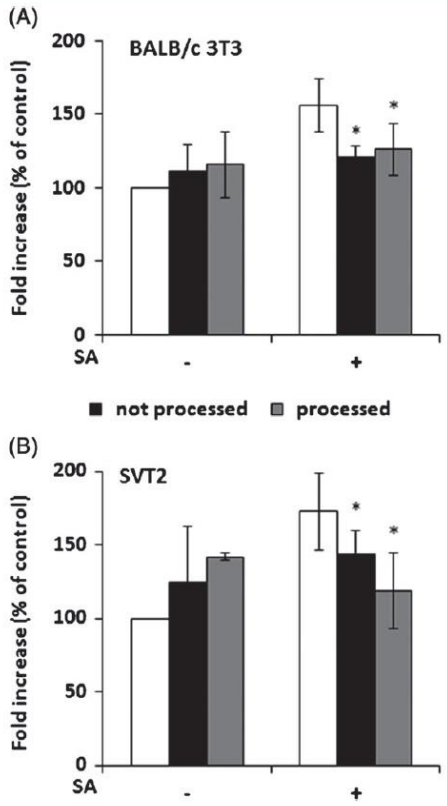

Figure 4. DCFDA assay for detection of intracellular ROS produced in response to oxidative stress in (A) normal and (B) cancer cells. Cells were pre-incubated with 0.6 mg mL^{-1} lipophilic tomato extracts from unprocessed (black bars) and processed (grey bars) samples for 48 h and then treated with 300 µmol L^{-1} SA for 2 h. White bars refer to control cells, untreated (–) or treated with SA (+). Values are expressed as fluorescence intensity compared with untreated cells. Asterisks (*) indicate values that are significantly different from SA-treated cells ($P < 0.01$) as determined by Student's *t* test.

carotenoids such as lycopene are mainly found in *trans* conformation in fresh tomato fruit, whereas they are normally transformed into the more bioactive *cis* form after food processing.[6]

Lipophilic tomato extracts prevent GSH depletion and lipid peroxidation

Since intracellular glutathione (GSH) is the most important antioxidant defence molecule and its depletion is the first hallmark of the progression of apoptosis, we evaluated GSH intracellular levels.

As shown in Fig. 5, pre-treatment of normal (Fig. 5A) and cancer (Fig. 5C) cells with lipophilic extracts had no significant effect on intracellular GSH levels. Oxidative stress induced by SA resulted in about 30% GSH depletion in both cell lines, but GSH intracellular levels were not affected when cells were pre-incubated with lipophilic extracts obtained from either processed or unprocessed samples.

GSH level is directly related to the degree of lipid peroxidation in the cell membrane,[33] as it participates in eliminating lipid peroxidation products by forming a GSH conjugate.[34] Therefore, we analysed lipid peroxidation levels in our experimental system by TBARS assay (Figs 5B and 5D). No lipid peroxidation was observed when cells were incubated in the presence of either unprocessed or processed lipophilic tomato extracts, whereas lipid peroxidation showed a 120 and 150% increase in normal and cancer cells respectively after SA treatment (Figs 5B and 5D). Noteworthy, pre-incubation of cells with lipophilic extracts completely abolished the effect of SA on lipid peroxidation, and no significant difference was observed between cells treated with extracts from processed or unprocessed samples. These results clearly indicate that treatment of cells with lipophilic extracts, either unprocessed or processed, is able to prevent the negative effect of SA-induced oxidative stress.

Lycopene role in protective effects of ZBR extracts

It has been hypothesized that lycopene was the compound responsible for the observed protective effect.

To verify the specific role of lycopene in protecting cells from oxidative stress, ROS production and intracellular GSH levels were analysed by following the same experimental procedure described above. The lycopene concentration used was 0.4 µg mL^{-1}, since this represents the amount of lycopene present in ZBR extracts when used at 0.6 mg mL^{-1}. As shown in Figs 6A and 6B, pre-treatment of cells with lycopene lowered ROS levels after SA treatment to 58% in normal cells and 33% in cancer cells. These values are in agreement with those reported for ZBR extracts. In Figs 6C and 6D, the results of intracellular GSH levels before and after SA treatment are reported. In cancer cells, a strong protective effect of lycopene from oxidative stress was found, as intracellular GSH levels were slightly higher than those of control cells in SA-treated samples. On the contrary, when normal cells were incubated in the presence of SA, no significant protective effect was observed after lycopene treatment. We hypothesize that the higher sensitivity of normal cells compared with cancer cells results in a lower ability of cells to rescue from stress. Altogether, these results demonstrated that other compounds are present in ZBR lipophilic extracts that could play a role in protecting cells, such as β-carotene and vitamin E, thus supporting the idea of a synergistic effect among structurally different lipophilic compounds.[35]

CONCLUSIONS

The results reported in this paper are particularly interesting since carotenoids are known to regulate different cellular pathways and functions,[8] but their bio-absorption is strongly influenced by several factors, including break-up of the food matrix and cooking temperatures. Here it was demonstrated that ZBR lipophilic extracts were able to counteract the detrimental effects induced by oxidative stress on different cell lines and that the high LAA exhibited by ZBR hybrid was mainly due to the presence of lycopene. However, it is noteworthy that ZBR extracts were more effective than lycopene alone in protecting cells, thus supporting the importance of a synergistic effect among antioxidants present in tomatoes.

To date, only a few reports are available on the protective effects of lipophilic tomato extracts on cells. A direct correlation between carotenoid content and antioxidant activity of tomatoes on rat cardiomyoblasts has been previously found.[7] In addition, it was demonstrated that tomato lipophilic and hydrophilic extracts protected cells from H_2O_2-induced cell death and that the antioxidant

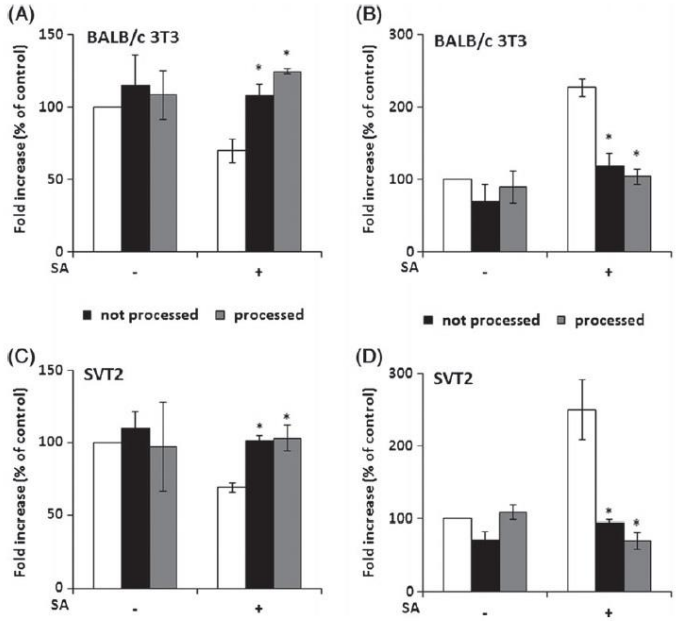

Figure 5. Determination of intracellular GSH and lipid peroxidation in (A, B) normal and (C, D) cancer cells. Cells were pre-incubated with 0.6 mg mL^{-1} lipophilic tomato extracts from unprocessed (black bars) and processed (grey bars) samples for 48 h and then treated with 300 µmol L^{-1} SA for 2 h. White bars refer to control cells, untreated (–) or treated with SA (+). A and C refer to intracellular GSH levels (DTNB assay) and B and D refer to lipid peroxidation levels (TBARS assay). In each experiment, values are expressed as fold increase compared with control (i.e. untreated) cells. Asterisks (*) indicate values that are significantly different from SA-treated cells ($P < 0.01$) as determined by Student's *t* test.

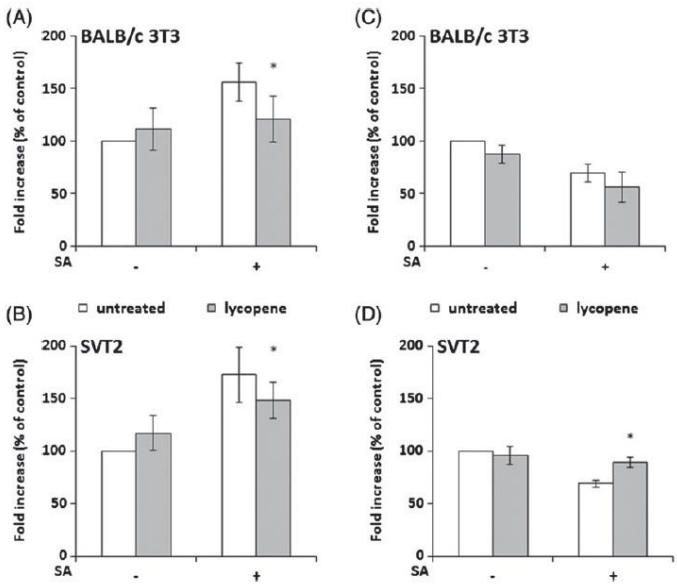

Figure 6. Protective effects of lycopene against oxidative stress in (A, C) normal and (B, D) cancer cells. Cells were pre-incubated with 0.4 µg mL^{-1} lycopene (light grey bars) for 48 h and then treated with 300 µmol L^{-1} SA for 2 h. White bars refer to control cells, untreated (–) or treated with SA (+). (A, B) DCFDA assay; (C, D) intracellular GSH levels. In both experiments, values are expressed as fold increase compared with control (i.e. untreated) cells. Asterisks (*) indicate values that are significantly different from untreated cells ($P < 0.05$) as determined by Student's *t* test.

activity did not change significantly after *in vitro* digestion, thus supporting the hypothesis that gastrointestinal digestion does not alter the antioxidant power of carotenoids.[36] Although many studies report the beneficial effects of lycopene and β-carotene on different cell lines after oxidative stress induction, as far as we know, this study is the first to demonstrate this ability by using lipophilic tomato extracts obtained from fruit before and after heat treatment. This work supports the beneficial role of carotenoids in ameliorating several chronic diseases in which oxidative stress can be considered a hallmark, thus suggesting a therapeutic potential for tomato-based products.

In the future, the study performed here on ZBR cultivar could be carried out also on other tomato genotypes characterized by high LAA in order to verify if they exhibit properties analogous to those exerted by ZBR on different cells. This analysis could be used by breeders to generate new hybrids characterized by higher nutritional levels.

ACKNOWLEDGEMENT

The authors thank GenoPOM-pro Project (PON02_00395_3082360) for the financial support of the activities reported in the present study.

REFERENCES

1 US Department of Agriculture, Economic Research Service, *Tomatoes* [Online]. (2008). Available: http://www.ers.usda.gov/ [September 2015].
2 Giovannucci E, Tomatoes, tomato-based products, lycopene, and cancer: review of the epidemiologic literature. *J Natl Cancer Inst* **91**: 317–331 (1999).
3 Hwang ES and Bowen PE, Effects of tomato paste extracts on cell proliferation, cell-cycle arrest and apoptosis in LNCaP human prostate cancer cells. *BioFactors* **23**:75–84 (2005).
4 Martínez-Valverde I, Periago MJ, Provan G and Chesson A, Phenolic compounds, lycopene and antioxidant activity in commercial varieties of tomato (*Lycopersicum esculentum*). *J Agric Food Chem* **82**:323–330 (2002).
5 Maiani G, Caston MJ and Catasta G, Carotenoids: actual knowledge on food sources, intakes, stability and bioavailability and their protective role in humans. *Mol Nutr Food Res* **53**:S194–S218 (2009).
6 Raiola A, Rigano MM, Calafiore R, Frusciante L and Barone A, Enhancing the health promoting effects of tomato fruit for biofortified food. *Mediators Inflamm* 2014:139873 (**2014**). DOI: 10.1155/2014/139873.
7 Li H, Deng Z, Liu R, Loewen S and Tsao R, Carotenoid compositions of coloured tomato cultivars and contribution to antioxidant activities and protection against H_2O_2-induced cell death in H9c2. *Food Chem* **136**:878–888 (2013).
8 Rao AV and Rao LG, Carotenoids and human health. *Pharmacol Res* **55**:207–216 (2007).
9 Kong KW and Ismail A, Lycopene content and lipophilic antioxidant capacity of by-products from *Psidium guajava* fruits produced during puree production industry. *Food Bioprod Process* **89**:53–61 (2011).
10 Renju GL, Kurup GM and Saritha Kumari CH, Effect of lycopene from *Chlorella marina* on high cholesterol-induced oxidative damage and inflammation in rats. *Inflammopharmacology* **22**:45–54 (2013).
11 Agarwal S and Rao AV, Carotenoids and chronic diseases. *Drug Metabol Drug Interact* **17**:189–210 (2000).
12 Johnson EJ, The role of carotenoids in human health. *Nutr Clin Care* **5**:47–49 (2002).
13 Tang G, Bioconversion of dietary provitamin A carotenoids to vitamin A in humans. *Am J Clin Nutr* **91**:1468S–1473S (2010).
14 Halliwell B and Cross CE, Oxygen-derived species: their relation to human disease and environmental stress. *Environ Health Perspect* **102**:5–12 (1994).
15 Gerster H, The potential role of lycopene for human health. *J Am Coll Nutr* **16**:109–126 (1997).
16 Graziani G, Pernice R, Lanzuise S, Vitaglione P, Anese M and Fogliano V, Effect of peeling and heating on carotenoid content and antioxidant activity of tomato and tomato-virgin olive oil systems. *Eur Food Res Technol* **216**:116–121 (2003).
17 Sanchez-Moreno C, Plaza L, de Ancos B and Cano MP, Impact of high pressure and traditional thermal processing of tomato puree on carotenoids, vitamin C and antioxidant activity. *J Sci Food Agric* **86**:171–179 (2006).
18 Friedman M, Anticarcinogenic, cardioprotective, and other health benefits of tomato compounds lycopene, α-tomatine, and tomatidine in pure form and in fresh and processed tomatoes. *J Agric Food Chem* **61**:9534–9550 (2013).
19 Ruggieri V, Francese G, Sacco A, D'Alessandro A, Rigano MM, Parisi M, *et al.*, An association mapping approach to identify favourable alleles for tomato fruit quality breeding. *BMC Plant Biol* **14**:337 (2014).
20 Zouari I, Salvioli A, Chialva M, Novero M, Miozzi L, Tenore GC, *et al.*, From root to fruit: RNA-Seq analysis shows that arbuscular mycorrhizal symbiosis may affect tomato fruit metabolism. *BMC Genomics* **15**:221 (2014).
21 Rigano MM, Raiola A, Tenore GC, Monti DM, Del Giudice R, Frusciante L, *et al.*, Quantitative trait loci pyramiding can improve the nutritional potential of tomato (*Solanum lycopersicum*) fruits. *J Agric Food Chem* **62**:11519–11527 (2014).
22 Wellburn AR, The spectral determination of chlorophylls *a* and *b*, as well as total carotenoids, using various solvents with spectrophotometers of different resolution. *J Plant Physiol* **144**:307–313 (1994).
23 Miller JN and Rice-Evans CA, Factors influencing the antioxidant activity determined by the $ABTS^{\bullet+}$ radical cation assay. *Free Radic Res* **26**:195–199 (1997).
24 Galano E, Arciello A, Piccoli R, Monti DM and Amoresano A, A proteomic approach to investigate the effects of cadmium and lead on human primary renal cells. *Metallomics* **6**:587–597 (2014).
25 Camera E, Mastrofrancesco A, Fabbri C, Daubrawa F, Picardo M, Sies H, *et al.*, Astaxanthin, canthaxanthin and β-carotene differently affect UVA-induced oxidative damage and expression of oxidative stress-responsive enzymes. *Exp Dermatol* **18**:222–231 (2009).
26 Frusciante L, Carli P, Ercolano MR, Pernice R, Di Matteo A, Fogliano V, *et al.*, Antioxidant nutritional quality of tomato. *Mol Nutr Food Res* **51**:609–617 (2007).
27 Capanoglu E, Beekwilder J, Boyacioglu D, Hall R and de Vos R, Changes in antioxidant and metabolite profiles during production of tomato paste. *J Agric Food Chem* **56**:964–973 (2008).
28 Re R, Bramley PM and Rice-Evans C, Effects of food processing on flavonoids and lycopene status in a Mediterranean tomato variety. *Free Radic Res* **36**:803–810 (2002).
29 Cano A, Costa M and Arnao MB, Hydrophilic and lipophilic antioxidant activity changes during on-vine ripening of tomatoes (*Lycopersicon esculentum* Mill.). *Postharv Biol Technol* **28**:59–65 (2003).
30 Toor RK and Savage GP, Antioxidant activity in different fractions of tomatoes. *Food Res Int* **38**:487–494 (2005).
31 Smedley PL and Kinniburgh DG, A review of the source, behavior and distribution of arsenic in natural waters. *Appl Geochem* **17**:517–568 (2002).
32 Paul S, Chakraborty S, Ali MN and Ray DP, Arsenic distribution in environment and its bioremediation: a review. *Int J Agric Environ Biotechnol* **8**:189–204 (2015).
33 Schneider LA, Dissemond J, Brenneisen P, Hainzl A, Briviba K, Wlaschek M, *et al.*, Adaptive cellular protection against UVA-1-induced lipid peroxidation in human dermal fibroblasts shows donor-to-donor variability and is glutathione dependent. *Arch Dermatol Res* **297**:324–328 (2006).
34 Tarozzi A, Marchesi A, Hrelia S, Angeloni C, Andrisano V, Fiori J, *et al.*, Protective effects of cyanidin-3-*O*-β-glucopyranoside against UVA-induced oxidative stress in human keratinocytes. *Photochem Photobiol* **81**:623–629 (2005).
35 Fernández-García E, Photoprotection of human dermal fibroblasts against ultraviolet light by antioxidant combinations present in tomato. *Food Funct* **5**:285–290 (2014).
36 Li H, Deng Z, Liu R, Loewen S and Tsao R, Bioaccessibility, *in vitro* antioxidant activities and *in vivo* anti-inflammatory activities of a purple tomato (*Solanum lycopersicum* L.). *Food Chem* **159**:353–360 (2014).

Journal of Photochemistry & Photobiology, B: Biology 163 (2016) 284–289

Contents lists available at ScienceDirect

Journal of Photochemistry & Photobiology, B: Biology

journal homepage: www.elsevier.com/locate/jphotobiol

An ascorbic acid-enriched tomato genotype to fight UVA-induced oxidative stress in normal human keratinocytes

Ganna Petruk [a], Assunta Raiola [b], Rita Del Giudice [a], Amalia Barone [b], Luigi Frusciante [b], Maria Manuela Rigano [b,*], Daria Maria Monti [a,c,**]

[a] Department of Chemical Sciences, University of Naples Federico II, Complesso Universitario Monte Sant'Angelo, via Cinthia 4, 80126 Naples, Italy
[b] Department of Agricultural Sciences, University of Naples Federico II, Via Università 100, 80055 Portici (Naples), Italy
[c] Istituto Nazionale di Biostrutture e Biosistemi (INBB), Rome, Italy

ARTICLE INFO

Article history:
Received 13 May 2016
Received in revised form 20 July 2016
Accepted 29 August 2016
Available online 31 August 2016

Keywords:
Antioxidants
Ascorbic acid
Tomato
Oxidative stress
UVA radiations
Eukaryotic cells

ABSTRACT

UVA radiations contribute up to 95% of the total UV exposure and are known to induce cell damage, leading to apoptosis. Since the benefic effects of ascorbic acid on human health are well known, a new tomato genotype (named DHO4), highly rich in ascorbic acid, has been recently obtained. Here, we compared the effects of ascorbic acid and hydrophilic DHO4 extracts in protecting human keratinocytes exposed to UVA stress. Keratinocytes were pre-incubated with ascorbic acid or with extracts from the ascorbic acid enriched tomato genotype and irradiated with UVA light. Then, ROS production, intracellular GSH and lipid peroxidation levels were quantified. Western blots were carried out to evaluate mitogen-activated protein kinases cascade, activation of caspase-3 and inflammation levels. We demonstrated that ROS, GSH and lipid peroxidation levels were not altered in cell exposed to UVA stress when cells were pre-treated with ascorbic acid or with tomato extracts. In addition, no evidence of apoptosis and inflammation were observed in irradiated pre-treated cells. Altogether, we demonstrated the ability of an ascorbic acid enriched tomato genotype to counteract UVA-oxidative stress on human keratinocytes. This protective effect is due to the high concentration of vitamin C that acts as free radical scavenger. This novel tomato genotype may be used as genetic material in breeding schemes to produce improved varieties with higher antioxidant levels.

1. Introduction

UV radiations are among the most harmful exogenous factor for the human skin due to ROS production and erythema development. Depending on their UV wavelength, incident photons may determine different damages in the target cells [1]. In particular, in the UVB range (280–295 nm), dimerization reactions between adjacent pyrimidine bases occur by direct light absorption by DNA, whereas UVA radiations (320–400 nm) are less absorbed by DNA, but excite other endogenous molecules, leading to DNA damage [2,3]. Particularly, UVA radiations increase the levels of free radicals/ROS, thus damaging cellular proteins, lipids, DNA, and eventually leading to apoptosis [4–6].

Nevertheless, in the last few years, UVA radiation has been used for cosmetic purposes, for example to cure gel nails, to dry traditional nail polish and for topcoats formulated to protect nails. The effects of UVA nail lamps on human health are still under debate. Some authors reported that UVA wavelengths are responsible for photoaging in human skin and long-term exposure to these lamps can increase skin cancer risk [7,8]. However, the internet market claims that the lamp has no effect on human health [9].

Ascorbic acid (AsA) shows significant ability as electron donor and potent antioxidant in humans; it exerts a relevant role in protecting DNA from damages induced by oxidant species and in the prevention of inflammation [10,11]. Darr and colleagues reported that the topical application of AsA significantly increased cutaneous levels of this vitamin in pigs, and it protected the skin from UVA and UVB damage, probably as a consequence of the reducing properties of this molecule [12].

Abbreviations: AsA, ascorbic acid; DCF, 2′,7′-dichlorofluorescein; DHO4, double homozygote; DTNB, 5,5′-dithiobis-2-nitrobenzoic acid; EDTA, 2-({2-[Bis(carboxymethyl) amino]ethyl}(carboxymethyl)amino)acetic acid; EGF, epidermal growth factor; ERKs, extracellular signal–regulated kinases; FW, fresh weight; H_2-DCFDA, 2′,7′-dichlorodihydrofluorescein diacetate; ICAM-1, intercellular adhesion molecule-1; IκB-α, inhibitor of nuclear factor kappa-B kinase subunit alpha; NF-κB, nuclear factor κB; PBS, phosphate buffered saline; P-p38, phosphorylated p38 MAP kinase; P-MAPKAPK-2, phosphorylated MAP kinase-activated protein kinase; ROS, reactive oxygen species; SAPK /JNKs, the stress-activated protein kinase/Jun.-amino-terminal kinase; TBA, thiobarbituric acid; TBARS, TBA reactive substances; TNB, 5-thio-2-nitrobenzoic acid.

* Correspondence to: M.M. Rigano, Department of Agricultural Sciences, University of Naples Federico II, Via Università 100, 80055 Portici (Naples), Italy.
** Correspondence to: D.M. Monti, Department of Chemical Sciences, University of Naples Federico II, Complesso Universitario Monte Sant'Angelo, via Cinthia 4, 80126 Naples, Italy.
E-mail addresses: mrigano@unina.it (M.M. Rigano), mdmonti@unina.it (D.M. Monti).

http://dx.doi.org/10.1016/j.jphotobiol.2016.08.047
1011-1344/

In addition, AsA is known to be a potent anti-inflammatory agent, since it suppresses nuclear factor κB (NF-κB) activation, a key molecule in the inflammatory process [13]. Noteworthy, humans have to introduce AsA with the diet, since they cannot synthesize it, due to mutations in the gene encoding gulonolactone oxidase, which catalyzes the last enzymatic step of the ascorbate biosynthetic pathway ([14] and references therein).

Tomatoes represent one of the most widely used and versatile fruit crop, consumed either fresh or processed (sauce, paste and juice) [15]. It has been reported that intake of tomato and tomato-based products is associated to benefic effects on human health due to the antioxidant compounds present in this fruit [16].

In this work we tested the antioxidant activity of hydrophilic extracts obtained from a novel tomato genotype, named DHO4, recently obtained in our laboratory and characterized by a high amount of AsA in the fruit. Previously, we demonstrated that hydrophilic extracts from the DHO4 genotype showed anti-proliferative activity specific for human cancer cells, as they did not affect the growth of normal cells [17]. Here, we compared the antioxidant activity of DHO4 hydrophilic extracts and of ascorbic acid in human keratinocyte-derived HaCaT cells exposed to UVA stress. We measured oxidative stress cascade, as well as the activation of caspase-3 and inflammation levels. Keratinocytes have been selected since these cells are normally present in the outermost layer of the skin and are more exposed to environmental stress, such as UVA irradiation [18], which contributes up to 95% of the total UV exposure.

2. Methods

2.1. Tomato Extracts and AsA Quantification

Hydrophilic extracts from the DHO4 fruit were obtained according to the procedure reported by Choi et al. [19] with minor changes. Briefly, frozen powder (2 g) was weighed, placed into a 50 mL Falcon tube, and extracted with 25 mL of 70% methanol into an ultrasonic bath (Branson 5200 Ultrasonic Corp.) for 60 min at 30 °C. The mixture was dried by rotovapor (R-210, Buchi), and re-dissolved in dimethyl sulfoxide (DMSO) 5% in PBS (1 mL).

Ascorbic acid quantification was carried out according to the colorimetric method reported by Stevens et al. [20] with modifications reported by Rigano et al. [17]. Briefly, 300 μL of ice cold 6% TCA were added to 500 mg of frozen powder. The mixture was incubated for 15 min on ice and centrifuged at 14,000 g for 20 min at 4 °C. Then, 20 μL of 0.4 M phosphate buffer (pH 7.4), 10 μL of double distilled (dd) H_2O and 80 μL of color reagent solution (prepared by mixing solution A (31% H_3PO_4, 4.6% (w/v) TCA and 0.6% (w/v) $FeCl_3$) with solution B (4% 2,2′-dipyridil (w/v) made up in 70% ethanol) at a proportion of 2.75:1 v/v) were added to 20 μL of supernatant. The mixture was incubated at 37 °C for 40 min prior measurement at 525 nm by a NanoPhotometer™ (Implen) using 6% TCA as reference. Three separated replicates for each sample were carried out, each one with three determinations. The concentration was expressed in nmol AsA according to the standard curve, designed over a range of 0–70 nmol; then the values were expressed in milligrams per 100 g FW.

2.2. Cell Culture

HaCaT cells (ATCC) were cultured in Dulbecco's Modified Eagle's Medium (Sigma-Aldrich), supplemented with 10% foetal bovine serum (HyClone), 2 mM L-glutamine and antibiotics, all from Sigma-Aldrich, in a 5% CO_2 humidified atmosphere at 37 °C. For sub-culturing HaCaT cells, the culture medium was removed and cells were rinsed with PBS, detached with trypsin-EDTA and diluted in fresh complete growth medium; sub-culture was done in a ratio of 1:4 every 72 h.

2.3. Oxidative Stress Analyses

To evaluate the protective effect of hydrophilic tomato extracts and of ascorbic acid against oxidative stress, cells were plated at a density of 4×10^4 cells/cm^2. 24 h after seeding, cells were incubated in the presence of 88 μM AsA (Sigma-Aldrich) or 3 mg/mL hydrophilic extracts for 2 h and treated with UVA light for 2 min (20 J/cm^2). In a preliminary experiment we determined that 2 min of UVA treatment were able to induce the highest level of oxidative stress (data not shown). Immediately after UVA treatment, ROS production and GSH levels were determined by DCFDA and DTNB assays, respectively. Lipid peroxidation and western blotting analyses were performed after 90 min incubation. Control experiments were performed by supplementing cell cultures only with identical volumes of DMSO.

2.4. DCFDA Assay

To determine cytosolic ROS levels, cells were incubated with cell permeable, redox-sensitive fluorophore 2′,7′-dichlorodihydrofluorescein diacetate (H_2-DCFDA, Sigma-Aldrich) at the concentration of 25 μM for 30 min at 37 °C. Cells were then washed with warm phosphate buffered saline (PBS) supplemented with 1 mM $CaCl_2$, 0.5 mM $MgCl_2$, 30 mM glucose (PBS plus) two times, detached by trypsin, centrifuged at 1000g for 10 min and resuspended in PBS plus at a cell density of 1×10^5 cells/mL. H_2-DCFDA is non-fluorescent until it is hydrolysed by intracellular esterases and readily oxidized to the highly fluorescent 2′,7′-dichlorofluorescein (DCF) in the presence of ROS. The DCF fluorescence intensity was measured at an emission wavelength of 525 nm and an excitation wavelength of 488 nm using a Perkin-Elmer LS50 spectrofluorimeter. Emission spectra were acquired at a scanning speed of 300 nm/min, with 5 and 5 slit widths for excitation and emission, respectively. ROS production was expressed as percentage of DCF fluorescence intensity of the sample under test, compared to the untreated sample. Three independent experiments were carried out, each one with three determinations.

2.5. DTNB Assay

To estimate glutathione levels, cells were detached by trypsin, centrifuged at 1000g for 10 min and resuspendend in lysis buffer (0.3 M NaCl, 0.5% NP-40 in 0.1 M TrisHCl, pH 7.4) containing protease inhibitors. After 30 min incubation on ice, lysates were centrifuged at 14,000g for 30 min at 4 °C. Supernatant protein concentration was determined by Bradford assay. Then, 50 μg of proteins were mixed with 3 mM EDTA, 144 μM 5,5′-dithiobis-2-nitrobenzoic acid (DTNB) in 30 mM TrisHCl pH 8.2, centrifuged at 14,000g for 5 min at room temperature and the absorbance of the supernatant was measured at 412 nm using a multiplate reader (Biorad).

The interaction of the sulfhydryl group of GSH and DTNB produced a yellow-coloured compound, 5-thio-2-nitrobenzoic acid (TNB). The rate of TNB production is directly proportional to the rate of this recycling reaction, which is in turn directly proportional to the concentration of GSH in the sample. Thus, the net absorbance at 412 nm yields an accurate estimation of the amount of GSH in the sample. GSH levels were expressed as percentage of TNB absorbance of the sample under test, compared to the untreated sample. Three independent experiments were carried out, each one with three determinations.

2.6. Measurement of Lipid Peroxidation

The levels of lipid peroxidation were determined by using the thiobarbituric acid reactive substances (TBARS) assay [21]. Briefly, cells were detached by trypsin, centrifuged at 1000g for 10 min and 5×10^5 cells were resuspendend in 0.67% thiobarbituric acid (TBA) and an equal volume of 20% trichloroacetic acid was added. The samples were then heated at 95 °C for 30 min, incubated on ice for 10 min and

centrifuged at 3000g for 5 min, at 4 °C. TBA reacts with the oxidative degradation products of lipids in samples, yielding red complexes that absorb at 532 nm. Lipid peroxidation levels were expressed as percentage of absorbance at 532 nm of the sample under test, compared to the untreated sample. Three independent experiments were carried out, each one with three determinations.

2.7. Western Blot Analyses

Cells were plated at a density of 2×10^4 cells/cm^2 in complete medium for 24 h and then treated as described above. Both untreated and treated cells were incubated for 30 or 90 min at 37 °C to detect IκB-α or ICAM-1 and p38 or MAPKAPK-2 phosphorylation levels, respectively. To prepare cell lysates, cells were scraped off in phosphate buffer, centrifuged at 1000g for 10 min and resuspended in lysis buffer (1% NP-40 in PBS, pH 7.4) containing protease and phosphatase inhibitors. After 30 min incubation on ice, lysates were centrifuged at 14,000g for 30 min at 4 °C. Upon determination of total protein concentration in the supernatant by the Bradford assay, samples were analyzed by SDS-PAGE and Western blotting using specific antibodies (Cell Signal Technology). To normalize to internal standard signals, antibodies against β-actin and GAPDH were used. The chemiluminescence detection system (SuperSignal® West Pico) was from Pierce.

2.8. Statistical Analyses

The biological replicates of samples were analyzed in triplicate. Quantitative parameters were expressed as the mean value ± SD. Significance was determined by Student's *t*-test at a significance level of 0.01.

3. Results and Discussion

3.1. Pre-treatment with AsA or Hydrophilic DHO4 Extracts Inhibits UVA-induced Damage in HaCaT Cells

A novel tomato genotype, DHO4, was previously produced in our laboratory, which contained a high content of ascorbic acid in the fruit. We demonstrated that hydrophilic extracts from the DHO4 genotype have anti-proliferative activity on human cancer cells whereas they don't affect the growth of normal cells [17].

To analyze the effects of hydrophilic DHO4 extracts on UVA stress-induced cells, we selected a concentration of the extract at which, in previous work, no cytotoxicity was observed (3 mg/mL), which corresponded to an AsA content of 88 μM [17]s.

For all the experiments, we used immortalized human keratinocyte cells (HaCaT) and UVA radiation as a source of stress. Cells were pretreated with 88 μM AsA or 3 mg/mL hydrophilic tomato extracts for 2 h and then oxidative stress was induced by UVA irradiation (20 J/cm^2). Immediately after UVA irradiation, ROS production and intracellular GSH levels were determined (Fig. 1A–B).

Incubation of cells with hydrophilic DHO4 extracts or with AsA did not alter ROS production (Fig. 1A, grey and white bar, on the left). We found that HaCaT cells exposed to UVA radiation showed a significant increase of fluorescence intensity levels (about 2-fold increase), which is related to ROS generation (Fig. 1A, black bars). Interestingly, when cells were pretreated with DHO4 extracts prior to UVA irradiation, no increase in ROS levels was observed after UVA exposure (Fig. 1A, grey bar, on the right). The same results obtained with DHO4 extracts were obtained by incubating HaCaT cells with AsA (Fig. 1A, white bars), thus suggesting that AsA contained in the DHO4 extract was responsible for the inhibition of ROS generation after UVA exposure.

Since the protective role of GSH from oxidative skin damage has been well documented, we measured intracellular GSH levels in both treated and untreated cells. When AsA or hydrophilic DHO4 extracts were added to the cells, no significant alteration in the GSH level was observed compared to untreated control cells (Fig. 1B, on the left). In UVA irradiated HaCaT cells we found a significant decrease (30%) in GSH level compared to untreated cells (Fig. 1B, black bars). Interestingly, when cells were treated with AsA or hydrophilic DHO4 extracts and then irradiated by UVA, the intracellular GSH level was similar to that observed in the absence of UVA treatment (Fig. 1B, grey and white bars, respectively). It has been reported that free radicals can cause irreversible damage to lipids and DNA, and resulted byproducts can be used as biomarkers of oxidative stress [22,23]. Therefore, we analyzed lipid peroxidation levels in HaCaT cells by measuring thiobarbituric acid reactive substances (TBARS), 90 min after UVA irradiation. We found that cells treated with AsA or hydrophilic tomato extracts did not show significant alteration in lipid peroxidation levels (Fig. 1C, on the left). A high increase (4-fold increase) in lipid peroxidation levels was measured in HaCaT cells upon UVA irradiation, compared to untreated control cells (Fig. 1C, black bars). Noteworthy, when cells were pretreated with AsA or DHO4 extracts and then irradiated by UVA, lipid peroxidation levels were found to be similar to those observed in not-irradiated cells (Fig. 1C, grey and white bars, respectively). A growing body of evidence suggests that UVA radiation generates ROS in the form of free radicals, such as superoxide anion and hydroxyl radical, as well as non-radical intermediates such as hydrogen peroxide [24,25]. Moreover, oxidative stress decrease intracellular levels of anti-oxidant molecules, including GSH, which participates in eliminating lipid

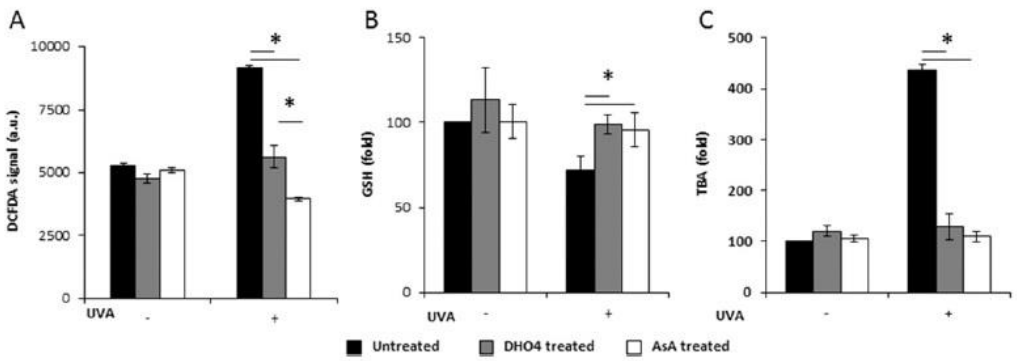

Fig. 1. AsA and DHO4 extracts suppress UVA-induced ROS production, GSH oxidation and lipid peroxidation in HaCaT cells. Cells were pre-incubated in the presence of 88 μM AsA (white bars) or 3 mg/mL DHO4 extracts (grey bars) for 2 h and then irradiated by UVA (20 J/cm^2). A, intracellular ROS levels were evaluated by DCFDA assay after UVA irradiation; B, intracellular GSH levels were determined immediately by DTNB assay; C, lipid peroxidation levels were evaluated after 90 min incubation, by TBARS assay. In B and C, values are expressed as fold increase with respect to control (i.e. untreated) cells. Data shown are the means ± S.D. of three independent experiments. Asterisks (*) indicate values that are significantly different ($p < 0.01$).

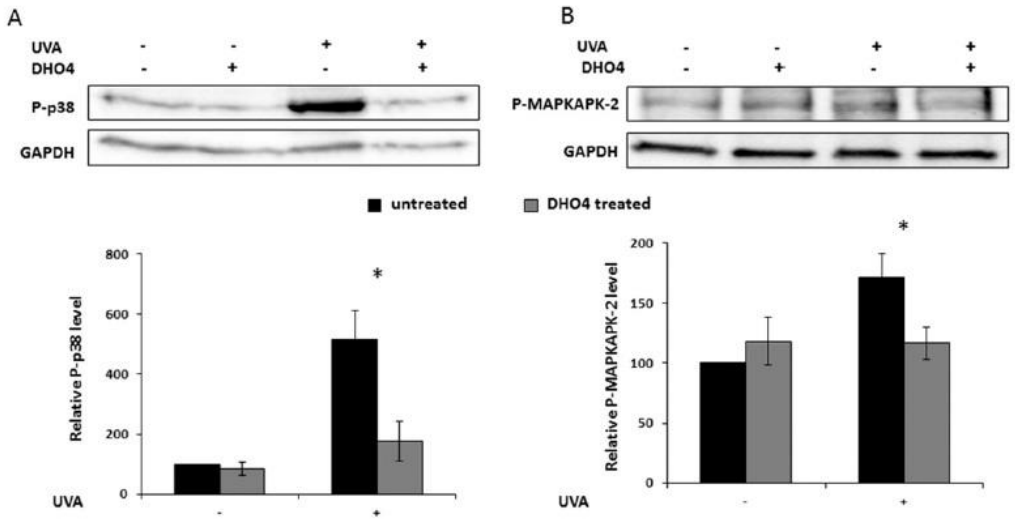

Fig. 2. Effect of DHO4 on UVA-induced oxidative stress markers in HaCaT cells. Cells were incubated with 3 mg/mL DHO4 extract 2 h prior to UVA (20 J/cm^2) irradiation for 2 min and then cells were incubated for 90 min. Western blots show the expression levels of p-p38 (A) and p-MAPKAPK-2 (B), with the relative densitometric analyses in the absence (black bars) or in the presence (grey bars) of DHO4. GAPDH was used as internal standard. Data shown are the means ± S.D. of three independent experiments. Asterisks (*) indicate values that are significantly different ($p < 0.01$).

peroxidation products, including 4-hydroxynonenal, by forming a GSH conjugate [23]. The finding that the AsA present in the tomato extracts is able to prevent alterations in ROS, GSH and lipid peroxidation levels in human keratinocytes irradiated by UVA, can be due to AsA free radical scavenger activity, exerted through its hydroxyl groups.

3.2. Activation of MAPK Cascade

Among the many signaling stress pathways induced by UVA, one involves the mitogen-activated protein kinases (MAPK) cascade. MAPK is a family of evolutionarily highly conserved enzymes that manage the response to growth stimulatory signals, such as insulin or epidermal growth factor (EGF), as well as adverse signals, such as cytotoxic and genotoxic substances or radiations. They include extracellular signal–regulated kinases (ERKs), stress-activated protein kinases, also known as c-jun *N*-terminal kinases (SAPK/JNKs), and the p38-MAPKs [26].

Therefore, we performed Western blot analyses to verify if the protective effect exerted by hydrophilic DHO4 extracts and by AsA from UVA-induced stress was related to MAPKs activation (Figs. 2 and 3). Treatment of cells with hydrophilic DHO4 extracts had no significant effect on p38 and MAPKAPK-2 (p38 target) phosphorylation levels (Fig. 2A and B, second lanes). When cells were irradiated by UVA, instead, we observed a significant increase in the phosphorylation levels of both p38 and MAPKAPK-2 (Fig. 2A and B, third lanes). Interestingly,

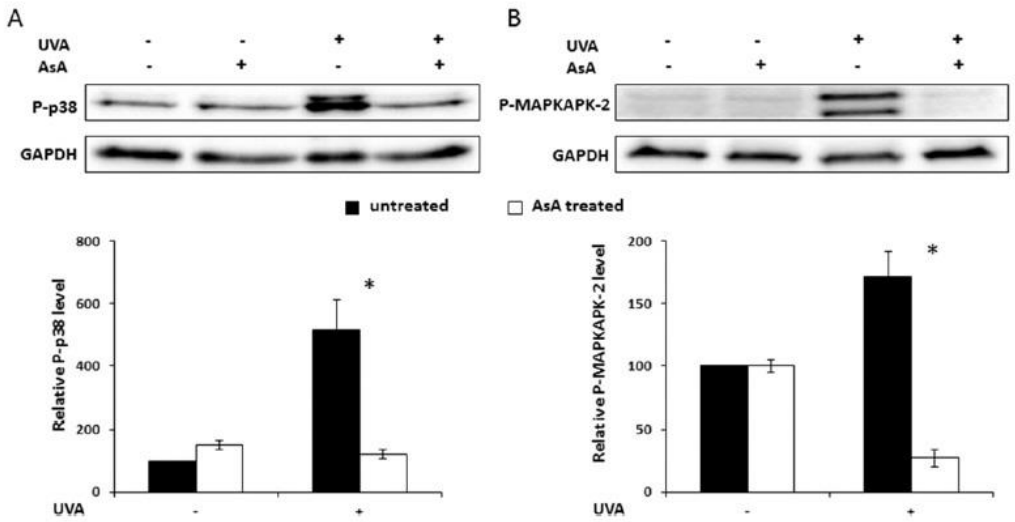

Fig. 3. AsA protects HaCaT cells from UVA-induced oxidative stress. Cells were incubated with 88 μM AsA 2 h prior to UVA (20 J/cm^2) irradiation for 2 min and then cells were incubated for 90 min. Representative western blots show the expression levels of p-p38 (A) and p-MAPKAPK-2 (B), with the relative densitometric analyses in the absence (black bars) or in the presence (white bars) of AsA. GAPDH was used as internal standard. Data shown are the means ± S.D. of three independent experiments. Asterisks (*) indicate values that are significantly different ($p < 0.01$).

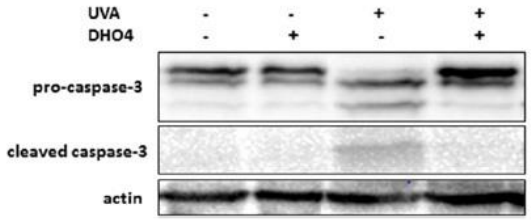

Fig. 4. DHO4 hydrophilic extracts protect HaCaT cells from UVA-induced apoptosis. Cells were pre-incubated with 3 mg/mL DHO4 extracts for 2 h, irradiated with UVA (20 J/cm^2) for 2 min and incubated for 90 min. Western blot was performed using anti-caspase-3, which recognizes both pro-caspase-3 and the activated form. β-actin was used as loading control.

when cells were pre-exposed to hydrophilic DHO4 extracts and then UVA irradiated, phosphorylation levels of both p38 and MAPKAPK-2 were similar to those observed in non-irradiated cells. (Fig. 2A and B, fourth lanes). The same results were obtained when cells were incubated with AsA (Fig. 3A and B), thus confirming that the DHO4 protective effect was due to the ascorbic acid contained in the DHO4 fruit.

ABTS analyses carried out in our laboratory demonstrated that AsA alone has an antioxidant activity comparable to that observed for DHO4 extracts (data not shown). However, treatment of cells with AsA prior to UVA irradiation was found to be more effective than DHO4 extract in preventing ROS production and MAPKAPK-2 phosphorylation levels. We hypothesize that the presence of other structurally different compounds present in DHO4 extracts could mask the AsA antioxidant activity observed on human keratinocytes.

Moreover, since it has been reported that UVA radiation entails, by activation of caspase-3, DNA damage and apoptosis [27,28], we analyzed activated caspase-3 levels in cells after UVA treatment. As shown in Fig. 4, DHO4 treatment had no effect on the activation of caspase-3, since cleaved caspase-3 was not observed. On the contrary, UVA exposure remarkably increased activation of caspase-3, as indicated by the presence of cleaved caspase-3 (Fig. 4, middle panel, third lane). It is worth to notice that when cells were pre-incubated in the presence of DHO4 extracts, no caspase-3 activation was observed, thus suggesting a protective role of DHO4 extracts from UVA irradiation. This result is in agreement with those reported by Ichihashi, who demonstrated that many epidermal skin cells, including keratinocytes, undergo apoptosis following UVA exposure as a result of DNA strand breaks [29].

3.3. DHO4 Protects HaCaT Cells from Inflammation

Finally, since it is known that UVA is also associated with induction of inflammation [30], we analyzed if DHO4 extracts could counteract the signaling pathway that leads to NF-κB activation. Among the signaling molecules that lead to inflammation, we chose IκB-α and ICAM-1, since they participate in the early events of the inflammation process [31]. IκB is the NF-κB inhibitor and its degradation leads to release of NF-κB for subsequent nuclear translocation. ICAM-1, instead, is a pro-inflammatory adhesion molecule whose expression is enhanced by NF-κB activation [31].

Cell lysates were analyzed by Western blotting using specific antibodies against IκB-α and ICAM-1. As shown in Fig. 5A, no differences were observed between DHO4-treated cells and untreated control cells. IκB-α was found to be degraded after UVA treatment. Interestingly, when cells were incubated with tomato extracts and then irradiated, IκB-α levels were similar to those observed in the absence of UVA treatment. ICAM-1 levels were found to be higher in cells exposed to oxidative stress compared to non-irradiated control cells. ICAM-1 levels were similar in cells pre-treated with the hydrophilic extracts and then exposed to oxidative stress and in non-irradiated cells (Fig. 5B). Our results are in line with the literature, since it has been reported that ROS can act as signal transduction molecules that induce pro-inflammatory cytokines and the NF-κB pathway [32]. Moreover, AsA is known to be a potent anti-inflammatory molecule that probably acts by suppressing the activation of transcription factor NF-κB that, in turn, inhibits tumor necrosis factor α_(TNF-α) [33].

Overall, our results suggest that DHO4 extracts are able to protect human normal cells from oxidative stress injury and inflammation process and that the protective effect is due to the high levels of AsA, that acts as an antioxidant molecule by donating its electrons, thus preventing other compounds from being oxidized. We believe that this novel genotype has a potential to be used as genetic material for breeding schemes in order to generate novel varieties with higher antioxidant levels. [17].

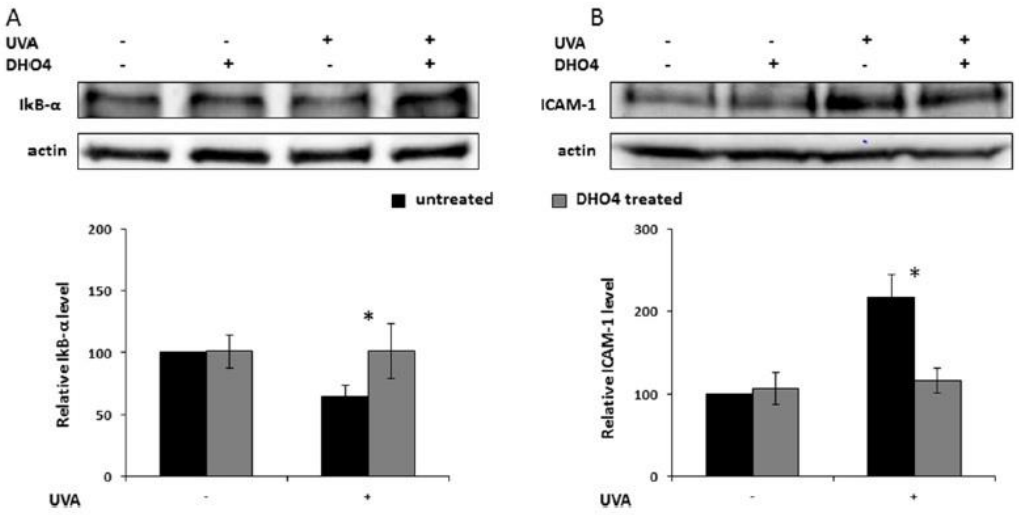

Fig. 5. Effects of DHO4 extracts on NF-kB signaling pathway in HaCaT cells. Cells were pre-treated with DHO4 extracts for 2 h, irradiated with UVA (20 J/cm^2) for 2 min and incubated for 30 min. Cell lysates were prepared and the levels of IκB-α (A) and ICAM-1 (B) were determined by Western blot analyses. β-actin was used as internal standard. The relative densitometric analyses, in the absence (black bars) or in the presence (grey bars) of DHO4, are reported. Data shown are the means ± S.D. of three independent experiments. Asterisks (*) indicate values that are significantly different ($p < 0.01$).

Stahl and Sies demonstrated that skin can be protected against UV-dependent lesions by supplying volunteers with tomato-based products [34]. Therefore, we believe that in the future novel tomato-based skin care products could be developed, including a dermatological lotion or a spray to be used on hands prior to nail care, to support the repair and regeneration of UVA-irradiated skin.

Conflict of Interest

The authors declare no competing financial interest.

Acknowledgement

The authors thank GenoPOM-pro Project (PON02_00395_3082360) for the financial support to the activities reported in the present study. The authors thank Carla Damiano for the work done during her master thesis.

References

[1] J.-L. Ravanat, T. Douki, J. Cadet, Direct and indirect effects of UV radiation on DNA and its components, J. Photochem. Photobiol. B Biol. 63 (2001) 88–102.
[2] J. Cadet, R. Teoule, Comparative study of oxidation of nucleic acid components by hydroxyl radicals, singlet oxygen and superoxide anion radicals, Photochem. Photobiol. 28 (1978) 661–665.
[3] J.-L. Ravanat, C. Saint-Pierre, P. Di Mascio, G.R. Martinez, M.H.G. Medeiros, J. Cadet, Damage to isolated DNA mediated by singlet oxygen, Helv. Chim. Acta 84 (2001) 3702–3709.
[4] T. Douki, A. Reynaud-Angelin, J. Cadet, E. Sage, Bipyrimidine photoproducts rather than oxidative lesions are the main type of DNA damage involved in the genotoxic effect of solar UVA radiation, Biochemistry 42 (2003) 9221–9226.
[5] D. Kulms, T. Schwarz, Molecular mechanisms of UV-induced apoptosis, Photodermatol. Photoimmunol. Photomed. 16 (2000) 195–201.
[6] R. Haywood, F. Rogge, M. Lee, Protein, lipid, and DNA radicals to measure skin UVA damage and modulation by melanin, Free Radic. Biol. Med. 44 (2008) 990–1000.
[7] M. Rosenbach, S. Kagan, S. Leventhal, Acrylic nail curing UV lamps: High-intensity exposure warrants further research of skin cancer risk, J. Am. Acad. Dermatol. 50 (2004) 50–54.
[8] B.L. Diffey, The risk of squamous cell carcinoma in women from exposure to UVA lamps used in cosmetic nail treatment, Br. J. Dermatol. 167 (2012) 1175–1178.
[9] D.F. Mac Farlane, C.A. Alonso, Occurrence of non melanoma skin cancers on the hands after UV nail light exposure, Arch. Dermatol. 145 (4) (2009) 447–449.
[10] J.A. Rodríguez, B. Nespereira, M. Pérez-Ilzarbe, E. Eguinoa, J.A. Páramo, Vitamins C and E prevent endothelial VEGF and VEGFR-2 overexpression induced by porcine hyper cholesterolemic LDL, Cardiovasc. Res. 65 (2005) 665–673.
[11] Y. Li, H.E. Schellhorn, New developments and novel therapeutic perspectives for vitamin C, J. Nutr. 137 (2007) 2171–2184.
[12] D. Darr, S. Combs, S. Dunston, T. Manning, S. Pinnell, Topical vitamin C protects porcine skin from ultraviolet radiation-induced damage, Br. J. Dermatol. 127 (1992) 247–253.
[13] P.K. Farris, Topical vitamin C: a useful agent for treating photoaging and other dermatologic conditions, Dermatol. Surg. 31 (2005) 814–818.
[14] G. Grosso, R. Bei, A. Mistretta, S. Marventano, G. Calabrese, L. Masuelli, M.G. Giganti, A. Modesti, F. Galvano, D. Gazzolo, Effects of Vitamin C on health: a review of evidence, Front. Biosci. 18 (2013) 1017–1029.
[15] S.A. de Santos, S.V. Borges, N. Ferreira Magalhães, H.V. Ricardo, A.D. Azevedo, Spray-dried tomato powder: reconstitution properties and colour, Braz. Arch. Biol. Technol. 51 (2008) 607–614.
[16] I. Martínez-Valverde, M.J. Periago, G. Provan, A. Chesson, Phenolic compounds, lycopene and antioxidant activity in commercial varieties of tomato (*Lycopersicum esculentum*), J. Sci. Food Agric. 82 (2002) 323–330.
[17] M.M. Rigano, A. Raiola, G.C. Tenore, D.M. Monti, R. Del Giudice, L. Frusciante, A. Barone, Quantitative trait loci pyramiding can improve the nutritional potential of tomato (*Solanum lycopersicum*) fruits, J. Agric. Food Chem. 62 (2014) 11519–11527.
[18] N.E. Fusenig, P. Boukamp, Multiple stages and genetic alterations in immortalization, malignant transformation, and tumor progression of human skin keratinocytes, Mol. Carcinog. 23 (1998) 144–158.
[19] S.H. Choi, H.R. Kim, H.J. Kim, I.S. Lee, N. Kozukue, C.E. Levin, M. Friedman, Free amino acid and phenolic contents and antioxidative and cancer cell-inhibiting activities of extracts of 11 greenhouse-grown tomato varieties and 13 tomato-based foods, J. Agric. Food Chem. 59 (2011) 12801-\.
[20] R. Stevens, M. Buret, C. Garchery, Y. Carretero, M. Causse, Technique for rapid small-scale analysis of vitamin C levels in fruit and application to a tomato mutant collection, J. Agric. Food Chem. 54 (2006) 6159–6165.
[21] E. Camera, A. Mastrofrancesco, C. Fabbri, F. Daubrawa, M. Picardo, H. Sies, W. Stahl, Astaxanthin, canthaxanthin and β-carotene differently affect UVA-induced oxidative damage and expression of oxidative stress-responsive enzymes, Exp. Dermatol. 18 (2009) 222–231.
[22] L.A. Schneider, J. Dissemond, P. Brenneisen, A. Hainzl, K. Briviba, M. Wlaschek, K. Scharffetter-Kochanek, Adaptive cellular protection against UVA-1-induced lipid peroxidation in human dermal fibroblasts shows donor-to-donor variability and is glutathione dependent, Arch. Dermatol. Res. 297 (2006) 324–328.
[23] A. Tarozzi, A. Marchesi, S. Hrelia, C. Angeloni, V. Andrisano, J. Fiori, G. Cantelli-Forti, P. Hrelia, Protective effects of cyanidin-3-O-β-glucopyranoside against UVA-induced oxidative stress in human keratinocytes, Photochem. Photobiol. 81 (2005) 623–629.
[24] R. Gniadecki, T. Thorn, J. Vicanova, A. Petersen, H.C. Wulf, Role of mitochondria in ultraviolet-induced oxidative stress, J. Cell. Biochem. 80 (2001) 216–222.
[25] Y. Miyachi, Photoaging from an oxidative standpoint, J. Dermatol. Sci. 9 (1995) 79–86.
[26] L.O. Klotz, C. Pellieux, K. Briviba, C. Pierlot, J.M. Aubry, H. Sies, Mitogen-activated protein kinase (p38-, JNK-, ERK-) activation pattern induced by extracellular and intracellular singlet oxygen and UVA, Eur. J. Biochem. 260 (1999) 917–922.
[27] A.G. Porter, U.J. Reiner, Emerging roles of caspase-3 in apoptosis, Cell Death Differ. 6 (1999) 99–104.
[28] Y.-C. Hseu, C.W. Chou, K.J. Senthil Kumar, K.T. Fu, H.M. Wang, L.S. Hsu, Y.H. Kuo, C.R. Wu, S.C. Chen, H.L. Yang, Ellagic acid protects human keratinocyte (HaCaT) cells against UVA-induced oxidative stress and apoptosis through the upregulation of the HO-1 and Nrf-2 antioxidant genes, Food Chem. Toxicol. 50 (2012) 1245–1255.
[29] M. Ichihashi, M. Ueda, A. Budiyanto, T. Bito, M. Oka, M. Fukunaga, K. Tsuru, T. Horikawa, UV-induced skin damage, Toxicology 189 (2003) 21–39.
[30] D. Rodrigues, A.C. Viotto, R. Checchia, A. Gomide, D. Severino, R. Itri, M.S. Baptista, W.K. Martins, Mechanism of *Aloe Vera* extract protection against UVA: shelter of lysosomal membrane avoids photodamage, Photochem. Photobiol. Sci. 15 (2016) 334–350.
[31] N. Fakhrudin, B. Waltenberger, M. Cabaravdic, A.G. Atanasov, C. Malainer, D. Schachner, E.H. Heiss, R. Liu, S.M. Noha, A.M. Grzywacz, J. Mihaly-Bison, E.M. Awad, D. Schuster, J.M. Breuss, J.M. Rollinger, V. Bochkov, H. Stuppner, V.M. Dirsch, Identification of plumericin as a potent new inhibitor of the NF-κB pathway with anti-inflammatory activity in vitro and in vivo, Br. J. Pharmacol. 171 (2014) 1676–1686.
[32] C. Gorrini, I.S. Harris, T.W. Mak, Modulation of oxidative stress as an anticancer strategy, Nat. Rev. Drug Discov. 12 (2013) 931–947.
[33] P.K. Farris, Topical vitamin C: a useful agent for treating photoaging and other dermatologic conditions, Dermatol. Surg. 31 (2005) 814–818.
[34] W. Stahl, H. Sies, Photoprotection by dietary carotenoids: concept, mechanisms, evidence and future development, Mol. Nutr. Food Res. 56 (2012) 287–295.

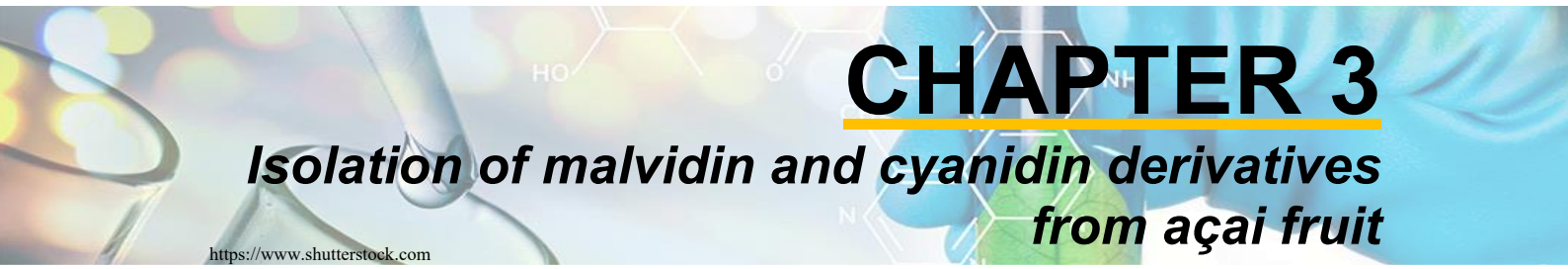

CHAPTER 3

Isolation of malvidin and cyanidin derivatives from açai fruit

https://www.shutterstock.com

Açai berries are considered to be the richest source of antioxidants in the world, thanks to the high content of polyphenols and flavonoids.
Açai has become famous for its anti-aging properties and clinical studies are providing promising evidence in support of heart and cardiovascular benefits as well as many other potential health benefits.[1]

[1]Barbosa, P. O., Pala, D., Silva, C. T., de Souza, M. O., do Amaral, J. F., Vieira, R. A. L., ... & de Freitas, R. N. (2016). Açai (Euterpe oleracea Mart.) pulp dietary intake improves cellular antioxidant enzymes and biomarkers of serum in healthy women. *Nutrition*, *32*(6), 674-680.

Journal of Photochemistry & Photobiology, B: Biology 172 (2017) 42–51

Contents lists available at ScienceDirect

Journal of Photochemistry & Photobiology, B: Biology

journal homepage: www.elsevier.com/locate/jphotobiol

Malvidin and cyanidin derivatives from açai fruit (*Euterpe oleracea Mart.*) counteract UV-A-induced oxidative stress in immortalized fibroblasts

Ganna Petruk[a], Anna Illiano[a], Rita Del Giudice[a], Assunta Raiola[b], Angela Amoresano[a], Maria Manuela Rigano[b], Renata Piccoli[a,c], Daria Maria Monti[a,c,*]

[a] Department of Chemical Sciences, University of Naples Federico II, Complesso Universitario Monte Sant'Angelo, via Cinthia 4, 80126 Naples, Italy
[b] Department of Agricultural Sciences, University of Naples Federico II, Via Università 100, 80055 Portici, Naples, Italy
[c] Istituto Nazionale di Biostrutture e Biosistemi (INBB), Rome, Italy

ARTICLE INFO

Keywords:
Euterpe oleracea
Antioxidants
Phenolics
Malvidin
Oxidative stress
UV-A radiations
Eukaryotic cells

ABSTRACT

UV-A radiations are known to induce cellular oxidative stress, leading to premature skin aging. Consumption of açai fruit (*Euterpe oleracea Martius*) is known to have many health benefits due to its high level of antioxidants. Herein, we analyzed the ability of phenolic compounds extracted from this fruit to attenuate UV-A-induced oxidative stress in immortalized fibroblast.

A methanol/water açai extract was fractionated by HPLC and each fraction tested for anti-oxidant stress activity. Immortalized fibroblasts were pre-incubated with açai fractions and then exposed to UV-A radiations. Açai extract was found to be able to strongly protect cells from oxidative stress. In particular, reactive oxygen species (ROS) production, GSH depletion, lipid peroxidation and no increase in the phosphorylation levels of proteins involved in the oxidative stress pathway was observed in cells pre-incubated with the extract and then irradiated by UV-A. Mass spectrometry analyses of HPLC fractionated extract led us to the identification of malvidin and cyanidin derivatives as the most active molecules able to counteract the negative effects induced by UV-A irradiation.

Our results indicate, for the first time, that açai fruit is a valuable natural source for malvidin and cyanidin to be used as anti-stress molecules and represent good candidates for dietary intervention in the prevention of age related skin damage.

1. Background

In the last few years, an increasing attention has focused on age-related diseases, including skin aging. Oxidative stress caused by aging is considered a general initiating factor of neurodegeneration and carcinogenesis [1]. Indeed, it is known that the skin is constantly exposed to oxidative stress induced by reactive oxygen species (ROS), generated by endogenous (i.e. enzyme activities) or exogenous sources [2,3].

UV radiation from sunlight is one of the most important health-related environmental factors because of its hazardous effects, which include generation of skin cancer, suppression of the immune system, and premature skin aging [2]. In particular, UV-A (400–315 nm) radiations are weakly absorbed by DNA, but rather excite endogenous chromophores, leading to DNA damage. This occurs through the production of reactive singlet oxygen that specifically reacts with guanine within the DNA molecule [4,5]. UV-A radiations may also promote the formation of hydroxyl radicals via the photosensitized production of superoxide anions. Because of their high reactivity and low specificity, hydroxyl radicals likely induce a wide range of DNA damage [6]. Fibroblasts, cells of the dermis, are continuously exposed to UV-A radiations, which are able to penetrate deeply in the skin. The cellular antioxidant defense system is composed of endogenously produced antioxidant molecules, but the intrinsic mechanism for antioxidant defense is gradually impaired with aging, resulting in an inability to deal with ROS generation [7]. A continuous and regular

Abbreviations: ABTS, 2,2′-azinobis(3-ethylbenzothiazoline-6-sulfonic acid); DCF, 2′,7′-dichlorofluorescein; DTNB, 5,5′-dithiobis-2-nitrobenzoic acid; EDTA, ethylene diamine tetra acetic acid; HAA, hydrophilic antioxidant activity; H_2-DCFDA, 2′,7′-dichlorodihydrofluorescein diacetate; MALDI, matrix-assisted laser desorption/ionization; MS, mass spectrometry; MTT, 3-(4,5-dimethylthiazol-2-yl)-2,5-diphenyltetrazolium bromide; P-HSP-27, phosphorylated heat shock protein; P-p38, phosphorylated p38 MAP kinase; P-MAPKAPK-2, phosphorylated MAP kinase-activated protein kinase; ROS, reactive oxygen species; r.t., room temperature; TBA, thiobarbituric acid; TBARS, TBA reactive substances; TFA, trifluoroacetic acid; TNB, 5-thio-2-nitrobenzoic acid

* Corresponding author at: Department of Chemical Sciences, University of Naples Federico II, Complesso Universitario Monte Sant'Angelo, via Cinthia 4, 80126 Naples, Italy.
E-mail address: mdmonti@unina.it (D.M. Monti).

http://dx.doi.org/10.1016/j.jphotobiol.2017.05.013
Received 27 February 2017; Received in revised form 5 May 2017; Accepted 9 May 2017
Available online 12 May 2017
1011-1344/

Table 1
Total phenolic acids, total flavonoids and hydrophilic antioxidant activity in açai extract.

Açai antioxidant determination	Value
Total phenols (mg/100 g DW)	192.41 ± 10.78
Total flavonoid (mg/100 g DW)	159.67 ± 7.65
HAA (mmol TE/100 g DW)	2.1 ± 0.17

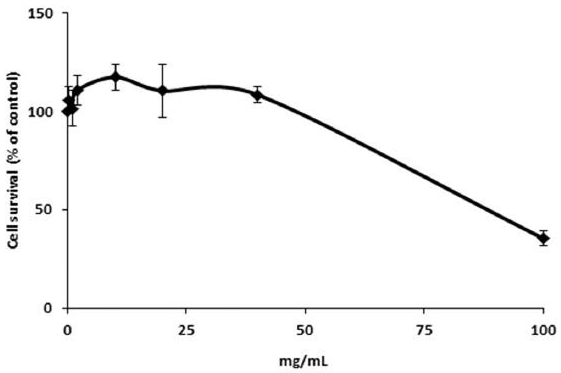

Fig. 1. Effect of açai extracts on the viability of BALB/3T3 fibroblasts. Dose-response curve of BALB/3T3 cells after 48 h incubation with increasing concentrations of açai extracts. Cell viability was assessed by the MTT assay and expressed as described in Materials and Methods section. Values are given as means ± S.D. (n ≥ 3).

intake of vitamins, trace metals, polyunsaturated fatty acids, and polyphenols from food sources contributes to counteract oxidative stress [8,9] and in preventing or retarding age-related diseases [10–12]. As an example, we recently report the beneficial effects of tomato extracts in counteracting oxidative stress in different cell lines [13,14]. Therefore, a continuous search for natural extracts highly rich in antioxidant molecules is needed to identify and provide novel natural drugs against aging-associated diseases.

Açai (*Euterpe oleracea Martius*) tree is a large palm found in the Amazon flood plain. The fruit of this palm is a small purple-black berry which reaches about 10 mm in diameter and is usually consumed in all states of Brazil since it is rich in α-tocopherol, fibers, lipids, polyphenols (including anthocyanins), and mineral ions [15,16]. The high polyphenol content, mostly composed of anthocyanins and flavones, is thought to confer to açai fruit several health-promoting effects, including anti-inflammatory, immunomodulatory, antinociceptive, and antioxidant properties [17–25]. In particular, açai extracts were shown to increase plasma antioxidant capacity [21], to decrease oxidative stress in endothelial cells [26], to attenuate tumor growth in mice affected by esophageal cancer [27] and to lower the level of blood cholesterol in animal models for hypercholesterolemia [28].

A positive role of açai in modulating ROS production and activating antioxidant genes expression in rat liver was also reported [29] and, more recently, Peixoto and colleagues demonstrated the beneficial effect of açai extract in counteracting oxidative stress and aging in *C. elegans* [18].

Although several reports on the spectrum of health benefits of açai have been reported, only few studies are available so far on the identification of the antioxidant molecules responsible for the reported beneficial effects on human health.

Here, a methanol/water extract from *Euterpe oleracea* fruits was analyzed for its antioxidant activity on fibroblasts exposed to UV-A-induced insults. A combined approach of bioassays and mass spectrometry analyses led to the identification of açai bioactive compounds.

2. Methods

2.1. Açai Extracts

Methanolic extracts from açai fruit were obtained as reported by Rigano et al. [30], starting from commercially available dried powder (2 g, Tuialimentos, Brasil). The mixture was dried in a rotovapor (R-210, Buchi), and dissolved in 5% dimethyl sulfoxide (DMSO) in PBS (1 mL).

2.2. Antioxidant Compounds Determination and Antioxidant Activity Analysis

Total phenols content was determined in the whole açai extract according to the method of Singleton et al. [31] modified as reported by Rigano et al. [30]. Briefly, an equal volume of Folin-Ciocalteu's phenol reagent and two volumes of ddH_2O were added to the hydrophilic extract. After 6 min, Na_2CO_3 was added (7% final concentration). After 90 min the absorbance was read at 760 nm. A standard curve was obtained by using gallic acid in the range 0–70 μg/mL. The total phenolic content was expressed as mg of gallic acid equivalents (GAE)/100 g dry weight (DW) of açai. Three independent analyses

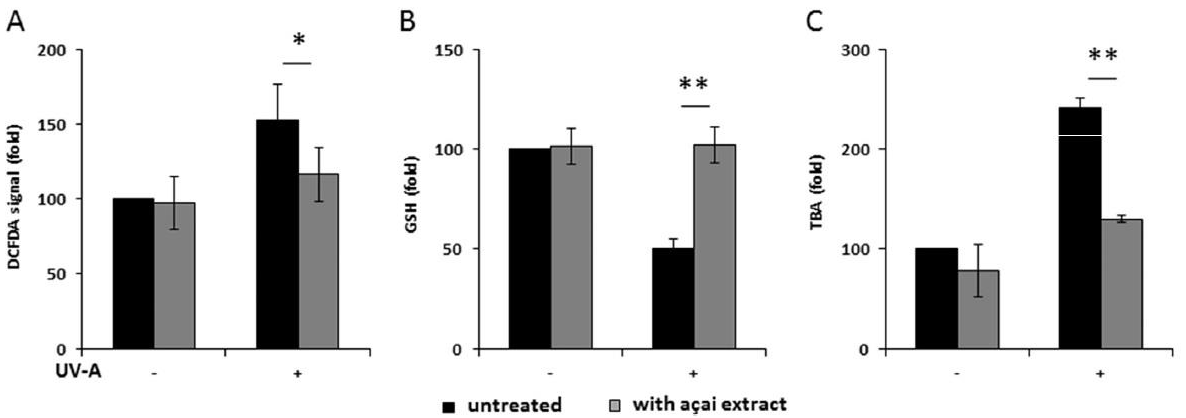

Fig. 2. ROS production, GSH oxidation and lipid peroxidation in BALB/3T3 cells irradiated by UV-A in the presence of açai extracts. Cells were pre-incubated in the presence of 10 mg/mL açai extract (grey bars) for 2 h and then irradiated by UV-A (100 J/cm^2). A, intracellular ROS levels were determined by DCFDA assay; B, intracellular GSH levels determined by DTNB assay; C, lipid peroxidation levels determined by TBARS assay. Values are expressed as fold increase with respect to control (i.e. untreated) cells. Data shown are the means ± S.D. of three independent experiments. * indicates $p < 0.01$; ** indicates $p < 0.001$.

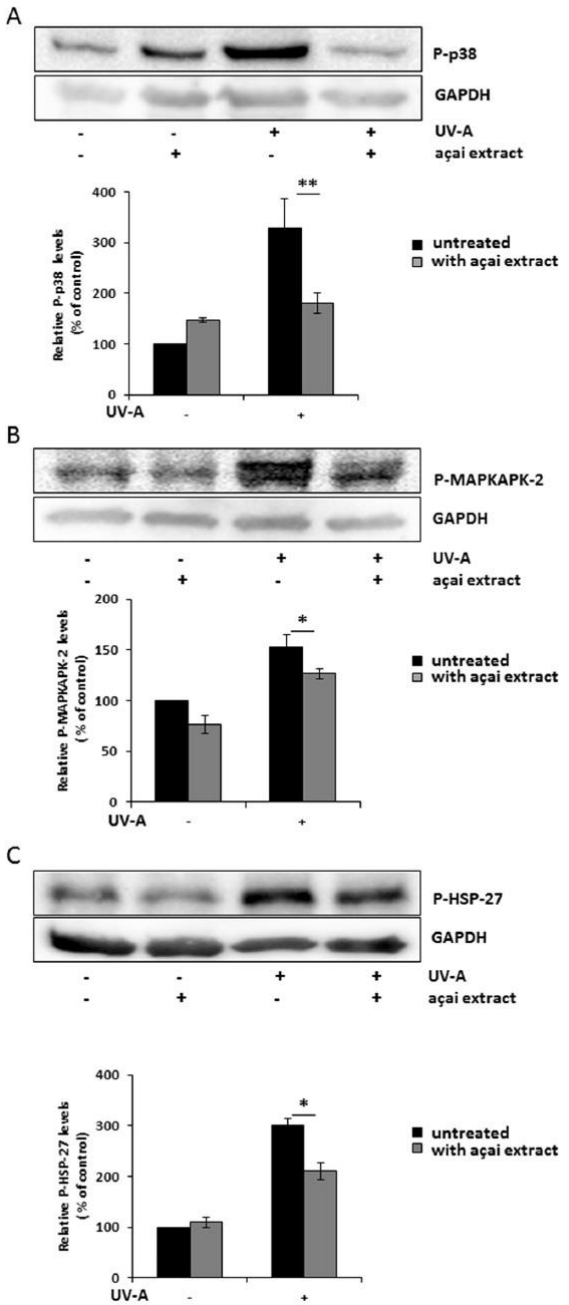

Fig. 3. Effect of açai extracts on UV-A-induced oxidative stress markers in BALB/3T3 fibroblasts. Cells were incubated with 10 mg/mL açaiextract2h prior to UV-A irradiation (100 J/cm^2) and then cells were incubated for 90 min. Western blots show the phosphorylation levels of p38 (A),MAPKAPK-2 (B) and HSP-27 (C), with the relative densitometric analysis in the absence (black bars) or in the presence (grey bars) of açai extract. GAPDH was used as internal standard. Data shown are the means ± S.D. of three independent experiments. * indicates $p < 0.01$; ** indicates $p < 0.001$.

were carried out.

Total flavonoids were estimated by the aluminum chloride colorimetric assay reported by Marinova et al. [32] with modifications reported by Raiola et al. [33]. Briefly, $NaNO_2$ (5%) was added to methanolic extract and, after 5 min incubation, $AlCl_3$ (10% w/v) was added. After 6 min, NaOH (1 M) was added and the absorbance measured at 510 nm. A standard curve was obtained by using quercetin in the range 0–100 μg/mL. Total flavonoids content was expressed as mg quercetin equivalents (QE)/100 g DW. Three independent analyses were carried out.

HAA was evaluated in the water-soluble fraction using the protocol described by Miller et al. [34] with modifications reported by Del Giudice et al. [35]. Briefly, methanolic extracts were allowed to react with an $ABTS^{\bullet+}$ solution for 2.5 min, and then the absorbance was measured at 734 nm using a spectrophotometer. A standard curve, obtained by using Trolox, was linear between 0 and 20 μM Trolox. Values were expressed as mmol TE/kg DW of açai. Three separate analyses were carried out with each sample.

2.3. Cell Culture and MTT Assay

BALB/3T3 fibroblasts (clone A31, from ATCC) were cultured in Dulbecco's Modified Eagle's Medium (Sigma-Aldrich, St Louis, Mo, USA), supplemented with 10% foetal bovine serum (HyClone), 2 mM L-glutamine and antibiotics, all from Sigma-Aldrich, in a 5% CO_2 humidified atmosphere at 37 °C.

Cells were seeded in 96-well plates (100 μL/well) at a density of 5×10^3/well. For dose-dependent cytotoxicity assays, 24 h after seeding, increasing volumes of açai methanolic extracts were added to the cells, to reach a final concentration ranging from 0.2 to 100 mg/mL. After 48 h incubation, cell viability was assessed by the MTT (3-(4,5-dimethylthiazol-2-yl)-2,5-diphenyltetrazolium bromide) assay, as described by Monti et al. [36]. Cell survival was expressed as the percentage of viable cells in the presence of extract compared to that of control samples. Two groups of cells were used as control, i.e. cells untreated with the extract and cells supplemented with identical volumes of DMSO. Each sample was tested in three independent analyses, each carried out in triplicates.

2.4. Oxidative Stress

To analyze oxidative stress, cells were plated at a density of 4×10^4 cells/cm^2. 24 h after seeding, cells were incubated for 2 h in the presence or absence of 10 mg/mL of açai extract, or equivalent amount of each isolated fraction, and then irradiated for 10 min with UV-A light (100 J/cm^2) (treatment before injury). In a second group of experiments, cells were irradiated for 10 min with UV-A (100 J/cm^2) and then incubated for 2 h in the presence or absence of açai extract or equivalent amount of each isolated fraction (treatment after injury).

2.5. DCFDA Assay

To estimate ROS production, the protocol described in [13] was followed. Briefly, at the end of incubation, cells were incubated with 2′,7′-dichlorodihydrofluorescein diacetate (H_2-DCFDA, Sigma-Aldrich). Fluorescence intensity was measured by a Perkin-Elmer LS50 spectrofluorimeter (525 nm emission wavelength, 488 nm excitation wavelength, 300 nm/min scanning speed, 5 slit width for both excitation and emission). ROS production was expressed as percentage of DCF fluorescence intensity of the sample under test, with respect to the untreated sample. Each value was assessed by three independent experiments, each with three determinations.

2.6. DTNB Assay

To estimate intracellular glutathione levels, a procedure previously described was followed [14]. Briefly, at the end of incubation, cells were detached by trypsin, lysed and protein concentration was determined by the Bradford assay. Then, 50 μg of proteins were incubated with 3 mM EDTA, 144 μM 5,5′-dithiobis-2-nitrobenzoic acid (DTNB) in

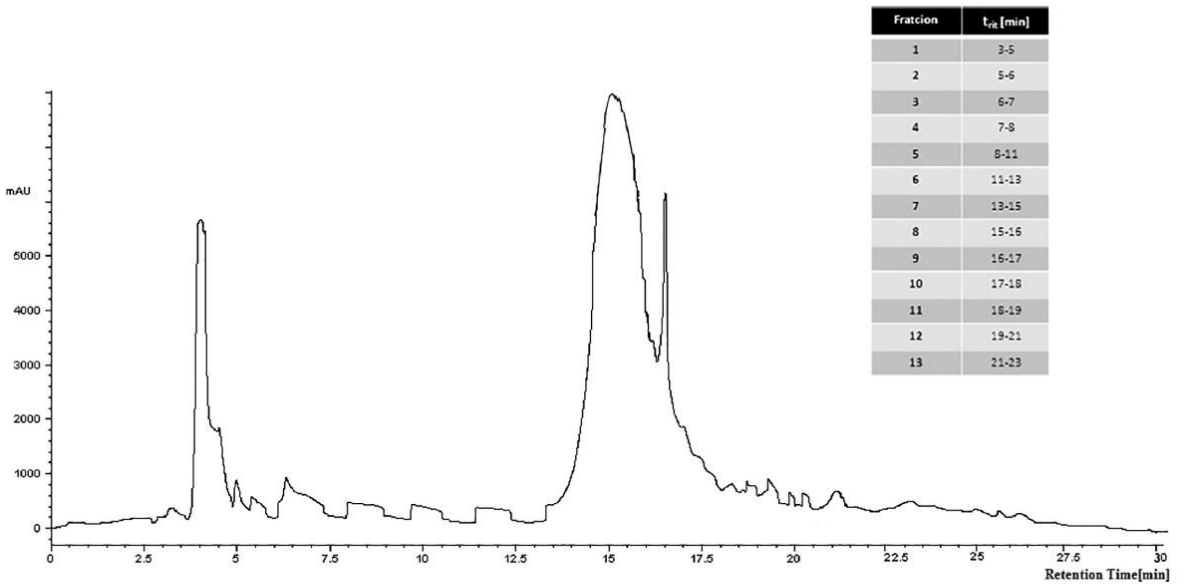

Fig. 4. Fractional analysis of açai extract by reverse-phase HPLC. Reverse phase C18 column was used with a linear gradient from 5% to 95% in 0.1% trifluoroacetic acid; elution was monitored at 278 nm. Thirteen fractions were manually collected.

30 mM TrisHCl pH 8.2, centrifuged at 14,000*g* for 5 min at 4 °C and the absorbance of the supernatant was measured at 412 nm by using a multiplate reader (Biorad). GSH levels were expressed as the percentage of TNB absorbance in the sample under test with respect to the untreated sample. Values are the mean of three independent experiments, each with triplicate determinations.

2.7. Measurement of Lipid Peroxidation

The thiobarbituric acid reactive substances (TBARS) assay was performed as described by Del Giudice et al. [13]. Briefly, after irradiation with UV-A, cells were kept for 90 min at 37 °C, then detached and suspended (5×10^4 cells) in 0.67% thiobarbituric acid (TBA) and 20% trichloroacetic acid (1:1 v/v). After heating and centrifugation at 3000*g* for 5 min at 4 °C, samples were read at 532 nm. Lipid peroxidation levels were expressed as the percentage of the absorbance at 532 nm of the sample under test, with respect to untreated cells (100%). Three independent experiments were carried out, each one with three determinations.

2.8. Western Blot Analyses

Cells were plated at a density of 2×10^4 cells/cm^2 in complete medium for 24 h and then treated as described above (paragraph 2.4). When açai extract was used before UV-A exposure, cells were incubated for further 90 min at 37 °C. Alternatively, following the induction of UV-A stress, cells were treated with the extract for 120 min at 37 °C. Cell lysates were then analyzed by Western blotting performed as reported by Galano et al. [37]. Phosphorylation levels of p38, MAPKAPK-2 or HSP-27 were detected by using specific antibodies purchased from Cell Signal Technology (Danvers, MA, USA). To normalize protein intensity levels, specific antibodies against internal standards were used, i.e. anti-β-actin (Proteintech, Manchester, UK) or anti-GAPDH (ThermoFisher, Rockford, IL, USA). The chemiluminescence detection system (SuperSignal® West Pico) was from Thermo Fisher.

2.9. Reverse-phase HPLC Analysis

Methanol/water açai extract (2 g/mL, 1 mL) was fractionated by reverse-phase HPLC on a Phenomenex Jupiter C18 column (250 × 2.00 mm 5 µm, 300 Å pore size) (Phenomenex, Torrance, California, USA) with a linear gradient from 5% to 95% acetonitrile (Sigma Aldrich,Saint Louis, USA) in 0.1% trifluoroacetic acid (TFA) (Carlo Erba Reagents S.r.l, Milan, Italy) over 40 min, at a flow rate of 200 µL/min; elution was monitored at 278 nm. The eluate was collected manually in thirteen fractions (1 mL). Fractions were lyophilized and dissolved in 5% DMSO in PBS, and their content identified by MALDI-TOF (AB SCIEX, Milan, Italy) analysis.

2.10. Mass Spectrometry Analyses

Matrix-assisted laser desorption/ionization (MALDI) mass spectrometry (MS) experiments were performed on a 5800 MALDI-TOF-TOF ABSciex equipped with a nitrogen laser (337 nm) (AB SCIEX, Milan, Italy). Aliquots of açai HPLC fractions (0.5 µL) were mixed (1:1, v/v) with 2.5 dihydroxybenzoic acid (10 mg/mL) (Sigma-Aldrich, Saint Louis, USA) in acetonitrile:water (90:10) solution. Calibration was performed by using AB SCIEX calibration mixture (Monoisotopic (M + nH)n$^+$: 904.46 Da des-Arg-Bradykinin, 1296.68 Da Angiotensin I, 1570.67 Da Glu-Fibrinopeptide B, 2093.08 Da ACTH (clip 1–17), 2465.19 Da ACTH (clip 18–39), 3657.92 Da ACTH (clip 7–38)). For polyphenols identification, MS and tandem mass (MSMS) spectra were acquired using a mass (*m/z*) range of 100–4000 Da.

2.11. Statistical Analyses

In all the experiments samples were analyzed in triplicate. Quantitative parameters were expressed as the mean value ± SD. Significance was determined by Student's *t*-test at a significance level of 0.01. Differences among fractions were determined by using SPSS (Statistical Package for Social Sciences) Package 6, version 15.0 (SSPS Inc., Chicago, IL, USA). Significance was determined by Duncan's-test at a significance level of 0.05.

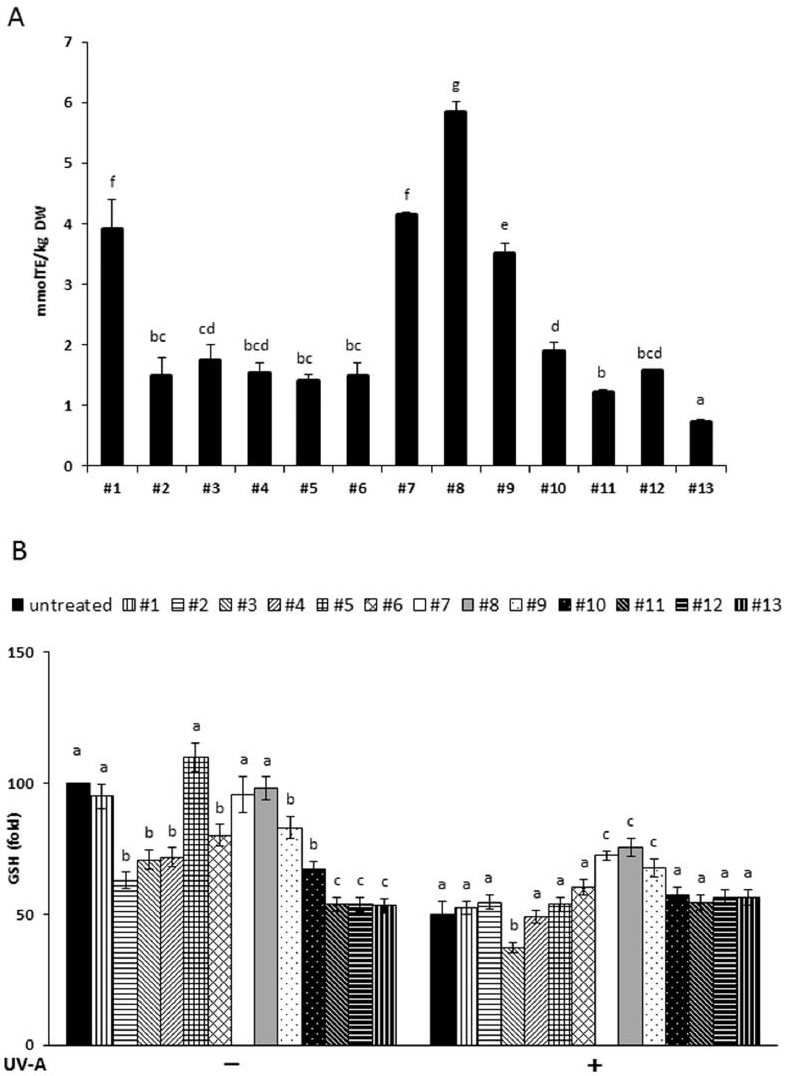

Fig. 5. Analysis of the antioxidant activity of açai fractions. A, Hydrophilic antioxidant activity (mmol TE/kg DW) in fractions evaluated by ABTS test. Data shown are the means ± S.D. of three independent experiments. Significance was determined by Duncan's-test at a significance level of 0.05. Values with different letters are significantly different. B, Changes in intracellular GSH levels of cells before (−) and after (+) UV-A treatment. Cells were incubated with açai extract, or equivalent amount of fractions obtained by HPLC, for 2 h prior to UV-A irradiation (100 J/cm^2). Data shown are the means ± S.D. of three independent experiments. Values with different letters are significantly different compared to untreated cells, indicated by black bars ($p < 0.05$).

3. Results

3.1. Antioxidant Compounds Determination

We first characterized the methanol/water açai extract by measuring its antioxidant compounds and determining the antioxidant activity. By colorimetric assays, the total phenol content was estimated to be 192.41 ± 10.78 mg GAE/100 g DW, whereas that of total flavonoids was found to be 159.67 ± 7.65 mg QE/100g DW. The mean antioxidant activity was 2.1 ± 0.17 mmol TE/100 g DW. Data are reported in Table 1.

3.2. Biocompatibility of Açai Extracts on Fibroblasts

The biocompatibility of the açai extract on BALB/3T3 fibroblasts was tested by a dose-response test, in a range from 0.2 to 100 mg/mL of extract. As shown in Fig. 1, cell viability was not affected up to 40 mg/mL, whereas at the highest concentration tested (100 mg/mL) a 50% reduction of cell viability was observed. On the basis of these results, subsequent experiments were carried out at 10 mg/mL of açai extract, corresponding to a flavonoid content of 0.16 mg QE/mL and to a phenolic content of 0.19 mg GAE/mL.

3.3. Pretreatment With Açai Extracts Inhibits UV-A-Induced Damage in BALB/3T3 Fibroblasts

In all the experiments reported below, BALB/3T3 fibroblasts were pretreated with açai extract for 2 h before the induction of oxidative stress by UV-A irradiation (100 J/cm^2). Immediately after UV-A irradiation, ROS production was determined by using H_2DCF-DA (2,7-

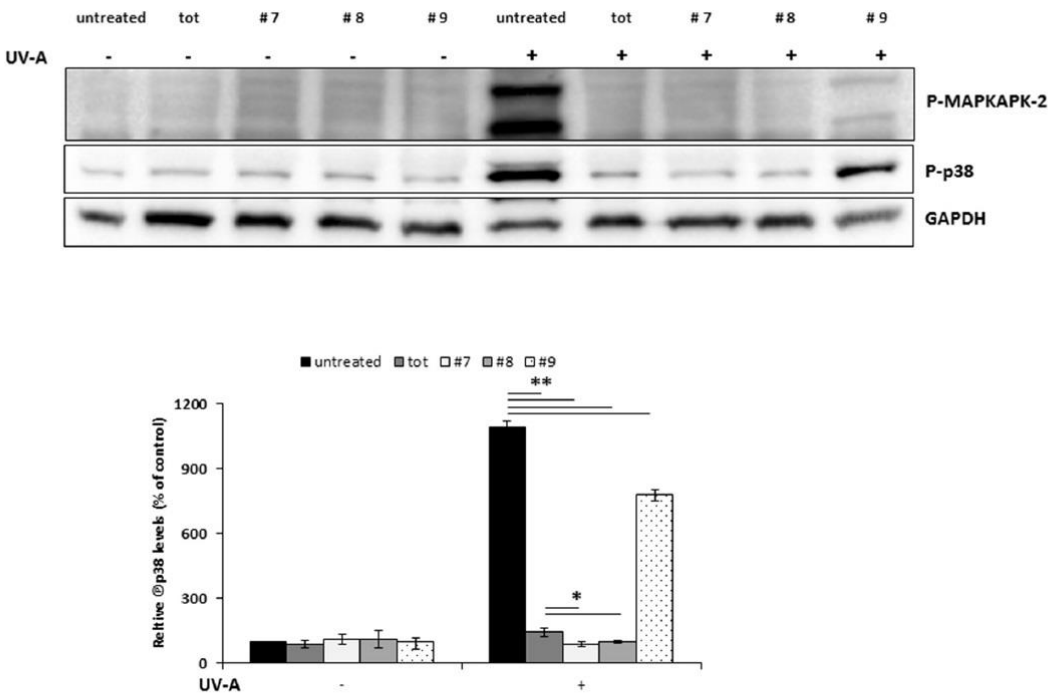

Fig. 6. Western blot analysis of UV-A-treated BALB/3T3 cells in the presence of HPLC fractions. Cells were incubated with different fractions for 2h prior to UV-A (100 J/cm^2) irradiation and then cells were incubated for further 90min at 37 °C. Representative western blots show the phosphorylation levels of p38 (A) and MAPKAPK-2 (B), with the relative densitometric analysis in the absence (black bars) or in the presence (white bars) of extract. GAPDH was used as internal standard. Data shown are the means ± S.D. of three independent experiments. * indicates $p < 0.01$, ** indicates $p < 0.001$.

dichlorofluorescin diacetate) (Fig. 2A). As expected, UV-A treatment significantly increased DCF fluorescence intensity, compared to the non-irradiated samples, whereas açai extract had no effect on ROS levels. Interestingly, pretreatment of cells with açai extract prior to UV-A exposure, resulted in the inhibition of ROS production. Moreover, following UV-A-oxidative stress induction, we found that intracellular GSH was significantly decreased with respect to untreated cells, whereas no alteration in intracellular GSH levels was observed when cells were pretreated with açai extract before being irradiated by UV-A (Fig. 2B). The protective effect of açai extract was confirmed by analyzing the lipid peroxidation levels after 90 min from irradiation. Lipid peroxidation level was measured by thiobarbituric acid reactive substances (TBARS). A significant increase in lipid peroxidation levels after UV-A treatment was observed but, noteworthy, this effect was abolished when cells were pretreated with açai extract. Again, pretreatment of cells with açai extract significantly counteracted the increase of lipid peroxidation (Fig. 2C).

The protective effect of açai extract was further confirmed by Western blot experiments, in which the phosphorylation levels of p38 and its direct target, MAPKAPK-2, were analyzed (Fig. 3). These proteins are directly involved in signaling stress pathways induced by UV-A [38]. When cells were UV-A irradiated, we observed a significant increase in the phosphorylation levels of p38 and MAPKAPK-2, as expected (Fig. 3A and B, third lane). Instead, although the treatment of non-irradiated cells with açai extract slightly altered the phosphorylation level of p38 (Fig. 3A, second lane), when cells were exposed to açai extract prior to UV-A treatment, the phosphorylation levels of p38 and MAPKAPK-2 were similar to those observed in non-irradiated cells (Fig. 3A and B, fourth lane). A similar trend was observed for HSP-27, a heat shock protein whose phosphorylation is directly related to oxidative stress [39,40] (Fig. 3C).

3.4. Antioxidant Activity of Açai Fractions

In order to identify which açai compounds were responsible for the antioxidant activity observed in irradiated fibroblasts, the extract was fractionated by HPLC on a reverse phase C18 column, from which the profile shown in Fig. 4 was obtained. 13 HPLC fractions were collected, as reported in the Figure, and their antioxidant activity was tested in vitro. The HAA analysis (Fig. 5A) revealed that the highest antioxidant activity was associated to fractions 7 and 8, for which the HAA mean values of 4.13 mmol TE/kg DW and 5.85 mmol TE/kg DW, respectively, were calculated. High antioxidant power was also identified in fractions 1 and 9, with HAA mean values of 3.92 and 3.49 mmol TE/kg DW, respectively. Lower values were detected in the other fractions, ranging from 0.72 mmol TE/kg DW (fraction 13) to 1.89 mmol TE/kg DW (fraction 10).

Then, we analyzed the intracellular GSH levels in BALB/3T3 cells pretreated with each HPLC fraction, before and after UV-A treatment. As shown in Fig. 5B, fractions 7 and 8 were able to contrast the detrimental effects of UV-A irradiation on GSH depletion, whereas fraction 9 was less efficient, in agreement with the HAA analysis. By contrast, fraction 1 did not show any protective effect from oxidative stress. Western blot experiments confirmed the strong antioxidant activity of fraction 7 and 8 on UV-A-stressed fibroblasts. In particular, the increase in p38 and MAPKAPK phosphorylation levels induced by UV-A irradiation was attenuated when cells were pretreated with açai fractions 7 and 8, whose effect was found to be slightly, but significantly, more pronounced than that of the whole extract (Fig. 6). Noticeable, a lower decrement in p38 phosphorylation level was observed when cells were pre-treated with fraction 9.

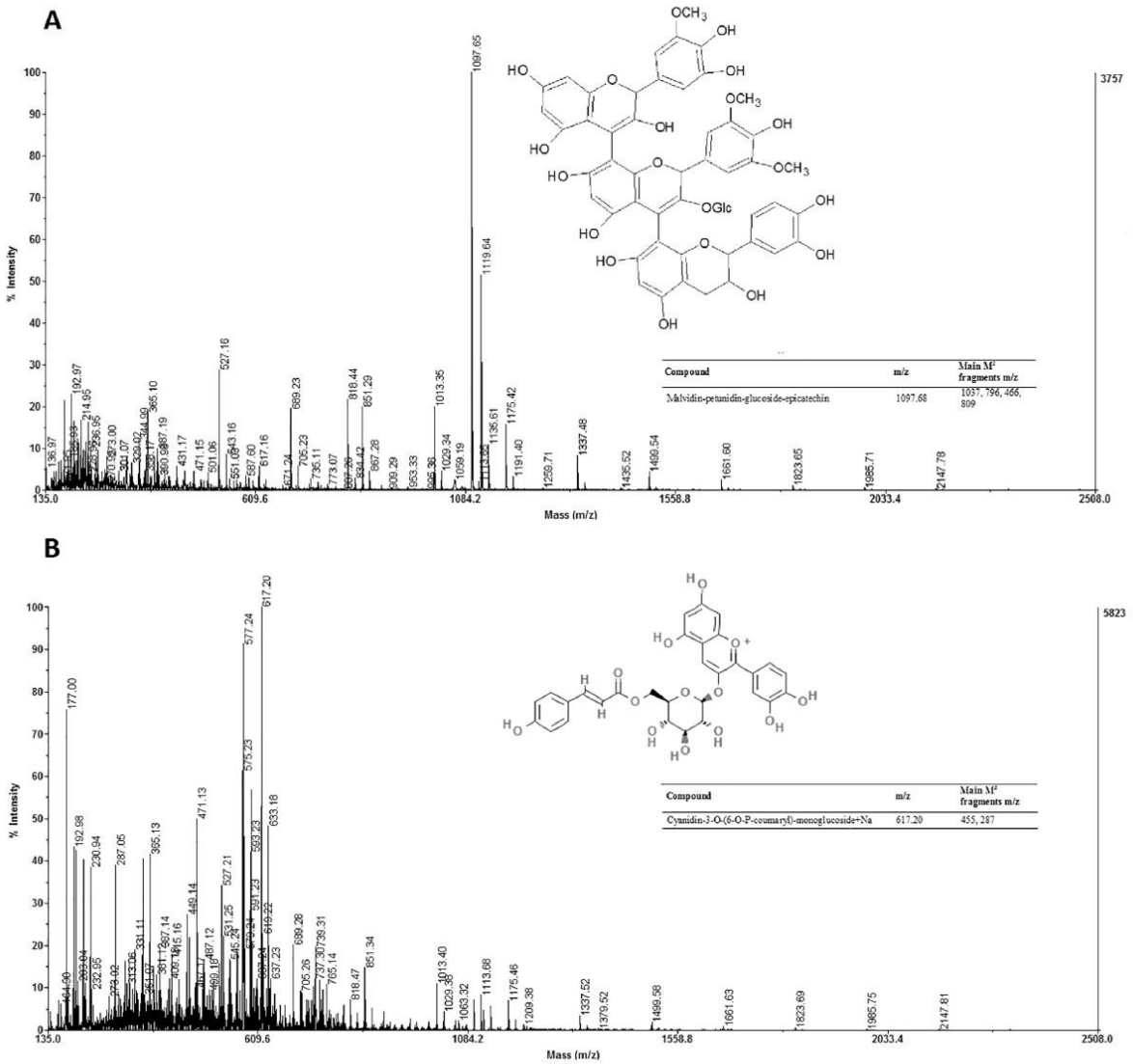

Fig. 7. MALDI-MS analysis of selected HPLC fractions from açai extract. The MALDIMS spectra of fractions 7 and 8 are reported in panels A and B, respectively. The attributions are reported.

3.5. Malvidin and Cyanidin are Responsible for the Açai Antioxidant Activity on Immortalized Fibroblasts

HPLC fractions 7 and 8 were submitted to MALDI-MS analysis, as described in the Material and Method section. The different species detected in the MALDI spectra (Fig. 7A-B) were identified on the basis of MSMS MALDI TOTOF analysis and compared with literature data [41]. Mass spectral identification is reported in Table 2. Qualitative and semi-quantitative differences can be appreciated in the MALDI spectra showing the presence of different flavonoids in açai fractions. Among them, malvidin-petunidin-glucoside-epicatechin was found to be the predominant compound in fraction 7, whereas cyanidin-3-O-(6-O-p-coumaryl)-monoglucoside was found to be the most abundant species in fraction 8. DCFDA assay indicated that malvidin and cyanidin enriched fractions were able to mitigate ROS production as well as the whole extract (Fig. 8A). However, the TBARS assay (Fig. 8B) revealed that the activity of malvidin enriched fraction was comparable to that of the whole extract, whereas cyanidin enriched fraction was lower.

Finally, to evaluate if malvidin and cyanidin derivatives protect cells after UV-A injury and to avoid any sunscreen effect, fibroblasts were first irradiated by UV-A (100 J/cm^2), and afterwards incubated for 2h with either açai extract or its fractions and then ROS, GSH levels and the phosphorylation levels of p38 were evaluated (Fig. 9). Interestingly, UV-A induced ROS production was mitigated by the presence of either açai extract or its active fractions. Furthermore, no alteration in intracellular GSH levels was measured and a significant decrease in the phosphorylation levels of p38 was also observed.

4. Discussion

Among the most severe environmental injuries to which humans are exposed, UV-A radiations are known to be the main cause of different

Table 2
MALDI mass spectral analysis of açai fractions after reverse-phase HPLC. The identified species and the relative percentages are reported (G = glucose).

Compound	*m/z*	Main M^2 fragments *m/z*	Fraction 7	Fraction 8
Petunidin-3-acetyl	365.10	305, 203	20%	43%
Peonidin-3-*O*-acetyl monoglucoside	527.19	467, 365, 203	32%	38%
Cyanidin-3-O-(6-O-P-coumaryl)-monoglucoside + Na	617.20	455, 287	10%	100%
Petunidin-3-acetyl diglucoside	689.23	527, 629	22%	20%
Malvidin-3-acetylglucose-ethil-catechin/ Petunidin-3-acetil triglucoside	851.31	791, 689	20%	17%
Petunidin-3-acetyl tetraglucoside	1013.35	952, 851	20%	14%
Malvidin-petunidin-glucoside-epicatechin	1097.68	1037, 796, 466, 809	100%	5%
Petunidin-3-acetyl + 5G	1175.42	1115, 1013	16%	8%
Petunidin-3-acetyl + 6G	1337.48	1277,1175	12%	5%
Petunidin-3-acetyl + 7G	1499.54	1439, 1337	8%	3%
Petunidin-3-acetyl + 8G	1661.6	1601, 1499	6%	3%
Petunidin-3-acetyl + 9G	1823.65	1763, 1661	6%	2%
Petunidin-3-acetyl + 10G	1985.71	1925, 1823	4%	1%
Petunidin-3-acetyl + 11G	2147.78	2087, 1985	2%	1%

detrimental effects on the skin, such as inflammation, premature skin aging and development of skin cancer [42,43]. In recent years, an increasing body of research has focused on antioxidants since they are able to counteract oxidative stress-induced pathological conditions. However, studies are usually conducted on commercial molecules, supposed to have antioxidant activity [43–45].

Here, we analyzed hydrophilic extracts from açai berries to evaluate their dermato-protective properties against UV-A irradiation. Açai is the name commonly used for the tree *Euterpe oleracea Martius*, a South American palm [25,46], whose berry is largely consumed since it shows several beneficial activities, including anti-inflammatory and antioxidant properties. These activities are mainly due to açai high content in polyphenol content, especially anthocyanins and flavones [20–25].

Immortalized fibroblasts, exposed to UV-A radiations, showed increased levels of intracellular ROS and lipid peroxidation, and decreased levels of intracellular GSH. Noteworthy, we found that a pre-treatment of cells with açai extracts clearly inhibited the detrimental effect of oxidative stress, since ROS generation, lipid peroxidation, intracellular GSH levels and p38 phosphorylation levels were all found to be almost unaltered with respect to UV-A unexposed cells. It is interesting to notice that the açai extract is able to efficiently protect immortalized, non-cancer cells from the deleterious effects of UV-A irradiation when tested at concentrations compatible with cell viability, i.e. non associated to any cytotoxicity. Moreover, we demonstrated that the protective effect of açai extract is not due to a sunscreen effect, as the extract was able to protect cells also after UV-A induced damage.

Mass spectrometry analyses of HPLC fractionated extract led us to the identification of the main agents responsible for the potent antioxidant activity of açai extracts on fibroblasts. These are two flavonoids, cyanidin and malvidin, both endowed with strong antioxidant activity, with malvidin the most active.

Cyanidin is considered the widest spread anthocyanin in the plant kingdom and it is known to be a strong natural antioxidant. Amorini and colleagues [47] demonstrated that cyanidin-3-glucoside, also known as kuromanin, has a remarkable antioxidant capacity in the model of Cu^{2+}-mediated human low density lipoprotein oxidation, even higher than resveratrol and ascorbic acid and independent from pH variations (from 4 to 7.4). In addition, it is reported that cyanidin-3-glucoside may attenuate obesity-associated insulin resistance and hepatic steatosis in high-fat diet-fed mice via the transcription factor FoxO1 [48].

Malvidin, normally present at high concentration in red wine and black rice, and responsible for their color, plays an important role in protecting plants from UV irradiation [49,50]. Accordingly, it has been reported that malvidin has antioxidant activity in vitro [51], as well as in neuronal and in endothelial cells [52,53]. Recently, it has been demonstrated that malvidin is also able to inhibit aging by attenuating oxidative stress in human diploid fibroblasts [54]. Moreover, several authors have shown that malvidin inhibits the growth of different tumor cell lines in vitro or in vivo [55–57].

Polyphenols are known to inhibit free radicals' production by donating hydrogen atoms, which break oxidation chains and chelate transition metal ions. Açai polyphenols may upregulate antioxidant enzymes by activating the Nrf2/Keap1 pathway [58], downregulate the expression of the pro-inflammatory transcription factor NF-kB, which in turn targets pro-inflammatory cytokines, and reduces the accumulation of intracellular lipids in differentiated adipocytes by downregulating the expression of adipogenic genes transcription factors [59]. Additionally, different studies performed on healthy women, which consumed 200 g/day of açai pulp for 4 weeks, revealed that some antioxidant enzymes, i.e. superoxide dismutase, catalase and glutathione, were increased [59–61].

Our findings now reveal that açai extract protects BALB/3T3 cells against UV-A irradiation by neutralizing the negative effects of stress induced by UV-A, as it interferes with ROS generation and keeps intracellular GSH and lipid peroxidation close to the normal cellular levels. This work reveals, for the first time, that malvidin present in açai

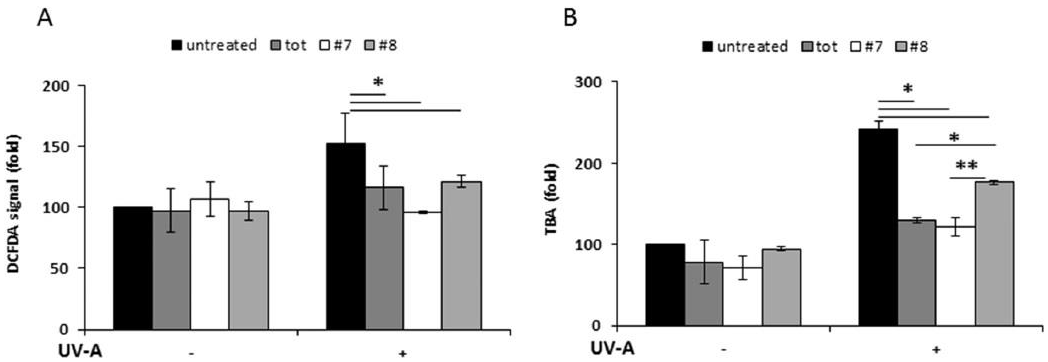

Fig. 8. ROS production and lipid peroxidation in UV-A-treated BALB/3T3 fibroblasts in the presence of açai fractions. Cells were pre-incubated with açai extract (dark grey bars), fraction 7 (white bars) and fraction 8 (light grey bars) for 2h and then irradiated by UV-A (100 J/cm^2). A, intracellular ROS levels; B, lipid peroxidation levels. Values are expressed as fold increase with respect to control (i.e. untreated) cells. Data shown are the means ± S.D. of three independent experiments. * indicates $p < 0.01$; ** indicates $p < 0.05$.

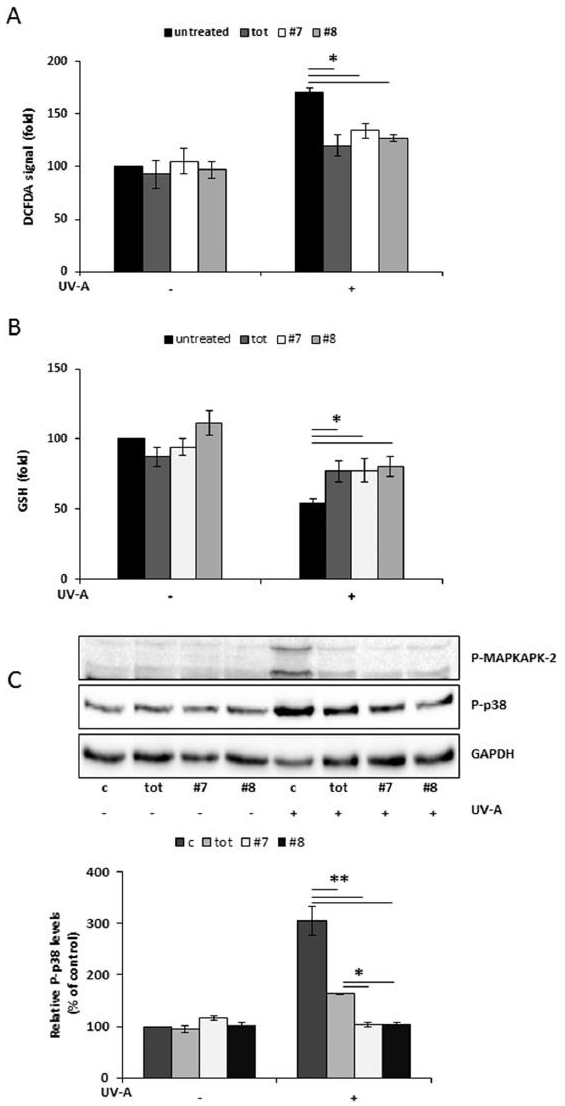

Fig. 9. Analysis of oxidative stress in BALB/3T3 fibroblasts incubated in the presence of açai fractions after UV-A treatment. Cells were irradiated by UV-A (100 J/cm^2) and then incubated with açai extract, fraction 7 or fraction 8 for 2h. A, intracellular ROS levels; B, intracellular GSH levels; C, Western blotting of the phosphorylation levels of p38 and MAPKAPK-2, with the relative densitometric analysis. GAPDH was used as internal standard. In all panels, untreated cells (named c in western blotting analysis) are represented by black bars, cells incubated with açai extract by dark grey bars, with fraction 7 by white bars and with fraction 8 by light grey bars. Values are expressed as fold increase with respect to control (i.e. untreated) cells. Data shown are the means ± S.D. of three independent experiments. * indicates $p < 0.05$; ** indicates $p < 0.01$.

extract can be considered as a good and safe candidate for dietary intervention in the prevention of age related diseases, since the use of anthocyanins as food additives (indicated as "E163") has been already approved in the European Union, Australia, and New Zealand [62].

Author contribution

G.P. and D.M.M. conceived, performed and analyzed cell biology experiments; A.R. and M.M.R. performed in vitro experiments; R.D.G. performed spectrophluorimetric experiments; A.A and A.I. conceived, performed and analyzed the HPLC and MS experiments; R.P. analyzed and discussed the data; D.M.M. wrote the paper with the contribution of all the authors.

Conflict of interest

The authors declare no competing financial interest.

Acknowledgement

The authors thank Dr. Carla Damiano for the work done during her master thesis.

References

[1] R. Thanan, S. Oikawa, Y. Hiraku, S. Ohnishi, N. Ma, S. Pinlaor, et al., Oxidative stress and its significant roles in neurodegenerative diseases and cancer, Int. J. Mol. Sci. 16 (2014) 193–217.
[2] D.R. Bickers, M. Athar, Oxidative stress in the pathogenesis of skin disease, J. Invest. Dermatol. 126 (2006) 2565–2575.
[3] S. Briganti, M. Picardo, Antioxidant activity, lipid peroxidation and skin diseases. What's new, J. Eur. Acad. Dermatol. Venereol. 17 (2003) 663–669.
[4] J. Cadet, R. Teoule, Comparative study of oxidation of nucleic acid components by hydroxyl radicals, singlet oxygen and superoxide anion radicals, Photochem. Photobiol. 28 (1978) 661–665.
[5] J.L. Ravanat, C. Saint-Pierre, P. Di Mascio, G.R. Martinez, M.H.G. Medeiros, J. Cadet, Damage to isolated DNA mediated by singlet oxygen, Helv. Chim. Acta 84 (2001) 3702–3709.
[6] T. Douki, A. Reynaud-Angelin, J. Cadet, E. Sage, Bipyrimidine photoproducts rather than oxidative lesions are the main type of DNA damage, Biochemistry 42 (2003) 9221–9226.
[7] S. Raha, B.H. Robinson, Mitochondria, oxygen free radicals, disease and ageing, Trends Biochem. Sci. 25 (2000) 502–508.
[8] L.A. Pham-Huy, H. He, C. Pham-Huy, Free radicals, antioxidants in disease and health, Int. J. Biomed. Sci. 4 (2008) 89.
[9] L. Gil del Valle, Oxidative stress in aging: theoretical outcomes and clinical evidences in humans, Biomed. Aging Pathol. 1 (2011) 1–7.
[10] A. Scalbert, I.T. Johnson, M. Saltmarsh, Polyphenols: antioxidants and beyond, Am. J. Clin. Nutr. 81 (2005) 215S–217S.
[11] B.E. van Wyk, M. Wink, Phytomedicines, Herbal Drugs, and Poisons, first ed., (2015) (Chicago, IL).
[12] M. Wink, Modes of action of herbal medicines and plant secondary metabolites, Fortschr. Med. 2 (2015) 251–286.
[13] R. Del Giudice, G. Petruk, A. Raiola, A. Barone, D.M. Monti, M.M. Rigano, Carotenoids in fresh and processed tomato (*Solanum lycopersicum*) fruits protect cells from oxidative stress injury, J. Sci. Food Agric. 97 (2017) 1616–1623, http://dx.doi.org/10.1002/jsfa.7910.
[14] G. Petruk, A. Raiola, R. Del Giudice, A. Barone, L. Frusciante, M.M. Rigano, D.M. Monti, An ascorbic acid-enriched tomato genotype to fight UV-A-induced oxidative stress in normal human keratinocytes, J. Photochem. Photobiol. B 163 (2016) 284–289.
[15] H. Rogez, Açai: Preparo, Composicao e Melhoramento da Conservacao, first ed., EDUFPA, Brazil, 2000.
[16] M.S.M. Rufino, J. Perez-Jimenez, S. Arranz, R.E. Alves, E.S. de Brito, M.S. Oliveira, F. Saura-Calixto, Açai (*Euterpe oleracea*)'BRS Para': a tropical fruit source of antioxidant dietary fiber and high antioxidant capacity oil, Food Res. Int. 44 (2011) 2100–2106.
[17] J. Holderness, I.A. Schepetkin, B. Freedman, L.N. Kirpotina, M.T. Quinn, J.F. Hedges, M.A. Jutila, Polysaccharides isolated from Açai fruit induce innate immune responses, PLoS One 6 (2011) e17301.
[18] H. Peixoto, M. Roxo, S. Krstin, T. Röhrig, E. Richling, M. Wink, An Anthocyanin-rich extract of açai (*Euterpe precatoria Mart.*) increases stress resistance and retards aging-related markers in *Caenorhabditis elegans*, J. Agric. Food Chem. 64 (2016) 1283–1290.
[19] M.M. dos Santos Dias, H.S.D. Martino, G. Noratto, A. Roque-Andrade, P.C. Stringheta, S. Talcott, A.M. Ramos, S.U. Mertens-Talcott, Anti-inflammatory activity of polyphenolics from açai (*Euterpe oleracea Martius*) in intestinal myofibroblasts CCD-18Co cells, Food Funct. 6 (2015) 3249–3256.
[20] R. Lichtenthaler, R.B. Rodrigues, J.G.S. Maia, M. Papagiannopoulos, H. Fabricius, F. Marx, Total oxidant scavenging capacities of *Euterpe oleracea Mart.*(Açai) fruits, Int. J. Food Sci. Nutr. 56 (2005) 53–64.
[21] S.U. Mertens-Talcott, J. Rios, P. Jilma-Stohlawetz, L.A. Pacheco-Palencia, B. Meibohm, S.T. Talcott, H. Derendorf, Pharmacokinetics of anthocyanins and antioxidant effects after the consumption of anthocyanin-rich açai juice and pulp (*Euterpe oleracea Mart.*) in human healthy volunteers, J. Agric. Food Chem. 56 (2008) 7796–7802.
[22] J. Kang, C. Xie, Z. Li, S. Nagarajan, A.G. Schauss, T. Wu, X. Wu, Flavonoids from açai (*Euterpe oleracea Mart.*) pulp and their antioxidant and anti-inflammatory activities, Food Chem. 128 (2011) 152–157.
[23] J. Kang, K.M. Thakali, C. Xie, M. Kondo, Y. Tong, B. Ou, G. Jensen, M.B. Medina,

A.G. Schauss, X. Wu, Bioactivities of açai (*Euterpe precatoria Mart.*) fruit pulp, superior antioxidant and anti-inflammatory properties to *Euterpe oleracea Mart*, Food Chem. 133 (2012) 671–677.

[24] H.A. Favacho, B.R. Oliveira, K.C. Santos, B.J. Medeiros, P.J. Sousa, F.F. Perazzo, J.C.T. Carvalho, Anti-inflammatory and antinociceptive activities of *Euterpe oleracea Mart.*, Arecaceae, oil, Rev. Bras 21 (2011) 105–114.

[25] A.G. Schauss, X. Wu, R.L. Prior, B. Ou, D. Huang, J. Owens, A. Agarwal, G.S. Jensen, A.N. Hart, E. Shanbrom, Antioxidant capacity and other bioactivities of the freeze-dried Amazonian palm berry, *Euterpe oleracea Mart.* (açai), J. Agric. Food Chem. 54 (2006) 8604–8610.

[26] G.D. Noratto, G. Angel-Morales, S.T. Talcott, S.U. Mertens-Talcott, Polyphenolics from açai (*Euterpe oleracea Mart.*) and red muscadine grape (*Vitis rotundifolia*) protect human umbilical vascular Endothelial cells (HUVEC)from glucose and lipopolysaccharide (LPS)-induced inflammation and target micro RN A-126, J. Agric. Food Chem. 59 (2011) 7999–8012.

[27] G.D. Stoner, L.S. Wang, C. Seguin, C. Rocha, K. Stoner, S. Chiu, A.D. Kinghorn, Multiple berry types prevent N-nitrosomethylbenzylamine-induced esophageal cancer in rats, Pharm. Res. 27 (2010) 1138–1145.

[28] M. Oliveira de Souza, M. Silva, M.E. Silva, R. de Paula Oliveira, M.L. Pedrosa, Diet supplementation with açai (*Euterpe oleracea Mart.*) pulp improves biomarkers of oxidative stress and the serum lipid profile in rats, Nutrition 26 (2010) 804–810.

[29] J.F. Ferreira da Costa Guerra, C.L. Lopes de Brito Magalhaes, D.C. Costa, M.E. Silva, M.L. Pedrosa, Dietary açai modulates ROS production by neutrophils and gene expression of liver antioxidant enzymes in rats, J. Clin. Biochem. Nutr. 49 (2011) 188–194.

[30] M.M. Rigano, A. Raiola, G.C. Tenore, D.M. Monti, R. Del Giudice, L. Frusciante, A. Barone, Quantitative trait loci pyramiding can improve the nutritional potential of tomato (*Solanum lycopersicum*) fruits, J. Agric. Food Chem. 62 (2014) 11519–11527.

[31] V.L. Singleton, J.A. Rossi, Colorimetry of total phenolics with phosphomolybdic-phosphotungstic acid reagents, Am. J. Enol. Vitic. 16 (1965) 144–158.

[32] D. Marinova, F. Ribarova, M. Atanassova, Total phenolics and total flavonoids in bulagrian fruits and vegetables, J. Univ. Chem. Technol. Metall. 40 (2005) 255–260.

[33] A. Raiola, R. Del Giudice, D.M. Monti, G.C. Tenore, A. Barone, M.M. Rigano, Bioactive compound content and cytotoxic effect on human cancer cells of fresh and processed yellow tomatoes, Molecules 21 (2016) 33.

[34] J.N. Miller, C.A. Rice-Evans, Factors influencing the antioxidant activity determined by the $ABTS^{\bullet+}$ radical cation assay, Free Radic. Res. 26 (1997) 195–199.

[35] R. Del Giudice, A. Raiola, G.C. Tenore, L. Frusciante, A. Barone, D.M. Monti, M.M. Rigano, Antioxidant bioactive compounds in tomato fruits at different ripening stages and their effects on normal and cancer cells, J. Funct. Foods 18 (2015) 83–94.

[36] D.M. Monti, D. Guarnieri, G. Napolitano, R. Piccoli, P. Netti, S. Fusco, A. Arciello, Biocompatibility, uptake and endocytosis pathways of polystyrene nanoparticles in primary human renal epithelial cells, J. Biotechnol. 10 (2015) 3–10.

[37] E. Galano, A. Arciello, R. Piccoli, D.M. Monti, A. Amoresano, A proteomic approach to investigate the effects of cadmium and lead on human primary renal cells, Metallomics 6 (2014) 587–597.

[38] L.O. Klotz, C. Pellieux, K. Briviba, C. Pierlot, J.M. Aubry, H. Sies, Mitogen-activated protein kinase (p38-, JNK-, ERK-) activation pattern induced by extracellular and intracellular singlet oxygen and UV-A, Eur. J. Biochem. 260 (1999) 917–922.

[39] W.R. Swindell, Heat shock proteins in long-lived worms and mice with insulin/insulin-like signaling mutations, Aging 1 (2009) 573.

[40] A. Strayer, Z. Wu, Y. Christen, C.D. Link, Y. Luo, Expression of the small heat-shock protein Hsp16 − 2 in Caenorhabditiselegans is suppressed by *Ginkgo biloba* extract EGb 761, FASEB J. 17 (2003) 2305–2307.

[41] R. Flamini, Mass spectrometry in grape and wine chemistry. Part I: polyphenols, Mass Spectrom. Rev. 22 (2003) 218–250.

[42] D. Kulms, T. Schwarz, Molecular mechanisms of UV-induced apoptosis, Photodermatol. Photoimmunol. Photomed. 16 (2000) 195–201.

[43] Y.-C. Hseu, C.W. Chou, K.J. Senthil Kumar, K.T. Fu, H.M. Wang, L.S. Hsu, Y.H. Kuo, C.R. Wu, S.C. Chen, H.L. Yang, Ellagic acid protects human keratinocyte (HaCaT) cells against UV-A-induced oxidative stress and apoptosis through the upregulation of the HO-1 and Nrf-2 antioxidant genes, Food Chem. Toxicol. 50 (2012) 1245–1255.

[44] Y.-C. Hseu, H.W. Lo, M. Korivi, Y.C. Tsai, M.J. Tang, H.L. Yang, Dermato-protective properties of ergothioneine through induction of Nrf2/ARE-mediated antioxidant genes in UV-A-irradiated human keratinocytes, Free Radic. Biol. Med. 86 (2015) 102–117.

[45] I.F. Almeida, A.S. Pinto, C. Monteiro, H. Monteiro, L. Belo, J. Fernandes, A.R. Bento, T.L. Duarte, J. Garrido, M.F. Bahia, J.M. Sousa Lobo, P.C. Costa, Protective effect of *C. sativa* leaf extract against UV mediated-DNA damage in a human keratinocyte cell line, J. Photochem. Photobiol. B 144 (2015) 28–34.

[46] A.G.V. Costa, D.F. Garcia-Diaz, P. Jimenez, P.I. Silva, Bioactive compounds and health benefits of exotic tropical red–black berries, J. Funct. Foods 5 (2013) 539–549.

[47] A.M. Amorini, G. Fazzina, G. Lazzarino, B. Tavazzi, D. Di Pierro, R. Santucci, F. Sinibaldi, F. Galvano, G. Galvano, Activity and mechanism of the antioxidant properties of cyanidin-3-O-βglucopyranoside, Free Radic. Res. 35 (2001) 953–966.

[48] H. Guo, M. Xia, T. Zou, W. Ling, R. Zhong, W. Zhang, Cyanidin 3-glucoside attenuates obesity-associated insulin resistance and hepatic steatosis in high-fat diet-fed and db/db mice via the transcription factor FoxO1, J. Nutr. Biochem. 23 (2012) 349–360.

[49] U. Matern, B. Grimmig, Polyphenols in plant pathology, Polyphenolic Phenomena. Paris: INRA Editions, 1993, pp. 143–147.

[50] E. Bognar, Z. Sarszegi, A. Szabo, B. Debreceni, N. Kalman, Z. Tucsek, B. Sumegi, F. GallyasJr, Antioxidant and anti-inflammatory effects in RAW264. 7 macrophages of malvidin, a major red wine polyphenol, PLoS One 8 (2013) e65355.

[51] R. Pop, M.N. Stefanut, A. Cata, C. Tanasie, M. Medeleanu, Ab initio study regarding the evaluation of the antioxidant character of cyanidin, delphinidin and malvidin, Cent. Eur. J. Chem. 10 (2012) 180–186.

[52] N. Matsunaga, S. Imai, Y. Inokuchi, M. Shimazawa, S. Yokota, Y. Araki, H. Hara, Bilberry and its main constituents have neuroprotective effects against retinal neuronal damage *in vitro* and *in vivo*, Mol. Nutr. Food Res. 53 (2009) 869–877.

[53] W. Huang, Y. Zhu, C. Li, Z. Sui, W. Min, Effect of blueberry *Anthocyanins Malvidin* and glycosides on the antioxidant properties in endothelial cells, Oxidative Med. Cell. Longev. (2016), http://dx.doi.org/10.1155/2016/1591803.

[54] H.R. Seo, M.J. Choi, J.M. Choi, J.C. Ko, J.Y. Ko, E.J. Cho, Malvidin protects WI-38 human fibroblast cells against stress-induced premature senescence, Eur. J. Cancer Prev. 21 (2016) 32–40.

[55] J.W. Hyun, H.S. Chung, Cyanidin and malvidin from *Oryza sativa* cv. Heugjinjubyeo mediate cytotoxicity against human monocytic leukemia cells by arrest of G2/M phase and induction of apoptosis, J. Agric. Food Chem. 52 (2004) 2213–2217.

[56] P.H. Shih, C.T. Yeh, G.C. Yen, Effects of anthocyanidin on the inhibition of proliferation and induction of apoptosis in human gastric adenocarcinoma cells, Food Chem. Toxicol. 43 (2005) 1557–1566.

[57] S.J. Patterson, J.G. Fischer, R.V. Dulebohn, DNA damage in HT-29 colon cancer cells is enhanced by high concentrations of the anthocyanin malvidin, FASEB J. 22 (2008) 890–900.

[58] W. Li, Y. Guo, C. Zhang, R. Wu, A.Y. Yang, J. Gaspar, A.N. Kong, Dietary phytochemicals and cancer chemoprevention: a perspective on oxidative stress, inflammation, and epigenetics, Chem. Res. Toxicol. 29 (2016) 2071–2095.

[59] H.S.D. Martino, M.M. dos Santos Dias, G. Noratto, S. Talcott, S.U. Mertens-Talcott, Anti-lipidaemic and anti-inflammatory effect of açai (*Euterpe oleracea Martius*) polyphenols on 3T3-L1 adipocytes, J. Funct. Foods 23 (2016) 432–443.

[60] P.O. Barbosa, D. Pala, C.T. Silva, M.O. de Souza, J.F. do Amaral, R.A.L. Vieira, G.A. Folly, A.C. Volp, R.N. de Freitas, Açai (*Euterpe oleracea* Mart.) pulp dietary intake improves cellular antioxidant enzymes and biomarkers of serum in healthy women, Nutrition 32 (2016) 674–680.

[61] D. Pala, P.O. Barbosa, C.T. Silva, M.O. de Souza, F.R. Freitas, A.C. Volp, R.C. Maranhão, R.N. Freitas, Açai (*Euterpe oleracea Mart.*) dietary intake affects plasma lipids, apolipoproteins, cholesteryl ester transfer to high-density lipoprotein and redox metabolism: a prospective study in women, Clin. Nutr. (2017), http://dx.doi.org/10.1016/j.clnu.2017.02.001.

[62] C.K. Singh, I.A. Siddiqui, S. El-Abd, H. Mukhtar, N. Ahmad, Combination chemoprevention with grape antioxidants, Mol. Nutr. Food Res. 60 (2016) 1406–1415.

CHAPTER 4

Characterization of the antioxidant activity of piscidic and eucomic acids from Opuntia ficus-indica L.cladodes

https://www.shutterstock.com

The prickly pear cactus (Opuntia ficus-indica) is an important nutrient and food source. Different plants of Opuntia produce edible fruits.
In addition, leaves and fruits of Opuntia are often used in traditional medicine for their benefic effects against arteriosclerosis, diabetes, gastritis, and hyperglycemia.[1].

[1]Aragona, M., Lauriano, E. R., Pergolizzi, S., & Faggio, C. (2017). Opuntia ficus-indica (L.) Miller as a source of bioactivity compounds for health and nutrition. *Natural Product Research*, 1-13.

Bioorganic & Medicinal Chemistry Letters 27 (2017) 5485–5489

Contents lists available at ScienceDirect

Bioorganic & Medicinal Chemistry Letters

journal homepage: www.elsevier.com/locate/bmcl

Protective effect of *Opuntia ficus-indica* L. cladodes against UVA-induced oxidative stress in normal human keratinocytes

Ganna Petruk [a,d], Flaviana Di Lorenzo [a,d], Paola Imbimbo [a], Alba Silipo [a], Andrea Bonina [b], Luisa Rizza [b], Renata Piccoli [a,c], Daria Maria Monti [a,c,*], Rosa Lanzetta [a,*]

[a] Department of Chemical Sciences, University of Naples Federico II, Complesso Universitario Monte Sant'Angelo, via Cinthia 4, 80126 Naples, Italy
[b] Bionap srl, R&D Contrada Fureria, ZIO 950125 Piano Tavola, Belpasso, Italy
[c] Istituto Nazionale di Biostrutture e Biosistemi (INBB), Rome, Italy

ARTICLE INFO

Article history:
Received 3 July 2017
Revised 5 October 2017
Accepted 19 October 2017
Available online 20 October 2017

Keywords:
Opuntia ficus-indica L.
Cladode water extracts
Antioxidants
UVA-induced oxidative stress
Eucomic acid
Piscidic acid

ABSTRACT

Opuntia ficus-indica L. is known for its beneficial effects on human health, but still little is known on cladodes as a potent source of antioxidants. Here, a direct, economic and safe method was set up to obtain water extracts from *Opuntia ficus-indica* cladodes rich in antioxidant compounds. When human keratinocytes were pre-treated with the extract before being exposed to UVA radiations, a clear protective effect against UVA-induced stress was evidenced, as indicated by the inhibition of stress-induced processes, such as free radicals production, lipid peroxidation and GSH depletion. Moreover, a clear protective effect against apoptosis in pre-treated irradiated cells was evidenced. We found that eucomic and piscidic acids were responsible for the anti-oxidative stress action of cladode extract. In conclusion, a bioactive, safe, low-cost and high value-added extract from *Opuntia* cladodes was obtained to be used for skin health/protection.

Natural products are receiving a great deal of interest by scientists and pharmacologists for their use in the prevention of oxidative stress-related pathologies, which include obesity, atherosclerosis, diabetes, cancer, neurodegenerative diseases, and aging.[1]

Opuntia is widely distributed in Mexico and in all American hemispheres, as well as in Africa and in the Mediterranean basin.[2] Among all the species, *Opuntia ficus-indica* (referred to here on as *Opuntia*) is the most widely distributed. The multiplicity of health-promoting properties of *Opuntia* are well known. Indeed, in traditional medicine it has been recognized as a source of prebiotics and phytochemicals.[3] Most of the studies report the protective effect of fruits and stems; for example, extracts from *Opuntia ficus-indica* var. *saboten* have been reported to protect against neuronal damage produced under oxidant conditions,[4] or against renal and hepatic alterations caused by mycotoxins.[5] On the other side, only few studies have been performed on the antioxidant, anti-inflammatory, wound healing, hypoglycemic and antimicrobial activities of *Opuntia* cladodes.[6,7] Lee and colleagues showed that an ethanol extract of cladodes decreased the oxidation of linoleic acid and DNA.[8] Recently, Avila demonstrated an increased antioxidant activity in plasma and blood in subjects consuming cladodes (300 g/day for 3 days).[9]

Given these premises, and taking into account the high annual productivity of biomass per hectare (10–40 tones dry weight), it is undeniable that *Opuntia* cladodes represent an economic and suitable substrate for isolation of antioxidants. However, it has to be considered that all the above studies have a common drawback, namely the use of organic solvents to extract bioactive compounds. Indeed, it was previously demonstrated that the extraction procedure, as well as the extraction solvent, notably affect the yield of natural products, their content as well as their antioxidant

Abbreviations: ABTS, 2,2-azinobis(3-ethylbenzothiazoline-6-sulfonic acid); CASP-3, caspase-3; CASP-7, caspase-7; DCF, 2′,7′-dichlorofluorescein; DTNB, 5,5′-dithiobis-2-nitrobenzoic acid; HAA, hydrophilic antioxidant activity; H_2-DCFDA, 2′,7′-dichlorodihydrofluorescein diacetate; MTT, 3-(4,5-dimethylthiazol-2-yl)-2,5-diphenyltetrazolium bromide; ORE, *Opuntia* raw extract; OSMF, *Opuntia* small molecular weight fraction; P-p38, phosphorylated p38 MAP kinase; P-MAPKAPK-2, phosphorylated MAP kinase-activated protein kinase; ROS, reactive oxygen species; SPF, sun protection factor; TEAC, Trolox equivalent antioxidant capacity; TBA, thiobarbituric acid; TBARS, TBA reactive substances; TNB, 5-thio-2-nitrobenzoic acid.

* Corresponding authors at: Department of Chemical Sciences, University of Naples Federico II, Complesso Universitario Monte Sant'Angelo, via Cinthia 4, 80126 Naples, Italy (R. Lanzetta, D.M. Monti).
E-mail addresses: mdmonti@unina.it (D.M. Monti), lanzetta@unina.it (R. Lanzetta).
[d] These authors contributed equally to the paper.

https://doi.org/10.1016/j.bmcl.2017.10.043
0960-894X/

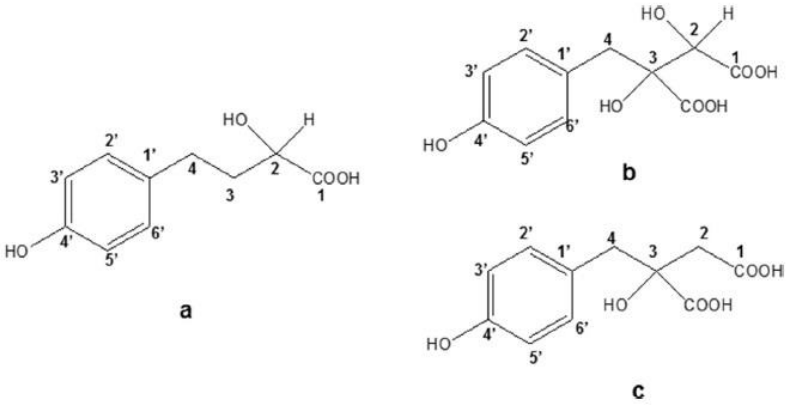

Fig. 1. Structure of 2-hydroxy-4-(4′-hydroxyphenyl)-butanoic acid (a) found in OSMF C, and of piscidic (b) and eucomic (c) acids found in OSMF D.

activity.[10] Furthermore, the use of organic solvents has elevated costs with the risk of contamination of the extract by solvent residues.

We previously reported that *Opuntia* extracts can be obtained by simple mechanical press and that the *Opuntia* raw extract (ORE) was constituted by two main components: i) a high molecular weight constituent consisting in two polysaccharide entities: a linear β-(1→4)-galactose polymer and a highly branched xyloarabinan; ii) a low molecular weight component consisting in lactic acid, D-mannitol and three phenolic derivatives, i.e. piscidic, eucomic and 2-hydroxy-4-(4′-hydroxyphenyl)-butanoic acids (Fig. 1).[6]

Phenolic compounds are used in several applications due to their proved antioxidant and potentially health-promoting properties.[11–13] Importantly, the chemical structure of phenolic compounds, in terms of their reducing properties as electron or hydrogen-donating agents, determines their potential for action as antioxidants.[14]

In this context, we investigated whether ORE is able to protect human keratinocytes against UVA-induced oxidative stress. UVA radiations are known to increase reactive oxygen species (ROS) production, thus causing oxidative damage of proteins, lipids and nucleic acids. These damages result in different detrimental effects on the skin, such as inflammation, premature aging and development of cancer.[15,16] Keratinocytes are essential components of skin and connective tissue, normally present in the outermost layer of the skin.[17] This prompted us to select cultured human keratinocytes (HaCaT cell line) as an excellent experimental model to test the protective role of *Opuntia* extracts against UVA radiations.

We first tested the *in vitro* antioxidant activity of the whole ORE and of each isolated fraction (OSMF A-D), obtained following the procedure described in Di Lorenzo et al.[6] and reported in Supplementary material.

By the ABTS colorimetric assay, we found that ORE is endowed with a significant antioxidant activity, as a low IC_{50} value was obtained (0.52 ± 0.01 mg/mL). Fraction OSMF A, namely the lactic acid component,[6] showed the highest IC_{50} value (1.4 ± 0.01 mg/mL), in agreement with findings obtained in a different experimental system by Lampe, who reported that lactic acid is able to scavenge free radicals.[18] The IC_{50} values of OSMF C (namely 2-hydroxy-4-(4′-hydroxyphenyl)butanoic acid, Fig. 1a) and D (namely piscidic and eucomic acids, Fig. 1b and c, respectively)[6] were found to be much lower (0.09 ± 0.02 and 0.03 ± 0.01, respectively) than those obtained for the whole extract and for OSMF B (D-mannitol,[6]) (IC_{50} = 0.79 ± 0.37 mg/mL). These results were confirmed by the TEAC (Trolox equivalent antioxidant capacity) test, from which much higher TEAC values were obtained for OSMF C and D, with respect to OSMF A and B, indicating a high content in antioxidants in the former two fractions (Table 1).

Table 1
Opuntia raw extract (ORE) and its fractions (OSMF A-D) were tested for their *in vitro* antioxidant properties. The antioxidant activity is expressed as the concentration required to scavenge 50% of free radical $ABTS^{\bullet+}$ (IC_{50}), Trolox equivalent antioxidant capacity (TEAC), and the ability to counteract UV radiations, expressed as sun protecting factor (SPF). Values are normalized to the concentration of each sample.

Sample	IC_{50} (mg/mL)	TEAC (μM/mg)	SPF
ORE	0.52 ± 0.01	43.2 ± 4.53	2.25 ± 0.5
OSMF A	1.4 ± 0.01	10.6 ± 3.39	1.4 ± 0.1
OSMF B	0.79 ± 0.37	24.08 ± 0.34	0.94 ± 0.11
OSMF C	0.09 ± 0.02	225.79 ± 15.85	0.2 ± 0.01
OSMF D	0.03 ± 0.01	749.65 ± 11.81	2.23 ± 0.41

We also tested the UV-protective properties of ORE and its OSMF fractions by measuring their sun protection factor (SPF) *in vitro*, according to a spectrophotometric method.[19] As shown in Table 1, while OSMF B and C did not show any significant protective effect, a value of about 2 was obtained when ORE or OSMF D

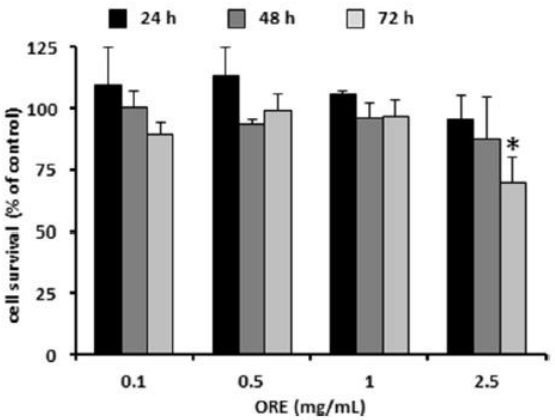

Fig. 2. Effect of ORE on the viability of human keratinocytes. Dose-response curve of HaCaT cells after 24 h (black bars), 48 h (dark grey bars) and 72 h (light grey bars) incubation in the presence of increasing concentrations of ORE. Cell viability was assessed by the MTT assay; the cell survival percentage was defined as described in Supplementary material. Values are given as means ± S.D. ($n \geq 3$). * indicates $p < 0.05$ with respect to untreated cells.

was tested; this value has been reported to correspond to 50% UV blockage. Therefore, these samples can be considered as having good sunscreen activity.[20] OSMF A showed an *in vitro* SPF of 1.4, in agreement with the results obtained by Kornhauser, who reported that lactic acid is commonly used in cosmetics for the improvement of photoaged skin.[21]

The biocompatibility of ORE on HaCaT cells was tested by performing a dose-response experiment, in which cells were exposed for different lengths of time to the extract within the range 0.1–2.5 mg/mL. We found that cell viability was not affected up to 1 mg/mL, even after 72 h incubation ($p > 0.05$) (Fig. 2), while after 72 h, at the highest concentration tested (2.5 mg/mL), about 30% cell death was observed. On the basis of these results and on previously reported data,[6] further experiments were carried out at 1 mg/mL ORE concentration.

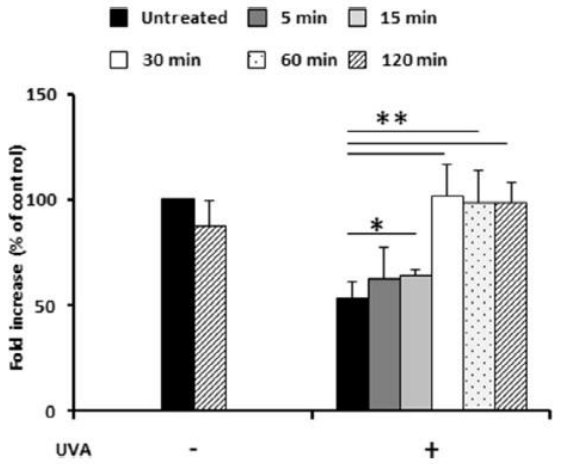

Fig. 3. GSH levels in HaCaT cells irradiated by UVA in the presence of ORE. Cells were pre-incubated in the presence of 1 mg/mL ORE (grey bars) for different lengths of time, irradiated by UVA (100 J/cm^2) and intracellular GSH levels determined by DTNB assay. Control cells, black bars; cells pre-treated with ORE are indicated by: dark grey bars (5 min of pre-incubation), light grey bars (15 min of pre-incubation), white bars (30 min of pre-incubation), spotted bars (60 min of pre-incubation) and dashed bars (120 min of pre-incubation). Values are expressed as fold increase with respect to control (i.e. untreated) cells. Data shown are the means ± S.D. of three independent experiments. * indicates $p < 0.05$; ** indicates $p < 0.001$.

To test if ORE was able to protect keratinocytes from oxidative stress, we performed a time course experiment in which cells were pre-treated with ORE (1 mg/mL) for different lengths of time (from 5 min to 2 h) before inducing oxidative stress by UVA irradiation (100 J/cm^2). Immediately after irradiation, intracellular GSH was evaluated by the DTNB assay (Fig. 3). As expected, UVA treatment significantly decreased intracellular GSH when compared to the non-irradiated samples (50% decrease), whereas ORE had no effect on intracellular GSH level. Interestingly, a pretreatment of cells with ORE, prior to UVA exposure, resulted in an inhibition of GSH oxidation in a time-dependent manner. In particular, we found that ORE was able to protect cells from GSH depletion after just 30 min incubation, and no difference was observed up to 2 h incubation. The efficacy of ORE at 1 mg/mL well correlates with the *in vitro* antioxidant assay (IC_{50} 0.52 mg/mL).

In order to identify the low molecular weight fraction from *Opuntia* extract responsible for the antioxidant activity of the whole extract, each fraction was tested by DTNB and DCFDA assays. For a direct comparison between the whole extract and its fractions, a suitable volume of each fraction was tested to reach the concentration of the single component in the whole extract tested at 1 mg/mL.[6] As shown in Fig. 4A, when cells were pre-incubated either with ORE or with the isolated fractions prior to be irradiated, ORE (dashed bars) and OSMF D (dotted bars) were found to be able to contrast the detrimental effects of UVA irradiation on GSH (GSH depletion), whereas the other fractions had no protective effect. In the absence of irradiation, instead, no effect on the intracellular GSH level was observed for any fraction. These results were also confirmed by the DCFDA assay (Fig. 4B), which showed no alteration in the redox state upon treatment with *Opuntia* samples. On the other hand, a significant increase in ROS production was observed when keratinocytes were irradiated by UVA (4-fold increase). Interestingly, the alteration in the redox state was fully counteracted when cells were pre-incubated either with ORE (dashed bars) or with OSMF D (dotted bars) prior to UVA

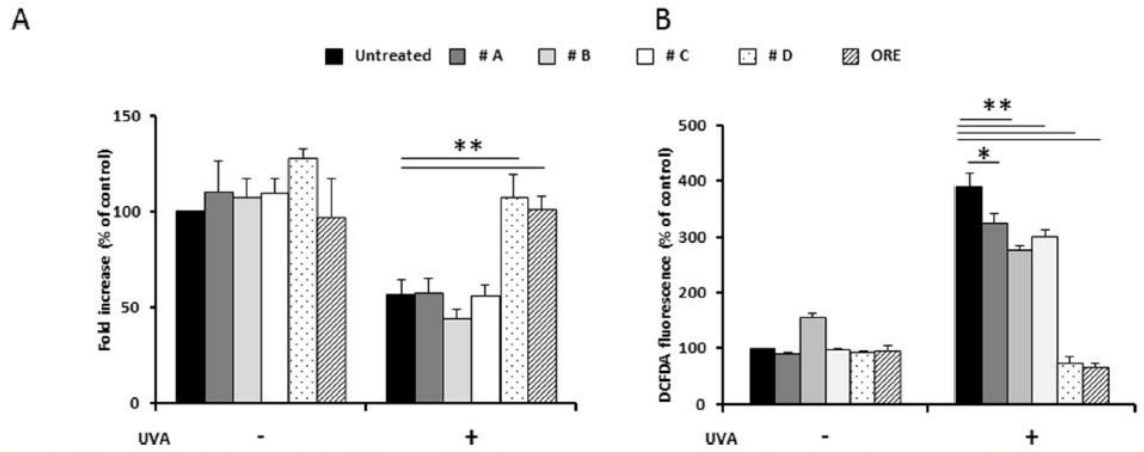

Fig. 4. GSH oxidation and ROS production in HaCaT cells irradiated by UVA in the presence of ORE and isolated fractions. A-B, Cells were pre-incubated in the presence of ORE (1 mg/mL) or equivalent amount of each *Opuntia* fraction for 30 min and then irradiated by UVA (100 J/cm^2). A, changes in intracellular GSH levels of cells before (–) and after (+) UVA treatment; B, intracellular ROS levels determined by DCFDA assay. Black bars, untreated cells; dark grey bars, fraction A (OSMF A, # A); light grey bars, fraction B (OSMF B, # B); white bars, fraction C (OSMF C, # C); spotted bars, fraction D (OSMF D, # D); dashed bars, ORE. Values are expressed as fold increase with respect to control (i.e. untreated) cells. Data shown are the means ± S.D. of three independent experiments. * indicates $p < 0.01$, ** indicates $p < 0.001$.

irradiation. A small, although significant, protective effect was observed with the other fractions. The slight antioxidant activity of lactic acid (present in OSMF A) is in line with Lampe and colleagues who found that lactic acid was effective in counteracting free radicals produced by a photoinitiator, but no effect was observed in the presence of hydrogen peroxide radicals, which are more reactive and able to enter the cell.[18] As for OSMF C, it is well known that the antioxidant activity of a phenolic compound must be related to the amount, position and number of the hydroxyl groups in the molecule.[22] In this context, piscidic and eucomic acids are richer in hydroxyl groups than 2-hydroxy-4-(4-hydroxyphenyl)-butanoic acid, the component of OSMF C (Fig. 1).

Based on these results, ORE and OSMF D were used to deeply analyze their antioxidant protective effect.

To this purpose, measurement of lipid peroxidation levels was performed (Fig. 5A).

We found that UVA treatment significantly increased lipid peroxidation levels when compared to a non-irradiated sample.

Noteworthy, a strong protective effect was observed when cells were pre-treated with ORE or OSMF D, since both values were comparable to those obtained in the absence of any treatment.

This result is in line with those obtained by Hfaiedh, who studied the effects of a water *Opuntia* extract in counteracting the negative effects of $NiCl_2$ in rats.[23]

The protective effect of ORE and OSMF D was further confirmed by Western blot experiments, in which the phosphorylation levels of p38 and its direct target, MAPKAPK-2, were analyzed (Fig. 5B). These proteins are directly involved in signaling stress pathways induced by UVA.[24,25] When cells were UVA irradiated, we observed a significant increase in the phosphorylation levels of the analyzed markers (Fig. 5B-C). On the contrary, when cells were exposed to ORE or OSMF D prior to UVA treatment, the phosphorylation levels of p38 and MAPKAPK-2 were similar to those observed in non-irradiated cells. These results are in agreement with those obtained by Zourgui and colleagues in mice using an ethanol:water extract.[5]

Furthermore, we verified whether ORE and OSMF D were able to protect cells against UVA-induced cell death. As shown in Fig. 6, a cell treatment with ORE did not induce apoptosis, since no cleavage of caspase-3 or caspase-7 was observed, while, as expected, upon UVA exposure, the activation of caspase-3 and -7 was remarkably increased, as indicated by the presence of the cleaved form of both proteins (Fig. 6, third lane). These results

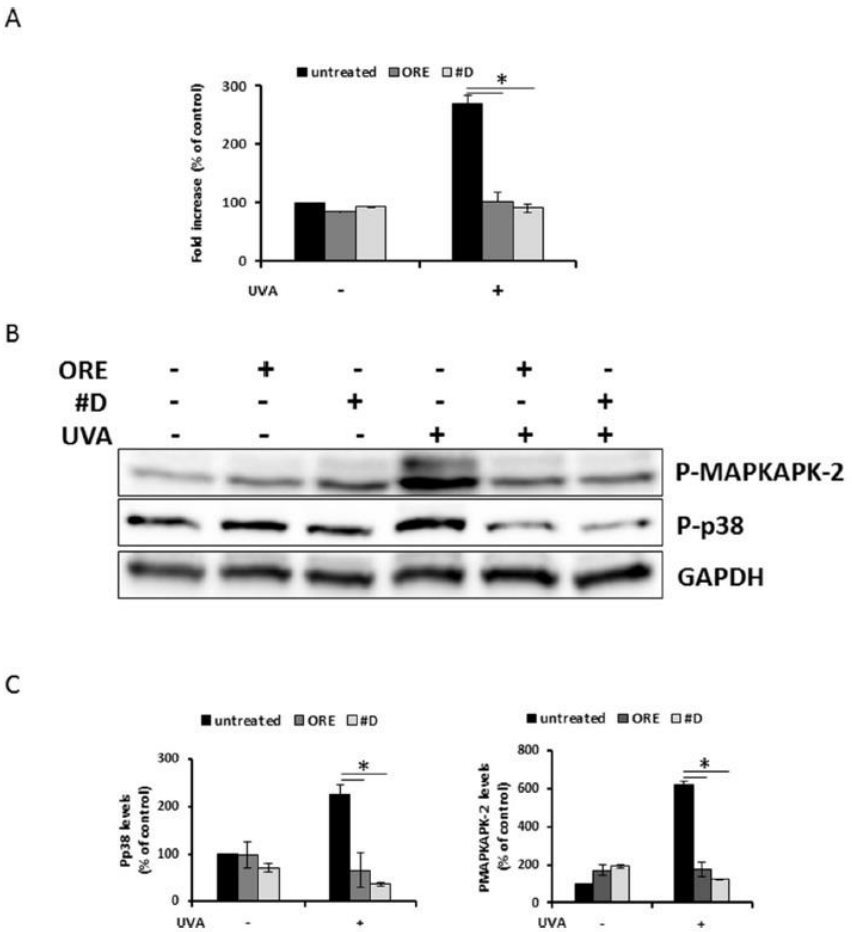

Fig. 5. Effect of ORE extract and OSMF D on UVA-induced oxidative stress markers in human keratinocytes. Cells were incubated with 1 mg/mL ORE or 0.15 mg/mL OSMF D for 30 min prior to UVA irradiation (100 J/cm^2) and then incubated for 90 min. A, lipid peroxidation levels determined by TBARS assay; B, Western blots. In Western blots the phosphorylation level of P-p38 and P-MAPKAPK-2 is reported, with the relative densitometric analysis (C) in the absence (black bars) or in the presence of ORE (dark grey bars) or OSMF D (light grey bars). GAPDH was used as internal standard. Data shown are the means ± S.D. of three independent experiments. * indicates $p < .005$.

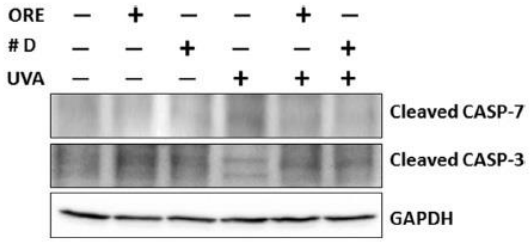

Fig. 6. ORE extract and OSMF D protect HaCaT cells from UVA-induced apoptosis. Cells were incubated with 1 mg/mL ORE or 0.15 mg/mL OSMF D for 30 min, irradiated with UVA (100 J/cm^2) and then grown for 24 h. Western blots were performed using anti-caspase-3 and -7, which recognize the activated forms of the proteins. GAPDH was used as loading control.

are in agreement with those reported by others, who demonstrated that many epidermal skin cells, including keratinocytes, undergo apoptosis following UVA exposure as a result of DNA strand breaks.[24,26] When, instead, keratinocytes were pre-incubated in the presence of ORE or OSMF D, and then exposed to UVA, no caspase-3 and -7 activation was observed, thus indicating a protective role of piscidic and eucomic acids from UVA-induced cellular stress.

The beneficial properties of *Opuntia* mucilage in producing a physical barrier on the cutis, favoring cutaneous reparative processes, is historically well known. Nowadays, given the enormous potential benefits on health of natural bioactive compounds isolated from *Opuntia* cladode extracts, intensive investigation is ongoing attracting the interest of food scientists and clinical pharmacologists. Some of the beneficial effects of *Opuntia* extracts have been attributed to fibers and polyphenols isolated from cladodes. However, all the studies published so far have been performed on extracts treated with organic solvents, which may not be completely removed with a potential danger for human health.

Here, we report the discover of an additional and intriguing beneficial property of water extracts from cladodes, i.e. a protective effect against UVA-induced oxidative stress and apoptosis, which has never been investigated so far. Altogether, our results demonstrate that ORE water extract has strong antioxidant properties, being able to counteract the negative effects induced in human keratinocytes by UVA radiations, and to protect cells from this common and pernicious source of stress. We demonstrated that the anti-stress effect of cladode extracts has to be ascribed to eucomic and piscidic acids, as these phenolic compounds are the sole components of fraction OSMF D, which fully retains the antioxidant activity of the whole extract. As widely known, the antioxidant potency of phenolic acids strongly depends on their structural features. Indeed, it has been demonstrated that the main structural characteristic responsible for the antioxidant activity of phenol derivatives is the number and location of the hydroxyl groups present in the molecule.[27] Two main mechanisms by which antioxidants can play their protective role have been proposed. Due to the presence of such hydroxy functions, phenols are able to easily donate hydrogen atoms to the free radicals thus blocking the chain propagation step occurring in the oxidation process (H-atom-transfer mechanisms).[14,28] Alternatively, the antioxidant can give an electron to the free radical becoming itself a radical cation (single-electron-transfer mechanisms). In addition, deprotonated carboxyl groups behave as electron-donating groups thus favoring the hydrogen atom transfer and electron-donating based radical scavenging.[29] Therefore, the potent antioxidant effect observed for both the piscidic and eucomic acids is clearly reflected in their structural features which promote the hydrogen atoms transfer to free radicals. The slight structural differences, as example, between the piscidic and the 2-hydroxy-4-(4′-hydroxyphenyl)-butanoic acid, namely the absence, in the latter, of one hydroxyl and one carboxyl group, could be reflected in the lower antioxidative power observed for OSMF C.

In our opinion the present study, shedding light on bioactive compounds responsible for *Opuntia* cladode antioxidant activity, represents an important step towards the therapeutic values of *Opuntia* properties.

It is important to underline that aqueous *Opuntia* antioxidant extracts can be obtained by simple mechanical press of cladodes, thus avoiding the use of expensive materials and of organic solvents, responsible for environmental pollution and persistence of residues dangerous for human health. Therefore, we obtained a bioactive, safe, low-cost and high value-added extract to be used in pharmaceutical and/or cosmetics applications for skin health/protection.

Conflict of interest

The authors declare no competing financial interest.

A. Supplementary data

Supplementary data associated with this article can be found, in the online version, at https://doi.org/10.1016/j.bmcl.2017.10.043.

References

1. Basaga H. *Biochem Cell Biol*. 1990;68:989–998.
2. Zorgui L, Ayed-Boussema I, Ayed Y, Bacha H, Hassen W. *Food Chem Toxicol*. 2009;47:662–667.
3. Coria Cayupán YS, Ochoa MJ, Nazareno MA. *Food Chem*. 2011;126:514–519.
4. Dok-Go H, Lee KH, Kim HJ, et al. *Brain Res*. 2003;965:130–136.
5. Zourgui L, Golli EEEI, Bouaziz C, Bacha H, Hassen W. *Food Chem Toxicol*. 2008;46:1817–1824.
6. Di Lorenzo F, Silipo A, Molinaro A, et al. *Carbohydr Polym*. 2017;157:128–136.
7. El-Mostafa K, El Kharrassi Y, Badreddine A, et al. *Molecules*. 2014;19:14879–14901.
8. Lee JC, Kim HR, Kim J, Jang YS. *J Agric Food Chem*. 2002;50:6490–6496.
9. Avila-Nava A, Calderón-Oliver M, Medina-Campos ON, et al. *J Funct Foods*. 2014;10:13–24.
10. Ammar I, Ennouri M, Attia H. *Ind Crops Prod*. 2015;64:97–104.
11. Kähkönen MP, Hopia AI, Vuorela HJ, et al. *J Agric Food Chem*. 1999;3954–3962.
12. Rice-Evans CA, Miller NJ, Paganga G. *Free Radic Biol Med*. 1996;20:933–956.
13. Dai J, Mumper RJ. *Molecules*. 2010;15:7313–7352.
14. Rice-Evans CA, Miller NJ, Paganga G. *Trends Plant Sci*. 1997;2:152–159.
15. Kulms D, Schwarz T. *Photodermatol Photoimmunol Photomed*. 2000;16:195–201.
16. Hseu YC, Chou CW, Senthil Kumar KJ, et al. *Food Chem Toxicol*. 2012;50:1245–1255.
17. Camera E, Mastrofrancesco A, Fabbri C, et al. *Exp Dermatol*. 2009;18:222–231.
18. Lampe KJ, Namba RM, Silverman TR, Bjugstad KB. *Biotechnol Bioeng*. 2009;103:1214–1223.
19. Mansur JS, Breder MNR, Mansur MCA, Azulay RD. *An Bras Dermatol, Rio Janeiro*. 1986;61:121–124.
20. Kale S, Gaikwad M, Bhandare S. *Int J Res Pharm Biomed Sci*. 2011;2:1220–1224.
21. Kornhauser A, Coelho SG, Hearing VJ. *Clin Cosmet Investig Dermatol*. 2010;3:135–142.
22. Biskup I, Golonka I, Gamian A, Sroka Z. *Postep Hig Med Dosw*. 2013;67:958–963.
23. Hfaiedh N, Allagui MS, Hfaiedh M, Feki AEl, Zourgui L, Croute F. *Food Chem Toxicol*. 2008;46:3759–3763.
24. Petruk G, Raiola A, Del Giudice R, et al. *Photochem Photobiol B Biol*. 2016;163:284–289.
25. Klotz L, Pellieux C, Briviba K, Pierlot C. *Eur J Biochem*. 1999;260:917–922.
26. Ichihashi M, Ueda M, Budiyanto A, et al. *Toxicology*. 2003;189:21–39.
27. Bendary E, Francis RR, Ali HMG, Sarwat MI, El Hady S. *Ann Agric Sci*. 2013;58:173–181.
28. Wright JS, Johnson ER, DiLabio GA. *J Am Chem Soc*. 2001;123:1173–1183.
29. Velika B, Kron I. *Free Radicals Antioxidants*. 2012;2:62–67.

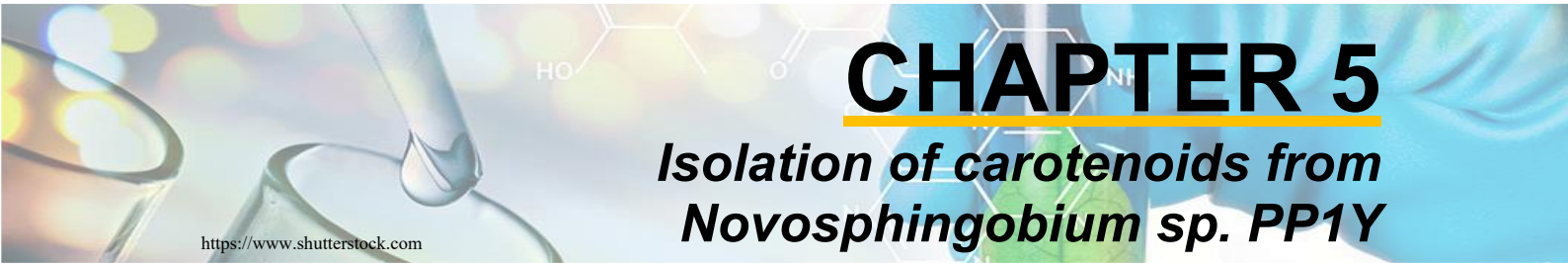

CHAPTER 5

Isolation of carotenoids from Novosphingobium sp. PP1Y

Novosphingobium puteolanum PP1Y *strain was isolated from sea water contaminated by aromatic compounds. To survive in such a high hostile environment, this bacterium has developed strategies to prevent oxidation.*[1]

[1]Notomista, E., Pennacchio, F., Cafaro, V., Smaldone, G., Izzo, V., Troncone, L., ... & Di Donato, A. (2011). The marine isolate Novosphingobium sp. PP1Y shows specific adaptation to use the aromatic fraction of fuels as the sole carbon and energy source. *Microbial ecology*, *61*(3), 582-594.

5.1 Introduction

It is well known that fruits, vegetables, grains, teas, wines, and some kinds of spices are natural sources of antioxidants[1]. But, in the last few years, the studies of possible new sources of antioxidants have become important, given that cosmetic and food industries require mostly antioxidants with natural origins and with higher power to counteract stress injury.

Marine animals are characterized by containing many polyunsaturated fatty acids, which are more susceptible to oxidation. The susceptibility of fatty acids to oxidation is thought to be directly dependent on their degree of unsaturation[2]. Therefore, in order to survive in a constantly stressed environment these organisms must have some “extraordinary” preventers of oxidation[3].

In 2011, a novel bacterial strain has been isolated and partially characterized, named *Novosphingobium puteolanum* PP1Y (herein indicated as PP1Y)[4,5]. The microorganism was isolated from the surface part of sea in Pozzuoli. This is a small dock bay in the harbor of which the storage of small boats is used and it is characterized by a severe pollution of the water by aromatic hydrocarbons. This microorganism shows the peculiar characteristic to be able to grow on a wide range of mono-and polycyclic aromatic substrates (i. e. pyrene, naphthalene and phenanthrene) and on complex mixtures of aromatic molecules dissolved in non-polar phases (such as diesel and gasoline). Despite these xenobiotic agents represent the sole source of carbon and energy for PP1Y, they are also, through redox cycling, inductors of the production of reactive oxygen species (ROS) in the organism[6]. Their over-production hereby leads to oxidative damage to DNA, proteins and lipids[1]. Therefore, PP1Y must to have an excellent reactive oxygen removal system to maintain cell homeostasis.

Notomista and colleagues observed that PP1Y colonies, during growth on solid rich mediums (LB-Agar) had a very light yellow color[4,] which in nature is normally due to the presence of pigments, such as carotenoids[7]. Moreover, UV-vis spectrum of the yellow pigment produced by *Novosphingobium puteolanum* PP1Y was found to be identical to that of nostoxanthin reported in literature[4]. This is not surprisingly, given that PP1Y belong to the family of *Sphingomonadales*, and it is know that several members of this family produce carotenoids. In addition, nostoxanthin is one of the most frequently found in this group of bacteria[8,9].

From a biotechnological and economical point of view, which are not be underestimated, the production of carotenoids by using microorganisms is very convenient and provide an alternative to chemical synthesis, responding to the market demand for natural antioxidants[7,10,11].

Here, the antioxidant activity and protective effect of a lipophilic extract, obtained from PP1Y, was tested. Benefic effect of this extract was studied *in vitro* (on epithelial colorectal adenocarcinoma cells) and *in vivo* (on *Caenorhabditis elegans*).

The nematode *C. elegans* has been proven to be a powerful invertebrate model organism to study many biological processes, including aging[12,13]. The fact that *C. elegans* lifespan is short, allows researchers to study the effects of different molecules over time. Moreover, as the genome of this worm is completely sequenced, it is possible to identify the molecular pathway involved in the pathology studied. Moreover, it is also possible to silence/modify different genes to confirm the involvement of a specific protein in response to drug treatment[14]. In addition, this organism offers other several advantages, such as low cost, straightforward maintenance and its transparency, which allows microscopy analyses without dissection[12].

In particular, in our study, the expression of stress response genes, such as sod-3::GFP and hsp- 16.2::GFP were analysed, as well as the determination of transcription factors involved in the activation of stress response.

5.2 Materials and methods

5.2.1 PP1Y cultivation and extract preparation

Novosphingobium sp. PP1Y microorganism was grown as described by De Lise et al.[15]. Briefly, a pre-inoculum in LB was grown at 30 °C over night under orbital shaking at 7000 *g* and then used to inoculate 1 L of Potassium Phosphate Minimal Medium (PPMM) and were maintained at 30 °C for other 28 h under orbital shaking. Then, cells were centrifuged at 5,524 *g* for 15 min at 4 °C and suspended in 2 mL of absolute methanol at a final concentration of 200 OD_{600nm}/mL. Cells were then disrupted by sonication (12 min, 30 sec ON and 30 sec OFF, on ice). The mixture was incubated to macerate at 4 °C over night under orbital shaking at 7000 *g*. Subsequently, the lysate was centrifuged at 22,100 *g* for 10 min at 4 °C and the soluble fraction was recovered and stored at 4 °C, whereas the pellet was processed again as described above. At the end, both soluble fractions were combined and dried by rotovapor (R-210, Buchi), and dissolved in 1 mL of dimethyl sulfoxide (DMSO).

5.2.2 Cell culture and analysis of cell viability

Human normal keratinocytes (HaCaT) and epithelial colorectal adenocarcinoma cells (LoVo and Caco-2) were from ATCC. Cells were cultured in Dulbecco's Modified Eagle's Medium (Sigma-Aldrich, St Louis, Mo, USA), supplemented with 10% foetal bovine serum (HyClone), 2 mM L-glutamine and antibiotics, all from Sigma-Aldrich, in a 5% CO_2 humidified atmosphere at 37 ºC. Every 48 h cells were sub-cultured in a ratio 1:5 for HaCaT and Caco-2 cells and 1:3 for LoVo cells. Briefly, the culture medium was removed and cells were rinsed with PBS and then detached with trypsin-EDTA. After centrifugation (5 min at 1000 *g*) cells were diluted in fresh complete growth medium.

Cells were seeded in 96-well plates (100 µL/well) at a density of 6 x 10^3/cm^2 for HaCaT cells and 9 x 10^3/cm^2 for other two cell lines. For dose-dependent cytotoxicity assays, 24 h after seeding, increasing volumes of PP1Y (0.1 to 1%, v/v) were added to the cells and cells were incubated for 24-48 h. Cell viability was assessed by the MTT (3-(4,5-dimethylthiazol-2-yl)-2,5-diphenyltetrazolium bromide) assay, as previously described[16].

5.2.3 C. elegans strains and culture conditions

Nematode strains were obtained from the Caenorhabditis Genetic Center (CGC). All C. elegans strains were cultured on solid nematode growth media (NGM) plates fed with living Escherichia coli OP50 and maintained at 20 °C in a temperature-controlled incubator. Prior to each assay eggs were isolated to obtain age synchronized cultures and kept in M9 buffer (3 g KH_2PO_4, 6 g Na_2HPO_4, 5 g NaCl, 1 mL 1 M $MgSO_4$, H_2O to 1 L) for hatching, as previously described[17].

5.2.4 Brood size

Synchronized N2 worms at L4 stage were sorted and placed one by one on individual NGM agar plates. In the treatment group, the bacterial lawn was supplemented with PP1Y extract (0.1% v/v). 100 µg/mL of epigallocatechin gallate (EGCG) (Sigma-Aldrich GmbH, Steinheim, Germany) was used as positive control,

whereas DMSO was used to verify that buffer was not responsible for side effects. Adult worms were transferred daily to fresh medium to separate them from their progeny. Eggs were counted every day for 5 days using a dissecting microscope. The results are presented as mean brood size.

5.2.5 C. elegans survival assay under oxidative stress

24 h after bleaching, N2 wild-type worms in L1 larval stage, were pre-treated with PP1Y extract (0.1% v/v) and maintained 48 h at 20 ºC. EGCG and DMSO were used as indicated above. In the adult stage, worms were transferred to fresh media and grouped in populations of approximately 80 individuals and treated with 80 µM juglone (5-hydroxy-1,4-naphthalenedione)[18]. After 24 h, dead and live worms were counted. The worms were scored dead when they did not respond to a gentle touch stimulus. The results are expressed as percentage of living worms.

5.2.6 Intracellular ROS accumulation in *C. elegans*

Synchronized N2 worms at L1 larval stage were pre-treated with PP1Y extract (0.1% v/v) and maintained 48 h at 20 ºC. EGCG and DMSO were used as indicated above. At the end of the treatment, worms were washed with M9 buffer and then incubated with 50 µM H_2DCFDA solution for 1 h at 20 °C. Worms were then mounted on a glass slide with a drop of 10 mM sodium azide (used to paralyze them) and photographed by the BIOREVO BZ-9000 fluorescent microscope (Keyence Deutschland 200 GmbH, Neu-Isenburg, Germany) equipped with a mercury lamp. Images were taken for at least 30 worms at constant exposure time (λ Ex 480/20 nm; λ Em 510/38 nm) using a 10 X objective lens. The relative fluorescence of the whole body was determined densitometrically by using ImageJ software 6.01. The results are expressed as percentage of fluorescence intensity of the worms under test compared to untreated worms.

5.2.7 Quantification of *hsp*-16.2::GFP and *sod*-3::GFP expression

The expression of *hsp*-16.2::GFP construct was quantified in the strain TJ375. Worms at larval stage L1 were pre-treated with PP1Y extract (0.1% v/v) and maintained 72 h at 20 °C. EGCG (50 µg/mL) and DMSO were used as indicated above. Then, worms were exposed to 20 µM juglone for 24 h and analyzed as described above.

The expression of *sod*-3::GFP construct was quantified in the strain CF1553. The worms at larval stage L1 were pre-treated with PP1Y extract (0.1% v/v) and maintained 72 h at 20 ºC. EGCG (100 µg/mL) was used as positive control, whereas DMSO was used as negative control. After treatment, the worms were analysed as described above.

5.2.8 Quantification of *DAF-16::GFP* and *SKN-1::GFP* localization

The nematode worms of transgenic strain TJ356 or LD1 at larval stage L1 were pre-treated with PP1Y extract (0.1% v/v) and maintained 24 h at 20 ºC and analyzed as described above. EGCG and DMSO were used as indicated above.

5.2.9 Analysis of oxidative stress in LoVo cells

To analyze oxidative stress LoVo cells were plated at a density of 2 x 10^4 cells/cm^2. 24 h after seeding, cells were incubated for 120 min with 0.1% of PP1Y extract, or equivalent amount of each isolated fraction. Then, 300 µM sodium arsenite (SA) was added to the cells and co-incubated for 45 min at 37 °C.

Changes in intracellular ROS levels in LoVo cells were determined by measuring the oxidative conversion of cell permeable 2′,7′-dichlorofluorescein diacetate (H_2-DCFDA, Sigma-Aldrich) to fluorescent dichlorofluorescein (DCF). In particular, the protocol described by Del Giudice and colleagues was used[19].

To estimate intracellular glutathione levels, a procedure previously described was followed[20].

LoVo cells were plated at a density of 9 x 10^4 cells/cm^2 in complete medium for 24 h and then treated as described above. After induction of oxidative stress, SA was removed and PP1Y extract added again to the cell culture for 90 min at 37 °C. Then, cell lysates were analysed by Western blotting performed as reported[21].

5.2.10 HPLC

Samples were analyzed using an HPLC system equipped with a Waters 1525 binary pump coupled to a Waters photodiode array detector. Samples were separated using a Waters symmetry C18 (4.6 x 7.5 mm) column. Separation was carried out at a flow rate of 1 mL/min by using a two solvent system consisting of water (solvent A) and methanol (solvent B). Compounds were separated using a 5 minutes isocratic eluition with 10% solvent B, followed by an initial 3 minutes linear gradient from 10% to 30% of solvent B, and then a 12 minutes linear gradient from 30% to 90% of solvent B and an isocratic 5 minutes step at 90% of solvent B.

5.2.11 Statistical analyses

The results are presented as mean of results obtained after at least three independent experiments (mean ± SEM or SD) and compared by t-test, one- or two-way ANOVA following Bonferroni's method (posthoc) using Graphpad Prism for windows, Version 6.01.

5.3 Results and discussion

5.3.1 Biocompatibility of PP1Y extract

PP1Y extract was tested on different human cells in order to evaluate its biocompatibility. One normal cell line, human keratinocytes (HaCaT), and two epithelial colorectal adenocarcinoma cells (Caco-2 and LoVo) were incubated with increasing amount of PP1Y extract (0.1-1%, v/v) for 24, 48 and 72 h. We found that cell viability was not affected at 0.1% of the extract after 24 and 48 h incubation, whereas a decrease in cell viability was observed at higher concentrations, even though we did not observe a dose-dependent toxicity (**Figure 1A-C**).

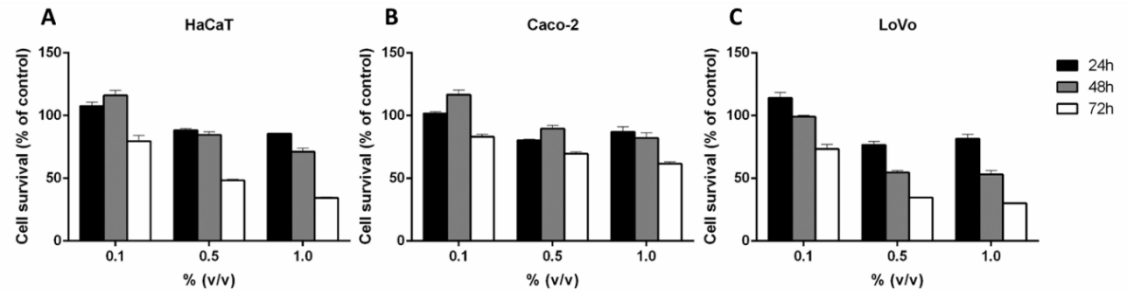

Figure 1: Effect of PP1Y on the viability of human cells. Dose-response curve of HaCaT (**A**), Caco-2 (**B**) and LoVo (**C**) cells after 24 h (black bars), 48 h (dark grey bars) and 72 h (light grey bars) incubation in the presence of increasing concentrations of PP1Y. Cell viability was assessed by the MTT assay; the cell survival percentage was defined as described in the Materials and Methods section. Values are given as means ± SEM (n ≥ 3).

Thus, we tested the biocompatibility of 0.1% PP1Y extract *in vivo*, i.e. using *C. elegans*. This nematode is normally used to understand the effects of antioxidants and their mechanism of action, as the worms are easy to cultivate, have a rapid life cycle and a well-established genetic pathway[18,22]. Moreover, they have many pathways in common with humans, thus representing a model organism[18,23].

We analyzed the variation of brood size, widely accepted as a toxicity marker 21 and found no significant effect on the fertility rate of PP1Y treated and untreated worms (176 ± 6 and 169 ± 7, respectively, p>0.5).

5.3.2 PP1Y extract inhibits oxidative stress in *C. elegans*

We then evaluated if PP1Y extract could act as antioxidant on an *in vivo* system, by protecting worms from oxidative stress induced by a lethal dose of 5-hydroxy-1,4-naphthalenedione (juglone). This molecule is widely used *in vivo* as an inducer of oxidative stress[25].

Wild-type (N2) worms were pretreated with 0.1% (v/v) PP1Y extract for 48 h and then transferred to new medium and exposed to a lethal dose of juglone (80 µM) for 24 h, after which the alive worms were counted. We found that the pretreatment of the N2 worms with PP1Y extract is indeed able to protect the organism against lethal oxidative stress (**Figure 2A**, white bar). The average of surviving worms after treatment with 80 µM juglone was 23 ± 2% and for the group pretreated with PP1Y for 48 h was 40 ± 2% (the increase rate was about 70%, p < 0.01). EGCG (100 µg/mL) was used as a positive control (**Figure 2A**, light grey bar).

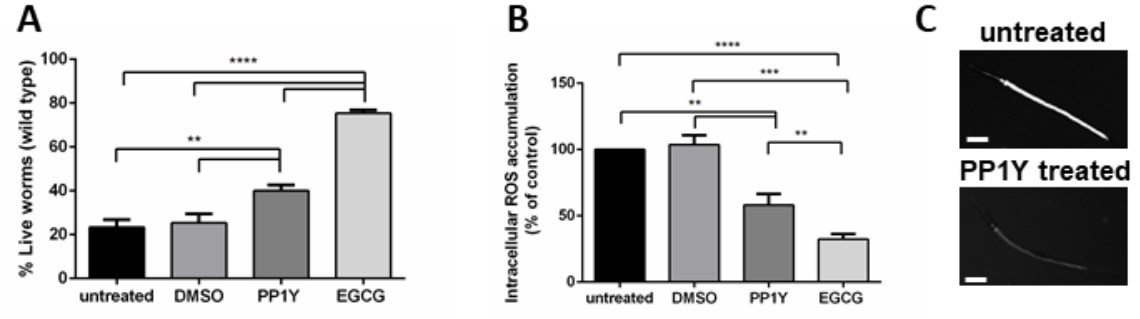

Figure 2: Protective effect of PP1Y extract against oxidative stress in C. elegans. A, N2 worms were incubated in the presence of 0.1 % (v/v) PP1Y extract (white bar) after juglone (80 µM) induced oxidative stress. The survival rate of wild type N2 worms is reported. Data are presented as mean ± SD (n=40, replicated at least 3 times). Buffer control is represented by DMSO (dark grey bar) and positive control is represented by EGCG (100 µM, light grey bar). **B-C**, Effect of PP1Y on intracellular ROS accumulation in N2 strain. Worms were incubated with 0.1 % (v/v) PP1Y extract (white bar) for 48 h. At the end of the experiment, intracellular ROS were measured by DCFDA. Data are presented as mean pixel intensity in percentage with respect to the control (represented by untreated worms, black bar and DMSO-treated worms, dark grey bar), (mean ± SD, n=40, replicated at least 3 times). **C**, Representative images of DCF fluorescence in untreated worms and in worms treated with the extract. Images were taken with BZ9000 from Keyence, scale bar = 100 µm. ** indicates p<0.005, *** indicates p<0.001, **** p< 0.0001.

We also found that PP1Y extract was able to counteract intracellular endogenous ROS accumulation. N2 worms were incubated with the extract for 48 h and then ROS levels were analyzed. As reported in **Figure 2B-C**, a significant lower fluorescence intensity was observed in nematodes treated with PP1Y extract (42% decrease, p<0.01) with respect to untreated control groups (represented by untreated and DMSO-treated worms).

The antioxidant activity was further confirmed by analyzing *hsp*-16.2 expression, which belong to the small heat shock proteins family, normally activated in the presence of oxidative stress. The TJ375 strain has a GFP reporter controlled by the *hsp*-16.2 promoter that is not active under standard conditions[26]. Following oxidative stress exposure, *hsp*-16.2 expression is induced, and worms exhibit an extensive GFP expression in the pharynx. When PP1Y extract was incubated with worms (72 h) before treatment with a non-lethal amount of juglone (20 µM, 24 h), *hsp*-16.2 expression was markedly inhibited with respect to juglone-treated worms. As shown in **Figure 3A**, a 52% decrease was observed with respect to the two control groups ($p<0.0001$). Surprisingly, no activation of *sod-3*, a protein usually activated by *daf*-16[27], was observed. In particular, we used CF1553 transgenic C. elegans strain, in which *sod*-3 is fused to GFP. After 72 h incubation with PP1Y extract, no increase in the fluorescence levels of *sod*-3 expression was observed between PP1Y treated worms and control-groups ($p>0.05$, **Figure 3B**).

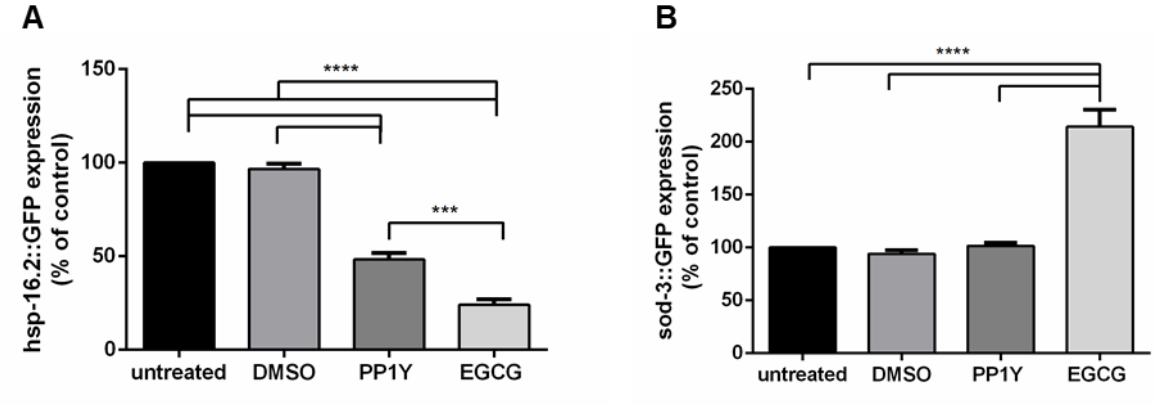

Figure 3: PP1Y extract protects worms from oxidative stress. **A**, TJ375 transgenic worms were incubated with 0.1 % DMSO (dark grey bar), 0.1 % PP1Y extract (white bar) or 50 µg/mL EGCG (light grey bar) for 72 h; then, 20 µM juglone was added to induce oxidative stress and worms were incubated for 24h. Head fluorescence was determined densitometrically by using ImageJ software and the hsp-16.2 expression was reported with respect to control worms. **B**, transgenic CF1553 worms were treated with 0.1% PP1Y extract for 72 h and then the expression of *sod-3*::GFP was evaluated. The relative fluorescence of the tails was determined densitometrically by using ImageJ software. In each panel, data are reported as mean ± SD, n=40, replicated at least 3 times.

5.3.3 P PP1Y extract protects worms from oxidative stress by *skn-1* pathway

To understand which mechanism of action was activated by PP1Y extract, experiments on transgenic worms (TJ356 and LD1) were performed. The TJ356 strain has *daf*-16 fused to GFP, whereas LD1 has *skn*-1 fused to YFP. Worms were treated with the extract for 24 h and then the translocation of each nuclear-transcription factor was analyzed. No nuclear translocation of *daf*-16 was observed in worms incubated with PP1Y extract (**Figure 4A**), whereas a slight (15 %) but significative ($p<0.005$) increase in *skn*-1 translocation was observed (**Figure 4B**). A totally different behavior was observed with EGCG, as already reported[28].

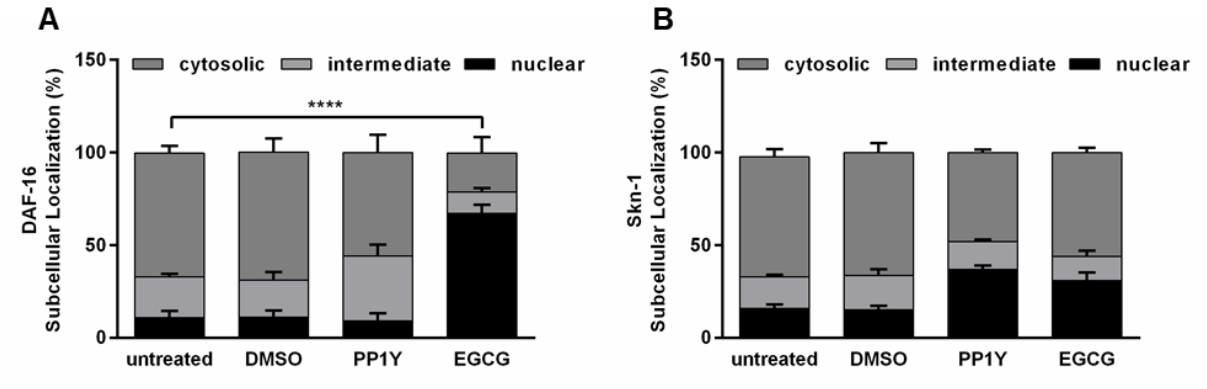

Figure 4. PP1Y extract protective effect is mediated by skn-1 pathway. TJ356 and LD1 transgenic worms were incubated as described above, but for 24 h and *daf-16* (**A**) or *skn-1* (**B**) localization was analyzed. The results are presented as percentage of worms exhibiting a protein sub-cellular localization pattern, namely cytosolic (dark grey bars), intermediate (light grey bars) and nuclear (black bars). In each panel, data are reported as mean ± SD, n=40, replicated at least 3 times

5.3.4 Antioxidant activity of PP1Y fractions

We then fractionated PP1Y extract by HPLC, and the profile is shown in **Appendix A** (**Figure S1**) was obtained. 5 HPLC fractions were collected, as reported in **Appendix A** (**Figure S1**), and their antioxidant activity was tested on LoVo cells by measuring the intracellular ROS and GSH levels in cells pretreated with each HPLC fraction, before and after SA treatment (**Figure 5A-B**). Cells were pre-treated with PP1Y extract (0.1%) or equivalent amount of each fraction for 120 min before inducing oxidative stress by SA treatment for 45 min. SA is a human carcinogen known to increase ROS production in human cells[29–31]. At the end of incubation, intracellular ROS levels were determined (**Figure 5A**). We found that no significant increase in ROS levels were observed when cells were pre-treated with PP1Y extract, whereas, as expected, a 100 % increase in ROS levels was observed in the presence of SA (**Figure 5A**, black bars). Moreover, we found that fraction 2 was the most effective in contrasting the detrimental effects of SA on ROS increase (light grey bars). Interestingly, when cells were incubated with the extract before inducing oxidative stress, no increase in ROS level was observed.

A similar behavior was observed when we analyzed the intracellular GSH levels in LoVo cells after SA-treatment (**Figure 5B**). Indeed, no GSH oxidation was observed after incubation with PP1Y extract and with fraction 2, but a significant increase in GSH level was observed after SA-treatment (80 and 71 % for PP1Y extract and fraction 2, respectively, with respect to stressed cells, $p<0.01$). Noteworthy, a small but significant effect of fraction 1 was observed (**Figure 5**, dark grey bars).

The protective effect was finally confirmed by Western blot experiments, in which the phosphorylation levels of p38 was analyzed (**Figure 5C**). It is known that, upon oxidative stress, this protein is phosphorylated[20]. When cells were stressed, we observed a significant increase in the phosphorylation levels of p38, whereas, when cells were exposed to PP1Y prior to stress, no alteration in the phosphorylation levels of p38 was observed.

Overall, these results indicate that PP1Y extract has a strong antioxidant activity both on human cells and in vivo since a protective effect against ROS production was observed on LoVo cells and in *C. elegans*.

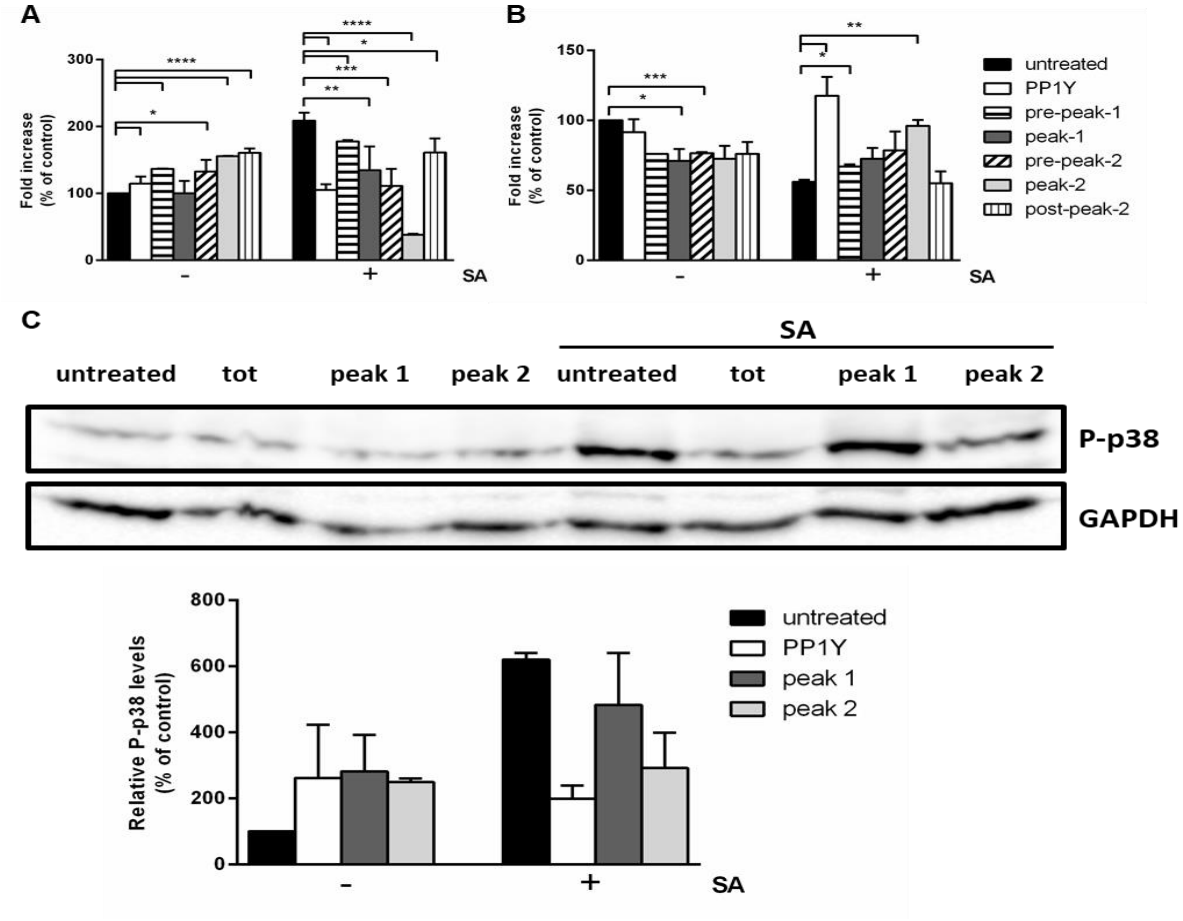

Figure 5: Analysis of the antioxidant activity of PP1Y extract and its fractions on LoVo cells after SA-induced oxidative stress. Cells were pre-incubated in the presence of 0.1 % PP1Y extract or equivalent amount of each fraction for 120 min and then cells were stressed by SA treatment (300 μM) for 45 min and intracellular ROS levels (**A**) and GSH levels (**B**) were determined. Untreated cells, black bars; cells pre-treated with: PP1Y extract, white bars; pre-peak-1, horizontal-line bars; peak 1, dark grey bars; pre-peak-2, diagonal-line bars; peak-2, light grey bars; post-peak-2, vertical-line bars. Values are expressed as fold increase with respect to control (i.e. untreated) cells. Data shown are the means ± S.D. of three independent experiments. * indicates $p<0.05$, ** indicates $p<0.01$, *** indicates $p<0.001$, **** indicates $p<0.0001$. **C**, Representative images of Western blots of cells incubated with PP1Y extract or the two HPLC peaks. Cells were treated as described above and, after SA-treatment, incubated for 90 min at 37 °C. In the Western blot, the phosphorylation level of P-p38 is reported. GAPDH was used as internal standard. Values are expressed as fold increase with respect to control (i.e. untreated) cells. Untreated cells, black bars; cells pre-treated with: PP1Y extract, white bars; peak 1, dark grey bars; peak-2, light grey bars. Data shown are the means ± S.D. of three independent experiments.

5.4 Conclusions

Novosphingobium puteolanum PP1Y, isolated from sea in Pozzuoli, is a member of *Sphingomonads*, which have been studied for their ability to degrade several aromatic compounds and to resist to oxidative stress induced by these xenobiotics. Here, taking advantages of the characteristics of PP1Y organism, we performed the extraction of active molecules from this bacterium. The data obtained demonstrated that cells and worms treated with the extracts were less sensitive to pro-oxidant agent. In the case of *C. elegans*, the resistance is conferred by the activation of Sk1 transcription factor. Moreover, we hypothesize that the benefic effect induced by PP1Y extract can be related to the presence of nosthoxantin, as the UV-vis

spectrum of the extract and of its active fraction have the same trend of the pure compound. Currently, to confirm our hypothesis the mass spectrometry analysis are underway.

From an economical point of view, this study suggest that PP1Y strain is a valid alternative to chemical synthesis, responding to the market demand for natural antioxidants.

5.5 References

1. Brewer, M. S. Natural antioxidants: Sources, compounds, mechanisms of action and potential applications. *Compr. Rev. Food Sci. Food Saf*. **10**, 221–247 (2011).

2. Richard, D., Kefi, K., Barbe, U., Bausero, P. & Visioli, F. Polyunsaturated fatty acids as antioxidants. *Pharmacol. Res.* **57**, 451–455 (2008).

3. Hermes-Lima, M. & Zenteno-Savín, T. Animal response to drastic changes in oxygen availability and physiological oxidative stress. *Comparative Biochemistry and Physiology - C Toxicology and Pharmacology* **133**, 537–556 (2002).

4. Notomista, E. … Di Donato, A. The marine isolate *Novosphingobium* sp. PP1Y shows specific adaptation to use the aromatic fraction of fuels as the sole carbon and energy source. *Microb. Ecol.* **61**, 582–594 (2011).

5. D'Argenio, V. … Di Donato, A. Complete sequencing of *Novosphingobium* sp. PP1Y reveals a biotechnologically meaningful metabolic pattern. *BMC Genomics* **15**, 384 (2014).

6. Valavanidis, A., Vlahogianni, T., Dassenakis, M. & Scoullos, M. Molecular biomarkers of oxidative stress in aquatic organisms in relation to toxic environmental pollutants. *Ecotoxicol. Environ. Saf.* **64**, 178–189 (2006).

7. Kaiser, P., Surmann, P., Vallentin, G. & Fuhrmann, H. A small-scale method for quantitation of carotenoids in bacteria and yeasts. *J. Microbiol. Methods* **70**, 142–149 (2007).

8. Davison, A. D. … Altavilla, N. *Sphingomonas paucimobilis* BPSI-3 mutant AN2 produces a red catabolite during biphenyl degradation. *J. Ind. Microbiol. Biotechnol.* **23**, 314–319 (1999).

9. Than, R. The pigment of *Pseudomonas paucimobitis* is a carotenoid. *Curr. Microbiol.* **3**, 4–7 (1979).

10. Misawa, N. & Shimada, H. Metabolic engineering for the production of carotenoids in non-carotenogenic bacteria and yeasts. *J. Biotechnol.* **59**, 169–181 (1998).

11. Sandmann, G. Combinatorial biosynthesis of carotenoids in a heterologous host: A powerful approach for the biosynthesis of novel structures. *ChemBioChem* **3**, 629–635 (2002).

12. Labuschagne, C. F. & Brenkman, A. B. Current methods in quantifying ROS and oxidative damage in *Caenorhabditis elegans* and other model organism of aging. *Ageing Res. Rev.* **12**, 918–930 (2013).

13. Antoshechkin, I. & Sternberg, P. W. The versatile worm: Genetic and genomic resources for *Caenorhabditis elegans* research. *Nat. Rev. Genet.* **8**, 518–532 (2007).

14. Waterston, R. Genome sequence of the nematode *C.elegans*: a platform for investigating biology (1998). Genome sequence of the nematode *C. elegans*: a platform for investigating biology. The *C. elegans* Sequencing Consortium. *Science (80-.)*. **282**, 2012–2018 (1998).

15. De Lise, F. … Izzo, V. RHA-P: Isolation, expression and characterization of a bacterial α-L-rhamnosidase from *Novosphingobium* sp. PP1Y. *J. Mol. Catal. B Enzym.* **134**, 136–147 (2016).

16. Monti, D. M. D. M. … Arciello, A. Biocompatibility, uptake and endocytosis pathways of polystyrene nanoparticles in primary human renal epithelial cells. *J. Biotechnol.* **193**, 3–10 (2015).

17. Stiernagle, T. Maintenance of *C. elegans*. *WormBook* (2006). doi:10.1895/wormbook.1.101.1

18. Abbas, S. & Wink, M. Green tea extract induces the resistance of *Caenorhabditis elegans* against oxidative stress. *Antioxidants* **3**, 129–43 (2014).

19. Del Giudice, R. … Rigano, M. M. Carotenoids in fresh and processed tomato (*Solanum lycopersicum*) fruits protect cells from oxidative stress injury. *J. Sci. Food Agric.* **97**, 1616-1623 (2016).

20. Petruk, G. … Monti, D. M. D. M. An ascorbic acid-enriched tomato genotype to fight UVA-induced oxidative stress in normal human keratinocytes. *J. Photochem. Photobiol. B Biol.* **163**, 284–289 (2016).

21. Galano, E., Arciello, A., Piccoli, R., Monti, D. M. D. M. & Amoresano, A. A proteomic approach to investigate the effects of cadmium and lead on human primary renal cells. *Metallomics* **6**, 587–97 (2014).

22. Brenner, S. The genetics of *Caenorhabditis elegans*. *Genetics* **77**, 71–94 (1974).

23. Kaletta, T. & Hengartner, M. Finding function in novel targets: *C. elegans* as a model organism. *Nat. Rev. Drug Discov.* **5**, 387 (2006).

24. Bischof, L., Huffman, D. & Aroian, R. Assays for toxicity studies in *C. elegans* with Bt crystal proteins. *C. elegans Methods Appl*. 139–154 (2006).

25. Dues, D. J. … Van Raamsdonk, J. M. Uncoupling of oxidative stress resistance and lifespan in long-lived isp-1 mitochondrial mutants in *Caenorhabditis elegans. Free Radic. Biol. Med.* **108**, 362–373 (2017).

26. Al-Amin, M., Kawasaki, I., Gong, J. & Shim, Y. Caffeine induces the stress response and up-regulates heat shock proteins in *Caenorhabditis elegans. Mol. Cells* **39**, 163 (2016).

27. Piazzesi, A., Papić, D., Bertan, F., Salomoni, P. & Nicotera, P. Replication-independent histone variant H3. 3 controls animal lifespan through the regulation of pro-longevity transcriptional programs. *Cell Rep.* **17**, 987–996 (2016).

28. Wang, E. & Wink, M. Chlorophyll enhances oxidative stress tolerance in *Caenorhabditis elegans* and extends its lifespan. *PeerJ* **4**, e1879 (2016).

29. Ruiz-Ramos, R., Lopez-Carrillo, L., Rios-Perez, A. D., De Vizcaya-Ruiz, A. & Cebrian, M. E. Sodium arsenite induces ROS generation, DNA oxidative damage, HO-1 and c-Myc proteins, NF-kappaB activation and cell proliferation in human breast cancer MCF-7 cells. *Mutat. Res.* **674**, 109–115 (2009).

30. Zhang, Z. … Shi, X. Reactive oxygen species mediate arsenic induced cell transformation and tumorigenesis through Wnt/beta-catenin pathway in human colorectal adenocarcinoma DLD1 cells. *Toxicol. Appl. Pharmacol.* **256**, 114–121 (2011).

31. Imlay, J. a. Pathways of oxidative damage. *Annu. Rev. Microbiol.* **57**, 395–418 (2003).

CHAPTER 6

Bacillus subtilis spores as antioxidants

https://www.shutterstock.com

Bacillus subtilis is ubiquitous.
Therefore, it has developed adaptive strategies to subsist in diverse environments.
Moreover, this bacterium is able to form spores, quiescent cells able to survive in adverse conditions[1].

[1]Ameisen, J. C. (2002). On the origin, evolution, and nature of programmed cell death: a timeline of four billion years. *Cell death and differentiation*, *9*(4), 367.

Submitted to Scientific Reports

Alternative use of spores from Bacillus subtilis: protection against environmental oxidative stress in human normal keratinocytes

Ganna Petruk[a], Giuliana Donadio[b], Mariamichela Lanzilli[b], Rachele Isticato[b], Daria Maria Monti [a,c]

[a]Department of Chemical Sciences, University of Naples Federico II, Complesso Universitario Monte Sant'Angelo, via Cinthia 4, 80126, Naples, Italy
[b]Department of Biology, University of Naples Federico II, Complesso Universitario Monte Sant'Angelo, via Cinthia 4, 80126, Naples, Italy
[c]Istituto Nazionale di Biostrutture e Biosistemi (INBB), Rome, Italy

Abstract

Inorganic trivalent arsenic is a major environmental pollutant and exposure to human results in many pathologies, including keratosis and carcinoma. Here, we analyzed the effects of *B. subtilis* spores on human normal keratinocytes in the presence of sodium arsenite oxidative stress. Pre-treatment of cells with spores before inducing oxidative stress was able to keep normal levels of intracellular ROS, GSH and lipid peroxidation, as well as to inhibit the activation of the MAPK cascade. Moreover, spores showed a positive effect on cell proliferation, probably due to their binding on the cell surface and the activation of intracellular catalases. We found that spores exert their protective effect by the nuclear translocation of Nrf-2, involved in the activation of stress response genes. This, in turn, resulted in a protective effect against sodium arsenite stress injury, as oxidative stress markers were reported to physiological levels when cells were stressed before incubating them with spores. Therefore, *B. subtilis* spores can be considered as a new agent to counteract oxidative stress on normal human keratinocytes.

Keywords

Bacillus subtilis, antioxidants, oxidative stress, eukaryotic cells, spores

.

6.1 Introduction

Arsenic is a natural element widely present in the food, water, air and soil[1]. The inorganic form exists predominantly in trivalent (As^{3+}, such as sodium arsenite and arsenic trioxide) or pentavalent (As^{5+}) form[2] and is generally considered more harmful than organic forms[3]. Epidemiological studies have shown that chronic exposure to trivalent arsenite is associated with dermal toxicity, neurodegenerative disorder, cardiovascular disease and the increased incidence of cancer in lung, skin, bladder, and liver[4–6]. Being a major form of trivalent arsenite, sodium arsenite (herein denoted as SA) contamination of water is a serious environmental problem worldwide due to the particularly high risk of SA for inducing human diseases[5,7]. SA is a human carcinogen and its carcinogenicity has been evaluated by International Agency for Research on Cancer (IARC) for the first time in 1973[3]. Indeed, it has been reported that the exposure of human cell lines to SA increases the production of reactive oxygen species (ROS)[8–10], which induce intracellular oxidative stress and result in oxidative DNA damage and end into apoptosis[11,12].

Cells are equipped with an array of antioxidant systems, as the superoxide dismutases (SODs), which catalyze the dismutation of superoxide anions into H_2O_2 and oxygen, maintaining a low intracellular ROS level. H_2O_2 is reduced by various systems, mainly by catalases and peroxidases. However, these endogenous systems are often insufficient for complete scavenging of ROS. Thus, scavengers of ROS or exogenous antioxidants have been proposed to be potentially beneficial in reducing SA-induced toxicity. However, a continuous search for new products able to prevent or retard stress-induced damages is still needed. Here, we propose the use of bacterial spores to counteract SA-induced damage.

Spore-forming bacteria are Gram-positive microorganisms belonging to different genera and including more than 200 species[13]. The common feature of these organisms is the ability to form the spore, a quiescent cellular type in response to harsh environments. The spore can survive in this dormant state for long periods, resisting to a vast range of stresses, such as high temperature, dehydration, absence of nutrients and presence of toxic chemicals[14]. When the environmental conditions ameliorate, the spore germinates, thus originating a vegetative cell able to grow and to sporulate again.

The *Bacillus* spore is resistant to oxidizing agents thanks to its outermost layer, as well as to the presence of enzymes, such as catalase, sod and lactase. Some Bacillus species are on the Food and Drug Administration's GRAS (generally regarded as safe) list. *Bacillus subtilis*, the model organism for spore formers, is currently used as an oral probiotic[15]; ingestion of significant amount of *B. subtilis* is thought to restore the normal microbial flora following extensive antibiotic use or illness[16]. *Bacillus* species (*Bacillus cereus*, *Bacillus clausii*, *Bacillus pumilus*) carried in five commercial probiotic products consisting of bacterial spores were characterized for potential attributes (colonization, immunostimulation, and antimicrobial activity) that could account for their claimed probiotic properties. *Bacillus* species are often identified in large numbers within the gut, where they exert their activity[17]. In particular, *B. subtilis* is a bacterium found on skin, in the digestive tract, in epithelial wounds, on extremities of the human body, in livestock and in soil[18,19]. Due to the fact that *B. subtilis* is ubiquitous, it has developed adaptive strategies to subsist in diverse environments via the production and secretion of a large number of genetically encoded molecules that control the growth of neighboring organisms[20,21]. In this article, the bacterial spores are used in a different field, i.e. that of exploiting their robust and dormant life form

endowed with formidable resistance properties. Keratinocytes have been selected since these cells are normally present in the outermost layer of the skin and are more exposed to environmental stress. The proof of concept developed in this work has been the design *B. subtilis* spores as a new agent to counteract sodium arsenite oxidative stress on normal human keratinocytes.

6.2 Materials and methods

6.2.1 Bacillus subtilis strains used and preparation of spores

B. subtilis wild type strain PY79 was used[22]. Sporulation was induced by exhaustion by growing cells in DSM (Difco Sporulation Medium) as described by Nicholson and Setlow[23]. After 30 h incubation at 37 °C, spores were collected, washed four times, incubated over night in water at 4 °C to lyse residual sporangial cells and purified on a step gradient of 20% to 50% of Gastrografin[24].

6.2.2 Cell culture and cell survival assay

Human normal keratinocytes (HaCaT) and epithelial colorectal adenocarcinoma cells (LoVo) were obtained from ATCC. Both cell lines were cultured as described in Materials and Methods of Chapter 5. Cells were seeded in 96-well plates (100 µL/well) at a density of 2 x 10^3/well (HaCaT cells). For dose-dependent survival assays, 24 h after seeding, increasing amount of spore (from 1:1 to 1:50) were added to the cells for 24-72 h. At the end of incubation, cells were detached by trypsin, centrifuged at 1000 g for 5 min at r.t. and the cell pellet was resuspended in 0.4% trypan blue buffer (Sigma-Aldrich) and counted in the hemocytometric chamber (Burker chamber, Sigma-Aldrich).

6.2.3 Oxidative stress

To analyze oxidative stress, cells were plated at a density of 4 x 10^4 cells/cm^2 (LoVo cells) and 2 x 10^4 cells/cm^2 (HaCaT cells). 24 h after seeding, cells were incubated for 30 min in the presence or absence of PY79 spores (1:50, cells:spore), and then incubated in the presence of 300 µM SA for 45 min at 37 °C (treatment before injury). In a second group of experiments, cells were stressed with 300 µM SA for 45 min at 37 °C and then cell medium was changed to remove SA and cells were incubated for 30 min in the presence or absence of spores (treatment after injury). In case of UVA treatment, 24 h after seeding, cells were incubated for 30 min in the presence or absence of spores and then the medium was removed and cells were washed twice with PBS. After washing, cells were covered with a thin layer of PBS and irradiated for 2 min with UVA light (20 J/cm^2). Subsequently to oxidative stress, cells were washed again with PBS and re-incubated with spores at 37 °C for 90 min.

6.2.4 Measurement of intracellular ROS levels

To estimate ROS production, the protocol described in[25] was followed.

6.2.5 Measurement of intracellular total GSH levels

Total activation of the GSH synthetic pathway was monitored by measuring GSH concentrations in the cells. Intracellular GSH levels were estimated as procedure previously was described[26].

6.2.6 Measurement of lipid peroxidation

The thiobarbituric acid reactive substances (TBARS) assay quantifies a by-product of lipid peroxidation, the malondialdehyde, that reacts with thiobarbituric acid (TBA) forming an abduct (MDA-TBA). We used the protocol described by Del Giudice et al[27].

6.2.7 Western blot analyses

HaCaT cells were plated at a density of 2 x 10^4 cells/cm^2 in complete medium for 24 h and then treated as described above (paragraph 6.2.4). After treatment, total cell lysate was obtained by resuspend each cell pellet in 50 µL of lysis buffer (100 mM Tris-HCl, 300 mM NaCl and 0.5% NP40 at pH 7.4, with addiction of inhibitors of proteases and phosphatases). Nuclear pellet was obtained after extracting cytosolic proteins with PBS buffer containg 0.1% triton and proteases inhibitors. Nuclear lysate was obtained by resuspending the pellet in RIPA buffer (150 mM NaCl, 1% NP-40, 0.1% SDS, proteases inhibitors in 50 mM Tris-HCl pH8.0). Lysates (100 µg of proteins) were then analyzed by Western blotting performed as reported by Galano et al[28]. Phosphorylation levels of p38, MAPKAPK-2, HSP-27 or Nrf-2 were detected by using specific antibodies purchased from Cell Signal Technology (Danvers, MA, USA). To normalize protein intensity levels, a specific antibody against anti-GAPDH or anti B-23 (ThermoFisher, Rockford, IL, USA) were used for cytosolic and nuclear extracts, respectively. The chemiluminescence detection system (SuperSignal® West Pico) was from Thermo Fisher.

6.2.8 Catalase assay

Quantitative determination of catalase activity of spores and of cells after spore incubation was measured by the loss of absorbance at 240 nm as previously described by Beers and Sizer[29]. Briefly, spores (5x10^8 or 1x10^9) or cell lysate (50 µg) were incubated for 30 min at room temperature in 1mL of hydrogen peroxide solution (50mM Potassium Phosphate Buffer, pH 7.0, 0.036% (w/w) H_2O_2). Then, samples were centrifuged for 1 min at 13000 g to remove the spores and the hydrogen peroxide concentration in solution was determined by measuring the absorbance at 240 nm. The percentage of peroxide removed was calculated as following:

% H_2O_2 red = 1-OD_{240nm} sample/OD_{240nm} standard

6.2.9 Adhesion assays

For adhesion assays, HaCaT cells were plated at a density of 3 x 10^4 cells/cm^2 in complete medium in a 24-well with cover glass for 24 h and then treated with spores previously bound with a red fluorescent protein[30] for 30 min (1:50, cells:spores). At the end of incubation, cells were washed 3 times with 500 µL PBS to remove non-adherent bacteria and then fixed in 4% paraformaldehyde in PBS for 15 min. To verify the specificity of the binding between cells and spores, in a parallel experiment cells were incubated with 0.6 M NaCl in PBS for 10 min[31] and then washed and fixed as described above. After fixing, cells were washed 3 times with 500 µL PBS and then observed with an Olympus BX51 fluorescence microscope. Images were captured using an Olympus DP70 digital camera equipped with Olympus U-CA Magnification Changer (100x) and processed with Image Analysis Software (Olympus) for minor adjustments of brightness, contrast and color balance and for creation of merged images.

To estimate the amount of spores bound to cells, the same experiment described above was performed, but instead of fixing cells, cells were detached in trypsin and resuspended in PBS (2 x 10^4 cells/mL). Fluorescence intensity of the cell

suspension was measured by a Perkin-Elmer LS50 spectrofluorimeter (540 nm excitation wavelength, 625 nm emission wavelength, 300 nm/min scanning speed, 5 slit width for both excitation and emission). Rhodamine fluorescence was expressed as percentage of red fluorescence intensity of the sample under test, with respect to untreated cells.

6.2.10 Statistical Analyses

In all the experiments samples were analyzed in triplicate. The results are presented as mean of results obtained after at least three independent experiments (mean ± SD, or mean ± SEM) and compared by one-way ANOVA following Tukey's multiple comparison test using Graphpad Prism for windows, Version 6.01.

6.3 Results and discussion

6.3.1 Effects of *B. subtilis* spores on human normal keratinocytes

Human keratinocytes were chosen because normally exposed to different environmental stress. The biocompatibility of wild type spores of *B. subtilis* (PY79) on HaCaT cells was tested by a time-course and doseresponse test, using a ratio from 1:1 to 1:50 (cells:spore). As shown in **Figure 1**, spore had a positive effect on cell viability, as an increase of about 60 % and 30 % was observed after 24 and 48 h, respectively, at the highest ratio used. No significant increase in cell viability was observed after 72 h, as normal cells are sensitive to the inhibition contact phenomenon, stopping their growth when they become confluent. On the basis of these results, subsequent experiments were carried out at a ratio 1:50.

It has been reported that *B. subtilis* spore are not able to properly germinate and outgrowth in cell culture medium for at least 5 hours[32].

In our experimental conditions, a partial loss of spore-refraction was observed after 24 hours of incubation in DMEM with 10% of fetal bovine serum in the presence or not of HaCaT cells. After 72 hours of incubation, the number of black spores represents the 90% of the total spores and no vegetative cells were observed. These data suggest that spores are able to start the germination process but not the outgrowth.

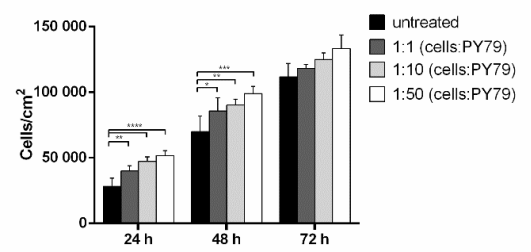

Figure 1: Effects of PY79 spores on human normal keratinocytes. Dose-response curve of HaCaT cells after 24, 48 and 72 h incubation in the presence of different concentrations of PY79 spores, in a ration from 1:1 to 1:50 (cells:spores). Cell survival percentage was defined as reported in Methods section (paragraph 4.2). Values are given as means ± SEM (n ≥ 3). * indicates p<0.05; ** indicates p<0.005, *** indicates p<0.001, **** indicates p<0.0001, with respect to untreated cells of each time point.

6.3.2 Pretreatment with *B. subtilis* spores inhibits SA-induced damage in eukaryotic cells

Trivalent inorganic arsenic (iAs^{3+}) is a toxic and carcinogenic environmental contaminant that humans are inadvertently exposed to every day through water, food and air. Epidemiological investigations demonstrate that long-term exposure to SA

leads not only to different types of cancer in skin, but also in lung, liver, kidney and bladder[5]. SA exerts its toxic effect through ROS generation that, produced in the mitochondria, causes loss of GSH homeostasis and oxidations of molecules (such as formation or lipid peroxides)[33]. To analyze the effects of *Bacillus* spores on cells subjected to oxidative stress, HaCaT cells were pre-treated with PY79 spores for 30 min before inducing oxidative stress by using 300 μM sodium arsenite (SA). Immediately after SA treatment, ROS production was determined by using H_2DCFDA (2,7-dichlorofluorescin diacetate). As expected, 45 min treatment with SA induced a 90% increase in ROS intracellular levels compared to control cells (**Figure 2A**). Interestingly, pre-treatment of cells with spores prior to SA exposure significantly suppressed SA-induced ROS production ($p<0.001$).

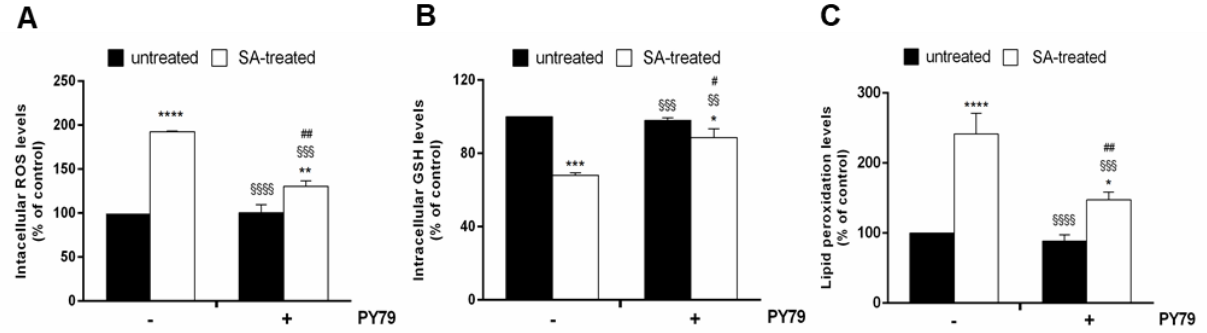

Figure 2: Analysis of the oxidative stress markers in HaCaT cells exposed to SA treatment in the presence of PY79 spores. Cells were pre-incubated in the presence of PY79 (1:50, cells:spores) for 30 min and then 300 μM SA was added to the culture medium for 45 min. **A**, intracellular ROS levels were determined by DCFDA assay; **B**, intracellular GSH levels determined by DTNB assay; **C**, lipid peroxidation levels determined by TBARS assay. Values are expressed as fold increase with respect to control cells. Data shown are the means ± S.D. of three independent experiments. * indicates $p<0.05$, ** indicates $p<0.005$, **** indicates $p<0.0001$, with respect to control cells; §§ indicates $p<0.005$, §§§ indicates $p<0.001$, §§§§ indicates $p<0.0001$, with respect to SA-treated cells; # indicates $p<0.05$; ## indicates $p<0.005$ with respect to PY79-treated cells.

This finding suggests that mitochondrial dysfunction, induced by SA treatment, may be counteracted by PY79 through a ROS-mediated signaling pathway. It is known that GSH is the most abundant[6] low molecular weight thiol that plays important roles in redox, nutrient metabolism, and regulation of cellular events[19], and is oxidized during oxidative stress. Thus, we analyzed intracellular GSH content in cells incubated in the presence of spores. Following SA-oxidative stress induction, we found a 30% decrease ($p<0.001$) in intracellular GSH levels with respect to control cells, whereas GSH levels were found to be unaltered when cells were co-treated with SA and spores (**Figure 2B**). The anti-stress activity of spores was further confirmed by TBARS assay, in which the peroxidation level of lipids was analyzed. The result of the experiment is reported in **Figure 2C** and it clearly shows that administration of spores to SA-stressed cells was able to keep unaltered the lipid peroxidation levels. In fact, cells pre-treated with spores and then exposed to SA stress showed significantly lower intracellular levels of lipid peroxidation (100%, $p<0.01$) if compared to untreated cells exposed to the stress.

The protective effect of *B. subtilis* spores was finally confirmed by Western blot experiments. In particular, we analyzed the phosphorylation levels of p38, of its direct target, MAPKAPK-2 and of HSP-27 (**Figure 3**). These proteins are important members of the mitogen-activated protein kinase (MAPK) family, and are directly involved in oxidative signaling stress pathways. Under stress conditions, we observed a significant increase in the phosphorylation levels of these three proteins, as expected (**Figure 3**, third lanes). On the other hand, co-treatment of cells with PY79 spores and SA resulted

in the inhibition of the phosphorylation of the analyzed markers (**Figure 3**, fourth lanes). easily counteracted by adding *B. subtilis* spores. This new use of spores would be a novel strategy to protect derma cells from SA toxicity.

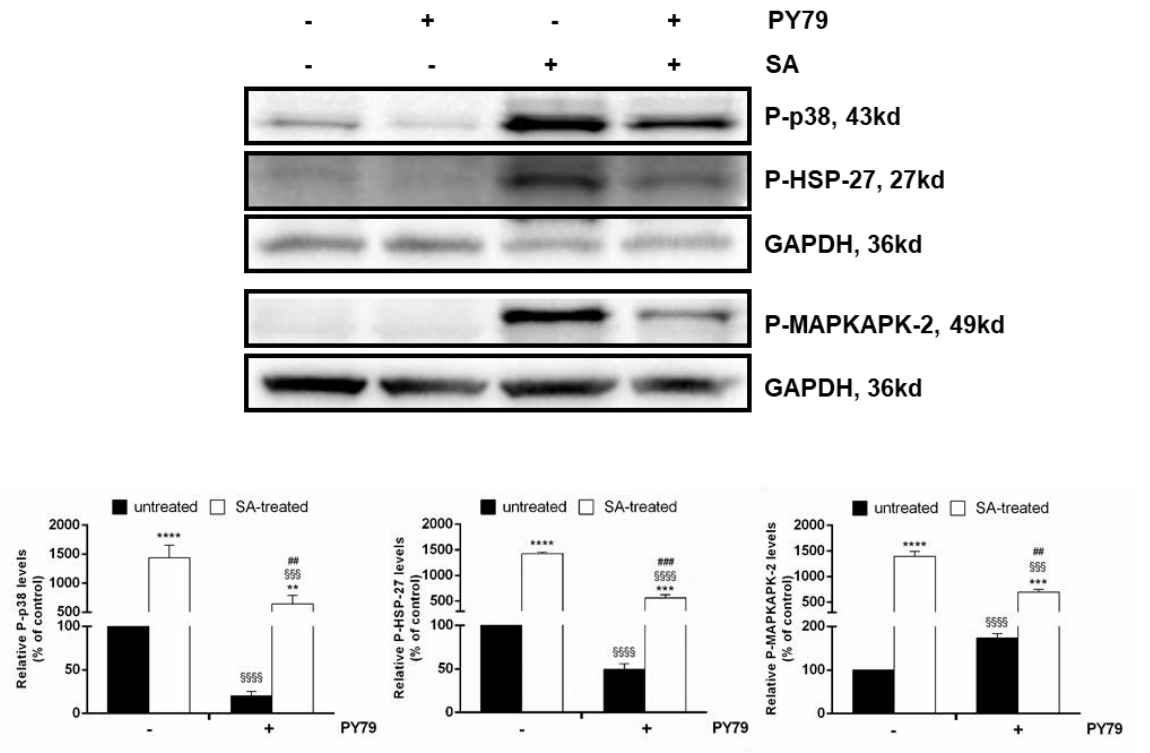

Figure 3: Effect of spores on SA-induced oxidative stress markers in HaCaT cells. Western blots show the phosphorylation levels of p38 (upper panel), HSP-27 -2 (middle panel) and MAPKAPK (lower panel), with the relative densitometric analysis in the absence (black bars) or in the presence (white bars) of SA. GAPDH was used as internal standard. ** indicates p<0.005, *** indicates p<0.001, **** indicates p<0.0001, with respect to control cells; §§§ indicates p<0.001, §§§§ indicates p<0.0001, with respect to SA-treated cells; ## indicates p<0.005, ### indicates p<0.001, with respect to PY79-treated cells.

To verify whether the observed protective effect of the spores was not specific for the cell line or the induced stress type, we repeated the experiments using a different oxidative stress inducer, i.e. UVA radiation, or a different cell line, i.e. human colon cancer (LoVo) cells. When UVA were used to induce stress, HaCaT cells were incubated with increasing number of spores (from ratio 1:1 to 1:50) for 30 min and then stress was induced by UVA irradiation (20 J/cm^2). After 90 min, cell lysates were analyzed by Western blotting. After UVA oxidative stress induction, we found a significant[7] increase in the phosphorylation level of p38, whereas the incubation of cells with spores prior UVA irradiation, resulted in a dose-dependent decrease of p38 phosphorylation level. In particular, in the ratio 1:50, this level was similar to that observed in non-irradiated cells (**Appendix B**, **Figure S1A**, p<0.0001).

As for LoVo cells, cells were co-treated with 300 µM SA and spores and intracellular ROS, GSH levels and lipid peroxidation were analyzed. As shown in **Appendix B** (**Figure S1B-D**), no alteration of these markers was observed during coexposure of cells to SA spores, suggesting a general efficacy of spores in counteracting oxidative stress.

6.3.3 B. subtilis spores are able to heal keratinocytes after SA injury

In the search of a general anti-stress application of spores, we evaluated if PY79 spores could restore cells after SA injury. To this purpose, cells were first stressed by SA for 45 min, incubated for 30 min with spores and then ROS production, GSH oxidation, activation of MAPK cascade and lipid peroxidation were evaluated (**Figure 4**). Interestingly, SA-induced alteration in ROS and GSH levels was suppressed by the presence of spores as these levels were similar to those obtained for untreated and spore-treated cells (**Figure 4A-B**). Accordingly, a decrease in lipid peroxidation and in the phosphorylation level of p38 levels was detected after SA injury and sporetreatment (**Figure 4C-D**).

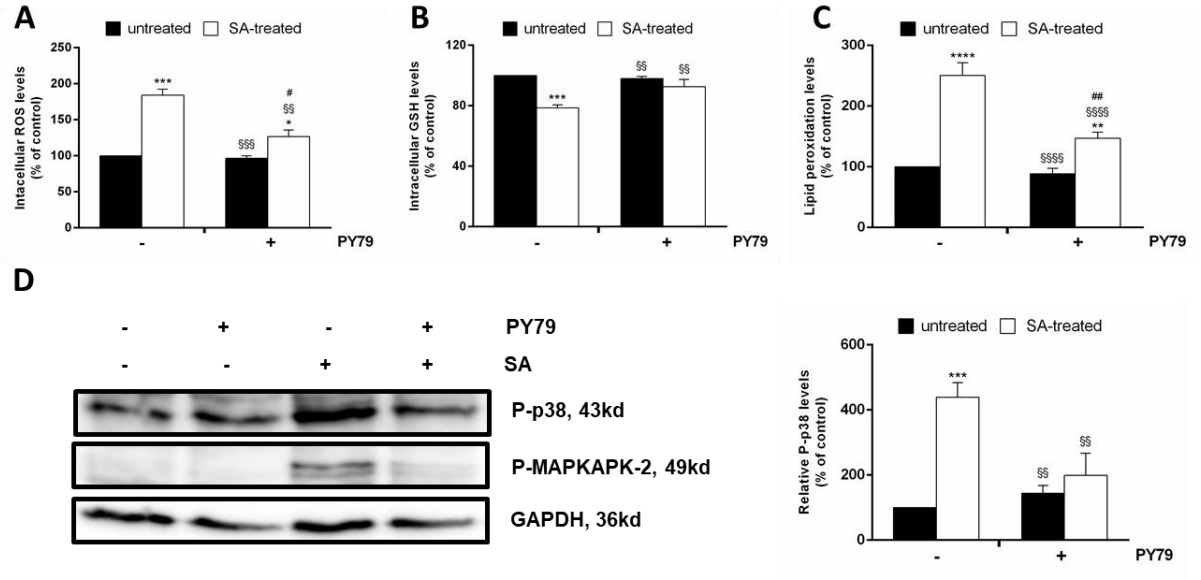

Figure 4: Ability of spores to heal SA-induced oxidative stress in HaCaT cells exposed to SA treatment. Cells were stressed by 300 μM SA for 45 min and then incubated in the presence of PY79 (1:50, cells:spores) for 30 min. **A**, intracellular ROS levels were determined by DCFDA assay; **B**, intracellular GSH levels determined by DTNB assay; **C**, lipid peroxidation levels determined by TBARS assay. Values are expressed as fold increase with respect to control cells; **D**, Western blots show the phosphorylation levels of p38 (upper panel), MAPKAPK-2 (middle panel), with the relative densitometric analysis in the absence (black bars) or in the presence (white bars) of SA. GAPDH was used as internal standard; Data shown are the means ± S.D. of three independent experiments. * indicates $p<0.05$, ** indicates $p<0.01$, *** indicates $p<0.001$, **** indicates $p<0.0001$, with respect to control cells; §§ indicates $p<0.005$, §§§ indicates $p<0.001$, §§§§ indicates $p<0.0001$, with respect to SA-treated cells; # indicates $p<0.05$, ## indicates $p<0.005$, with respect to PY79-treated cells.

6.3.4 The spore-induced antioxidant activity is regulated by Nrf-2 nuclear translocation

In order to get insights into the molecular mechanism of *B. subtilis* spores-protective effect, we analyzed the involvement of the transcription factor Nrf-2. Under normal physiological conditions, Nrf-2 is associated to Keap-1, which keeps Nrf-2 in the cytosol and directs it to proteasomal degradation. Upon either oxidative stress induction and/or in the presence of antioxidants, Keap-1 dissociates from Nrf-2 which is translocated to the nucleus where it binds to antioxidant responsive element (ARE) sequences and activates the transcription of several phase-II detoxifying enzymes[35]. It has been recently reported that *lactobacilli*, well-known probiotics, can elicit their beneficial effect by inducing the generation of non-dangerous levels of ROS in intestinal epithelium cells, upon NOX binding[36,37]. This ROS near threshold level is

sufficient to induce Nrf-2 nuclear translocation with the consequent induction of cell proliferation[36,37]. Thus, we incubated HaCaT cells in the presence of PY79 spores for different length of time (from 5 min to 30 min) and lysates were analyzed by Western Blotting using a Nrf-2 antibody (**Figure 5A**).

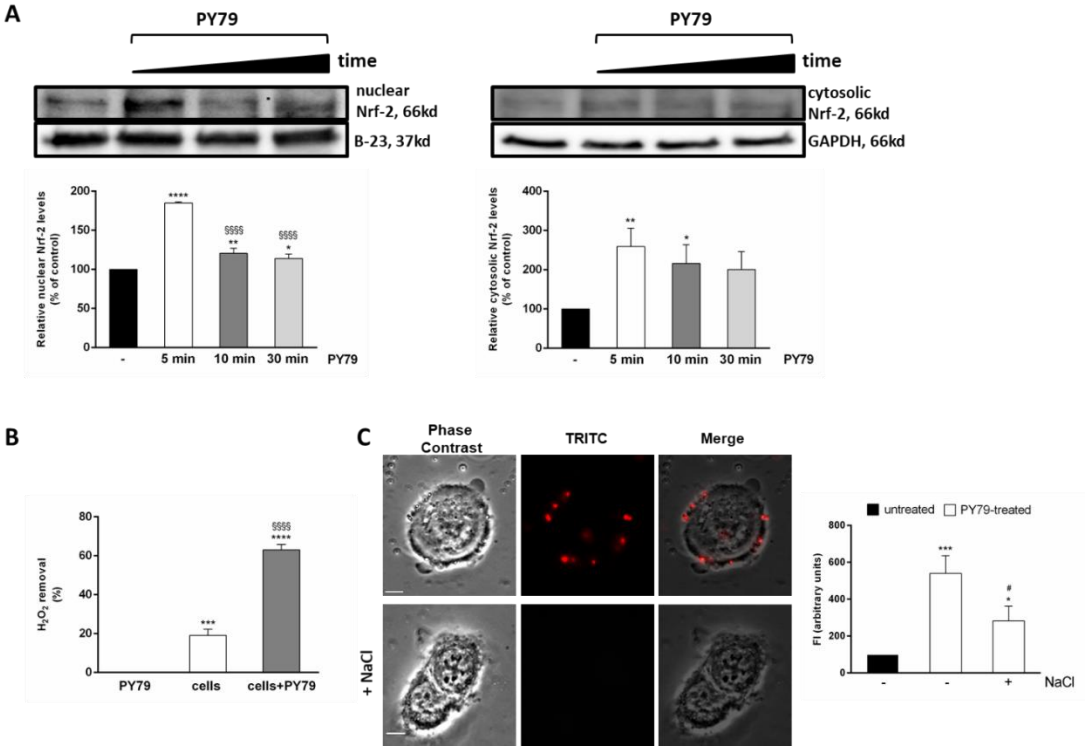

Figure 5: PY79 spores effects on HaCaT cells. A, Western blot analysis for Nrf-2 was performed on cytosolic and nuclear proteins obtained from HaCaT cells after incubation with spores (ratio 1:50) for 5 min (white bars), 15 min (dark grey bars) and 30 min (light grey bars). Nrf-2 was quantified by densitometric analysis and normalized to GAPDH (cytosol) or B-23 (nucleus). Data shown are the means ± S.D. of three independent experiments. * indicates p<0.05, ** indicates p<0.005, **** indicates p<0.0001, with respect to control cells; §§§§ indicates p<0.0001, with respect to PY79-treated cells for 5 min. **B**, Catalase assay on HaCaT cells in the presence of PY79 spores. Cells were exposed to spores (1:50) for 30 min and then 50 µg of cell lysates were incubated with 0.036% (w/w) H_2O_2. Then, H_2O_2 concentration in solution was determined by measuring the absorbance at 240 nm. The experiments were performed in triplicate and the data were expressed as the mean of three independent experiments. *** indicates p<0.001, **** indicates p<0.0001, with respect to spores; §§§§ indicates p<0.0001, with respect to control cells. **C**, Adhesion of spores to HaCaT cells. Cells were incubated with PY79 fluorescent spores (1:50, cells:spores) for 30 min, treated in the presence or absence of 0.6 M NaCl in PBS, washed, fixed and observed by fluorescence microscopy, as described in Methods section (paragraph 6.2.9). A representative image is reported for both the experimental conditions tested. The same field has been observed by phase contrast and fluorescence microscopy. Merged panels are reported. The exposure time was of 200 ms. Scale bar 1 mm. Histograms on the right represent quantitative data obtained by spectrofluorimetric analysis. Values are expressed as fold increase with respect to control cells. Data shown are the means ± S.D. of three independent experiments. * indicates p<0.05, *** indicates p<0.001, with respect to control cells; # indicates p<0.05, with respect to PY79-treated cells without NaCl treatment.

As shown in **Figure 5A**, an increase in both cytosolic and nuclear Nrf-2 levels was observed after 5 min incubation, and then the nuclear signal decreased over time. As one of the results of Nrf-2 activation is the activation of enzymes involved in antioxidant response, we evaluated the catalase activity of cells incubated with spores in the ratio 1:50 (1.5×10^7 cells: 7.5×10^8 spore), by measuring the H_2O_2 consumption. As reported in **Figure 5B**, a higher catalase activity was detected in keratinocyte lysate

after incubation with spores than in untreated cells ($p<0.0001$), thus confirming that spores are able to induce the activation of the antioxidant pathway on HaCaT cells. One should consider that no catalase activity was detected in *B. subtilis* spores when 1 x 10^9 spores were tested (**Figure 5B**). Moreover, the antioxidant activity observed is not related to spores' intracellular enzymes, as spores are resistant to the lysis procedure followed for eukaryotic cells[23]. Finally, we measured the amount of spores bound to the surface of HaCaT cells by using TRITC-fluorescent spores[30]. Cells were incubated as described above, in the presence or absence of 0.6 M NaCl in order to remove specifically bound spores. The results shown in **Figure 5C** indicated that fluorescently analysed spores were bound to the cell surface, as a 4.5-fold increase in fluorescence was observed with respect to untreated cells ($p<0.001$) and that the binding was specific, as, after incubation with NaCl, a significant decrease in fluorescence intensity was observed ($p<0.05$).

6.4 Conclusions

Trivalent arsenite is considered one of the most severe environmental injury to which humans are normally exposed, and it has been associated with many disorders, from cardiovascular to cancer[4–6]. Human population is mostly exposed to SA through inhalation, ingestion and dermal contact[38]. Several lines of evidence demonstrated that exposure of human cell lines to SA induces an increase in ROS levels, DNA damage and leads to apoptosis[8–12]. In this context, we investigated the possibility of an alternative and innovative use of *B. subtilis* spores. In particular, using an array of biochemical methodologies, we analysed the protective effect of spores in counteracting the SA-induced oxidative stress on human normal keratinocytes. Spores clearly induced a positive effect both in the prevention of stress as well as when used to heal cells after stress injury. This applicability was found to be independent from the cell type used and from the source of stress, as the same protective effect was observed when colon cells were stressed by SA and when UVA was used on HaCaT cells (see **Appendix B, Figure S1**). It is worth to notice that the protective effect exerted by spores is not only due to the antioxidant activity of the spore, but to the activation of Nrf-2, a nuclear transcription factor, actively involved in oxidative stress response[35]. As already reported, Gut bacteria (as *B. subtilis* and *L. plantarum*) stimulate ROS production in epithelial cells by an enzymatic mechanism analogous to the pathogen-induced respiratory burst in phagocytes[36,39]. Interestingly, enzymatically generated ROS in the epithelia is stimulated not only by potential pathogens, but also by symbiotic bacteria, especially members of the lactobacilli taxon, and promotes cell proliferation and migration[40,41], accelerates restitution post injury[42], and modifies epithelial NF-kB signaling[43]. Authors demonstrated that the presence of this bacteria was able to slightly increase ROS production just enough to promote the dissociation between Keap-1 and Nrf-2[37]. The increase in ROS levels is mediated by the catalytic action of NADPH oxidases, such as Nox-1, present on the cell membrane. The expression of Nox enzymes has been found in barrier cells, including phagocytes, colon, lung and kidney epithelium, as well as in keratinocytes and it seems to have a role in the defense of the organism, since it is activated by microorganisms or inflammatory mediators[44]. The finding that spores are able to bind HaCaT cells suggest an activation of Nox, which will result in an increase of ROS levels and consequently in the nuclear translocation of Nrf-2. Accordingly, in our experimental system, no difference in p38 phosphorylation level was observed between control cells and cells incubated with spores after 75 min incubation (**Figure 3**), whereas a small, although

significant increase was observed after 30 min incubation (**Figure 4**). This result is in line with the hypothesis that the interaction between spores and cells gives rise a to a transient, small increase, not toxic, of the oxidative stress pathway. The activation of the antioxidant system through the up-regulation of Nrf-2 is critical for the protection of skin cells from oxidative stress-induced damage. Suppressed oxidative stress by spores may be useful in the treatment of skin damage, photo-aging, and skin cancers. Thus, our findings suggest that spores can be an effective component in skin care products.

6.5 References

1. Chen, C., Jiang, X., Zhao, W. & Zhang, Z. Z. Dual role of resveratrol in modulation of genotoxicity induced by sodium arsenite via oxidative stress and apoptosis. *Food Chem. Toxicol.* **59**, 8–17 (2013).

2. Rossman, T. G. Mechanism of arsenic carcinogenesis: An integrated approach. *Mutation Research - Fundamental and Molecular Mechanisms of Mutagenesis* **533**, 37–65 (2003).

3. Hughes, M. F., Beck, B. D., Chen, Y., Lewis, A. S. & Thomas, D. J. Arsenic exposure and toxicology: A historical perspective. *Toxicol. Sci.* **123**, 305–332 (2011).

4. Cui, X., Kobayashi, Y., Akashi, M. & Okayasu, R. Metabolism and the paradoxical effects of arsenic: carcinogenesis and anticancer. *Curr. Med. Chem.* **15**, 2293–2304 (2008).

5. Smith, A. H. … Smith, M. T. Cancer risks from arsenic in drinking water. *Environ. Health Perspect.* **97**, 259–267 (1992).

6. Rahman, M. M., Ng, J. C., & Naidu, R. Chronic exposure of arsenic via drinking water and its adverse health impacts on humans. *Environ. Geochem. Health* **31**, 189–200 (2009).

7. Brown, K. G. & Ross, G. L. Arsenic, drinking water, and health: a position paper of the American Council on Science and Health. *Regul. Toxicol. Pharmacol.* **36**, 162–174 (2002).

8. Ruiz-Ramos, R., Lopez-Carrillo, L., Rios-Perez, A. D., De Vizcaya-Ruiz, A. & Cebrian, M. E. Sodium arsenite induces ROS generation, DNA oxidative damage, HO-1 and c-Myc proteins, NF-kappaB activation and cell proliferation in human breast cancer MCF-7 cells. *Mutat. Res.* **674**, 109–115 (2009).

9. Zhang, Z. … Shi, X. Reactive oxygen species mediate arsenic induced cell transformation and tumorigenesis through Wnt/beta-catenin pathway in human colorectal adenocarcinoma DLD1 cells. *Toxicol. Appl. Pharmacol.* **256**, 114–121 (2011).

10. Imlay, J. a. Pathways of oxidative damage. *Annu. Rev. Microbiol.* **57**, 395–418 (2003).

11. Hei, T. K. & Filipic, M. Role of oxidative damage in the genotoxicity of arsenic. *Free Radic. Biol. Med.* **37**, 574–581 (2004).

12. Wang, T. S., Kuo, C. F., Jan, K. Y. & Huang, H. Arsenite induces apoptosis in Chinese hamster ovary cells by generation of reactive oxygen species. *J. Cell. Physiol.* **169**, 256–268 (1996).

13. Cutting, S. M., Hong, H. a, Baccigalupi, L. & Ricca, E. 18. Oral vaccine delivery by recombinant spore probiotics. *Int. Rev. Immunol.* **28**, 487–505 (2009).

14. Isticato, R. … Ricca, E. Non-recombinant display of the B subunit of the heat labile toxin of *Escherichia coli* on wild type and mutant spores of Bacillus subtilis. *Microb. Cell Fact.* **12**, 98 (2013).

15. Green, D. H. … Cutting, S. M. Characterization of two *Bacillus* probiotics characterization. *App. Envir. Microbiol*. *65*, 8–12 (1999).

16. Mazza, P. The use of *Bacillus subtilis* as an antidiarrhoeal microorganism. *Boll. Chim. Farm.* **133**, 3–18 (1994).

17. Rhee, K.-J., Sethupathi, P., Driks, A., Lanning, D. K. & Knight, K. L. Role of commensal bacteria in development of gut-associated lymphoid tissues and preimmune antibody repertoire. *J. Immunol.* **172**, 1118–24 (2004).

18. Ara, K. et al. Foot odor due to microbial metabolism and its control. *Can. J. Microbiol.* **52**, 357–364 (2006).

19. Earl, A. M., Losick, R. & Kolter, R. Ecology and genomics of *Bacillus subtilis*. *Trends in Microbiol.* **16**, 269–275 (2008).

20. Stein, T. *Bacillus subtilis* antibiotics: Structures, syntheses and specific functions. *Mol. Microbiol.* **56**, 845–857 (2005).

21. Liu, W.-T. et al. Imaging mass spectrometry of intraspecies metabolic exchange revealed the cannibalistic factors of *Bacillus subtilis*. *Proc. Natl. Acad. Sci. U. S. A.* **107**, 16286–16290 (2010).

22. Youngman, P., Perkins, J. B. & Losick, R. A novel method for the rapid cloning in *Escherichia coli* of *Bacillus subtilis* chromosomal DNA adjacent to Tn917 insertions. *Mol. Gen. Genet.* **195**, 424–33 (1984).

23. Colin R. Harwood, S. M. C. *Molecular biological methods for Bacillus*. (1990).

24. Henriques, A. O., Melsen, L. R. & Moran, C. P. Involvement of superoxide dismutase in spore coat assembly in *Bacillus subtilis. J. Bacteriol.* **180**, 2285–2291 (1998).

25. Del Giudice, R. … Rigano, M. M. Carotenoids in fresh and processed tomato (*Solanum lycopersicum*) fruits protect cells from oxidative stress injury. *J. Sci. Food Agric.* **97**, 1616–1623 (2016).

26. Petruk, G. … Monti, D. M. D. M. An ascorbic acid-enriched tomato genotype to fight UVA-induced oxidative stress in normal human keratinocytes. *J. Photochem. Photobiol. B Biol.* **163**, 284–289 (2016).

27. Del Giudice, R. … Rigano, M. M. Antioxidant bioactive compounds in tomato fruits at different ripening stages and their effects on normal and cancer cells. J. *Funct. Foods* **18**, (2015).

28. Galano, E., Arciello, A., Piccoli, R., Monti, D. M. & Amoresano, A. A proteomic approach to investigate the effects of cadmium and lead on human primary renal cells. *Metallomics* **6**, 587–597 (2014).

29. Beers, R. & Sizer, I. A spectrophotometric method for measuring the breakdown of hydrogen peroxide by catalase. *J. Biol. Chem.* **195**, 133–140 (1952).

30. Beers, R. & Sizer, I. A spectrophotometric method for measuring the breakdown of hydrogen peroxide by catalase. *J. Biol. Chem.* **195**, 133–140 (1952).

31. Arciello, A. … Piccoli, R. Insights into the fate of the N-terminal amyloidogenic polypeptide of ApoA-I in cultured target cells. *J. Cell. Mol. Med.* **15**, 2652–2663 (2011).

32. Alebouyeh, M. … Zali, M. R. Characterization of the interaction of undomesticated *Bacillus subtilis* spores with Caco-2 cell line. *Ann. Microbiol.* **59**, 273–277 (2009).

33. Simon, H.-U., Haj-Yehia, A. & Levi-Schaffer, F. Role of reactive oxygen species (ROS) in apoptosis induction. *Apoptosis* **5**, 415–418 (2000).

34. Anderson, M. E. Glutathione: An overview of biosynthesis and modulation. *Chem. Biol. Interact.* **111–112**, 1–14 (1998).

35. Ma, Q. Role of nrf2 in oxidative stress and toxicity. *Annu. Rev. Pharmacol. Toxicol.* **53**, 401 (2013).

36. Jones, R. M. … Neish, A. S. Symbiotic *lactobacilli* stimulate gut epithelial proliferation via Nox-mediated generation of reactive oxygen species. *EMBO J.* **32**, 3017–3028 (2013).

37. Jones, R. M. … Neish, A. S. *Lactobacilli* modulate epithelial cytoprotection through the Nrf2 pathway. *Cell Rep.* **12**, 1217–1225 (2015).

38. Singh, N., Kumar, D. & Sahu, A. P. Arsenic in the environment: effects on human health and possible prevention. *J. Environ. Biol.* **28**, 359–65 (2007).

39. Alam, A. … Neish, A. S. Redox signaling regulates commensal-mediated mucosal homeostasis and restitution and requires formyl peptide receptor 1. *Mucosal Immunol.* **7**, 645–655 (2014).

40. Wentworth, C. C., Jones, R. M., Kwon, Y. M., Nusrat, A. & Neish, A. S. Commensal-epithelial signaling mediated via formyl peptide receptors. *Am. J. Pathol.* **177**, 2782–2790 (2010).

41. Wentworth, C. C., Alam, A., Jones, R. M., Nusrat, A. & Neish, A. S. Enteric commensal bacteria induce extracellular signal-regulated kinase pathway signaling via formyl peptide receptor-dependent redox modulation of dual specific phosphatase. *J. Biol. Chem.* **286**, 38448–38455 (2011).

42. Swanson, P. A. … Neish, A. S. Enteric commensal bacteria potentiate epithelial restitution via reactive oxygen species-mediated inactivation of focal adhesion kinase phosphatases. *Proc. Natl. Acad. Sci.* **108**, 8803–8808 (2011).

43. Kumar, A. … Neish, A. S. Commensal bacteria modulate cullin-dependent signaling *via* generation of reactive oxygen species. *EMBO J.* **26**, 4457–4466 (2007).

44. Lambeth, J. D. NOX enzymes and the biology of reactive oxygen. *Nat. Rev. Immunol.* **4**, 181–9 (2004).

CHAPTER 7

Simultaneous production of antioxidants and starch from microalga Clorella sorokiniana

https://www.shutterstock.com

Microalgae are microscopic photosynthetic organisms that are found in both marine and freshwater environments.
Microalgae can be used to produce a wide range of metabolites such as proteins, lipids, carbohydrates, carotenoids or vitamins for health, food and feed additives, cosmetics and for energy production[1].

[1]Priyadarshani, I., & Rath, B. (2012). Commercial and industrial applications of micro algae–A review. *J algal biomass utln*, *3*(4), 89-100.

Submitted to EMBO Reports

Simultaneous production of antioxidants and renewable molecules from microalga Chlorella sorokiniana

Ganna Petruk[a], Imma Gifuni[b], Anna Illiano[a], Mariana Roxo[c], Gabriella Pinto[a], Angela Amoresano[a], Antonio Marzocchella[b], Renata Piccoli[a,d], Michael Wink[c], Giuseppe Olivieri[b], Daria Maria Montia,[d]

[a]Department of Chemical Sciences, University of Naples Federico II, Complesso Universitario Monte Sant'Angelo, via Cinthia 4, 80126, Naples, Italy
[b] Department of Chemical Engineering, of Materials and Industrial Production, University of Napoli "Federico II", Napoli , Italy;
[c]Institute of Pharmacy and Molecular Biotechnology, University of Heidelberg, Heidelberg, Germany;
[d]Istituto Nazionale di Biostrutture e Biosistemi (INBB), Rome, Italy

Abstract

In recent years, microalgae have gained considerable importance as potential source of biofuels and bioplastics. However, these markets are still developing, as the high cost of cultivation ask for exploiting microalgae into new areas and with a biorefinery approach towards a multicomponent cascade extraction process. To exploit microalgae as a multicomponent source, starch was extracted with high yield from *Chlorella sorokiniana* in biocompatible conditions. Then, to minimize waste production, the extract residue was tested as a potential source of antioxidants. We found that it was able to elicit a strong protective activity towards oxidative stress either *in vitro* on human colon cancer cells and in *vivo on C. elegans* worms, by inhibiting ROS production and activating DAF-16/FOXO transcription factor pathway. We observed that a pool of molecules from three different classes (fatty acids, photosynthetic pigments and carotenoids) were synergistically responsible for this activity. To our knowledge, this is the first report on the obtainment, from a "waste" fraction, of a high value product endowed with antioxidant activity tested in a cell-based model and *in vivo*.

Keywords

Antioxidants; *Chlorella sorokiniana*; eukaryotic cells; microalgae; *C. elegans*

7.1 Introduction

The circular bioeconomy, based on the biorefinery approach, seems to be a good and long-term solution to harmonise the use of natural resources with the sustain of the economic growth, ensure human wellness, reduce the increase of CO_2 concentration in the air and reduce waste production. Microalgae have been often indicated as a potential candidate for biorefinery as they are an incredible reservoir of compounds endowed with biological activities that could be used in different fields[1].

Microalgal biomass is renewable, as the industrial byproduct CO_2 and the sun light energy, are both required for their growth. As no competition exists with food culture on the use of arable land, many recent studies have been focused on the exploitation of various microalgal component in order to obtain the maximum economic benefit, as the conversion of biomass into different products produces minimal waste to the environment. Currently, the research is mainly focused on the use of microalgae as sources of lipids for biodiesel production[2], carbohydrates for methane production via anaerobic fermentation[3], proteins for animal nutrition[4] and food additives. On one hand, several process alternatives to exploit microalgal components in a multi-product biorefinery have been proposed in literature[5], but most of them have been tested as raw fractions not characterized in their single components to validate them as potential products in the market. As an example, it is frequently claimed that the pigment fraction can turn positive the economic balance of the whole process (cultivation plus biorefinery), by assuming that all the pigments can potentially be sold at an antioxidant like price. But if this is the case, or if only a small fraction of the extracted pigments can have these properties, is far to be verified.

We recently reported the use of *Chlorella sorokiniana* to extract starch carbohydrates for bioplastics production[6]. However, from the economic point of view, the exploitation of other components apart from starch is mandatory to render the process more attractive. In particular, *C. sorokiniana*, during nitrogen depletion conditions (required for starch accumulation) increases the production of pigments endowed with antioxidant activity[7]. Indeed, microalgae are normally exposed to high oxygen and radical stress in their natural environment, thus they have developed several efficient protective systems against reactive oxygen species (ROS) and free radicals[8]. For this reason, pigments from microalgae, such as chlorophylls carotenoids, xanthophylls and phycobiliproteins, could be used in food, cosmetic, nutraceutical and pharmaceutical industries[7]. In particular, astaxanthin, β-carotene, zeaxanthin and lutein are endowed with antioxidants activity higher than α-tocopherol[9]. However, to date, the main bottleneck of microalgal exploitation as a multicomponent source is to separate the raw extract in different fractions preserving the activity of their components.

Here, taking advantage of the extraction technique we recently reported to obtain starch from *C. sorokiniana*[6] , we used the waste material as a starting point for antioxidant production. We found that this material was rich in molecules endowed with antioxidant activity which were validated as potential products by testing their properties in a real applicative environment, i.e. either on a cell-based model and *in vivo* on a *C. elegans* model.

7.2 Materials and methods

7.2.1 Microalgal strain and culture conditions

Chlorella sorokiniana Shihiraet Krauss strain ACUF 318 (http://www.acuf.net) is a fresh water terrestrial alga. The culture medium used was Bold's Basal Medium (BBM) containing $NaNO_3$ as nitrogen source at concentration of 0.25 g L^{-1}. The growth was carried out in inclined square bubble column photo-bioreactors, as reported by Olivieri *et al*.[10]. The culture was continuously irradiated with white fluorescent lamps on the front side of the reactors with a light intensity of 300 µmol m^{-2} s^{-1}. Aeration and mixing was provided by feeding air supplemented with 2% of CO_2. Gas flow rate was set at 0.2 vvm. The temperature was maintained at 25 °C by air-conditioning system. Nitrogen depletion was reached after the regular uptake of $NaNO_3$ for biomass growth and the biomass was harvested in the second day of nitrogen depletion, optimal condition for starch accumulation and productivity (Gifuni et al. manuscript in preparation)[11].

7.2.2 Pigments extraction

A conventional solvent extraction method was performed in order to determine the antioxidant activity of *C. sorokiniana* extract. Pure ethanol (99.8%, Sigma-Aldrich) was used as solvent. The extraction protocol follows that reported by Aremu et al.[12] with some modifications. Briefly, the microalgal biomass was dried and ground to 0.150 mg powder. 200 mg of microalgal powder were suspended in 2 mL of ethanol and disrupted by bead beater (2000 *g* for 3 cycles of 1 min space out with 2 min breaks in ice) equipped by 0.5 mm glass beads. The disrupted biomass was moved to dark flaks and the beads were washed twice with ethanol and the final volume was led to 20 mL. The mixture was shaken for 24 h at 250 rpm in the dark on a magnetic stirrer. Then the mixture was centrifuged at 12000 *g* for 10 min. The supernatant, dried using N_2 stream, represents the ethanol extract (EE). Then, the extract was solubilized in 1 mL of DMSO for further analysis on ca cell-based model and in vivo. The remaining pellet (EEP) was also collected and dried to assay the recovered starch.

7.2.3 Biochemical composition

Initial microalgal biomass and the pellet after extraction were characterized in terms of lipids, proteins, total sugars, starch and proteins. The extracts were assayed for pigments, proteins and total sugars concentration, lipids were calculated as difference between the biomass content and the pellet content using mass balance.

Lipids were extracted according to the protocol by Breuer et al.[13] followed by gravimetric quantification of the chloroform extract, previously dried at 100°C for 1 h.

Proteins were assayed by BCA Protein Assay Kit (Thermo Scientific). 10 mg of sample (biomass and dried pellet) was dissolved in 1 mL of lysis buffer (60 mM Tris, 2% SDS) and disrupted by bead beater (700 *g* for 3 cycles of 4 min space out with 1 min breaks in ice) equipped by 0.5 mm glass beads. The samples were incubated at 100 °C for 30 min for the extraction of membrane proteins and then centrifuged at 2500 g for 10 min. Supernatants were analyzed by BCA Kit.

Total sugars concentration was measured by spectrophotometric method of Anthrone modified with respect to that described by Chen and Vaidyanathan[14]. In particular, the disruption of the biomass and of the pellet was carried out according to the procedure described for proteins.

Starch was measured using Total Starch kit by Megazyme (Wicklow, Ireland) and according the manufacture's protocol with some modifications. The amount of

sample was set at 10 mg the microalgal samples and the cells disruption was carried out by the bead beater, as previously reported[15].

Pigments were directly measured by spectrophotometric measurements at 663, 646 and 470 nm. chlorophyll a, b and carotenoids concentration were calculated according to Wellburn[16].

The composition assays were performed in triplicates.

Simple sugars are calculated as difference between total sugars concentration and starch concentration.

The recovery yields of the biomolecules were calculated through mass balances. The recovery yield (Y,%) is defined as reported in the following formula:

$$Y = \frac{m_{x\ EP}}{m_{x\ initial}} \cdot 100\%$$

Where $m_{x\ EP}$ is the amount (mg) of the compound x (proteins, lipids, total sugars, starch) in EP and $m_{x\ initial}$ is the amount (mg) of the compound x in the initial biomass.

7.2.4 Cell culture and cell survival assay

Human epithelial colorectal adenocarcinoma cells (LoVo) were obtained from ATCC and cultured as described in Materials and Methods section of Chapter 5.

For dose-dependent survival assays cells were seeded in 96-well plates (100 µL/well) at a density of 4 x 10^4 cells per cm^2. 24 h after seeding, increasing amount of microalgae extract (from 20 µg mL^{-1} to 2 mg mL^{-1}) were added to the cells for 24-48 h. At the end of treatment, cells were incubated with 3-(4,5-dimethylthiazol-2-yl)-2,5-diphenyl tetrazolium bromide (MTT) reagent and the cells were incubated for 4 h at 37 °C in a humidified 5% CO_2 incubator. At the end of the incubation, medium was removed and the converted dye was solubilized with isopropanol containing 0.01 mol L^{-1} HCl (100 µL per well). Absorbance was measured at a wavelength of 570 nm using an automatic plate reader (Microbeta Wallac 1420, PerkinElmer, Waltham, MA, USA). Cell survival was expressed as percentage of viable cells in the presence of the microalgae extract under test compared with control cells grown in the absence of the extract. The assay was carried out in triplicates for at least 3 times. Control experiments were performed either by growing cells in the absence of the extract or by adding to the cell cultures identical volumes of DMSO. The method used avoids any possibility of a DMSO effect on the final results.

7.2.5 Oxidative stress

To analyze if EE was able to protect cells from oxidative stress, LoVo cells were plated at a density of 4 x 10^4 cells per cm^2. 24 h after seeding, cells were incubated for different length of time (24 or 48 h) in the presence or absence of EE (200 µg mL^{-1}), and then incubated in the presence of 300 µM SA for 45 min at 37 °C. At the end of treatment, cell viability was assessed by the MTT assay as reported above.

To detect the minimal pre-treatment time, cells were plated as reported above and then incubated for different length of time (5-120 min) with EE (200 µg mL^{-1}). Then, cells were exposed to oxidative stress as reported above and a DTNB assay was performed (described more in detail in paragraph 7.2.6). The result of the experiment is reported in **Appendix C** (**Figure S1**).

Once defined the minimum pre-treatment, in all further experiments cells were pre-treated with EE for 30 min and then exposed to SA for 45 min. After incubation, different assays were performed, as reported below.

7.2.6 Measurement of intracellular total GSH levels

Total reduced glutathione levels were estimated by using the procedure previously described[17].

7.2.7 Measurement of intracellular ROS levels on cells

ROS intracellular levels were evaluated by using a cells permeable probe, 2',7'-dichlorodihydrofluorescein diacetate (H_2-DCFDA, Sigma-Aldrich). In particular the protocol described in[18] was followed.

7.2.8 Western blot analyses

LoVo cells were plated at a density of 4 x 10^4 cells per cm^2 in complete medium for 24 h and then treated as described above (paragraph 7.2.5). After treatment time, cells were detached and lysed in 100 mM Tris-HCl, 300 mM sucrose with addiction of inhibitors of proteases and phosphatases. These lysates were analyzed by Western blotting as reported by Del Giudice et al[19]. Phosphorylation levels of p38 and MAPKAPK-2 were detected by using specific antibodies purchased from Cell Signal Technology (Danvers, MA, USA). To normalize protein intensity levels, a specific antibody against anti-GAPDH (ThermoFisher, Rockford, IL, USA) was used. The chemiluminescence detection system (SuperSignal® West Pico) was from Thermo Fisher.

7.2.9 In vivo experiments on *Caenorhabditis elegans*

The importance of *C. elegans*, as the model organism, in studying antioxidant properties of natural extracts is described in Introduction section in Chapter 5. Whereas, its stains and methods more in detail are reported in Materials and Methods section in Chapter 5.

7.2.16 Reverse-phase HPLC Analyses

Metabolites from ethanol extracts were separated by reverse-phase HPLC on a Phenomenex Jupiter C18 column (250 × 2.00 mm 5 µm, 300 Å pore size) (Phenomenex, Torrance, California, USA) at a flow rate of 200 µL/min. A linear gradient from 5% to 95% acetonitrile in 0.1% formic acid (Sigma Aldrich, Milan, Italy) was used over a time of 40 min and a wavelength of 278 nm was used for monitoring the elution. The eluate was collected in thirteen fractions to be directly analyzed by MALDI-TOF and LC-MS.

7.2.17 Mass Spectrometry Analyses

Matrix-assisted laser desorption/ionization (MALDI) mass spectrometry (MS) experiments were performed on a 5800 MALDI-TOF-TOF ABSciex equipped with a nitrogen laser (337 nm) (AB SCIEX, Milan, Italy). Aliquots of HPLC fractions (0.5 µL) were mixed (1:1, v/v) with a solution of 2.5 dihydroxybenzoic acid (DHB, Sigma Aldrich, Milan, Italy) at a concentration of 10 mg/mL in acetonitrile:water (90:10) solution. Standards Kit for Calibration of AB SCIEX MALDI-TOF was from AB SCIEX calibration mixture. For metabolite identification, MS and tandem mass (MSMS) spectra were acquired in reflector positive mode, by using a mass (m/z) range of 100–4000 Da. Laser power was set to 3500 V for MS spectra acquisition. Each spectrum represents the sum of 3000 laser pulses from randomly chosen spots per sample position. For CID experiments, ambient air was used as collision gas with medium pressure of 10−6 Torr. The data were reported as monoisotopic masses. LCMS analyses were performed by LC-MS equipped by an Agilent HPLC system (1260 Series) on a reverse-

phase C18 column (Agilent Life Sciences Extend-C18, 2.1x50mm,1.8 µm) coupled to an Agilent 6230 TOF mass spectrometer. The HPLC separation was carried out by using water and acetonitrile as mobile phases A and B, respectively, both acidified with 0.1% formic acid. A linear gradient was employed over 40 min (0–2 min: 2% B, 2–8 min: 2-40% B, 8–20 min: 40%-60% B, 20-30 min: 60-80%, 30-40 min, 80-95) at a flow rate of 0.3 mL min^{-1}. The injection volume was 20 µL and The MS source was an electrospray ionization (ESI) interface in the positive ion mode with capillary voltage of 3000 V, gas temperature at 325 °C, dry gas (N_2) flow at 5 l min−1 and the nebulizer at 35 psi. The MS spectra were acquired in a mass range of 150-1000 m/z with a rate of 1 spectrum/s, time of 1000 ms/spectrum and transient/spectrum of 9961.

7.2.16 Statistical Analyses

In all the experiments samples were analyzed in triplicate. The results are presented as mean of results obtained after three independent experiments (mean ± SD) and compared by one-way ANOVA following Bonferroni's method (posthoc) using Graphpad Prism for windows, Version 6.01.

7.3 Results and discussion

Recently, a laboratory scale protocol for starch purification by Gifuni et al.[6] highlighted the need of removing pigments form the microalgal biomass before recovering starch. Taking into account that in a biorefinery perspective each component of the microalgal biomass should be valorized, the extraction of pigments from the microalgal biomass was performed not to obtain the highest amount of pigments, but with the aim of extracting interesting antioxidant molecules without damaging, or drastically reducing, the starch recovery yield. For the same reason, ethanol, already proved not to damage starch, was used. Moreover, ethanol belongs to the permitted solvents exploitable for the extraction of compounds used in food industries (law 2009/32/CE), thus suggesting the possibility to use the extracted antioxidants, or the molecules recovered from the pellet, also as food additives. Finally, this solvent has a low evaporation temperature (78 °C), so it can be easily recovered by evaporation and with low energetic investment.

7.3.1 Pigments extraction

The microalgal biomass was harvested and dried at the early stage of nitrogen depletion. Pigments extraction was performed by using ethanol on dried biomass, as reported in Materials and Methods section. The composition in starch, simple sugars, proteins and lipids was analysed on the initial biomass and on the extracted biomass pellet (herein denoted as EP), and is reported in **Table I**. The microalgal biomass was found to be composed by starch (39.2 ± 1.0%), proteins (29.1 ± 1.1%), lipids (19.8 ± 0.4%) and simple sugars (10.0 ± 0.3%). After pigments extraction, the weight loss of the EP was about 35%, with respect to the initial biomass. In particular, the EP composition with respect to the initial biomass dry weight (**Table I**), showed that starch content was 26.4 ± 0.6%, proteins were 18.5 ± 0.1%, simple sugars were 13.7 ± 0.4%. Lipid content was 4.1 ± 0.1%, thus indicating that lipids were almost completely extracted by the solvent. With the extraction protocol proposed, it was possible to recover 82.9% of the initial starch, and a significant amount of proteins (78.3%). Only 17.0% of the initial lipid content remained in the pellet after the extraction. Therefore, starch recovery was considered satisfying. Simple sugars seem to increase in the pellet with respect to the untreated biomass, probably because part of the initial starch

is reduced in simple sugars during the treatment. The composition in proteins and lipids of EP suggests applications as feedstock for bioplastics or as feed or food complements without further treatments. By introducing further separation steps, all the components of the pellet could be separated and exploited as biochemicals in different industrial fields, with higher profit. For example, proteins could be used for animal feed[22], starch as bulk chemicals in food or pharmaceutical industries[6] and lipids as food emulsifier or for biofuel production.

When the ethanol extracted fraction (herein denoted as EE) was analyzed, besides the presence of lipids (29.5 ± 3.6 mg), proteins (12.5 ± 1.3 mg) and sugars (4.9 ± 0.8 mg), carotenoids, chlorophyll a and b were detected (0.17 ± 0.23 mg, 0.79 ± 0.11 mg and 0.66 ± 0.09 mg, respectively). Thus, the EE was chosen to test the protective antioxidant activity on human cells against oxidative stress injury.

Table I. Total composition of biomass, of the extracted biomass pellet (EP) and of ethanol extracted fraction (EE).

	Biomass composition (%DW)	EP composition (%DW)	EE composition (mg)
Simple sugars	10.0 ± 0.3	13.7 ± 0.4	4.9 ± 0.8
Starch	39.2 ± 1.0	26.4 ± 0.6	-
Proteins	29.1 ± 1.1	18.5 ± 0.1	50.2 ± 1.3
Lipids	18.8 ± 0.4	4.1 ± 0.1	65.8 ± 3.6
Weight loss	0	35	-
Chl a	-	0	0.79 ± 0.23
Chl b	-	0	0.66 ± 0.11
Carotenoidi	-	0	0.17 ± 0.09

7.3.2 In vitro biocompatibility and antioxidant activity of microalgae extract

Human cancer colon cells (LoVo) were chosen as a proof of concept to study the protective effects of EE. For this reason, we first evaluated the biocompatibility of EE by treating cells for 24 and 48 h with increasing amounts (from 20 μg mL^{-1} to 2 mg mL^{-1}) of the extract. At the end of incubation, cell viability was assessed by the 3-(4,5-dimethylthiazol-2-yl)-2,5-diphenyl tetrazolium bromide (MTT) reduction assay, used as an indicator of metabolically active cells, as only alive cells are able to convert MTT to formazan salts. The results of dose-response experiments are reported in **Figure 1A**. In particular, no toxicity was observed up to 200 μg mL^{-1} of microalgae extract at any time analysed, whereas, at higher concentrations (1 and 2 mg mL^{-1}), cell viability was found to be significantly lower in a dose- and time- dependent manner.

Based on these results, we selected 200 μg mL^{-1} microalgae extract as the optimal concentration to analyse the ability of the extract to protect cells from oxidative stress induced by sodium arsenite (SA). Cells were pre-treated with 200 μg mL^{-1} EE for 24 h (**B**, grey bars) or 48 h (**C**, grey bars) in the presence or absence of 300 μM SA and cell viability was measured. As shown in **Figure 1**, cells incubated in the presence of SA, showed a low survival rate (67 and 61% after 24 and 48 h, respectively) when compared to untreated cells (**Figure 1B** and **C**, black bars). Interestingly, the treatment of cells with EE before inducing oxidative stress was able to keep unaltered cell viability, which was found to be comparable to that of untreated cells (**Figure 1B** and **C**, grey bars). As it is well documented that SA induces high ROS production and consequently GSH oxidation in eukaryotic cells[23,24], we analysed EE ability to maintain unaltered intracellular ROS and GSH levels. As shown in **Figure 1D**, the pre-treatment of LoVo cells with the extract reduced ROS levels of about 3.5 times with respect to cells exposed to SA. Similarly, total intracellular GSH levels were significantly higher

(about 40%) in cells pre-treated with microalgae extract and then exposed to the stress, compared to cells exposed to SA (**Figure 1E**).

Finally, we analyzed the phosphorylation levels of p38 and its direct target MAPKAPK-2 (**Figures 1F-G**). These proteins belong to the family of mitogen-activated protein kinases (MAPK) and are directly involved in oxidative signaling stress pathways. Consistently with the results reported above, we observed a significant increase in the phosphorylation level of both proteins after oxidative stress injury (**Figure 1F**, third lane). On the other hand, the pre-treatment of cells with the microalgae extract prior to SA resulted in the inhibition of the phosphorylation of the above mentionated markers (**Figure 1F**, fourth lanes). It is worth to notice that, in all the experiments described, no induction of oxidative stress was observed when cells were incubated with the microalgae extract.

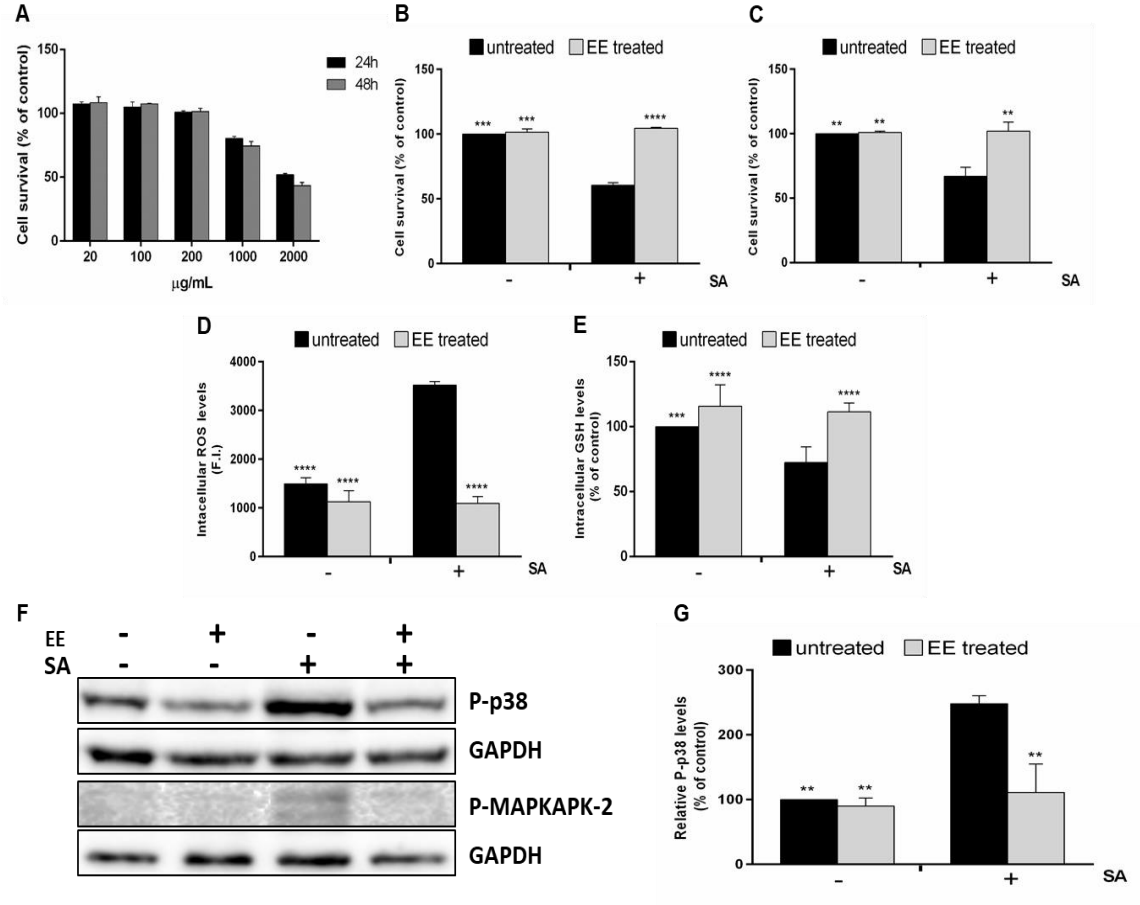

Figure 1: **In vitro antioxidant activity of microalgae extract. A**, LoVo cells were treated with increasing concentrations of EE (from 20 to 2000 µg mL^{-1}) for 24 (black bars) and 48 h (grey bars). Cell viability was assessed by the MTT assay. **B**, **C**, LoVo cells were pre-incubated with 200 µg mL^{-1} EE (grey bars) for 24 (**B**) and 48 h (**C**) and then treated with 300 µM SA for 45 min. Cell viability was assessed by the MTT assay. **D**, **E**, LoVo cells were incubated with of 200 µg mL^{-1} EE prior to be stressed by 300 µM sodium arsenite (SA) for 45 min at 37 °C. **D**, Intracellular ROS levels were determined by DCFDA assay. Values are expressed as fold increase with respect to control (i.e. untreated) cells. **E**, intracellular GSH levels determined by DTNB assay. **F**, Representative images of Western blots of cells incubated with EE. Cells were treated as described above and, after SA-treatment, incubated for 90 min at 37 °C. In Western blots the phosphorylation level of P-p38 and P-MAPKAPK-2 is reported. GAPDH was used as internal standard. In **B**, **C**, **D**, **E**, **G** histograms, black bars refer to control cells, grey bars refer to cells pre-treated with EE, untreated (−) or treated with SA (+). Values are expressed as fold increase with respect to control (i.e. untreated) cells. Data shown are the means ± S.D. of three independent experiments. ** indicates $p<0.005$; *** indicates $p<0.001$; **** indicates $p<0.0001$.

7.3.3 In vivo biocompatibility and antioxidant activity of microalgae extract

The protective activity of EE against oxidative stress was then evaluated on an *in vivo* system, i.e. Caenorhabditis elegans. We first analyzed the variation of brood size, widely accepted as a toxicity marker[25], after treatment with the microalgae extract, and we did not find any significant difference with respect to untreated worms (169 ± 7 vs 177 ± 6, respectively).

Then, the antioxidant activity was evaluated by treating N2 wild-type worms, in L1 larval stage, with EE (200 µg mL-1), for 48 h at 20 °C. Epigallocatechin-3-gallate (EGCG) 100 µg mL-1 was used as positive control, whereas DMSO was used to verify that buffer was not responsible for side effects. In the adult stage, worms were transferred to fresh media and grouped into populations of approximately 80 individuals and treated with lethal dose of 80 µM 5-hydroxy-1,4-naphthalenedione (juglone)[26]. After 24 h, dead and live worms were counted. The worms were considered dead when they did not respond to a gentle touch stimulus.

As showed in **Figure 2A**, worms pre-treated with EE showed a significantly higher survival rate (46 ± 7 worms, light grey bar) with respect to worms treated with juglone (23 ± 4 worms, black bar) or juglone and DMSO (25 ± 4 worms, dark grey bar).

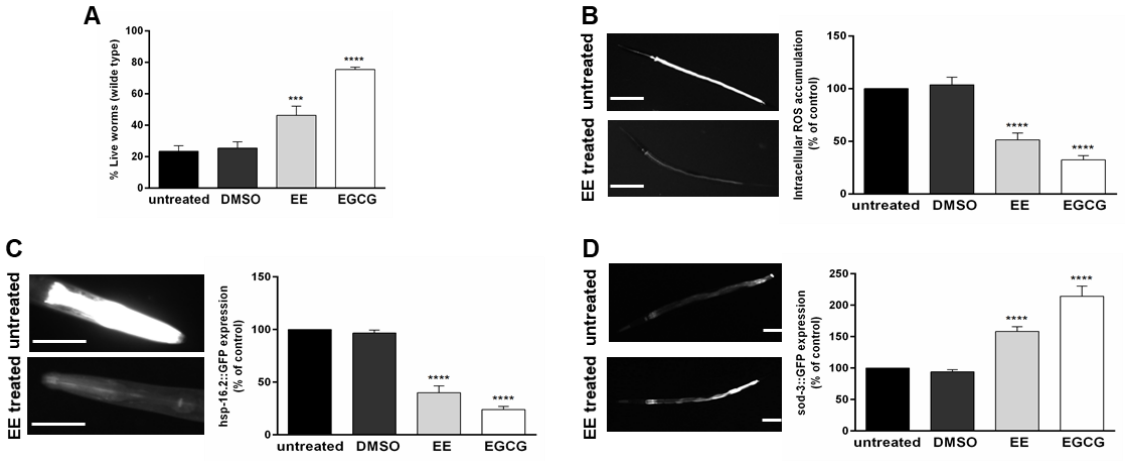

Figure 2: In vivo antioxidant activity of microalgae extract. A, wild type N2 worms were treated with 200 µg mL^{-1} EE extract for 48 h and then exposed to lethal dose of juglone (80 µM). After 24 h, alive and dead worms were counted and survival rate were reported in histograms. **B**, wild type N2 worms were treated with 200 µg mL^{-1} EE extract for 48 h and then incubated with DCF fluorescent probe. After 1 h incubation, accumulation of intracellular ROS levels was evaluated. On the left, representative images of DCF fluorescence in untreated worms (up) and in worms treated with EE (below); On the right, quantification of the fluorescence intensity of the whole body determined densitometrically by using ImageJ software. **C**, transgenic TJ375 worms were treated with 200 µg mL-1 EE extract for 72 h and then exposed to juglone (20 µM). After 24 h, the expression of GFP::hsp-16.2 was evaluated. On the left, representative images of GFP fluorescence in untreated worms (up) and in worms treated with extract (below); On the right, the relative fluorescence of the heads determined densitometrically by using ImageJ software. **D**, transgenic CF1553 worms were treated with 200 µg mL-1 EE extract for 72 h and then the expression of GFP::sod-3 was evaluated. On the left, representative images of GFP fluorescence in untreated worms (up) and in worms treated with extract (below); On the right, the relative fluorescence of the tails determined densitometrically by using ImageJ software. In the Figure, black bars refer to control worms, light grey bars refer to worms treated with EE, white bars refer to worms treated with EGCG (used as positive control), whereas dark grey bars refer to worms treated with buffer (DMSO). In **B**, **C** and **D** histograms data are presented as percentage of the mean pixel intensity of each treatment, with respect to control worms (mean ± SD, n=40, replicated at least 3 times). Images were taken with BZ9000 from Keyence, scale bar = 100 µm. *** indicates $p < 0.001$, **** indicates $p < 0.0001$, compared to the untreated worms by one-way ANOVA followed by Bonferroni (post-hoc).

Afterwards, the ability of EE in counteracting ROS production was evaluated. As reported in the histograms of **Figure 2B**, significant lower fluorescence intensity was observed in nematodes N2 treated with EE (about 50%, light grey bar) with respect to the untreated control group (black and darker grey bars).

Subsequently, the expression of heat shock protein *hsp-16.2* was evaluated. The family of HSPs proteins is found in almost all living organisms and its expression is mainly induced by heat shock or oxidative stress[27]. Thus, the mutant strain TJ375, which has a *hsp-16.2* promoter fused to a GFP reporter was incubated with EE (72 h) in the presence of 20 µM juglone (24 h). Worms pre-treated with the extract showed extremely low expression of *hsp-16.2* (about 60%, **Figure 2C**, light grey bar) when compared to stressed worms (**Figure 2C**, black and dark grey bars).

As SOD is believed to act as the first line of defense in the disposal of ROS, the effect of EE (72 h) on *sod-3* expression was analyzed by using the mutant strain CF1553, which has a *sod-3* promoter fused to a GFP reporter. A significant higher expression of *sod-3::GFP* was detected in worms treated with EE (about 42% increase, **Figure 2D**, light grey bar) in comparison with control worms (**Figure 2D**, black and dark grey bars).

Therefore, these results indicate that EE extract exerts its antioxidant activity not only by scavenging ROS production, but also by modulating the expression of stress response genes, such as *sod-3* and *hsp-16.2*.

Finally, we analyzed the subcellular localization of *daf-16/FOXO*, which is the main transcription factor involved in the regulation of stress response genes (**Figure 3A**).

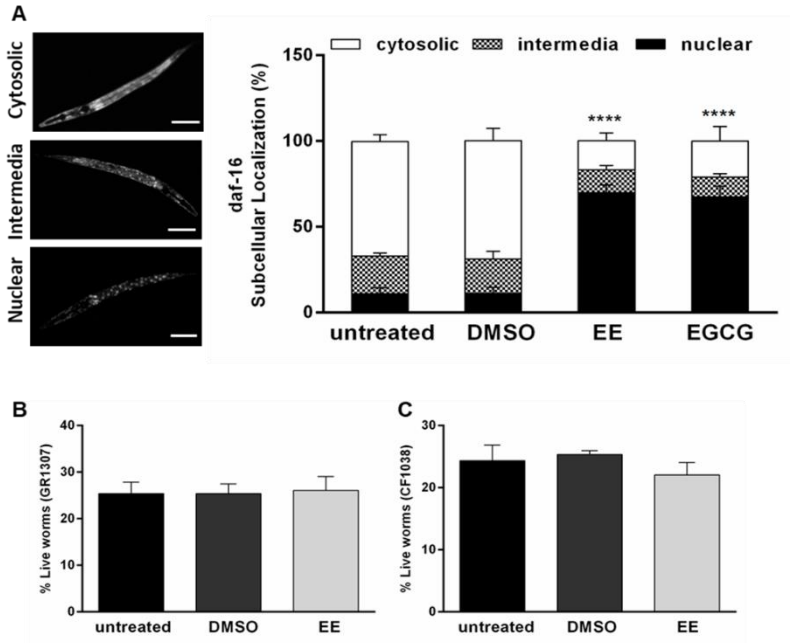

Figure 3: Pathway activated by EE in *C. elegans*. A, transgenic TJ356 worms were treated with 200 µg mL^{-1} EE extract for 24 h and then *GFP::daf-16* localization was evaluated. On the left, representative images of different GFP localization. On the right, histograms reporting the percentage of worms exhibiting a DAF-16 sub-cellular localization pattern, namely cytosolic (white bars), intermediate (checked bars) and nuclear (black bars). Data are presented as mean ± SD (n=40, replicated at least 3 times). Images were taken with BZ9000 from Keyence, scale bar = 100 µm. **** indicates p< 0.0001, compared to the untreated worms by one-way ANOVA followed by Bonferroni (post-hoc). **B-C**, a *daf-16* null mutant (GR1307) and *daf-16* loss-of-function mutant (CF1038) worms were treated with 200 µg mL^{-1} EE extract (light grey bars) for 48 h and then exposed to lethal dose of juglone (80 µM). After 24 h, alive and dead worms were counted and the survival rate was reported. Data are presented as mean ± SD (n=40, replicated 3 times).

Under physiological conditions, DAF-16/FOXO remains inactive in the cytosol, whereas, some environmental or stress conditions can stimulate its translocation to the nucleus, where it induces the expression of different genes involved in stress response, metabolism and longevity.

The mutant strain TJ356 has a *daf-16* fused withto a GFP reporter and was used to detect *daf-16::*GFP localization. As shown in Figure 3A, worms pretreated in the presence of EE (24 h) showed a higher percentage of *daf-16*::GFP nuclear localization (about 70%), with respect to untreated worms (12%). This pathway was further confirmed by performing survival assays with a *daf-16* loss-of-function mutant (CF1038) and a d*af-16* null mutant (GR1307) grown in the presence of EE (48 h). In both cases, the extract had no effect on the survival rate of the worms (**Figure 3B** and **C**, light grey bars), in contrast to the results obtained with N2 worms (**Figure 2A**).

7.3.4 Identification of active compounds

EE was then fractionated by HPLC and the elution profile is shown in **Figure S2A, Appendix C**. Thirteen fractions were manually collected and tested for antioxidant activity on LoVo cells by measuring intracellular GSH in the presence or absence of oxidative stress (300 µM SA). As shown in **Appendix C** (**Figure S2B**), fractions 8, 9, 11 and 12 had no effect on GSH levels when tested alone, but showed a high protective effect against oxidative stress. To verify the occurrence of additive effects, the active fractions were combined and tested on LoVo cells, in the presence or absence of SA damage, and the results, shown in **Appendix C** (**Figure S2B**), suggested the presence of additive effects.

The active fractions were further analyzed by LC-MS and MALDI-TOF/TOF for the identification of the main agents responsible for their bioactivity. The LC-MS TIC chromatogram of each fraction is reported in **Appendix C** (**Figure S2C-F**). A similar profile for the four fractions was observed, although relevant differences in their relative abundance were recorded. The base peak chromatogram of an ethanol extract with the identification of the most abundant peaks is reported in **Appendix C** (**Figure S3**) while mass spectral identification of each peak is reported in **Appendix C (Table I)**. The assignment of species to each mass peak is based on the interpretation of MALDI-TOF/TOF spectra and on the comparison with literature data[29-31]. By LC-TOF analysis, we found several saturated and polyunsaturated chain fatty acids, consisting of their radical species, dimeric forms and sodium adducts (**Appendix C, Table I**) as shown as an example in **Appendix C** (**Figure S4**). This finding is not surprising, as Bergé et colleagues[32] reported the analysis of fatty acids (FAs) from different microalgae strains. Although a variable content of proteins and lipids depending on the specific algal strain and growth conditions was detected in microalgae[33], they show a high amount of lipids[34]. In this context, Richards et al. demonstrated that long chain polyunsaturated fatty acids (LC-PUFAs) of the omega-3 series act as indirect antioxidants *in vitro*[35].

Besides FAs, different antioxidant molecules, well documented in literature, were identified by LC-TOF analysis and confirmed by tandem MS. In particular, carotenoids, such as astaxanthin and its sodiated form (596.4 Da,), and porphyrins, as chlorophyll c2 (609.3 Da), pheophorbide a (593.3 Da) and thioether porphyrin (611.4 Da) were found to be present[36,37]. A MALDI-TOF/TOF spectrum is reported for chlorophyll C2, with the structures drawn for the most intense fragments (**Appendix C, Figure S5**). Interestingly, the chlorophylls esterified with unsaturated long chain fatty acid, e.g. Pheophytin a' (871.2 Da, **Appendix C, Figure S6**) and hydroxylated chlorophyll a (908.9 Da, **Appendix C, Figure S7**), were detected only by MALDI.

The other fragmentation spectra were collected in **Appendix C** (**Figures S8-11**). Finally, a derivate quercetin and some triacylglycerols were found exclusively in fractions 8 and 9, respectively.

7.4 Conclusions

In this study, a new strategy for a sequential recovery of starch and antioxidants was proposed and validated. We found that, after starch extraction from *C. sorokiniana*, the waste product was able to counteract oxidative stress, both in a cell-based model and in vivo, as many carotenoids, chlorophylls and FAs are present. While the antioxidant activity of the first two class of molecules identified is well documented, the literature is still quiescent on the FAs antioxidant activity. However, some studies are reported on the impact of polyunsaturated fatty acids (PUFAs) intake on oxidative stress, as omega-3 PUFAs have been shown to reduce lipoperoxidation levels, advance glycation end products, increase SOD/CAT enzymatic ratio in the livers of diabetic rats fed with a high fat thermolyzed diet (rich in advanced glycation end-products)[35,38]. These properties, together with the reported inhibition of hepatic lipogenesis afforded by EPA and DHA[39], suggest a multifaceted healthful activity of omega-3 fatty acids supplementation in liver disorders. We still do not know to which class of molecules the antioxidant activity is due, or if there is a synergistic effect among them, and further analysis will be performed to shed light on this issue. It has to be taken into account, however, that, to date, papers claim the multiproduct biorefinery of algae, but no cascade or validation of the obtained products are reported[5,40,41]. The physic-chemical characterization of the starch granules, extracted with the method here reported, was already carried out[6] and its properties suggest interesting industrial application: emulsifier for food and pharmaceuticals, bioplastics, textiles and paper preservation. The novelty of the present work is in the proved feasibility of the cascade approach to isolate two different high value products, starch and antioxidants in developing markets.

7.5 References

1. Chew, K. W. … Chang, J.-S. Microalgae biorefinery: High value products perspectives. *Bioresour. Technol.* **229**, 53–62 (2017).

2. Monari. C., Righi, S. & Olsen, S. I. Greenhouse gas emissions and energy balance of biodiesel production from microalgae cultivated in photobioreactors in Denmark: A life-cycle modeling. *J. Clean. Prod.* **112**, 4084–4092 (2016).

3. Santos-Ballardo, D. U., Rossi, S., Reyes-Moreno, C. & Valdez-Ortiz, A. Microalgae potential as a biogas source: current status, restraints and future trends. *Rev. Environ. Sci. Bio/Technology* **15**, 243–264 (2016).

4. Carboni, S., Clegg, S. H. & Hughes, A. D. The use of biorefinery by-products and natural detritus as feed sources for oysters (Crassostrea gigas) juveniles. *Aquaculture* **464**, 392–398 (2016).

5. Ruiz, J. … Barbosa, M. J. Towards industrial products from microalgae. *Energy Environ. Sci.* **9**, 3036–3043 (2016).

6. Gifuni, I. … Marzocchella, A. Microalgae as new sources of starch: Isolation and characterization of microalgal starch granules. *Chem. Eng. Trans.* **57**, 1423–1428 (2017).

7. Goiris, K. … Muylaert, K. Impact of nutrient stress on antioxidant production in three species of microalgae. *Algal Res.* **7**, 51–57 (2015).

8. Pulz, O. & Gross, W. Valuable product from biotechnology of microalgae. *Appl. Microbiol. Biotechnol.* **65**, 635–648 (2004).

9. Shimidzu, N., Goto, M. & Miki, W. Carotenoids as singlet oxygen quenchers in marine organisms. *Fish. Sci.* **62**, 134–137 (1996).

10. Olivieri, G. … Pollio, A. Effects of photobioreactors design and operating conditions on *Stichococcus bacillaris* biomass and biodiesel production. *Biochem. Eng. J.* **74**, 8–14 (2013).

11. I. Gifuni, A. Pollio, G. Olivieri, A. Marzocchella. Identification of an industrial microalgal strain for starch production in biorefinery context: the effect of nitrogen and carbon concentration on starch accumulation. *New Biotechnol. J.* (2017).

12. Aremu, A. O. … Van Staden, J. Changes in phytochemical content and pharmacological activities of three Chlorella strains grown in different nitrogen conditions. *J. Appl. Phycol.* **28**, 149–159 (2016).

13. Breuer, G. … Lamers, P. P. Analysis of fatty acid content and composition in microalgae. *J. Vis. Exp.* (2013). doi:10.3791/50628

14. Chen, Y. & Vaidyanathan, S. Simultaneous assay of pigments, carbohydrates, proteins and lipids in microalgae. *Anal. Chim. Acta* **776**, 31–40 (2013).

15. Gifuni, I., Olivieri, G., Pollio, A., Franco, T. T. & Marzocchella, A. Autotrophic starch production by *Chlamydomonas* species. *J. Appl. Phycol.* 1–10 (2016). doi:10.1007/s10811-016-0932-2

16. Wellburn, A. R. The spectral determination of chlorophylls a and b, as well as total carotenoids, using various solvents with *Spectrophotometers* of different resolution. *J. Plant Physiol.* **144**, 307–313 (1994).

17. Petruk, G. … Monti, D. M. D. M. An ascorbic acid-enriched tomato genotype to fight UVA-induced oxidative stress in normal human keratinocytes. *J. Photochem. Photobiol. B Biol.* **163**, 284–289 (2016).

18. Del Giudice, R. … Rigano, M. M. Carotenoids in fresh and processed tomato (Solanum lycopersicum) fruits protect cells from oxidative stress injury. *J. Sci. Food Agric.* **97**, 1616–1623 (2016).

19. Del Giudice, R. … Rigano, M. M. Antioxidant bioactive compounds in tomato fruits at different ripening stages and their effects on normal and cancer cells. *J. Funct. Foods* **18**, (2015).

20. Stiernagle, T. Maintenance of *C. elegans*. *WormBook* (2006). doi:10.1895/wormbook.1.101.1

21. Abbas, S. & Wink, M. Green tea extract induces the resistance of *Caenorhabditis elegans* against oxidative stress. *Antioxidants* **3**, 129–43 (2014).

22. Zhu, L. Biorefinery as a promising approach to promote microalgae industry: An innovative framework. *Ren. Sust. Ener. Rev.* 41: 1376–1384 (2015).

23. Akanda, M., Tae, H., Kim, I., Ahn, D. & Tian, W. Hepatoprotective role of hydrangea macrophylla against sodium arsenite-Induced mitochondrial-dependent oxidative stress via the inhibition of MAPK/ Caspase-3 Pathways. *Int. J. Mol. Sci.* **18**, 1–15 (2017).

24. Maheshwari, N., Khan, F. & Mahmood, R. Sodium meta-arsenite induced reactive oxygen species in human red blood cells: impaired antioxidant and membrane redox systems, haemoglobin oxidation, and morphological changes. *Free Radic. Res.* **51**, 1–49 (2017).

25. Bischof, L. J., Huffman, D. L. & Aroian, R. V. Assays for toxicity studies in *C. elegans* with Bt crystal proteins. *Methods Mol. Biol.* **351**, 139–54 (2006).

26. Abbas, S. & Wink, M. Green tea extract induces the resistance of *Caenorhabditis elegans* against oxidative stress. *Antioxidants* **3**, 129–43 (2014).

27. Santoro, M. G. (2000) Heat shock factors and the control of the stress response. *Biochem.Pharmacol.* **59**, 55–63.

28. Juin, C., Bonnet, A., Nicolau, E., Bérard, J. & Devillers, R. UPLC-MSE Profiling of phytoplankton metabolites: Application to the identification of pigments and structural analysis of metabolites in porphyridium. *Mar. Drugs* **13**, 2541–2558 (2015).

29. Gilbert-López, B., Mendiola, J. & Fontecha, J. Downstream processing of *Isochrysis galbana*: a step towards microalgal biorefinery. *Green Chem.* **17**, 4599–4609 (2015).

30. Lang, I., Hodac, L. & Friedl, T. Fatty acid profiles and their distribution patterns in microalgae: a comprehensive analysis of more than 2000 strains from the SAG culture collection. *BMC Plant Biol.* **11**, 124 (2011).

31. Flamini, R. & Traldi, P. Mass Spectrometry in grape and wine analysis. *Mass Spectrometry Rev.* **22**, (2010).

32. Bergé, J. P. & Barnathan, G. Fatty acids from lipids of marine organisms: Molecular biodiversity, roles as biomarkers, biologically active compounds, and economical aspects. *Adv. Biochem. Engin./Biotechnol.* **96**, 49–125 (2005).

33. Duong, V. T. … Schenk, P. M. High protein- and high lipid-producing microalgae from northern australia as potential feedstock for animal feed and biodiesel. *Front. Bioeng. Biotechnol*. **3**, 53 (2015).

34. Sharma, K., Li, Y. & Schenk, P. UV-C-mediated lipid induction and settling, a step change towards economical microalgal biodiesel production. *Green Chem.* **16**, 3539–3548 (2014).

35. Richard, D., Kefi, K., Barbe, U., Bausero, P. & Visioli, F. Polyunsaturated fatty acids as antioxidants. *Pharmacol. Res.* **57**, 451–455 (2008).

36. Serrano, Gustavo A., M. N. Natural astaxanthin, antioxidant protection power for healthy eyes. *Agro. FOOD Ind. Hi Tech* **25**, (2014).

37. Wang, E. & Wink, M. Chlorophyll enhances oxidative stress tolerance in *Caenorhabditis elegans* and extends its lifespan. *PeerJ* **4**, e1879 (2016).

38. de Assis, A. M. … Moreira, J. C. Ω3-Polyunsaturated fatty acids prevent lipoperoxidation, modulate antioxidant enzymes, and reduce lipid content but do not alter glycogen metabolism in the livers of diabetic rats fed on a high fat thermolyzed diet. *Mol. Cell. Biochem.* 1–10 (2011). doi:10.1007/s11010-011-1099-4

39. Lamaziere, A., Wolf, C., Barbe, U., Bausero, P. & Visioli, F. Lipidomics of hepatic lipogenesis inhibition by omega 3 fatty acids. Prostaglandins Leukot. *Essent. Fat. Acids* **88**, 149–154 (2013).

40. Laurens, L. M. L. … Pienkos, P. T. Development of algae biorefinery concepts for biofuels and bioproducts; a perspective on process-compatible products and their impact on cost-reduction. *Energy Environ. Sci.* **10**, 1716–1738 (2017).

41. Safi, C. … Pontalier, P.-Y. A two-stage ultrafiltration process for separating multiple components of *Tetraselmis suecica* after cell disruption. *J. Appl. Phycol.* **26**, 2379–2387 (2014).

.

CHAPTER 8

General discussion

https://www.shutterstock.com

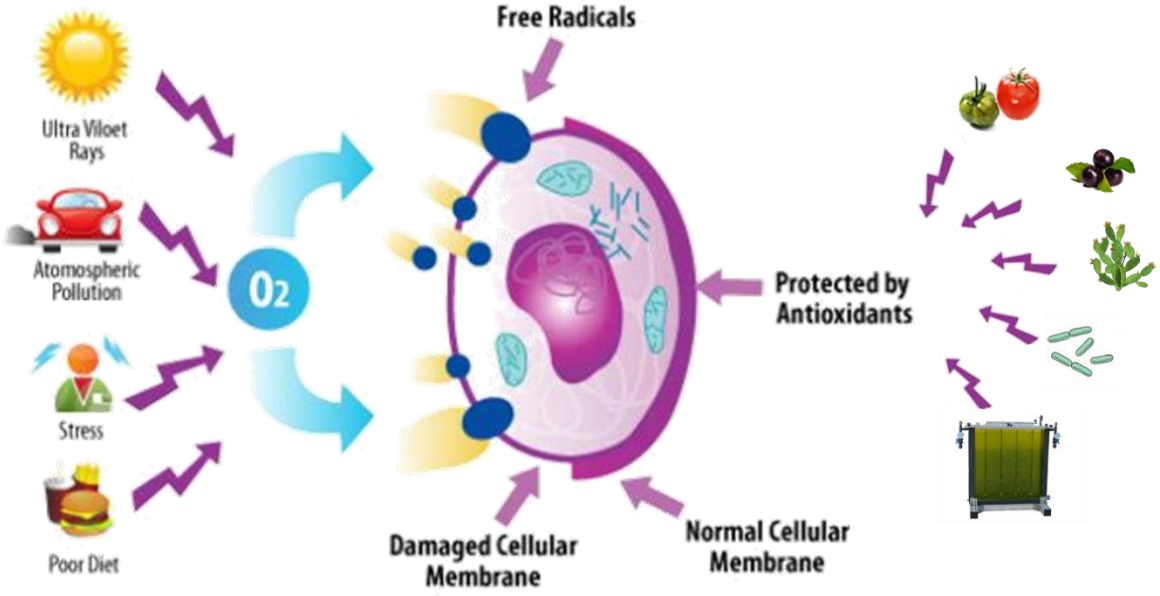

Image taken from http://www.in-corpore.ch

General discussion

The search, characterization and application of antioxidants remains in the focus of numerous research teams all over the world. In particular, the interest in natural antioxidants is increasing in the last years, mostly because of the elevated production costs and the potential toxicity of synthetic antioxidants, as well as because of a general consumer preference towards natural food additives[1]. Moreover, natural molecules show a wide range of applications, which comprise the use of anti-oxidative phytochemicals as functional ingredients for pharmaceuticals, functional foods, dietary supplements, animal feed, cosmetics and other products.

Of course, in the case of synthetic antioxidants, it is relatively easy to find which antioxidant and which dose can be considered as safe, as the safety tests are easy to be done[2]. Instead, in the case of antioxidants extracted from natural sources, the presence of mixtures with several active substances make the identification and quantification of the single contribute of each molecule particularly difficult. In addition to active substances, natural products contain other components, the safety of which is often not completely known. However, it is assumed that products consumed since a long time are safe, as people have adapted them as a part of the diet and no acute toxicity has been observed so far, even if the effects of long-time exposure on health has not been examined in detail.

The aim of the present PhD project was to analyse the antioxidant activity of extracts obtained from different natural sources or microorganisms, in order to study their beneficial effects against oxidative stress injury and to characterize their chemical composition to obtain molecules with potential applications in food or cosmetic industry.

Fruits and vegetables are rich in antioxidants and are thought to be able to prevent chronic human diseases, such as cancer and cardiovascular diseases, acting as free radical scavengers[3,4]. One of the products continuously consumed in the so-called Mediterranean and Asian diet, considered as healthy feeding habits, is tomato[5–7]. This vegetable, rich in different active molecules, is consumed either fresh or processed into a wide range of manufactured products[8]. Therefore, the attention was focused on studying the beneficial extracts from two different type of tomatoes:

- Zebrino (ZBR), a commercial variety;
- a new hybrid (DHO), obtained through quantitative trait loci pyramiding.

The antioxidant activity of lipophilic ZBR tomato extracts, before and after thermal processing, was analyzed. It is known that some antioxidants loose their activity when cooked[9], but lycopene is absorbed more efficiently from processed tomato products compared to raw tomatoes. This is due to the degradation *via* isomerization of the *all -trans* to the *cis*-form, and it is known that the bioavailability of *all –cis*-isomers in foods is higher than that of *all –trans* –isomers[10]. The lipophilic extract from this cultivar, before and after processing, had no effect on the growing of different cell lines, and it showed a protective effect when cells were exposed to oxidative stress injury. It was also found that lycopene was the molecule responsible for counteracting damage caused by oxidative stress, even if to a lower extent with respect to the whole extract, thus supporting the idea of synergism between the molecules present in the analyzed tomato cultivar.

Then, the attention was focused on a new tomato hybrid, obtained by pyramiding specific loci of *S. pennellii* into *S. lycopersicum* genome. These loci are responsible for high AsA and phenolic compounds production. These lines have been crossed to obtain a double homozygote (DHO). DHO hydrophilic extracts were tested on normal human keratinocytes. The extract had anti-proliferative activity on human cancer cells whereas it was not toxic on normal cells[11]. In addition, it clearly showed protective effects from oxidative stress damage and inflammation induced by UVA radiations on human normal cells. It was found that AsA was the molecule responsible for the beneficial effect.

The extract from the Brazilian berry açai (*Euterpe oleracea* Martius) was then analyzed as its consumption is known, among local people, to have pro-healthy effects. The berry is highly rich in anthocyanins, molecules endowed with antioxidant activity and known to be responsible for the "French Paradox", which indicates anthocyanins as the antioxidants that protect French people from heart disease[12–17]. French are known to consume large amounts of coffee, nicotine, sugar, white flour, cheese and saturated fats, yet they have a very low rate of heart disease compared to neighbouring, such as the English and Danish. The reason for this low rate is thought to be in the consume of red wine, rich in anthocyanins. Noteworthy, red wine has lower amount of anthocyanins with respect to the açai berry. Moreover, açai is rich in other phenols, vitamins B, minerals, fiber, proteins, omega-3 fatty acids and oleic acid (omega-9)[18,19]. Thus, the hydrophilic extract from açai fruits was used to study its health benefits also on fibroblasts exposed to UVA radiations. After having evaluated its excellent antioxidant activity, the extract was fractionated by reverse HPLC and mass spectral identification showed the presence of two different predominant compounds, malvidin-petunidin-glucoside-epicatechin and cyanidin-3-O-(6-O-p-coumaryl)-monoglucoside. These molecules, characterized by a different number of aromatic rings, were able to protect fibroblasts from the negative effects induced by UVA. It is well documented that the effectiveness of natural antioxidants is due to their aromatic rings, and their antioxidant power is generally proportional to the number of −OH groups present on the aromatic ring(s)[20]. This extract, as well as its partially purified fractions, were also added to the cells, after exposure to UVA radiations, to verify their ability to heal cells from the damage caused by the exposure to a stress agent. The results were surprisingly good, as the extract and its fractions were able to restore normal intracellular ROS and GSH levels and to inhibit MAPK cascade activation. This finding opens the way to new prospects for its use: as additive in food or in after-sun creams.

Despite all the excellent evidence obtained with the extracts from the above-mentioned products, it has to be considered that organic solvents were used to extract antioxidants. To date, solvent extractions are the most commonly used procedures to prepare extracts from plant materials due to their ease of use, efficiency, and wide applicability. It is generally known that the yield of chemical extraction depends on the polarity of the solvent, the extraction time and temperature, sample-to-solvent ratio as well as on the chemical composition and physical characteristics of the sample. Therefore, there is no universal extraction procedure suitable for extraction of all plant active molecules[21]. However, there are some inconveniences in using organic solvents:

1. they can extract some unwanted components, such as sugars, organic acids and fats, so that consequently additional steps maybe required to remove those;

2. organic solvents have elevated costs and they require energy to remove them, with a consequent increase in the costs;
3. some of them are toxic, even if present in traces, on human health.

In order to avoid the toxicity of commonly used solvents (methanol, hexane, acetonitrile), açai active molecules were extracted with different solvents, such as ethanol and isopropanol, which are considered as safe (law 2009/32/CE) and then the antioxidant activity was evaluated on cells. Different experimental conditions (light, time of incubation, temperature, buffer) were evaluated on stressed cells and a good antioxidant activity was recovered after up to 10 weeks incubation at room temperature in the dark (**Appendix D**).

Starting from these promising results, the attention was focused on a previously reported water extract from the cladodes of *Opuntia ficus-indica*[22], which represents the non-edible part of the plant. Authors demonstrated that the *Opuntia* raw extract (ORE), obtained by simple mechanical press, was rich in phenolic derivatives, i.e. piscidic, eucomic and 2-hydroxy-4-(4'-hydroxyphenyl)-butanoic acids[22]. ORE and its active molecules were thus tested for their ability to protect human keratinocytes from UVA induced oxidative stress. The results obtained clearly showed the antioxidant activity of the extract on the cell-based model. Moreover, the presence of carbohydrates in the extract is very useful, as their capability to form a molecular network and to retain huge amount of water can act as a protective layer on mucosal surfaces accelerating the re-epithelization of dermal wound[23–25].

Plants and their fruits are not the only source of antioxidants, but they are also metabolites produced by microbes[26–28]. For instance, recently, some *Streptomyces* bacteria strains were isolated and an *in vitro* antioxidant characterization was performed[29–31]. In this context, two bacteria were evaluated for their antioxidant activity: a member of *Sphingomonadales* and a *Bacillus subtilis*. While in the first case antioxidants from the bacterium were extracted, in the second case the whole spore from the bacterium was used as antioxidant.

Novosphingobium sp. PP1Y isolated and microbiologically characterized[32,33], is part of a group of Gram-negative α-proteobacteria, whose genomes show the presence of a great abundance of glycosyl hydrolases, glycosyltransferases and carotenoids. Lipophilic extract of this bacteria was used to analyse its antioxidant activity *in vitro* (eukaryotic cells) as well as *in vivo* (*C. elegans*). In both cases, it showed excellent antioxidant capacity in the protection of cells and worms against different stress inductors. In addition, the whole extract was fractionated and the active fractions were analyzed by mass spectrometry. It was found that the antioxidant activity of this extract was probably due to the presence of nostoxanthin.

Bacillus subtilis is a bacterium found on skin, in the digestive tract, in epithelial wounds, on extremities of the human body, in livestock and in soil[34,35]. As it is ubiquitous, it has developed adaptive strategies to subsist in diverse environments *via* the production and secretion of a large number of genetically encoded molecules that control the growth of neighbouring organisms[36,37]. For this reason, *B. subtilis* is commercially sold as a skincare product, a food ingredient for human consumption, animal feed, fertilizer, an antibiotic substitute and oral probiotic[38]. In fact, ingestion of *B. subtilis* can restore the normal microbial flora. Therefore, it was hypothesized an alternative usage of this microorganism by exploiting its resistance properties against adverse conditions. *B. subtilis* spores were used as antioxidants on human normal keratinocytes in the presence of oxidative stress and then different oxidative stress markers were studied to confirm spores' protective effects. Interestingly, the cells were

able to resist to stress damage not because the spores reduced ROS production, but because the incubation with spores induced the activation of Nrf-2 pathway in cells. This result was not surprising, as Gut bacteria (as *B. subtilis* and *L. plantarum*) stimulate ROS production in epithelial cells by an enzymatic mechanism analogous to the pathogen-induced respiratory burst in phagocytes[39,40]. Interestingly, enzymatically generated ROS in the epithelia is stimulated not only by potential pathogens but also by symbiotic bacteria, especially members of the *lactobacilli* taxon, and promotes cell proliferation and migration[41,42], accelerates restitution post injury[43], and modifies epithelial NF-kB signaling[44]. Jones and collaborators demonstrated that lactobacilli can induce proliferation in cells of the intestinal epithelium by generation of physiological levels of ROS[40]. These low levels of ROS, induced the dissociation of Keap1 from Nrf2, which translocates to the nucleus and binds to Antioxidant Response Element (ARE) sequences and initiates the transcription of antioxidant enzymes and detoxifying proteins[45].

Finally, minimizing the dependence on fossil-based resources and reducing the generation of solid and liquid wastes represent one of the main challenges for the modern society[46]. In fact, the European Union is committed to fostering resource efficiency and reducing its reliance on fossil resources, in favour of a circular and regenerative model that uses resources in a smart and efficient way, developing a circular economy and broadening the Union's bio-economy. In this context, microalgae have gained considerable importance due to potential exploitation in several markets, from simple biomass production for food and feed to high-value added product applications[47,48]. However, the market of these applications is still developing and prudent strategies must be adopted to compensate the high cost of cultivation: the exploitation of the several components of microalgae according to the biotechnological route is a potential strategy[49]. A practical case is the valorisation of starch fraction for food and other applications: the production cost is expected to be too high to be competitive. Therefore, in the idea of circular bio-economy, a new extraction technique to obtain starch from *Chlorella sorokiniana* Shihiraet Krauss has been exploited[47], given that the discarded fraction after this extraction process is very rich in antioxidants. The extract obtained from *C. sorokiniana* was analyzed on an *in vivo* system (*C. elegans*) and it was able to rescue worms from oxidative stress by activating DAF-16/FOXO transcription factor, which plays a role similar to Nrf-2 in mammals. Long chain polyunsaturated fatty acids (PUFA), carotenoids, porphyrins, a derivate of quercetin and some triacylglycerols were found to be the molecules responsible for the antioxidant activity.

In conclusion, in the present PhD thesis, many antioxidants from natural sources have been isolated and tested, and these extracts have a similar antioxidant power with respect to the isolated molecules. This opens the way to the use of the whole extract in food or cosmetic industries, avoiding the high costs for the purification of single compounds and in accordance with the increasing demand of natural products endowed with pro-healthy effects. In particular, it has to be taken into account that during storage and transport, fresh fruit is exposed to mould spoilage, which is the main cause of postharvest decay, which results in a great economic loss. In this context, one should keep in mind that many natural antioxidant extracts, rich in polyphenols, are endowed with antimicrobial activity[50-52].Therefore, the use of natural extracts would be a valid alternative to synthetic fungicides, normally used to prevent postharvest disease in fruit and vegetables. In addition, coating fresh fruit with natural extracts may avoid or delay the oxidation process, increasing their shelf life[53].

In the case of food industry, adding the whole extract to edible biofilms, would protect food from oxidation processes and increase its nutritional values.

Finally, it will be also interesting to combine different extracts to study additive/synergistic effects. However, the approach is really complex, given that most free-radical scavengers act in oxidation-reduction reactions that are reversible, and some of them (e.g. ascorbate) can act both as antioxidants and pro-oxidants, depending on the conditions. In addition, given the role of ROS as mediators of normal signalling processes, the determination of the optimal dosage requires a fine tuning, to avoid side effects due to the perturbation of the redox balance required for the maintenance of normal cell functions. Therefore, an extensive study at a molecular level is required to develop an effective and side effect-free product.

Bibliography

1. Papas, A. M. Diet and antioxidant status. *Food Chem. Toxicol.* **37**, 999–1007 (1999).

2. Kroon, P. & Williamson, G. Polyphenols: Dietary components with established benefits to health? *J. Sci. Food Agric.* **85**, 1239–1240 (2005).

3. Russell, R. M. & Paiva, S. A. R. β-Carotene and other carotenoids as antioxidants. *J. Am. Coll. Nutr.* **18**, 426–433 (1999).

4. Astorg, P., Gradelet, S., Bergès, R. & Suschetet, M. Dietary lycopene decreases the initiation of liver preneoplastic foci by diethylnitrosamine in the rat. *Nutr. Cancer.* **29**, 60–8 (1997).

5. Li, Q. … McClements, D. J. Potential physicochemical basis of Mediterranean diet effect: Ability of emulsified olive oil to increase carotenoid bioaccessibility in raw and cooked tomatoes. *Food Res. Int.* **89**, 320–329 (2016).

6. E., Roemmich, J. & Claycombe, K. Federation of American Societies for Experimental Biology., Federation proceedings. *The FASEB Journal* **29**, (2015).

7. Xu, X. … Xie, L. Tomato consumption and prostate cancer risk: a systematic review and meta-analysis. *Sci. Rep.* **6**, 37091 (2016).

8. De Sousa, A. S., Borges, S. V., Magalhães, N. F., Ricardo, H. V. & Azevedo, A. D. Spray-dried tomato powder: Reconstitution properties and colour. *Brazilian Arch. Biol. Technol.* **51**, 807–814 (2008).

9. Thane, C. & Reddy, S. Processing of fruit and vegetables: effect on carotenoids. *Nutr. Food Sci.* **97**, 58–65 (1997).

10. Friedman, M. Anticarcinogenic, cardioprotective, and other health benefits of tomato compounds lycopene, α-tomatine, and tomatidine in pure form and in fresh and processed tomatoes. *J. Agric. Food Chem.* **61**, 9534–9550 (2013).

11. Rigano, M. M. … Barone, A. Quantitative trait loci pyramiding can improve the nutritional potential of tomato (*Solanum lycopersicum*) fruits. *J. Agric. Food Chem.* **62**, 11519–11527 (2014).

12. Lichtenthaler, R. … Marx, F. Total oxidant scavenging capacities of *Euterpe oleracea* Mart. (Açai) fruits. *Int. J. Food Sci. Nutr.* **56**, 53–64 (2005).

13. Mertens-Talcott, S. U. … Derendorf, H. Pharmacokinetics of anthocyanins and antioxidant effects after the consumption of anthocyanin-rich açai juice and pulp (*Euterpe oleracea* Mart.) in human healthy volunteers. *J. Agric. Food Chem.* **56**, 7796–7802 (2008).

14. Kang, J. … Wu, X. Bioactivities of açaí (*Euterpe precatoria* Mart.) fruit pulp, superior antioxidant and anti-inflammatory properties to *Euterpe oleracea* Mart. *Food Chem.* **133**, 671–677 (2012).

15. Kang, J. … Wu, X. Flavonoids from acai (*Euterpe oleracea* Mart.) pulp and their antioxidant and anti-inflammatory activities. *Food Chem.* **128**, 152–157 (2011).

16. Peixoto, H. … Wink, M. An anthocyanin-rich extract of açai (*Euterpe precatoria* Mart.) increases stress resistance and retards aging-related markers in *Caenorhabditis elegans*. *J. Agric. Food Chem.* (2016). doi:10.1021/acs.jafc.5b05812

17. Dias, M. M. dos S. … Mertens-Talcott, S. U. Anti-inflammatory activity of polyphenolics from açai (*Euterpe oleracea* Martius) in intestinal myofibroblasts CCD-18Co cells. *Food Funct*. **6**, 3249–3256 (2015).

18. Rufino, M. do S. M. … Saura-Calixto, F. Açaí (*Euterpe oleraceae*) 'BRS Pará': A tropical fruit source of antioxidant dietary fiber and high antioxidant capacity oil. *Food Res. Int.* **44**, 2100–2106 (2011).

19. Noratto, G. D., Angel-Morales, G., Talcott, S. T. & Mertens-Talcott, S. U. Polyphenolics from Açai (*Euterpe oleracea* Mart.) and red muscadine grape (*Vitis rotundifolia*) protect human umbilical vascular endothelial cells (HUVEC) from glucose- and lipopolysaccharide (LPS)-induced inflammation and target microRNA-126. *J. Agric. Food Chem.* **59**, 7999–8012 (2011).

20. Brewer, M. S. Natural antioxidants: Sources, compounds, mechanisms of action and potential applications. *Compr. Rev. Food Sci. Food Saf.* **10**, 221–247 (2011).

21. Dai, J. & Mumper, R. J. Plant phenolics: Extraction, analysis and their antioxidant and anticancer properties. *Molecules* **15**, 7313–7352 (2010).

22. Di Lorenzo, F. … Lanzetta, R. The polysaccharide and low molecular weight components of Opuntia ficus indica cladodes: Structure and skin repairing properties. *Carbohydr. Polym.* **157**, 128–136 (2017).

23. Galati, E. M., Monforte, M. T., Tripodo, M. M., D'Aquino, A. & Mondello, M. R. Antiulcer activity of *Opuntia ficus indica* (L.) Mill. (*Cactaceae*): Ultrastructural study. *J. Ethnopharmacol.* **76**, 1–9 (2001).

24. Galati, E. M., Pergolizzi, S., Miceli, N., Monforte, M. T. & Tripodo, M. M. Study on the increment of the production of gastric mucus in rats treated with *Opuntia ficus indica* (L.) Mill. cladodes. *J. Ethnopharmacol.* **83**, 229–233 (2002).

25. Kaur, M., Kaur, A. & Sharma, R. Pharmacological actions of *Opuntia ficus indica* : *A Review*. http://www.japsonline.com/counter.php?aid=541 2, 15–18 (2012).

26. Juan, M. Y. & Chou, C. C. Enhancement of antioxidant activity, total phenolic and flavonoid content of black soybeans by solid state fermentation with *Bacillus subtilis* BCRC 14715. *Food Microbiol.* **27**, 586–591 (2010).

27. Rakesh, O. D., Pathak, R., Dhaker, A. S., Arora, R., Kumar, R., Rajaram, R., & Gautam, H. K. Biology, I. Isolation , characterization , and bioactivity of deep sea bacteria with special reference to induction of antibacterial and antioxidant metabolites. *Can. J. Pure Appl. Sci.* **5**, 1363–1370 (2011).

28. Sadrati, N., Daoud, H., Zerroug, A., Dahamna, S. & Bouharati, S. Screening of antimicrobial and antioxidant secondary metabolites from endophytic fungi isolated from wheat (*Triticum Durum*). *J. Plant Prot. Res.* **53**, 128–136 (2013).

29. Rao, A. V. & Rao, L. G. Carotenoids and human health. *Pharmacol. Res.* **55**, 207–216 (2007).

30. Ser, H. L. … Lee, L. H. Presence of antioxidative agent, Pyrrolo[1,2-a]pyrazine-1,4-dione, hexahydro- in newly isolated *Streptomyces mangrovisoli* sp. nov. *Front. Microbiol.* **6**, 854 (2015).

31. Tan, L. T.-H. … Goh, B.-H. Investigation of antioxidative and anticancer potentials of *Streptomyces* sp. MUM256 isolated from Malaysia mangrove soil. *Front. Microbiol.* **6**, 1316 (2015).

32. Notomista, E. … Di Donato, A. The marine isolate *Novosphingobium* sp. PP1Y shows specific adaptation to use the aromatic fraction of fuels as the sole carbon and energy source. *Microb. Ecol.* **61**, 582–594 (2011).

33. D'Argenio, V. … Di Donato, A. Complete sequencing of *Novosphingobium* sp. PP1Y reveals a biotechnologically meaningful metabolic pattern. *BMC Genomics* **15**, 384 (2014).

34. Ara, K. … Tomita, F. Foot odor due to microbial metabolism and its control. *Can. J. Microbiol.* **52**, 357–364 (2006).

35. Earl, A. M., Losick, R. & Kolter, R. Ecology and genomics of Bacillus subtilis. *Trends in Microbiol.* **16**, 269–275 (2008).

36. Liu, K.-F., Chiu, C.-H., Shiu, Y.-L., Cheng, W. & Liu, C.-H. Effects of the probiotic, *Bacillus subtilis* E20, on the survival, development, stress tolerance, and immune status of white shrimp, Litopenaeus vannamei larvae. *Fish Shellfish Immunol.* **28**, 837–844 (2010).

37. Stein, T. *Bacillus subtilis* antibiotics: Structures, syntheses and specific functions. Molecular *Microbiol.* **56**, 845–857 (2005).

38. Green, D. H. … Cutting, S. M. Characterization of two *Bacillus* probiotics. *Appl. Environ. Microbiol.* **65**, 4288–4291 (1999).

39. Alam, A. … Neish, A. S. Redox signaling regulates commensal-mediated mucosal homeostasis and restitution and requires formyl peptide receptor 1. *Mucosal Immunol.* **7**, 645–655 (2014).

40. Jones, R. M. … Neish, A. S. Symbiotic lactobacilli stimulate gut epithelial proliferation via Nox-mediated generation of reactive oxygen species. *EMBO J.* **32**, 3017–3028 (2013).

41. Wentworth, C. C., Jones, R. M., Kwon, Y. M., Nusrat, A. & Neish, A. S. Commensal-epithelial signaling mediated *via* formyl peptide receptors. *Am. J. Pathol.* **177**, 2782–2790 (2010).

42. Wentworth, C. C., Alam, A., Jones, R. M., Nusrat, A. & Neish, A. S. Enteric commensal bacteria induce extracellular signal-regulated kinase pathway signaling *via* formyl peptide receptor-dependent redox modulation of dual specific phosphatase. *J. Biol. Chem.* **286**, 38448–38455 (2011).

43. Swanson, P. A. … Neish, A. S. Enteric commensal bacteria potentiate epithelial restitution via reactive oxygen species-mediated inactivation of focal adhesion kinase phosphatases. *Proc. Natl. Acad. Sci.* **108**, 8803–8808 (2011).

44. Kumar, A. … Neish, A. S. Commensal bacteria modulate cullin-dependent signaling via generation of reactive oxygen species. *EMBO J.* **26**, 4457–4466 (2007).

45. Jones, C. L. HHS Public Access. 33, 395–401 (2015).

46. Liguori, R. & Faraco, V. Biological processes for advancing lignocellulosic waste biorefinery by advocating circular economy. *Biores.Technol.* **215**, 13–20 (2016).

47. Priyadarshani, I. & Rath, B. Commercial and industrial applications of micro algae – *A review*. *J. Algal Biomass Util.* **3**, 89–100 (2012).

48. Eppink, M. H. M. … Wijffels, R. H. From current algae products to future biorefinery practices: *A Review*. 1–25 (2017). doi:10.1007/10_2016_64

49. Villalobos, M. del C. … Córdoba, M. de G. Antioxidant and antimicrobial activity of natural phenolic extract from defatted soybean flour by-product for stone fruit postharvest application. *J. Sci. Food Agric.* **96**, 2116–2124 (2016).

50. Chen, J., Zhang, S. & Yang, X. Control of brown rot on nectarines by tea polyphenol combined with tea saponin. *Crop Prot.* **45**, 29–35 (2013).

51. Kossah Zhang, H., Chen,W., R. Antimicrobial and antioxidant activities of Chinese sumac (Rhustyphina L.) fruit extract. *Food Control* **22**, 128–132 (2011).

52. Gatto, M. A. … Di Venere, D. Activity of extracts from wild edible herbs against postharvest fungal diseases of fruit and vegetables. *Postharvest Biol. Technol.* **61**, 72–82 (2011).

53. Feliziani, E., Santini, M., Landi, L. & Romanazzi, G. Pre- and postharvest treatment with alternatives to synthetic fungicides to control postharvest decay of sweet cherry. *Postharvest Biol. Technol.* **78**, 133–138 (2013).

APPENDIX

List of Scientific publications:

I- Del Giudice, R., Arciello, A., Itri, F., Merlino, A., Monti, M., Buonanno, M., Penco, A., Canetti, D., **Petruk, G.**, Monti, S.M., Relini, A., Pucci, P., Piccoli, R., Monti, D.M., "*Protein conformational perturbations in hereditary amyloidosis: Differential impact of single point mutations in ApoAI amyloidogenic variants*". Biochim. Biophys. Acta - Gen. Subj., **2016**,1860(2), 434–444. doi.org/10.1016/j.bbagen.2015.10.019

II- Ferraro, G., Monti, D.M., Amoresano, A., Pontillo, N., **Petruk, G**, Pane, F., Amoresano, A., Merlino, A., "*Gold-based drug encapsulation within a ferritin nanocage: X-ray structure and biological evaluation as a potential anticancer agent of the Auoxo3-loaded protein*", Chem. Com., **2016**, 52, doi.org/10.1039/c6cc02516a

III- Petruk, G., Raiola, A., Del Giudice, R., Barone, A., Frusciante, L., Rigano, M.M., Monti, D.M., "*An ascorbic acid-enriched tomato genotype to fight UVA-induced oxidative stress in normal human keratinocytes*". J. Photochem. Photobio. B: Bio., **2016**, 163, 284-289, doi.org/10.1016/j.jphotobiol.2016.08.047 (**CHAPTER 2**)

IV- Del Giudice, R.*, **Petruk, G.***, Raiola, A., Barone, A., Monti, D.M., Rigano, M.M., "*Carotenoids in fresh and processed tomato (Solanum lycopersicum) fruits protect cells from oxidative stress injury*". J. Sci. Food Agri., **2017**, 97(5), 1616-1623, doi.org/10.1002/jsfa.7910 (**CHAPTER 2**)
* These authors equally contributed to this manuscripts

V- Petruk, G., Illiano, A., Del Giudice, R., Raiola, A., Amoresano, A., Rigano, M.M., Monti, D.M., "*Malvidin and cyanidin derivatives from açai fruit (Euterpe oleracea Mart.) counteract UV-A-induced oxidative stress in immortalized fibroblasts*". J. Photochem. Photobio. B: Bio., **2017**, 172, 42-51, doi.org/10.1016/j.jphotobiol.2017.05.013 (**CHAPTER 3**)

VI- Monti, D.M., Ferraro G., **Petruk, G.**, Maiore, L., Pane, F., Amoresano, A., Cinellu, M.A., Merlino, A., "*Ferritin nanocages loaded with gold ions induce oxidative stress and apoptosis in MCF-7 human breast cancer cells*", Dalton Trans., **2017**, doi.org/10.1039/C7DT02370G

VII- Petruk, G., Di Lorenzo, F., Imbimbo, P., Silipo, A., Bonina, A., Riza, L., Piccoli, R., Monti, D.M., Lanzetta, R., "*Protective effect of Opuntia ficus-indica L. cladodes against UVA-induced oxidative stress in normal human keratinocytes*", Bioorg. Med. Chem. Lett. -**2017** 27(24), 5485-5489. (**CHAPTER 4**)

VIII- Raiola, A., Errico, A., **Petruk, G.**, Monti, D.M., Barone, A., Rigano, M.M., "*Bioactive compounds in Brassicaceae vegetables with a role in the prevention of chronic diseases*", Molecules, **2018** 23(1), 15; doi:10.3390/molecules23010015

IX- Sobeh, M., Esmat, A., **Petruk, G.**, Abdelfattah, M.A.O., Dmirieh, M., Monti, D.M., Abdel-Naim, A.B., Wink, M., "*Phenolic compounds from Syzygium jambos (Myrtaceae) exhibit distinct antioxidant and hepatoprotective activities in vivo*", J. Funct. Foods, -**2018** 41, 223-231, doi.org/10.1016/j.jff.2017.12.055

X- Sobeh, M., Youssef, F.S., Esmat, A **Petruk, G.**, El-Khatib, A.H., Monti, D.M., Ashourb, M.L., Wink, M., "*High resolution UPLC-MS/MS profiling of the polyphenolics in the methanol extract of Syzygium samarangense leaves and its hepatoprotective activity in rats with CCl4-induced hepatic damage",* Food Chem. Toxic., - **Minor revisions**

List of Scientific communications:

- ✓ **Petruk, G.**, Raiola, A., Del Giudice, R., Barone, A., Rigano, M. M., & Monti, D. M. "*A new tomato hybrid to fight UVA-induced (ultraviolet) oxidative stress"* 17th International Conference on Oxidative Stress Reduction, Redox Homeostasis & Antioxidants (Paris, France, 13-15 June). Journal of ISANH Volume 3: Special Issue for Paris Redox 2016 DOI: http://dx.doi.org/10.18143/JISANH_v3i3_1155.

- ✓ Ferraro, G., Monti, D.M., Amoresano, A., Pontillo, N., **Petruk, G.**, Pane, F., Cinellu, M.A., and Merlino, M. (2016) "*Encapsulation of gold-based drugs inside the ferritin nanocage*" XLIV Congresso della Divisione di Chimica Fisica della SCI (Naples, Italy, 20-23 September).

- ✓ Monti, M., Del Giudice, R., Arciello, A., Merlino, A., Buonanno, M., Penco, A., Canetti, D., **Petruk, G.**, Monti, S.M., Monti D.M. (2016) *"The impact of a single point mutation in the ApoAI triggering renal systemic amyloidosis"* International Conference: The kidney in genetic and rare deseases (Naples, Italy, 27-29 Octobre).

- ✓ **Petruk, G.**, Gifuni, I., Roxo, M., Olivieri, G., Marzocchella, A., Piccoli, A., Wink, M., Monti, D.M. "*Microalgae in circular economy: from waste to high value products*" 19th International Conference on Oxidative Stress Reduction, Redox Homeostasis and Antioxidants, (Paris, France, 26-27 June) Journal of ISANH Archive -Volume 5 Special Issue for Paris Redox 2017 DOI: 10.13140/RG.2.2.17132.05764.

- ✓ **Petruk, G.**, Del Giudice, R., Imbimbo, P., Di Lorenzo, F., Rigano, M.M., Lanzetta, R., Piccoli, R., Monti, D.M. "*Fighting UVA-induced oxidative stress with natural antioxidants*" I° GIORNATA S.I.R.R. 2017 – NAPOLI (Naples, Italy, 31 May), - **speaker**

- ✓ **Petruk, G.**, Gifuni, I., Roxo, M., Olivieri, G., Marzocchella, A., Piccoli, A., Wink, M., Monti, D.M. "*Microalgae in circular economy: from waste to high value products*" SIB 2017 – 59th Congress – Italian Society of Biochemistry and Molecular Biology (Caserta, Italy, 20-22 September)

- ✓ **Petruk, G.**, Del Giudice, R., Imbimbo, P., Di Lorenzo, F., Rigano, M.M., Lanzetta, R., Piccoli, R., Monti, D.M. "*Natural products as a source of antiaging molecules*" SIB 2017 – 59th Congress – Italian Society of Biochemistry and Molecular Biology (Caserta, Italy, 20-22 September)

Scientific activities in foreign laboratory: In 2016, from July 1st to September 30th in the laboratory of Prof. Michael Wink, Institute of Pharmacy and Molecular Biotechnology, Heidelberg, Germany.

List of Supplementary Informations:

A- Chapter 5 "*Isolation of carotenoids from Novosphingobium sp.* PP1Y"

B- Chapter 6 "*Bacillus subtilis spores as antioxidants*"

C- Chapter 7 "*Simultaneous production of antioxidants and starch from microalga Chlorella sorokiniana*"

D- Chapter 8 "*General discussion*"

Isolation of carotenoids from Novosphingobium puteolanum PP1Y

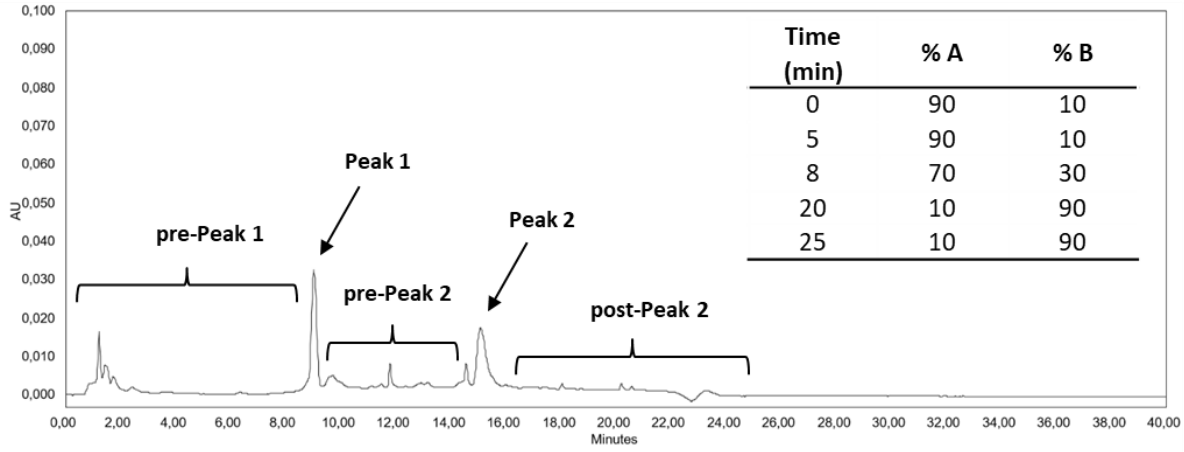

Time (min)	% A	% B
0	90	10
5	90	10
8	70	30
20	10	90
25	10	90

Figure S1. Fractional analysis of PP1Y extract by reverse-phase HPLC.

Submitted to Scientific Reports

Alternative use of spores from Bacillus subtilis: protection against environmental oxidative stress in human normal keratinocytes

Ganna Petruk[a], Giuliana Donadio[b], Mariamichela Lanzilli[b], Rachele Isticato[b]*, Daria Maria Monti [a,c]*

[a]Department of Chemical Sciences, University of Naples Federico II, Complesso Universitario Monte Sant'Angelo, via Cinthia 4, 80126, Naples, Italy
[b]Department of Biology, University of Naples Federico II, Complesso Universitario Monte Sant'Angelo, via Cinthia 4, 80126, Naples, Italy
[c]Istituto Nazionale di Biostrutture e Biosistemi (INBB), Rome, Italy

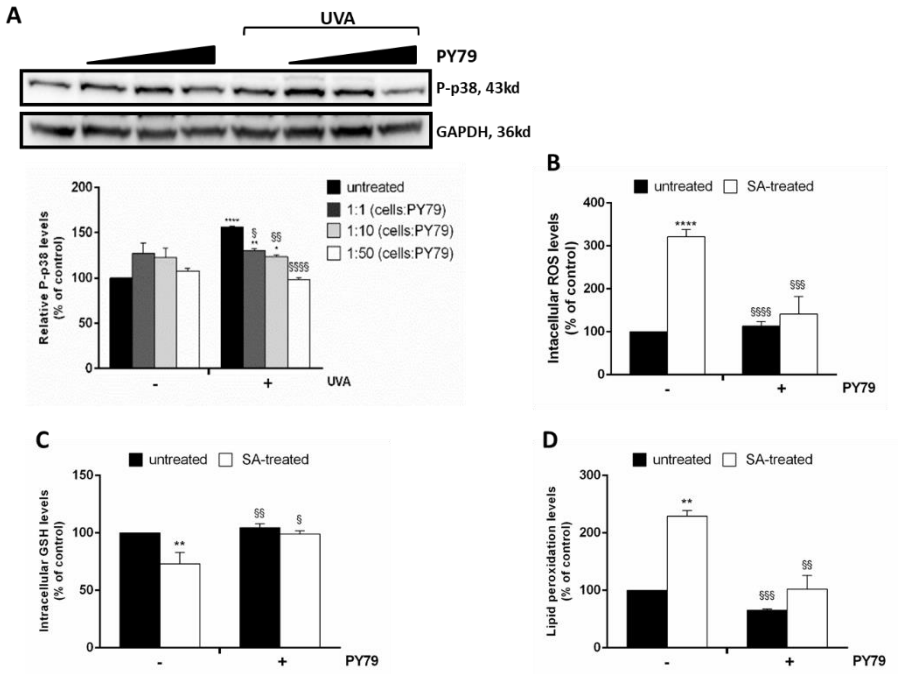

Figure S1: Analysis of oxidative stress in HaCaT cells exposed to UVA treatment and LoVo cells stressed by SA in the presence of PY79 spores. **A**, HaCaT cells were pre-incubated in the presence of increasing amount of PY79 (from 1:1 to 1:50, cells:spores) for 30 min and then irradiated by UVA (20 J/cm^2). Western blots show the phosphorylation level of p38, with the relative densitometric analysis in the absence (-) or in the presence (+) of UVA stress. GAPDH was used as internal standard. * indicates $p<0.05$, ** indicates $p<0.01$, **** indicates $p<0.0001$, with respect to control cells; § indicates $p<0.05$, §§ indicates $p<0.01$, §§§§ indicates $p<0.0001$, with respect to UVA-treated cells. **B-D**, LoVo cells incubated with PY79 (1:50, cells:spores) for 30 min before treatment with 300 µM SA for 45 min. **B**, DCFDA assay; **C**, DTNB assay; **D**, TBARS assay. Values are expressed as fold increase with respect to control cells. Data shown are the means ± S.D. of three independent experiments. ** indicates $p<0.005$, **** indicates $p<0.0001$, with respect to control cells; § indicates $p<0.05$, §§ indicates $p<0.01$, §§§ indicates $p<0.001$, §§§§ indicates $p<0.0001$, with respect to SA-treated cells.

Submitted to EMBO Reports

Simultaneous production of antioxidants and renewable molecules from microalga Chlorella sorokiniana

Ganna Petruk[a], Imma Gifuni[b], Anna Illiano[a], Mariana Roxo[c], Gabriella Pinto[a], Angela Amoresano[a], Antonio Marzocchella[b], Renata Piccoli[a,d], Michael Wink[c], Giuseppe Olivieri[b]*, Daria Maria Montia,[d]*

[a]Department of Chemical Sciences, University of Naples Federico II, Complesso Universitario Monte Sant'Angelo, via Cinthia 4, 80126, Naples, Italy
[b] Department of Chemical Engineering, of Materials and Industrial Production, University of Napoli "Federico II", Napoli , Italy;
[c]Institute of Pharmacy and Molecular Biotechnology, University of Heidelberg, Heidelberg, Germany;
[d]Istituto Nazionale di Biostrutture e Biosistemi (INBB), Rome, Italy

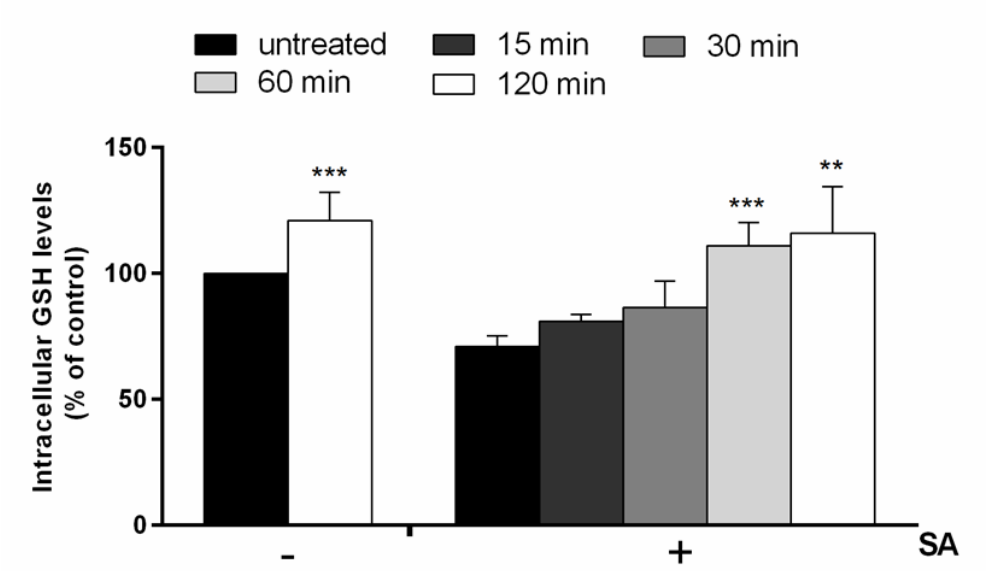

Figure S1: GSH levels in LoVo cells stressed by SA in the presence of EE. Cells were pre-incubated in the presence of 200 μg mL^{-1} EE for different lengths of time prior to be stressed by 300 μM SA for 45 min. Intracellular GSH levels determined by DTNB assay. Control cells, black bars; cells pre-treated with EE are indicated by: dark grey bars (15 min of pre-incubation), grey bars (30 min of pre-incubation), light grey bars (60 min of pre-incubation) and white bars (120 min of pre-incubation). Values are expressed as fold increase with respect to control (i.e. untreated) cells. Data shown are the means ± S.D. of three independent experiments. ** indicates $p<0.005$, *** indicates $p<0.001$.

A

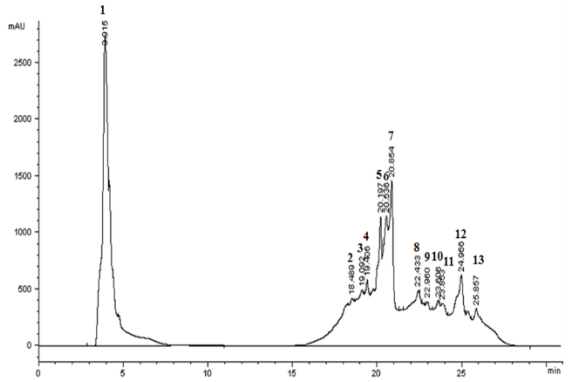

B

Cells incubated with:	% of intracellular GSH levels (with respect to untreated cells)	
	Unstressed cells	**SA-stressed cells**
untreated	100	69 ± 2
EE	100 ± 10	113 ± 9
#1	75 ± 9	62 ± 1
#2	71 ± 6	60 ± 8
#3	63 ± 4	76 ± 5
#4	59 ± 5	67 ± 5
#5	74 ± 2	82 ± 3
#6	66 ± 6	94 ± 3
#7	75 ± 3	74 ± 2
#8	92 ± 5	91 ± 8
#9	82 ± 8	99 ± 3
#10	82 ± 8	82 ± 13
#11	95 ± 2	95 ± 3
#12	80 ± 1	105 ± 4
#13	85 ± 2	58 ± 1
mix #7,8,11 and 12	113 ± 10	115 ± 11

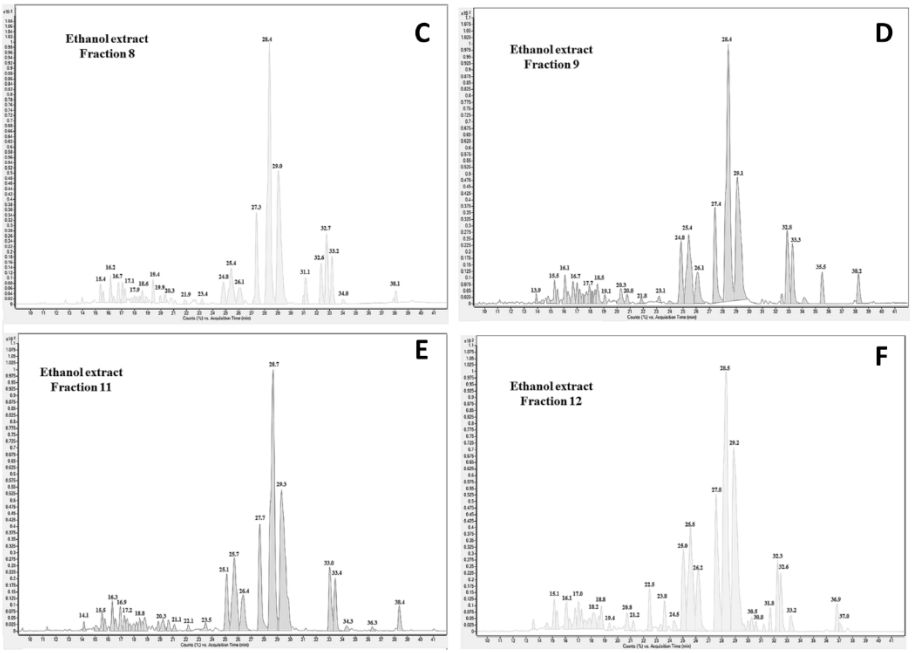

Figure S2: Characterization of EE. A, HPLC chromatogram of EE, in which eluted fractions are marked in the profile. **B**, Analysis of the antioxidant activity of microalgae fractions by DTNB assay. LoVo cells were pre-incubated in the presence of 200 µg mL^{-1} EE or equivalent amount of each fraction after HPLC for 120 min and then cells were stressed by SA treatment (300 µM) for 45 min and intracellular GSH levels determined, as described in Materials and Methods section. Values are reported as % of untreated cells. **C-F**, TIC chromatogram of the fractions with the highest biological activity.

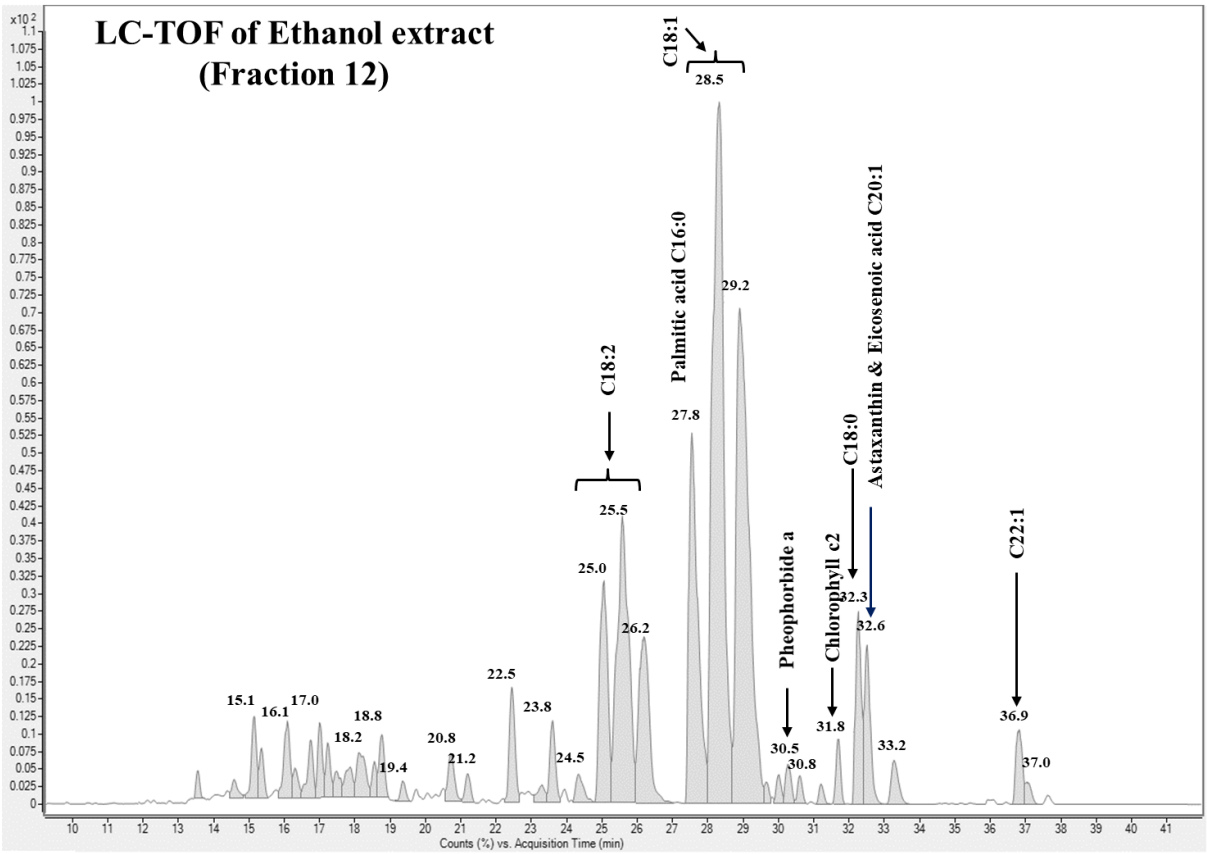

Figure S3: LC-TOF of EE (Fraction 12)

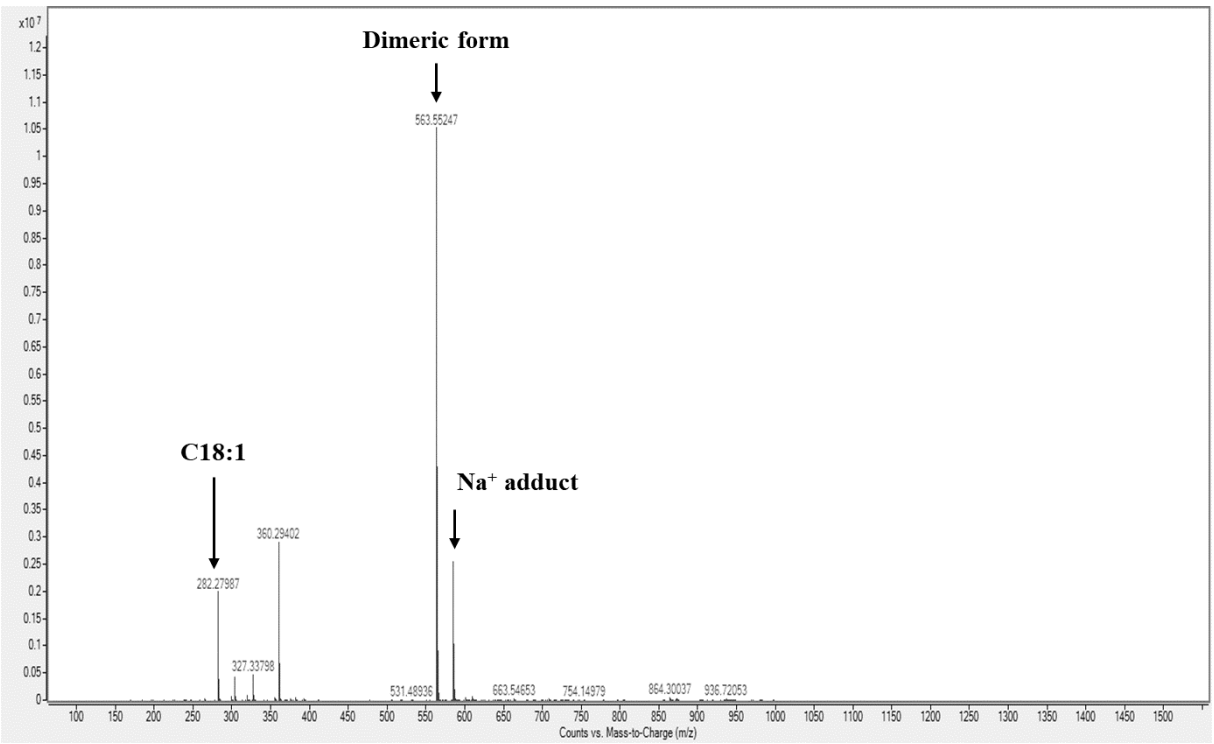

Figure S4: LC-TOF spectrum of ethanol extract (Fraction 12) at 28.5 min

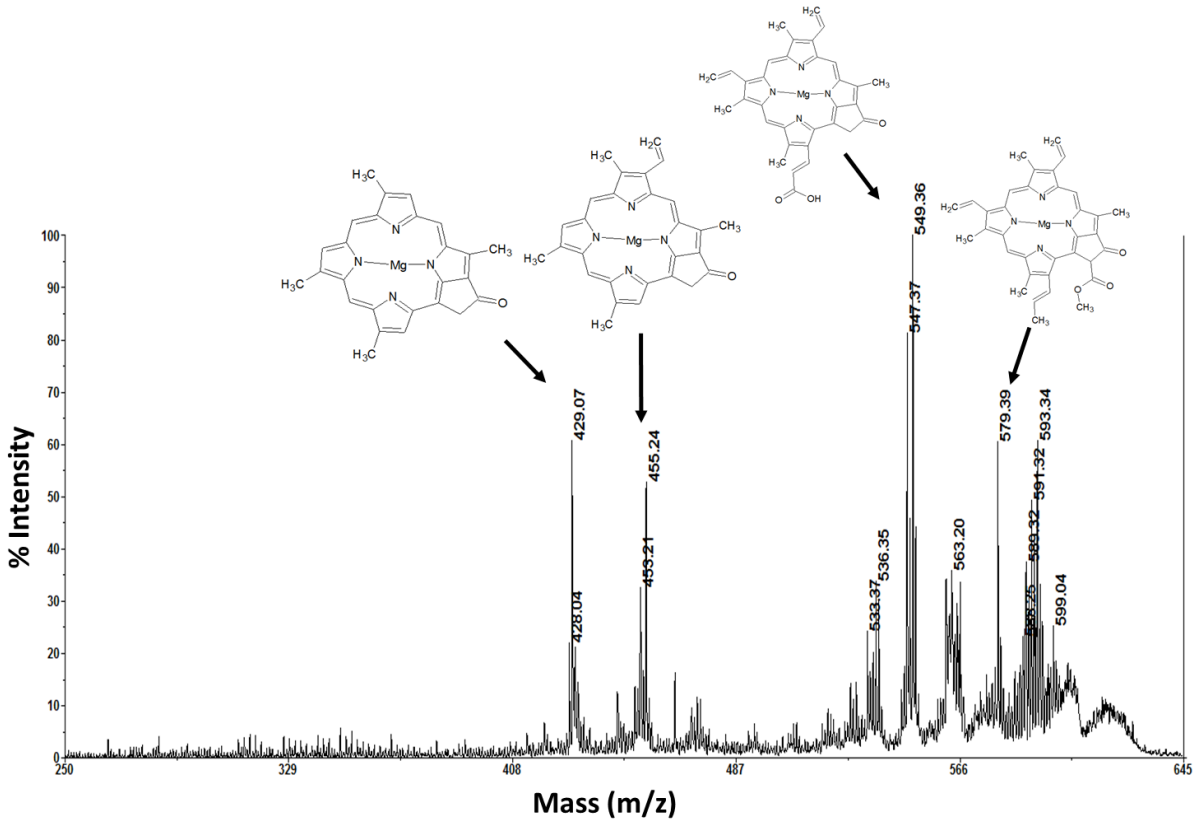

Figure S5: MALDI-TOF/TOF spectrum of Chlorophyll C2 (609.3 Da)

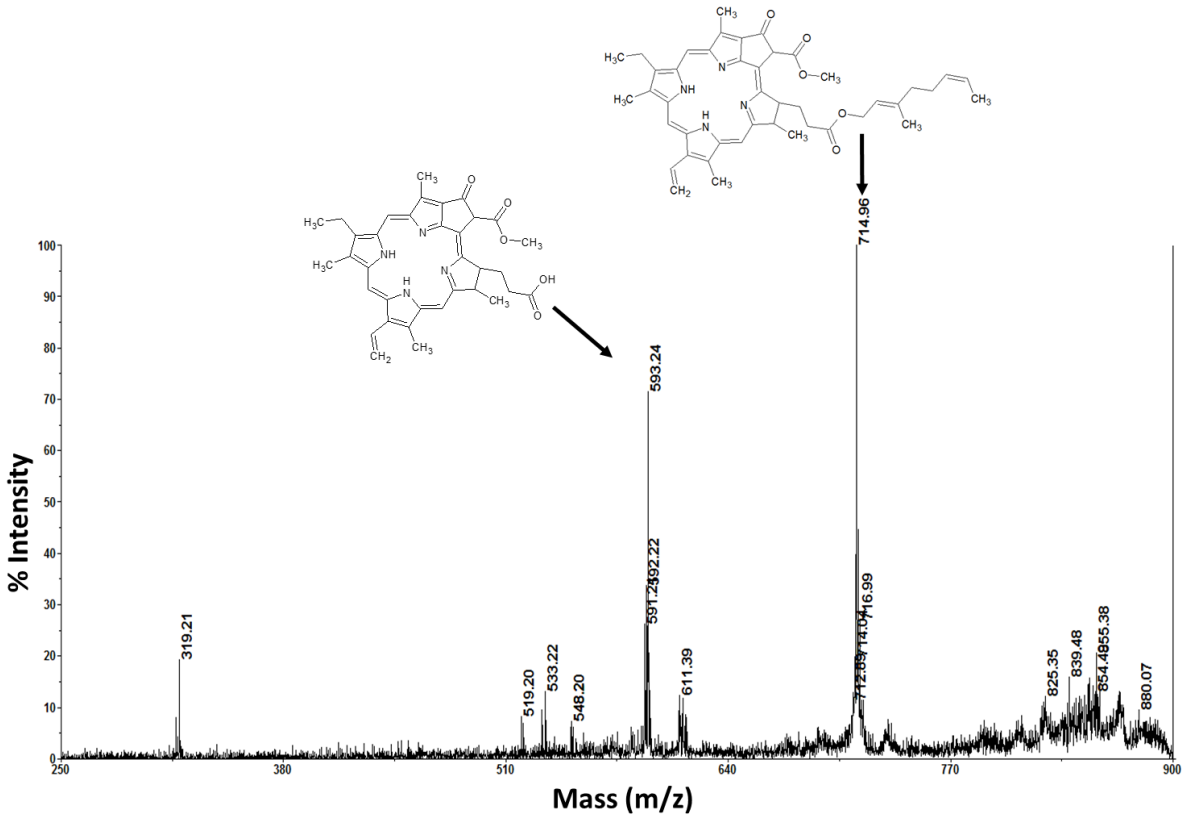

Figure S6: MALDI-TOF/TOF spectrum of Pheophytin a' (871.2 Da)

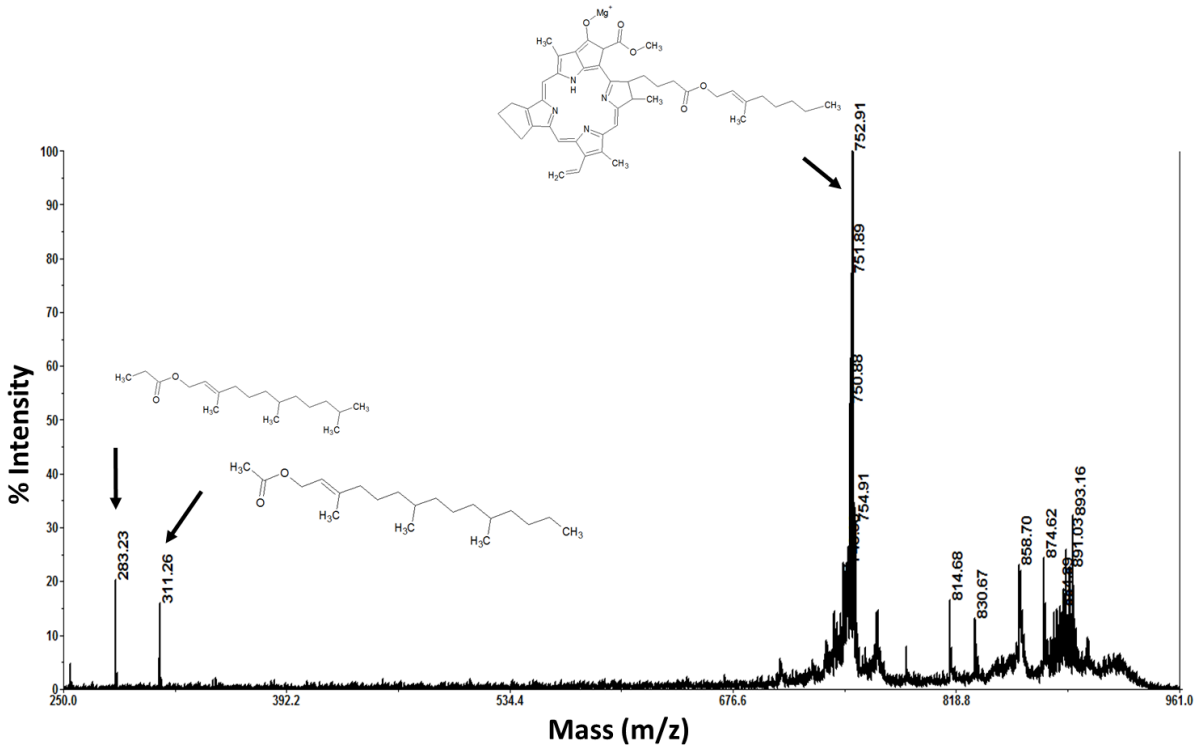

Figure S7: MALDI-TOF/TOF spectrum of hydroxylated chlorophyll a (908.9 Da)

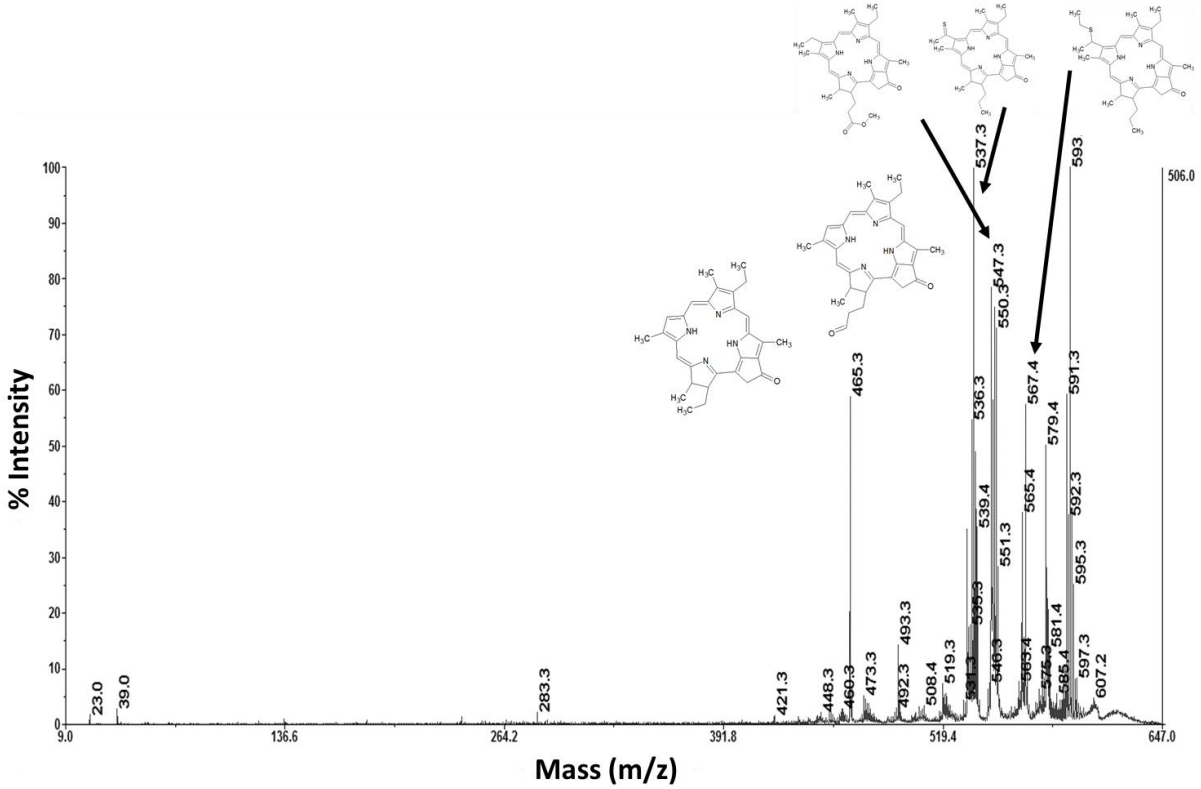

Figure S8: MALDI-TOF/TOF spectrum of S-Et Porphyrin at 611.3 Da

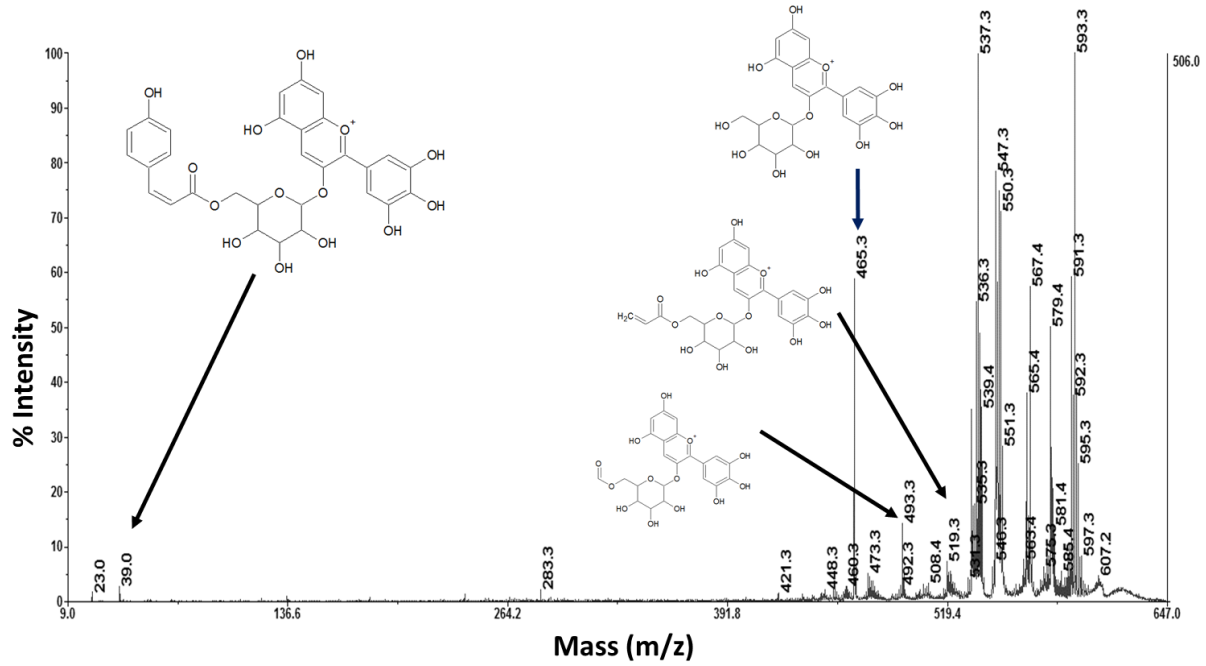

Figure S9: MALDI-TOF/TOF spectrum of Delfinidin – p-coumaroyl glucoside at 611.3 Da

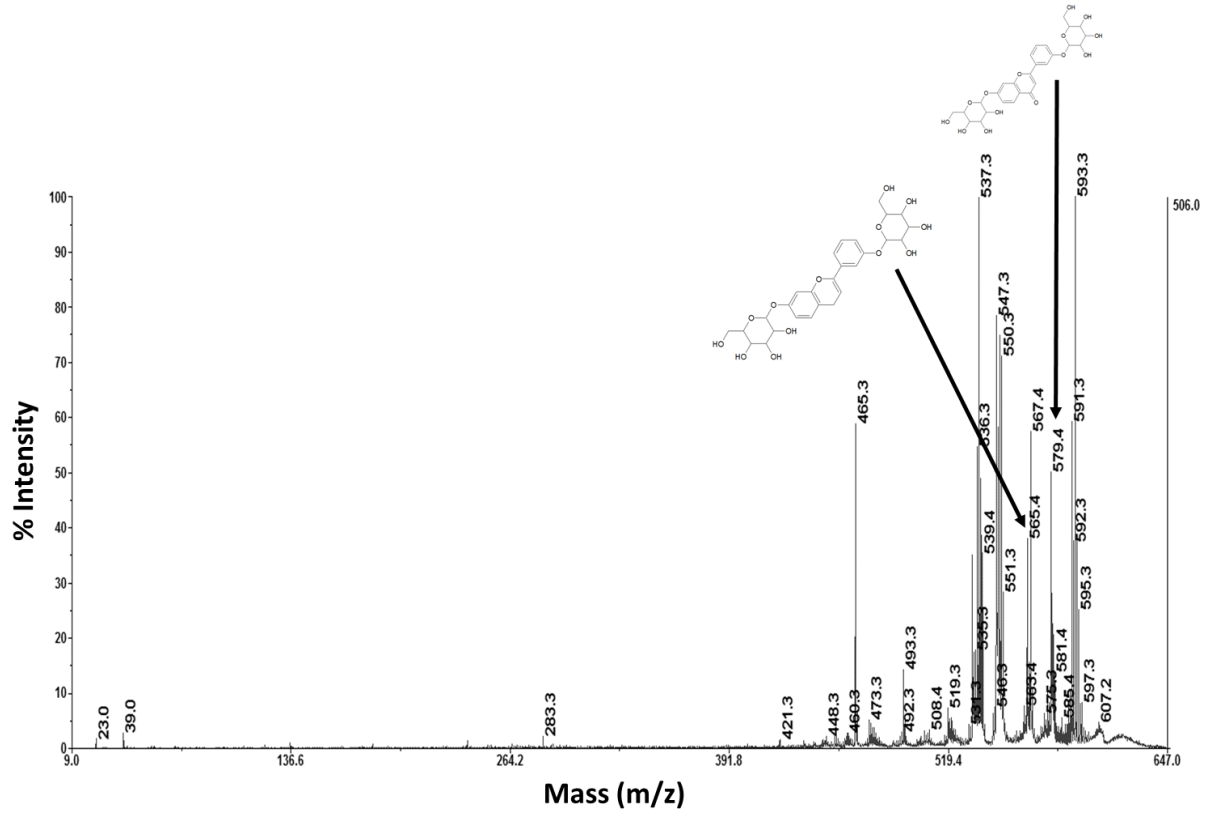

Figure S10: MALDI-TOF/TOF spectrum of Luteolin dihexoside at 611.3 Da

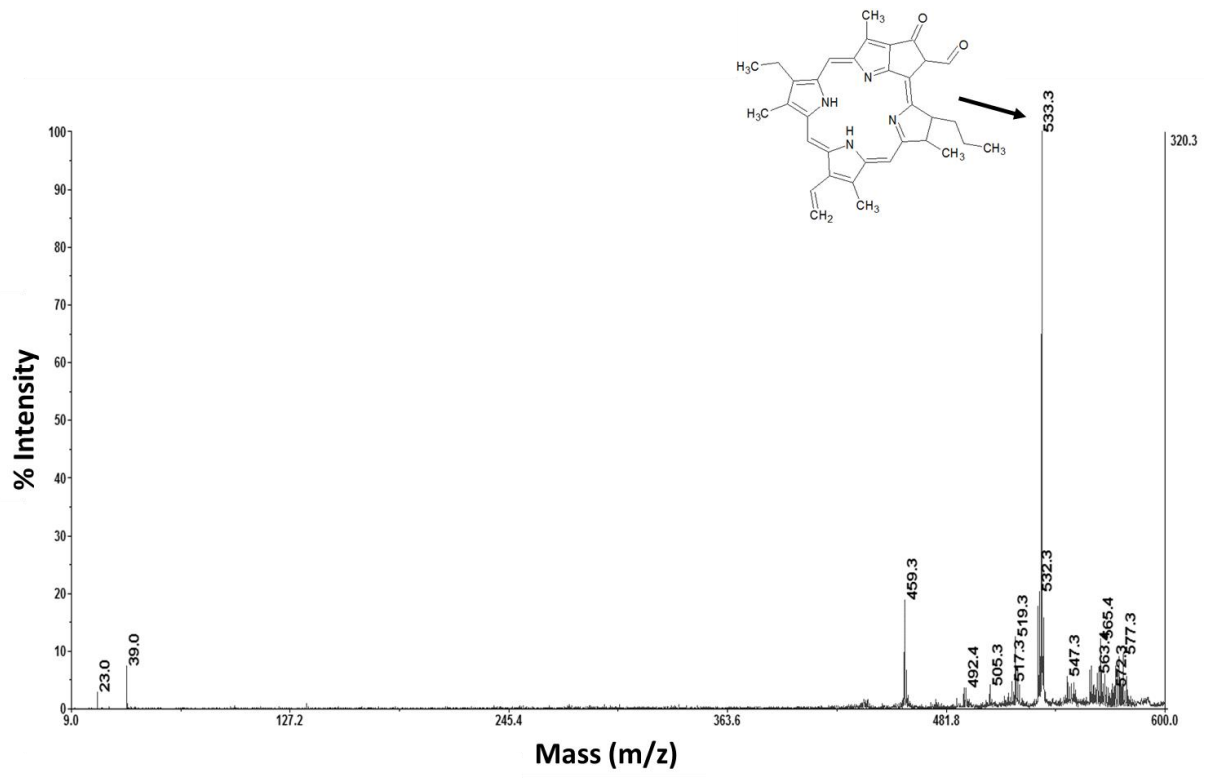

Figure S11: MALDI-TOF/TOF spectrum of pheophorbide at 593.3 Da

Table I. Identification of each peak of TIC chromatogram with relative retention time and relative abundance.

Species	Measured m/z	Detected Ion	MALDI-TOF/TOF Fragments	Rt (min)	Relative abundance (%)			
					8	9	11	12
Fatty acid C18:3	278.2	$M^{\bullet+}$		15.4	1.5	3.1	2.4	2.5
Dimeric form of C18:3	555.5	$[M+H]^+$						
Fatty acid C19:2	294.2	$M^{\bullet+}$		16.2/16.7	3.1	3.7	3.6	2.8
Dimeric form of Fatty acid C19:2	587.4 609.3	$[M+H]^+$, $[M+Na]^+$						
Dimeric form of C19:0	595.5 617.5	MH^+ $[M+Na]^+$		17.1	1.9	1.7	0.7	1.8
Fatty acid C19:1	296.2	$M^{\bullet+}$		18.6	0.8	2.4	1.4	0.3
Dimeric form of Fatty acid C19:1	591.5	$[M+H]^+$, $[M+Na]^+$						
Fatty acid C18:3	279.3	$[M+H]^+$		18.9	0.4	n.d.	n.d.	n.d.
S Porphyrin (SEt)	611.3	$[M+H]^+$	567.4 Da, 547.3 Da, 537.3 Da, 493.3 da, 465.3 Da	19.4	1.7	n.d.	1.4	n.d.
Luteolin dihexoside	611.4	$[M+H]^+$	579.4 Da, 565.4 Da					
Delphinidine 3-O p-coumaroyl-monoglucoside	611.4	$[M+H]^+$	519.3 da, 465.31, 493.3 (malvidine 3-0 monoglucoside)					
Fatty acid C18:4	277.2	$[M+H]^+$		19.9	0.4	n.d.	1.4	n.d.
Fatty acid C19:2	295.2	$[M+H]^+$						
Fatty acid C22:5	330.2	$M^{\bullet+}$						
S-Porphyrin (SEt)	611.4	$[M+H]^+$	567.4 Da, 547.3 Da, 537.3 Da, 493.3 da, 465.3 Da					
Luteolin dihexoside	611.4	$[M+H]^+$	579.4 Da, 565.4 Da					
Delphinidine 3-O p-coumaroyl-monoglucoside	611.4	$[M+H]^+$	519.3 da, 465.31, 493.3 (malvidine 3-0 monoglucoside)					
Fatty acid C19:0	298.2	$M^{\bullet+}$		20.3	0.5	1.9	1.1	1.3
Dimeric form of Fatty acid C19:0	595.5 617.5	$[M+H]^+$ $[M+Na]^+$						
Fatty acid C14:0	228.2	$M^{\bullet+}$		21.9	0.3	0.3	0.3	2.3
Dimeric form of C14:0	455.4	$[M+H]^+$						
Fatty acid C16:1	254.2 $M^{\bullet+}$	$M^{\bullet+}$		23.4	0.3	0.4	0.6	1.9

Fatty acid C22:4	332.2	M^{+}						
Dimeric form of C16:1	507.5	$[M+H]^{+}$						
Fatty acid C18:2	280.2	M^{+}		24.8	2.3	4.8	4.3	5.2
Dimeric form of C18:2	559.5	$[M+H]^{+}$ $[M+Na]^{+}$		25.4 26.2	5.2 2.4	8.6 3.7	8.7 4.0	9.6 5.2
Fatty acid C16:0	256.3	M^{+}		27.5	7.7	7.3	8.5	9.7
Dimeric form of C16:0	511.5 533.5	$[M+H]^{+}$ $[M+Na]^{+}$						
Fatty acid C18:1	282.3	M^{+}		28.3 29.0	32.0 20.3	27.6 16.6	28.5 20.9	23.2 18.6
Dimeric form of C18:1	563.5 585.5	$[M+H]^{+}$ $[M+Na]^{+}$						
Fatty acid C17:0	270.3	M^{+}		32.6	n.d.	n.d.	n.d.	0.7
Dimeric form of C17:0	539.5 561.5	$[M+H]^{+}$ $[M+Na]^{+}$						
Quercetin 3-(2"-p-hydroxybenzoyl-4"-p-coumarylrhamnoside)	715.3	$[M+H]^{+}$	699.1 Da, 669.1 Da, 561.1 Da, 311.4 Da, 283.4 Da	30.9	0.4	n.d.	n.d.	n.d.
Chlorophyll c2	609.3	$[M+H]^{+}$	579.4 Da, 549.4 Da, 455.3 Da, 429.05 Da	31.1	5.7	0.5	n.d.	1.3
Pheophorbide a	593.3	$[M+H]^{+}$	533.3 Da, 459.3 Da	32.8 33.8	n.d.	n.d.	n.d.	0.7 0.3
Fatty acid C18:0	284.4	M^{+}		32.7	6.4	5.8	4.8	3.2
Dimeric form of C18:0	567.6 589.5	$[M+H]^{+}$ $[M+Na]^{+}$						
Fatty acid C20:1	310.3	M^{+}		33.2	3.7	4.2	n.d.	2.8
Pheophorbide a	593.3	$[M+H]^{+}$	533.3 Da, 459.3 Da					
Dimeric form of C20:1	619.6 641.6	$[M+H]^{+}$ $[M+Na]^{+}$						
Pheophytin a'	871.2	$[M+H]^{+}$	593.2 Da, 714.9 Da					
Hydroxylated Chloronhyll a	908.9	$[M+H]^{+}$	752.9 Da ,311.3 Da ,283.2 Da					
Fatty acid C20:1	310.3	M^{+}		34.0	0.4	0.6	0.4	0.9
Astaxanthin	596.4	$[M+H]^{+}$						
Dimeric form of C20:1	619.6 641.6	$[M+H]^{+}$ $[M+Na]^{+}$						
TG(16:0/18:1(9Z)/18:2	874.7	$[M+NH_4]^{+}$		35.5	n.d.	1.9	n.d.	n.d.
TG(18:1(9Z)/18:1(9Z)/18:1(9Z)	902.7	$[M+NH_4]^{+}$						
Fatty acid C22:1	338.3	M^{+}		38.0	0.8	1.9	1.6	1.8
Dimeric form of C22:1	675.7 697.5	$[M+H]^{+}$ $[M+Na]^{+}$						

Table I: stability test of açai extract by measuring intracellular ROS levels in HaCaT cells exposed to sodium arsenite (SA). The extract was obtained by using ethanol or 2-propanol as solvents. After extraction the samples were dried by rotovapor and then resuspended in H_2O or in PBS. The antioxidant activity of the extract was analysed after different time of incubation at different temperatures, in the presence or absence of the light. Cells were pre-incubated with 0.5% (v/v) of acai extracts for 2 h and then exposed to SA for 1 h. After incubation intracellular ROS levels were determined by DCFDA assay. Values are expressed as fold increase with respect to control (i.e. untreated) cells. Data shown are the means ± S.D. of three independent experiments.

untreated	100
SA treated	155±5

Açai stability		extracted in Ethanol		extracted in 2-propanol	
		resuspended in H_2O	resuspended in PBS	resuspended in H_2O	resuspended in PBS
incubation t_0		118±7	118±29	117±16	117±17
incubation 72 h	4 °C	93±12	108±14	123±17	82±13
	−20° C	135±47	166±28	111±8	121±14
	TA in the light	106±15	94±12	106±38	89±15
	TA in the dark	130±45	98±3	102±7	87±15
	37 °C	137±2	103±31	78±18	101±33
incubation 1 week	4 °C	216±99	216±37	123±18	109±3
	−20° C	77±73	84±36	136±20	93±23
	TA in the light	40±44	169±31	164±8	89±39
	TA in the dark	50±57	142±23	124±4	96±13
	37 °C	78±39	208±53	140±36	105±23
incubation 2 weeks	4 °C	114±30	116±7	71±2	77±17
	−20° C	158±18	136±11	70±7	59±13
	TA in the light	126±15	147±10	60±37	63±13
	TA in the dark	114±24	109±5	67±18	73±9
	37 °C	143±1	94±11	125±7	84±19
incubation 3 weeks	4 °C	57±22	194±33	181±15	170±7
	−20° C	144±23	168±9	151±5	156±42
	TA in the light	198±31	162±12	161±11	146±14
	TA in the dark	114±3	147±10	150±4	147±5
	37°C	159±5	149±30	165±30	137±18
incubation 10 weeks	4 °C	148±17	158±4	149±10	130±22
	−20° C	147±14	141±1	135±10	128±16
	TA in the light	126±4	145±5	121±26	157±67
	TA in the dark	129±6	118±12	133±42	266±113

Biochimica et Biophysica Acta 1860 (2016) 434–444

Contents lists available at ScienceDirect

Biochimica et Biophysica Acta

journal homepage: www.elsevier.com/locate/bbagen

Protein conformational perturbations in hereditary amyloidosis: Differential impact of single point mutations in ApoAI amyloidogenic variants

Rita Del Giudice [a], Angela Arciello [a,e], Francesco Itri [a], Antonello Merlino [a,b], Maria Monti [a,e], Martina Buonanno [b,c], Amanda Penco [d], Diana Canetti [a,e], Ganna Petruk [a], Simona Maria Monti [b], Annalisa Relini [d,e], Piero Pucci [a,e], Renata Piccoli [a,e], Daria Maria Monti [a,e,*]

[a] Department of Chemical Sciences, University of Naples Federico II, 80126 Naples, Italy
[b] Institute of Biostructures and Bioimaging-CNR, Via Mezzocannone 16, 80134 Naples, Italy
[c] Dipartimento di Scienze e Tecnologie Ambientali, Biologiche e Farmaceutiche, Seconda Università di Napoli, Caserta, Italy
[d] Department of Physics, University of Genoa, Genoa, Italy
[e] Istituto Nazionale di Biostrutture e Biosistemi (INBB), Rome, Italy

ARTICLE INFO

Article history:
Received 17 July 2015
Received in revised form 15 October 2015
Accepted 23 October 2015
Available online 26 October 2015

Keywords:
Apolipoprotein A I
Protein stability
Amyloidosis
Conformational diseases

ABSTRACT

Amyloidoses are devastating diseases characterized by accumulation of misfolded proteins which aggregate in fibrils. Specific gene mutations in Apolipoprotein A I (ApoAI) are associated with systemic amyloidoses. Little is known on the effect of mutations on ApoAI structure and amyloid properties. Here we performed a physico-chemical characterization of L75P- and L174S-amyloidogenic ApoAI (AApoAI) variants to shed light on the effects of two single point mutations on protein stability, proteolytic susceptibility and aggregation propensity. Both variants are destabilized in their N-terminal region and generate fibrils with different morphological features. L75P-AApoAI is significantly altered in its conformation and compactness, whereas a more flexible and pronounced aggregation-competent state is associated to L174S-AApoAI. These observations point out how single point mutations in ApoAI gene evocate differences in the physico-chemical and conformational behavior of the corresponding protein variants, with the common feature of diverting ApoAI from its natural role towards a pathogenic pathway.

1. Background

Amyloidoses are characterized by protein aggregation in insoluble fibrils and their deposition in tissues and organs, with consequent alteration of their functionality. To date, almost 30 amyloidogenic proteins have been identified [1]; although these proteins do not show any sequence or structure homology, they have the ability to give rise to amyloid fibrils characterized by a highly ordered and rigid structure [2–5].

Apolipoprotein A I (ApoAI) is the main component of high density lipoproteins (HDL) and is mostly involved in the removal of cholesterol from peripheral tissues and its transfer, via the plasma, to the liver, where it is either recycled back to plasma as a component of newly formed lipoproteins, or excreted from the body via bile [6]. Due to ApoAI conformational plasticity, in its lipid-free or lipid-poor form, this protein is able to bind to phospholipids and to unesterified cholesterol to give rise to nascent HDL [7].

Some of the mutations in ApoAI gene are associated with hereditary systemic amyloidoses, characterized by extracellular fibrillar deposits in specific tissues, mainly heart, liver, kidneys and testes [8–10]. It has been reported that in the HDLs of heterozygous patients, in which both the wild-type protein and an amyloidogenic variant (L75P-AApoAI, L174S-AApoAI or L64P-AApoAI) are present, the wild-type protein is more abundant than the variant [11–13]. This finding is in line with our recent observation that in stably transfected human hepatic cells over-expressing L75P-AApoAI the secretion of the amyloidogenic variant is down-regulated [14], which in turn is in line with the observation of Marchesi and coworkers, who reported a decreased secretion efficiency of L75P- and L174S-AApoAI variants in transiently transfected COS cells [15]. Moreover, it has been hypothesized that AApoAI variants have a lower affinity for HDLs when compared to the wild-type protein; this would shift the ApoAI distribution from HDL-bound to lipid-poor/free state, which is relatively unstable and susceptible to proteolysis. The

Abbreviations: ANS, 8-anilino-1-naphthalensulfonic acid; ApoAI, apolipoprotein A I; AApoAI, amyloidogenic apolipoprotein A I; CD, circular dichroism; DLS, dynamic light scattering; GdnHCl, guanidine hydrochloride; HDL, high-density lipoproteins; MD, molecular dynamics; ThT, thioflavin T; TM-AFM, tapping mode atomic force microscopy; LC-MS, liquid chromatography-mass spectrometry.

* Corresponding author at: Department of Chemical Sciences, University of Naples Federico II, 80126 Naples, Italy.
E-mail address: mdmonti@unina.it (D.M. Monti).

http://dx.doi.org/10.1016/j.bbagen.2015.10.019
0304-4165/

resolution at 2.2 Å of the crystal structure of lipid-free Δ(185–243)-ApoAI revealed that ApoAI associates in domain swapped dimers held together by two four-helix bundles each constituted by the N-terminus of one subunit and the C-terminus of its partner. Interestingly, all the 19 amyloidogenic mutations so far identified cluster in two regions: the amino-terminus (residues 1–100) and within residues 173–178 [16], which, in the dimeric structure, define a 3D hot-spot mutation site [17]. To date, only few full-length AApoAI variants, out of 19 identified so far, have been investigated, which show significant peculiarities on the conformational transitions [18–21]. Recently, a model has been proposed, prompting that AApoAI mutations perturb one of the 4 predicted hot spots of the protein (14–22, 53–58, 69–72 and 227–232), with consequent full-length protein aggregation via the N-terminal region. This event would be followed by proteolytic cleavage at the exposed loop (83–100) and release of the N-terminal fibrillogenic polypeptide [21], which has been found to be the main protein constituent of ex-vivo fibrils [8]. It has been hypothesized that perturbation in the hot spots is one of the prerequisite for AApoAI misfolding, even though other factors may influence this process [21]. Here we analyzed the effects of two point mutations, L75P and L174S, on AApoAI conformational stability, being the former an "inside" mutation, i.e. located within the N-terminal fibrillogenic polypeptide, and the latter an "outside" mutation. Leu 75 is located in the middle of the short helix 70–76 that contributes to define the relative helical orientation in the four-segment bundle, whereas Leu 174 is located in the "bottom" of the hydrophobic cluster [22]. The variant with leucine to proline substitution at position 75 (L75P-AApoAI) is associated with a hereditary systemic amyloidosis characterized by preferential accumulation of fibrils in the kidneys and liver [11]. Instead, in the case of leucine to serine substitution at position 174 (L174S-AApoAI), a predominant accumulation of fibrils in the heart, skin, testes and larynx was observed [12]. The molecular basis of this differential localization of amyloid fibrils is still unknown.

We report structural stability, proteolytic susceptibility and aggregation propensity of full-length recombinant, lipid-free, human AApoAI harboring L75P or L174S mutation, to reveal the effects of a single point mutation on AApoAI structure and amyloidogenic potential.

This study is aimed to add knowledge to the largely unknown field of systemic amyloidoses. Starting from the general hypothesis suggesting that single point mutations, occurring in the 3D hot spot mutation site, direct the protein towards an amyloidogenic pathway, our study is aimed at revealing common and different impacts of mutations on protein stability.

2. Methods

2.1. Production of recombinant proteins

A bacterial expression system consisting of ApoAI expressing pET20 plasmid in *Escherichia coli* strain BL21(DE3) pLysS (Invitrogen) was used to prepare AApoAI proteins, as previously described [18]. Primer-directed PCR mutagenesis was used to introduce the L75P and L174S mutations. The mutation was verified by dideoxy automated fluorescent sequencing. Human ApoAI proteins were purified from bacterial cell lysate by immobilized metal affinity chromatography (HiTrap columns, GE Healthcare, Waukesha, WI) under denaturing conditions (4 M urea). Following binding, an extensive wash with 500 mM NaCl and 4 M urea in sodium phosphate buffer, 20 mM, pH 7.4 (wash buffer) was performed and bound proteins were then eluted with 500 mM imidazole in wash buffer. Proteins were dialyzed versus refolding buffer (50 mM Tris–HCl, pH 7.4), concentrated with 30 kDa molecular weight cut-off Amicon Ultra centrifugal filter devices (Millipore), and stored at −20 °C.

Purity and identity of the wild-type and variants were confirmed by LC–MS analyses, as reported below. Chromatographic traces recorded for each protein preparation, showed a single sharp peak, corresponding to the recombinant protein and the measured molecular masses were in agreement with the theoretical ones, according to the amino acid sequences of his-tagged expressed constructs (wild-type ApoAI: measured molecular mass: 29,799.6 ± 1.1 Da, theoretical molecular mass: 29,798.5 Da; L75P-AApoAI: measured molecular mass: 29,783.0 ± 1.8 Da, theoretical molecular mass: 29,782.5 Da; L174S-AApoAI: measured molecular mass: 29,772.8 ± 1.5 Da, theoretical molecular mass: 29,772.4 Da). For all the experiments His-tag containing proteins were used, as in preliminary conformational analyses (data not shown) we did not observe any significant difference comparing the His-tag containing wild-type protein to the protein after His-tag removal, or to commercial ApoAI (Sigma-Aldrich).

2.2. CD spectroscopy

Circular dichroism (CD) measurements were performed on a Jasco J815 spectropolarimeter (Jasco, Essex, UK), equipped with a temperature control system, using a 1-mm quartz cell in the far-UV range 194–260 nm (50 nm/min scan speed). Each spectrum was the average of three scans with the background of the buffer solution subtracted. Measurements were performed at 25 °C at a protein concentration of 0.15 mg/mL in 50 mM Tris HCl pH 7.4. Raw spectra were corrected for buffer contribution and converted to mean residue ellipticity, θ (mdeg cm^2 $dmol^{-1}$). Estimation of the secondary structure was carried out according to the Variable Selection Method (CDSSTR) using DICHROWEB [23].

2.3. Intrinsic fluorescence analysis

Emission fluorescence spectra were recorded in the range 300–450 nm, following excitation at 280 (tyrosine/tryptophan) or 295 nm (tryptophan). Measurements were carried out at 25 °C in a 10 mm cell by using a Perkin-Elmer LS50 spectrofluorimeter. Emission spectra were acquired at a scanning speed of 300 nm/min, with 10 and 5 slit widths for excitation and emission, respectively. Proteins (3 μM) were analyzed in 50 mM Tris HCl at pH 7.4.

2.4. Dye-binding assays

2.4.1. ThT binding assay

Proteins (0.3 mg/mL) were incubated at 25 °C in 50 mM Tris HCl at pH 7.4 in the presence of 10 μM thioflavin T (ThT). ThT fluouorescence emission spectra were acquired in the range 470–490 nm at 1 h intervals with scan speed of 300 nm/min, upon excitation at 450 nm. Excitation and emission slits were set at 5 and 10 nm, respectively. Fluorescence intensity values at 482 nm were plotted as a function of time. The determination of apparent $t_{1/2}$ values was obtained by non-linear regression fit of the data according to a double Boltzmann equation. The reported values represent the means from three independent experiments.

2.4.2. 1-Anilinonaphthalene-8-sulfonic acid (ANS) binding assay

Emission fluorescence spectra of recombinant proteins (3 μM) were acquired in the presence of the dye ANS (350 μM). Analyses were performed in 50 mM Tris HCl at pH 7.4, at 25 °C. Emission fluorescence spectra were recorded in the range 400–600 nm, following excitation at 380 nm. Excitation and emission slits were set at 5 and 10 nm, respectively.

2.5. Protein stability to denaturing agents

2.5.1. Chemical denaturation

Equilibrium denaturation was carried out on samples using guanidine (GdnHCl) and urea. Proteins were incubated for 24 h at 4 °C at 0.05 mg/mL prior to addition of denaturant. Incubated proteins were combined with denaturant, diluted from 8 M stock solutions. Samples were stored at 4 °C for 24 h prior to data collection. Changes in tryptophan fluorescence were recorded. The unfolding transition was

monitored by recording the wavelength at maximum fluorescence intensity (λ_{max}). The λ_{max} of triplicate dilutions of each sample was averaged and plotted against the denaturant concentration. Experimental points, describing sigmoidal curves, were fitted using the Boltzmann equation and $D_{1/2}$ (the concentration of denaturant at which the protein is half folded) was calculated. Assuming a two-state model (folded and unfolded), the free energy of denaturation was calculated as described by Petrlova et al. [18] by using the equation: $\Delta G_D^\circ = -RT\ln K_D$. ΔG_D° and m values were obtained by plotting ΔG_D versus denaturant concentration to give the linear equation [24] $\Delta G_D = \Delta G_D^\circ - m[\text{denaturant}]$, where ΔG_D° is the free energy of protein folding in water (0 M denaturant), and m the cooperativity of denaturation.

2.5.2. Thermal denaturation

Temperature-induced denaturation of proteins (0.05 mg/mL) was performed as a function of increasing temperature (20–100 °C). Protein samples were incubated at the desired temperature for 15 min before taking the measurements. Denaturation of proteins was performed by recording changes in tryptophan fluorescence.

2.6. Homology modeling and molecular dynamics simulations

The starting structure of wild-type ApoAI for molecular dynamics simulation was taken from the protein data bank (PDB) file 3R2P [17]. The structure, which has been solved at 2.2 Å resolution, includes residues 3–182 of two chains. Based on the evidence of dynamic light scattering experiments, this dimeric structure was considered as representative of the protein conformation in solution. Models of the mutants were built on the structure of wild-type ApoAI by manual residue replacement.

Molecular dynamics (MD) and trajectory analysis were performed with the software package GROMACS 4.6.6 [25–27] using the Gromos43a1 force field. Appropriate number of counterions (Na^+) was added to neutralize the systems. The structures were immersed in a rectangular box filled with SPC water molecules at a density of 1000 kg/m^3 [28] with periodic boundary conditions. Long-range electrostatic interactions were treated with the particle-mesh Ewald method with a grid spacing of 12 Å and cutoff of 8 Å. [29]. The molecules were submitted to initial energy minimisation with the steepest descent for 5000 steps followed by 500 ns NVT and 500 ps NPT equilibration with position restraints. Production runs were performed for 10 ns with a 2 fs step. To the best of our knowledge, these simulations are the first ever performed on mutants of ApoAI.

Temperature and pressure coupling were obtained with the v-rescale [30] and the Parrinello-Rahman [31] algorithms, respectively. Bond lengths were constrained using LINCS [32]. The overall flexibility of the systems was evaluated comparing the traces obtained by diagonalizing the covariance matrix of the coordinate fluctuations, as previously described [33]. Only Cα atoms were included in the definition of the covariance matrices. Figures were prepared with Pymol (www.pymol.org).

2.7. Complementary proteolysis experiments and mass spectrometry analysis

Complementary proteolysis experiments were carried out by treating 0.4 mg/mL solutions of proteins with trypsin, chymotrypsin, and endoproteinase Glu-C in 50 mM Tris HCl, pH 7.4. Different E:S ratios were optimized for each proteolytic probe as reported: 1:8000 for chymotrypsin and trypsin, 1:10,000 for endoprotease Glu-C. The extent of digestion was monitored on a time-course basis by sampling the reaction mixture at 15 and 30 min and blocking the reactions with 2% trifluoroacetic acid (TFA). Peptide mixtures were analyzed by liquid chromatography-mass spectrometry (LC–MS) onto a QuattroMicro LC-MS system (Micromass, Waters) interfaced with a 1100 HPLC (Agilent Technologies, Palo Alto, CA). Peptide mixtures from the different proteolysis experiments were fractionated by reverse-phase HPLC on a Phenomenex Jupiter C18 column (250 mm × 2.1 mm, 300 Å pore size) and eluted by using a step gradient from 5% to 60% of solvent B (5% formic acid and 0.05% TFA in acetonitrile) over 60 min and from 60% to 95% in 5 min (solvent A 5% formic acid and 0.05% TFA in water). The flow rate was kept at 200 μL/min and directly introduced in the mass spectrometers ESI source. Horse heart myoglobin was used to calibrate the instrument (average molecular mass 16,951.5 Da) at 5 scans/s.

2.8. Determination of critical concentration

Proteins were incubated at different concentrations (from 0.15 to 2 mg/mL) in 50 mM Tris HCl pH 7.4 for 14 days at 37 °C. Then, samples were centrifuged at 14,000 *g* for 30 min at r.t., supernatants were filtered with a 20 nm cut off filter and the absorbance at 280 nm measured.

2.9. Dynamic light scattering

Dynamic light scattering (DLS) measurements were carried out using a Malvern nano zetasizer (Malvern, UK) [34]. Proteins (0.55 mg/mL) were diluted in 50 mM Tris HCl at pH 7.4, filtered with a 0.22 μm cut off filter and incubated at 37 °C over time. Samples were placed in a disposable cuvette and held at 25 °C during analysis. The aggregation rate was monitored at time 0 and after 24 h, 48 h and 7 days of incubation. For each sample, spectra were recorded six times with 11 sub-runs using the multimodal mode. The Z average diameter was calculated from the correlation function using the Malvern technology software.

2.10. Atomic force microscopy

For AFM inspection, ApoAI samples were incubated at 0.3 mg/mL at 37 °C. Incubation times in the range from 4 to 7 weeks were considered. At the end of incubation, proteins were centrifuged at 1700 *g* for 10 min, the pellet was suspended in an equal volume of water, and a 10 μL aliquot was deposited on freshly cleaved mica and dried under mild vacuum. Tapping mode AFM images were acquired in air using a Multimode SPM, equipped with "E" scanning head (maximum scan size 10 μm) and driven by a Nanoscope V controller, and a Dimension 3100 SPM, equipped with a 'G' scanning head (maximum scan size 100 μm) and driven by a Nanoscope IIIa controller (Digital Instruments, Bruker AXS GmbH, Karlsruhe, Germany). Single beam uncoated silicon cantilevers (type OMCL-AC160TS, Olympus, Tokyo, Japan) were used. The drive frequency was between 290 and 340 kHz, the scan rate was between 0.3 and 0.8 Hz. Aggregate sizes were estimated from the heights in cross section of the topographic AFM images.

3. Results

3.1. Effects of amyloidogenic mutations on ApoAI secondary structure

The secondary structure content of AApoAI variants was estimated by far-UV CD spectroscopy at pH 7.4, at 0.15 mg/mL protein concentration to approximate physiological conditions. As shown in Fig. 1, wild-type ApoAI and the two amyloidogenic variant proteins were predominantly in an α-helical state, with a slightly lower α-helix content of the variants with respect to the wild-type protein (Table 1). When the proteins were incubated at 37 °C over time, no significant changes in the spectra of the wild-type protein were observed, consistently with literature data [18 and references therein]; on the contrary, the α-helicity of both variants decreased over time accompanied by an increase in β-strand, indicating an alteration of the protein native conformation towards an aggregation competent state.

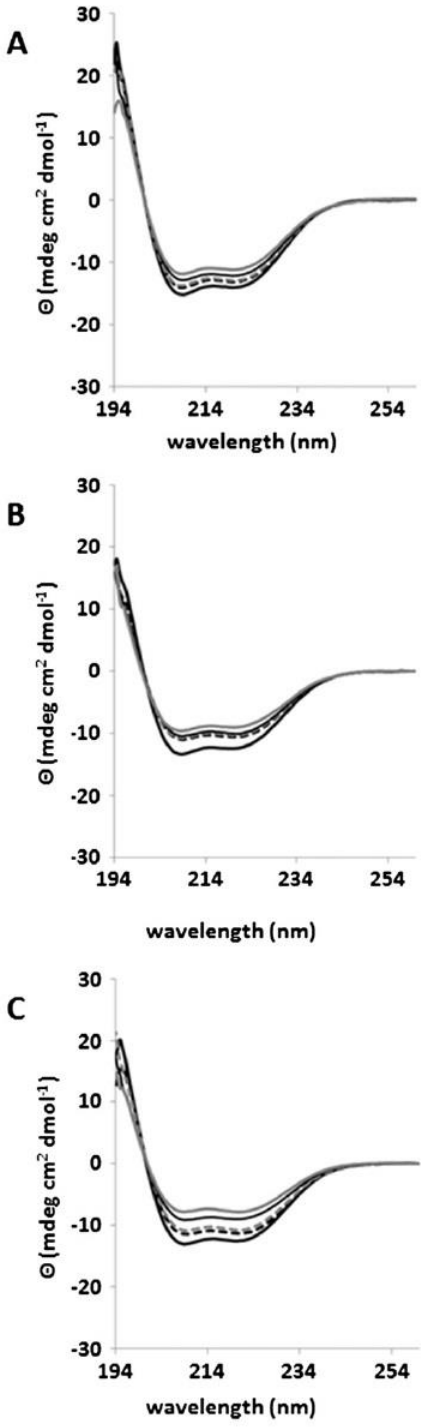

Fig. 1. Far-UV CD spectra of wild-type ApoAI and its amyloidogenic variants upon incubation at 37 °C. A, wild-type ApoAI; B, L75P-AApoAI; C, L174S-AApoAI. Spectra were acquired at 25 °C with 0.15 mg/mL protein concentration in 50 mM TrisHCl buffer, pH 7.4. Spectra were recorded at time 0 (bold black line), after 24 h (black dashed line), 48 h (gray dashed line), 72 h (black fine line) and after 7 days (bold gray line) incubation.

Table 1
α-Helix and β-strand contents (%) for wild-type ApoAI and its amyloidogenic variants, upon incubation at 37 °C. Data shown are the means from three independent experiments. The accuracy of the secondary structure content estimation is approximately 2% for wild-type ApoAI and 4% for its amyloidogenic variants.

Incubation time (h)	Wild-type ApoAI		L75P-AApoAI		L174S-AApoAI	
	α-Helix (%)	β-Strand (%)	α-Helix (%)	β-Strand (%)	α-Helix (%)	β-Strand (%)
0	49	29	40	36	45	28
24	49	28	34	36	40	21
48	47	29	32	39	35	37
72	40	34	31	39	29	41
168	38	33	29	40	20	53

3.2. Effects of amyloidogenic mutations on ApoAI conformation

During amyloid formation protein aggregation leads to an increase in the exposure of hydrophobic regions to the aqueous environment. ANS binding studies revealed a 3-fold increase of ANS fluorescence intensity in the presence of wild-type ApoAI (Fig. 2A, black line), due to the exposure of ANS accessible hydrophobic surfaces, as previously reported [35–38]. A larger increase of ANS fluorescence was measured for both variants compared to wild-type ApoAI, particularly evident for L174S-AApoAI variant, indicating that both mutations trigger the exposure of hydrophobic regions (Fig. 2A, gray line and dashed line for L75P-AApoAI and L174S-AApoAI, respectively).

To compare the tertiary structure of AApoAI variants with that of the wild-type protein, the intrinsic fluorescence emission intensity was registered and the shift of maximum emission wavelength (λ_{max}), due to changes in solvent exposure of tyrosine and tryptophan residues, was evaluated. As the four Trp residues of the wild-type protein (at positions 8, 50, 72 and 108), as well as the five Tyr residues (at positions 18, 29, 100, 115, 166), are located within the four-helix bundle domain and are all conserved in the amyloidogenic variants under study, this analysis is a measure of the stability of AApoAI N-terminal region. Fluorescence spectra were collected either upon excitation at 295 nm, where the contribution of tyrosine residues is negligible (Fig. 2B), or upon excitation at 280 nm, where both Tyr and Trp residues significantly contribute to the absorption (Fig. 2C). As shown in Fig. 2B, in the case of L75P-AApoAI (gray line) the maximum fluorescence intensity emission wavelength ($\lambda_{max} = 344.7 \pm 0.3$ nm) is higher than that of wild-type ApoAI ($\lambda_{max} = 335.7 \pm 0.6$ nm). These data suggest that the substitution L75P is able to induce changes in the conformation of the N-terminal domain with consequent exposure of hydrophobic protein surfaces, since proline is known to interrupt protein α-helical structure. On the contrary, L174S-AApoAI (Fig. 2B, dashed line) showed a $\lambda_{max} = 336.3 \pm 1.2$ nm, a value similar to that recorded for wild-type ApoAI. Similar results were observed when the contribution of both Tyr and Trp was analyzed (Fig. 2C and Table S1).

3.3. Effects of mutations on ApoAI stability

To get insights into the structural features that favor AApoAI amyloidogenicity, we compared the folding of the L75P-AApoAI and L174S-AApoAI to that of wild-type ApoAI by investigating protein stability in the presence of chemical denaturing agents, such as guanidine hydrochloride (GdnHCl) and urea. Upon excitation at 295 nm, the unfolding transition was monitored by evaluating the change in λ_{max} as a function of chemical agent concentration. As the equilibrium unfolding of wild-type ApoAI by GdnHCl has been well characterized, it can be used as a reference for the stability of the variants. As shown in Fig. 3(A–B), sigmoidal curves (filled squares) were obtained in the case of wild-type protein, confirming a cooperative unfolding pattern that well fits the two-state model [18,39]. As shown in Table 2, the mid-point of the denaturation process ($D_{1/2}$ values), ΔG_D° and

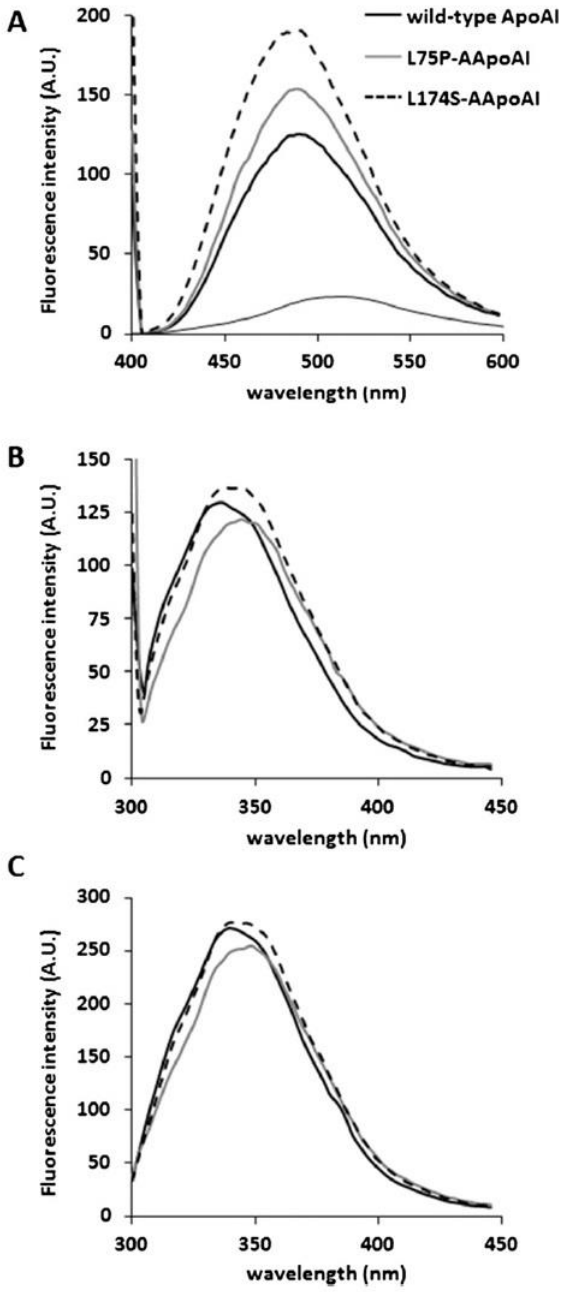

Fig. 2. Fluorescence analyses of AApoAI variants. A, binding of ANS to wild-type ApoAI (black line) and to its amyloidogenic variants L75P (gray line) and L174S (dashed line). ANS spectrum is reported as a fine black line. ANS emission fluorescence spectra were recorded in the range from 400 to 600 nm at the excitation wavelength of 395 nm. ANS emission was monitored at pH 7.4. B and C, tryptophan and tyrosine emission spectra at pH 7.4 of wild-type ApoAI (bold black line), L75P-AApoAI (gray line) and L174S-AApoAI (dashed line). Fluorescence was excited at 295 nm (B) and at 280 nm (C).

cooperativity (m) values were similar to those previously reported [18 and references therein].

A completely different behavior was observed in the case of L75P-AApoAI and L174S-AApoAI, as the denaturation curves are shifted to lower denaturant concentrations compared to wild-type ApoAI, indicating a decreased structural stability. In particular, for L75P-AApoAI variant (empty circles in Fig. 3 (A–B), protein unfolding was found not to be a cooperative process and a higher λ_{max} was recorded even in the absence of the denaturing agent. On the other hand, for

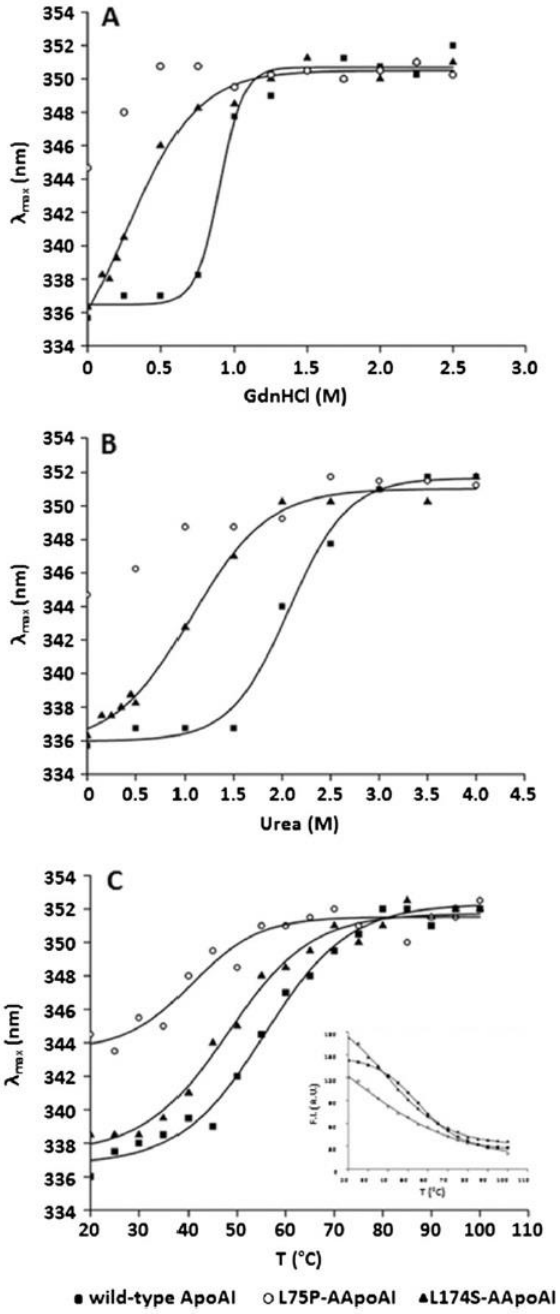

Fig. 3. Unfolding of wild-type ApoAI (filled squares) and of its amyloidogenic variants L75P (empty circles) and L174S (filled triangles) induced by the addition of increasing amounts of GdnHCl (A), urea (B), or by temperature changes (C). Following excitation at 295 nm, emission spectra were recorded and curves were obtained by reporting the maximum emission fluorescence as a function of the denaturing agent concentration value. Tryptophan fluorescence intensity as a function of temperature is reported as an inset in C.

Table 2
Denaturation parameters for the unfolding of AApoAI variants. Data shown are the means from three independent experiments.

Protein	$D_{1/2}$ (M)	ΔG_D° (kcal/mol)	m	$D_{1/2}$ (M)	ΔG_D° (kcal/mol)	m	Tm (°C)	ΔH (kcal/mol)
	GdnHCl			Urea			Temperature	
Wild-type ApoAI	0.90 ± 0.01	2.9 ± 0.5	2.76 ± 0.32	2.1 ± 0.3	4.4 ± 0.4	2.0 ± 0.1	55.3 ± 0.5	26.9 ± 0.1
L75P-AApoAI	n.a.	n.a.	n.a.	n.a.	n.a.	n.a.	40.8 ± 2.2	15.0 ± 0.4
L174S-AApoAI	0.39 ± 0.01	0.20 ± 0.04	0.9 ± 0.2	1.1 ± 0.4	1.3 ± 0.2	1.0 ± 0.2	43.5 ± 4.6	22.4 ± 0.4

L174S-AApoAI variant, a hyperbolic curve (filled triangles in Fig. 3A) was obtained in the presence of GdnHCl, indicative of a fast and non-cooperative unfolding process. Following the addition of increasing amounts of urea, a sigmoidal curve was obtained for L174S variant (Fig. 3B, filled triangles) even though less pronounced when compared to the wild-type protein, indicating a loss in unfolding cooperativity. Denaturation parameters for the unfolding process of AApoAI variants are reported in Table 2. The lower GdnHCl $D_{1/2}$ values obtained for wild-type ApoAI and L174S variant, compared to urea $D_{1/2}$, may suggest the importance of electrostatic interactions, efficiently weakened by GdnHCl, in the stabilization of the two proteins [40]. Loss in cooperativity during denaturation is a common feature of amyloidogenic variants, as variants G26R and L178H [18], and the recently published R173P [20] share this behavior.

Finally, by thermal denaturation (Fig. 3C) we observed that the proteins are all structurally stable up to 50 °C, although enthalpy and midpoint values, reported in Table 2, were found to be lower for the variants than for wild-type ApoAI, confirming their lower stability with respect to the native protein.

3.4. Structural features of wild-type ApoAI, L75P-AApoAI and L174S-AApoAI: a molecular dynamics study

To address differences in the structural features of the two variants when compared to the wild-type protein, models of the variants were obtained and used as inputs for a molecular dynamics (MD) study. In wild-type ApoAI, L75 is located in the middle of the short helix 70–76 that contributes to define the relative helical orientation in the four-segment bundle and interacts with L14 in the "bottom" hydrophobic cluster formed by V11, L14, F71 and L82. L174, instead, is located in the packed "bottom" hydrophobic cluster so that its substitution with Ser was expected to disrupt this cluster [17,22]. On the other hand, from the MD simulations it emerged that the replacement of L174 with a Ser has only a moderate effect on the overall structure of the protein. In fact, in the L174S variant, the serine side chain can be well accommodated within the helix 141–180, since it can form a hydrogen bond with the carbonylic oxygen of Y170 (Fig. 4A). On the contrary, the L75P substitution has a stronger destabilizing effect, since the presence of Pro breaks helix 70–76 and disturbs the stabilizing hydrophobic interactions that play a major role in orienting the helices of the four-segment bundle (Fig. 4B).

During the MD simulations, no significant changes in the overall structure from the corresponding crystal structure occurred in wild-type ApoAI, while the two variants show subtle, but significant variations. In particular, the average structures extracted from the trajectories for the three proteins suggest that L174S-AApoAI, which has an overall structure similar to that of wild-type protein, presents a slight reduced radius of gyration (5.91 ± 0.02 nm vs 5.98 ± 0.03 nm of wild-type ApoAI), while L75P-AApoAI adopts a less compact structure (+2% in the total solvent accessible surface area), with a significant loss of α-helical content (about −2%). These differences well reflect in the average distances between donor and acceptor atoms involved in the formation of 3_{10}-, α- and π-helices (Table S2). These data are in overall agreement with those obtained by CD spectra (Fig. 1).

To verify if the conformational changes induced by the mutations also affects the overall dynamics of the proteins, the trace of the covariance matrix of CA atoms for the three structures, which is a measure of the overall flexibility [33], has been evaluated. The values for wild-type ApoAI, L75P-AApoAI and L174S-AApoAI were 75 nm^2, 105 nm^2 and 98 nm^2, respectively. These data clearly indicate that the mutations enhance the overall flexibility of the protein.

To obtain a more detailed picture of the observed differences, the percentage of α-helical content of each residue (helicity) during the simulation was plotted as a function of the residue number (Fig. S1). Interestingly, although the plots have an overall similar profile for the three proteins, some differences can be evidenced: wild-type ApoAI is generally more structured; however in the regions encompassing residues 18–30, 80–81 and 126–131 it is slightly less structured than the two variants. L75P-AApoAI shows a lower helical content in correspondence of residues 66–73, 135–137, 157–160 and 172–177, but it is more structured than both wild-type ApoAI and L174S in the regions 125–129 and 140–142. L174S-AApoAI has a lower α-helical content in correspondence of residues 107–110, 140–141, but it is more structured in the regions 77–80 and 158–160. These differences are associated with slight variations also in the solvent accessible surface area per residue. Notably, although in the L75P variant the region encompassing residues 135–137 presents a lower helical content when compared to the other proteins (Fig. S1), it becomes more buried than in L174S-AApoAI and the wild-type protein, as the average solvent accessible surface area of residue 136 is: 76, 62 and 76 $Å^2$, in wild-type, L75P-AApoAI and L174S-AApoAI, respectively.

3.5. Complementary proteolysis experiments

In order to define ApoAI regions structurally altered by the presence of mutations, the surface topology of wild-type protein, L75P-AApoAI and L174S-AApoAI variants was investigated by a complementary proteolysis approach coupled with mass spectrometry identification of cleavage sites (LC–MS) [41]. Complementary proteolysis refers to limited proteolysis experiments carried out in conditions able to generate a single proteolytic event on the protein which originates two "complementary" peptides. Further cleavages occurring on the two complementary peptides are not considered. Conformational changes induced by mutations and affecting protein topology were monitored by the appearance of preferential cleavage sites located in exposed and flexible regions of the proteins, which become more susceptible to proteolysis [42,43]. Complementary proteolysis experiments were performed using trypsin, chymotrypsin and endoprotease Glu-C as conformational probes. All reactions were carried out in parallel on the three proteins by using the same E:S ratio and were monitored on a time-course basis by sampling the incubation mixture after 15 and 30 min of hydrolysis. Following this time course approach, primary and secondary cleavage sites, always produced by a single proteolytic event, were only defined on kinetic basis. The LC–MS profiles showed that both variants were more susceptible to proteases than the wild-type protein, as demonstrated by the higher number of peptides released at the same hydrolysis time (data not shown). This observation suggests that both AApoAI variants are more flexible and/or less structured than the wild-type protein, in agreement with both spectroscopic and molecular dynamics data.

The distribution of the proteolytic sites is outlined in Fig. 4C. A similar pattern of proteolytic accessibility could be observed in all the

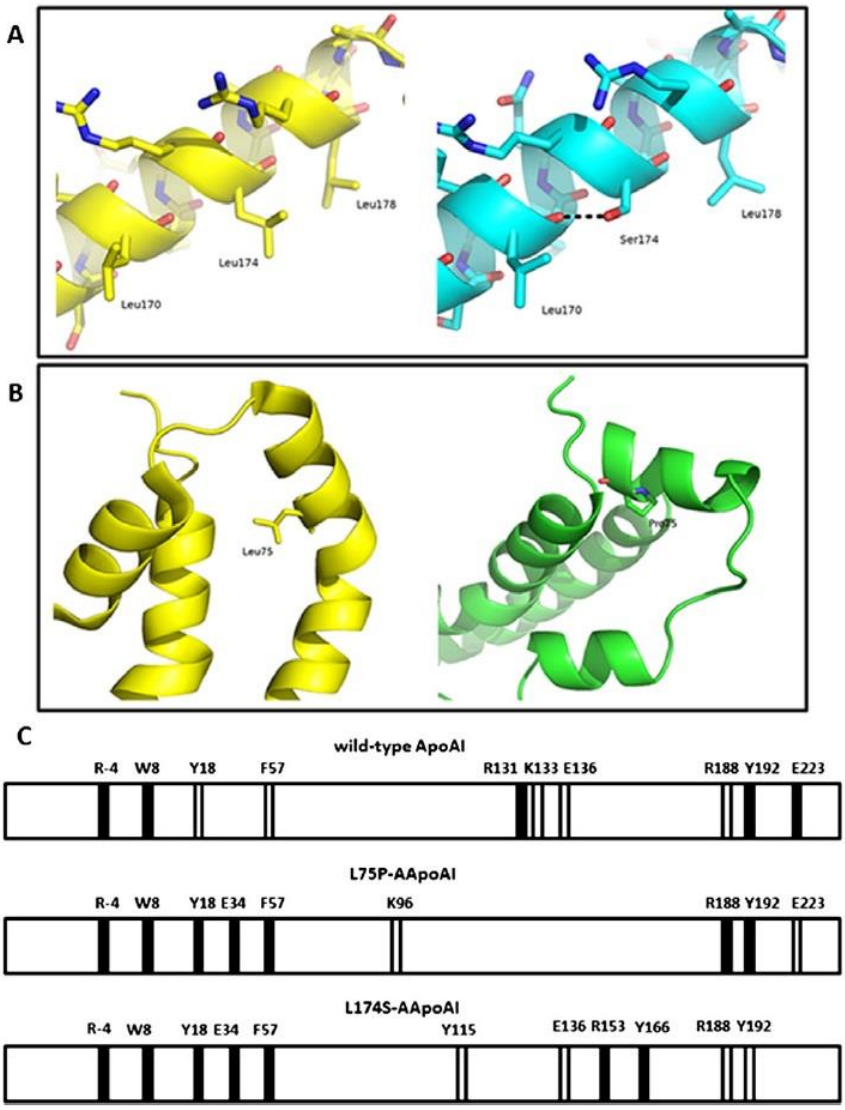

Fig. 4. Structural features of AApoAI variants. A, insight of the structure of helix encompassing residues 141–180 in wild-type ApoAI (yellow) and in L174S variant (cyan). B, ribbon representation of the helix bundle in proximity of L75 in the structure of wild-type ApoAI (yellow) and of L75P variant (green). For sake of clarity, one helix from the second chain of the dimer was removed. C, pattern of preferential proteolytic sites in native and AApoAI variants. Schematic representation of the results obtained from limited proteolysis experiments on wild-type ApoAI (upper), L75P-AApoAI (middle) and L174S-AApoAI (lower). Proteolytic sites are designed as primary (filled) or secondary sites (empty) merely on kinetic basis. The R-4 cleavage site was not taken in consideration, as it is located in the his-tag peptide sequence occurring in the recombinant proteins.

proteins, with preferential cleavage sites gathering at both the N- and C-terminal regions. However, hydrolysis at Y18 and F57 occurred much faster in the mutants than in wild-type ApoAI and E34 was not recognized in the native protein, suggesting a higher flexibility in the N-terminal region of the variants. Moreover, cleavage at K96 and Y115, in L75P- and L174S-AApoAI, respectively, suggests a slight conformational change in the region including the putative proteolytic site in AApoAI variants, responsible for the release of the fibrillogenic polypeptide. On the contrary, in wild-type ApoAI this region, as reported in the crystal structure [17], is in a predominantly α-helical structure, which protects the protein from proteolytic cleavage.

Also at the C-terminus, wild-type ApoAI and L75P variant are characterized by a quite similar proteolytic profile, showing accessibility at residues R188, Y192 and E223. This region seems to be protected in the L174S variant, as showed by the disappearance of the E223 cleavage site and by a slower kinetic of hydrolysis at level of R188 and Y192 residues, thus suggesting that a slight conformational change occurred in this region. Further differences in the proteolytic patterns of the three proteins were located in the region encompassing the 131–136 sequence that was exposed in the wild-type ApoAI, as demonstrated by cleavages at R131, K133 and E136. On the contrary, this region became completely inaccessible in the L75P variant, in perfect agreement with the molecular dynamics simulation. The accessibility of this sequence changed also in the L174S variant, where E136 was still recognized, but with slow kinetics and the appearance of new cleavage sites at R153 and Y166 was detected. It is noteworthy that these cleavages occurred quite close to the mutation site 174, indicating a higher accessibility of this region, as suggested by molecular dynamics calculations.

From MD and complementary proteolysis experiments we can conclude that both L75P- and L174S-AApoAI variants have an increased exposure of the N-terminal region.

3.6. Effects of mutations on ApoAI aggregation

As structural and conformational alterations have been associated with the presence of a single point mutation, the impact of pathogenic substitutions on the aggregation propensity of full-length AApoAI was investigated by using different approaches. First, to get information about the critical concentration [44] of AApoAI variants, proteins were incubated at different concentrations for 14 days at 37 °C. Their final concentration (c_f) was measured spectrophotometrically following the removal of aggregated species, as described in the Methods section. In the graph (Fig. S2), we reported $1 - c_f / c_i$ versus c_i, where c_i is the initial protein concentration and $1 - c_f / c_i$ is a measure of protein aggregated species. We calculated a critical concentration of 0.18 ± 0.05 mg/mL for L75P variant and 0.15 ± 0.04 mg/mL for L174S variant. No aggregation occurred for the wild-type protein.

Next, we measured the kinetics of aggregation of AApoAI variants by ThT binding assays. Proteins were incubated (0.3 mg/mL) at pH 7.4 in the presence of ThT, and the increase of ThT emission fluorescence at 482 nm was measured over time (Fig. 5A). A much higher increase in ThT fluorescence intensity was observed in the case of L174S-AApoAI variant with respect to L75P-AApoAI, whereas no aggregation of the wild-type protein was observed, in line with previous results [18]. For both AApoAI variants, a double-sigmoidal curve of ThT emission was observed, less evident in the case of L75P-AApoAI variant (inset of Fig. 5A). For both variants, the first transition occurred with a smaller amplitude increase in ThT fluorescence intensity with respect to the second one. The apparent $t_{1/2}$ values were: 29 ± 9 h and 96 ± 10 h for L75P-AApoAI and 35 ± 6 h and 83 ± 7 h for L174S-AApoAI. In agreement with data reported by Grudzielanek and coworkers on insulin aggregation [45], we hypothesize that the first transition is associated to with the formation of partially folded species able to bind ThT, whereas the second transition can be due to the formation of amyloid nuclei (Fig. 5A). Similar results were obtained in the presence of physiological amount of NaCl (0.15 M). Hence, in our experimental conditions, low salt concentration has no significant effect on the aggregation propensity of AApoAI variants.

Then, we analyzed the stability of protein tertiary structure upon incubation at 37 °C, as destabilization represents a crucial step during fibrillogenesis [46]. Proteins were incubated at 37 °C up to 1 week and at time intervals ANS binding experiments and intrinsic fluorescence analyses were performed (Fig. S3). In the presence of either amyloidogenic variants an increase in ANS fluorescence, more evident for L174S-AApoAI (Fig. S3C, gray line), was detected after 72 h, suggesting conformational changes leading to the exposure of hydrophobic surfaces. A decrease in ANS binding was observed after a prolonged incubation (1 week, Fig. S3C, dashed lines), suggesting shielding of hydrophobic patches due to their direct involvement in fibril formation. No changes in ANS binding was observed instead in the case of wild-type ApoAI (Fig. S3A). These results were confirmed by intrinsic fluorescence experiments (Fig. S3D–I and Table S1), showing a decrease of the emission maximum after 72 h incubation to be related to protein aggregation. As a consequence, Trp residues are hindered and remain buried instead of being exposed to the solvent.

Furthermore, we evaluated the apparent hydrodynamic diameter of the three proteins by means of dynamic light scattering (DLS). For wild-type ApoAI we obtained an apparent hydrodynamic diameter of 11.0 ± 1.1 nm, consistent with the size of a protein dimer, as previously reported by X-ray crystallography [22]. The hydrodynamic diameter of the

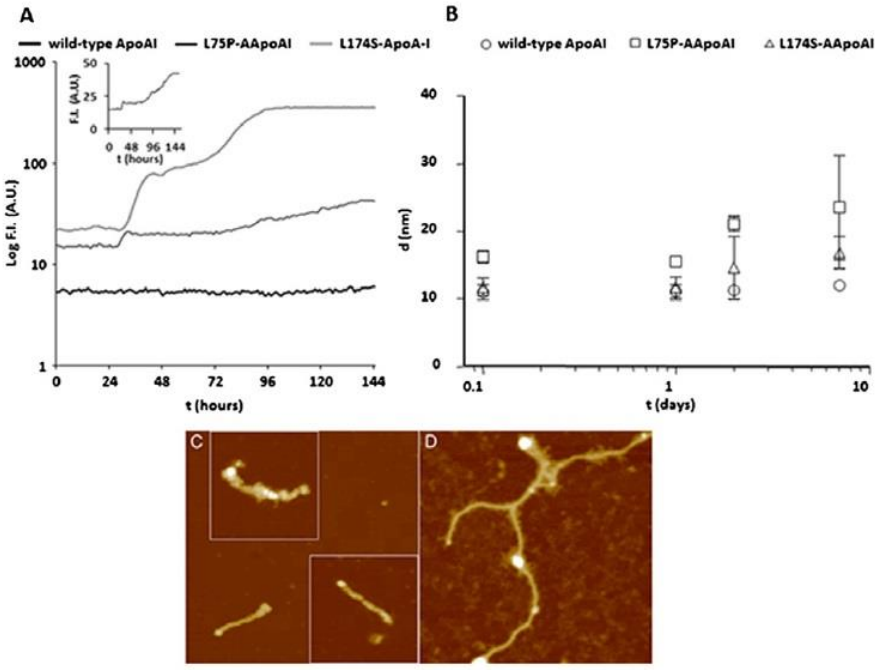

Fig. 5. AApoAI aggregation. A, ThT binding assay. Proteins under test were incubated for 144 h at 25 °C in 50 mM Tris HCl, pH 7.4. During the incubation, emission fluorescence values at 482 nm were recorded every 60 min. A typical curve for wild-type ApoAI (black bold line), L75P-AApoAI (black fine line) and L174S-AApoAI (gray bold line) are shown. The inset shows an enlargement of L75P-AApoAI curve. B, apparent hydrodynamic diameter of AApoAI variants over time. Wild-type ApoAI (empty circles), L75P-AApoAI (empty squares) and L174S-AApoAI variant (empty triangles) were incubated at 37 °C for different length of time. The hydrodynamic diameter, d(nm), is reported as a function of time, t(days), expressed as logarithm of time. C, D, tapping mode AFM images (height data) of L75P-AApoAI (C) and L174S-AApoAI (D) aggregates obtained after seven weeks incubation. Scan size 750 nm, Z range 29 nm (C and insets), 12 nm (D). The insets in C are at the same scale of the background image (inset scan size, 500 nm).

L174S-AApoAI variant was 11.8 ± 1.4 nm, similar to the value obtained for the wild-type protein, whereas the L75P-AApoAI variant showed a diameter of 16.3 ± 0.9 nm, consistent with a less-compact structure than the native protein, according to intrinsic fluorescence experiments and MD simulations (Fig. 2B-C). When proteins were analyzed after 24 h incubation, no formation of higher molecular aggregated species were detected in the three samples, as indicated in Fig. 5B, where the diameter values are plotted as a function of the incubation time. Indeed, wild-type ApoAI showed a constant apparent diameter up to 7 days (Fig. 5B) in agreement with ANS binding experiments, intrinsic fluorescence analyses and ThT binding (Figs. 2 and 5A), thus confirming no aggregation for the wild-type protein. On the contrary, the variants showed a different behavior with respect to ApoAI, with peculiar characteristics differentiating one from the other. The apparent diameter of L174S-AApoAI gradually increased up to 16.9 ± 2.4 nm after 7 days incubation, whereas L75P-AApoAI reached an apparent diameter value of 23.6 ± 7.8 nm, suggesting a pronounced decrease of protein compactness over time.

Finally, AFM experiments were performed to inspect the aggregate morphology after incubation times ranging from 4 to 7 weeks. We found that L75P-AApoAI formed scanty, short fibrils with length of 200–350 nm and height of 4–6 nm (Fig. 5C). These fibrils exhibit a beaded morphology, resulting from the assembly of different subunits of variable size, with not very regular packing. The L174S-AApoAI variant displayed a higher density of fibrillar aggregates as compared to L75P-AApoAI. These aggregates were generally smoother, longer and thinner than those formed by L75P-AApoAI, exhibiting typical lengths between 200 nm and 4 μm and heights between 1 and 3 nm; Fig. 5D shows L174S-AApoAI fibrils detected after 7 weeks incubation. In addition, a minority of thick, beaded fibrils (length 400–500 nm, height 5–6 nm) was also observed (not shown). No fibrils were detected for wild-type ApoAI in the same conditions. All the data collected indicate that the AApoAI variants are prone to aggregate and generate fibrils qualitatively similar to the fibrillar structures reported in the literature for other AApoAI variants [18,19].

4. Discussion

Using an array of independent methodologies, the effects of the "inside mutation" L75P and the "outside mutation" L174S on ApoAI propensity to undergo an amyloidogenic pathway have been analyzed with the aim of elucidating common and different features of amyloidogenic mutations in the development of the disease. We found that both variants display: (i) a slightly lower α-helical content with respect to the native protein and a time dependent increase of β-strand structure; (ii) more exposed hydrophobic regions, particularly evident for L174S variant; (iii) reduced stability and loss of unfolding cooperativity; (iv) increased flexibility; and (v) enhanced susceptibility to protease cleavage in the N-terminal region.

Nevertheless, the two variants show significant differences, which contribute to add knowledge to the emerging picture of the cause and effect relationship in ApoAI associated amyloidosis. As supposed, the substitution of L75 with proline has a destabilizing effect, as it breaks helix 70–76. This helix overlaps with one of the three predicted N-terminal amyloid "hot spots", whose perturbation has been recently suggested to be a prerequisite for misfolding [21]. This leads to the exposure of hydrophobic residues mainly located in the N-terminal region, as demonstrated by the increased intrinsic fluorescence intensity and ANS binding, as well as by the exposure of a proteolytic site at Y18, belonging to the major hot spot 14–22, as also found for G26R and L178H variants [18]. Furthermore, the accessibility of further proteolytic sites at E34 and F57 (the latter belonging to the minor hot spot 53–58), both hindered in the native protein, is the consequence of the propagation of the local perturbation (helix 70–76) to the other two predicted hot spots and the cause of the decreased protein compactness. In fact, DLS measurements of the hydrodynamic diameter demonstrated that the L75P variant is a much less compact protein with respect to both the wild-type protein and the L174S variant, with an increased diameter of 50%. Therefore, as a response to the occurrence of the "internal" mutation L75P, the protein acquires a "looser" structure at the N-terminal domain, with significant alteration of protein conformation and compactness, while the "external" mutation L174S is responsible for a less destabilized but more flexible structure to which a more pronounced aggregation-competent state is associated.

In the 3D structure, residue 174 is in close proximity to hot spot 14–22 which appears to be destabilized, as indicated by the appearance of a cleavage site at Y18. This perturbation could affect the hot spot 53–58, in line with cleavage at F57. Moreover, in the L174S variant cleavages at R153 and Y166 occur. The structural differences between L75P- and L174S-AApoAI variants are mainly due to differences in the exposed regions of the proteins. We believe that in L75P variant the N-terminal region is more unstructured, as indicated by Trp intrinsic fluorescence (Fig. 2B) and suggested by DLS measurements (Fig. 5B) and MD simulations (Fig. 4B), whereas in L174S the region encompassing residues 153–166 seems to be more unstructured, as demonstrated by limited proteolysis experiments (Fig. 4C).

We propose that these structural features represent the molecular basis of the different aggregation propensity of the two variants. Following incubation at 37 °C, L174S shows a higher propensity to aggregate than the L75P variant, as demonstrated by CD and fluorescence analyses, ThT binding and AFM imaging. The time-dependent increase of β-sheet structure, shown by L75P and L174S variants, is similar to that of G26R-AApoAI [18], whereas for L178H-AApoAI an increase in the α-helical content has been described over time, accompanied by the formation of very short fibrillar structures [18]. Upon 7 days incubation at 37 °C, DLS measurements revealed an over time increase of protein diameter by about 50% and 44% for the L75P and L174S variants, respectively, compared to the wild-type protein. Noteworthy, L75P-AApoAI lower compactness well correlates with the beaded morphology of its fibrils, whereas even though L174S-AApoAI is relatively compact and less unstructured than the other variant, it presents higher aggregation propensity than L75P-AApoAI. It is likely that in this case a balance between protein compactness, partial unfolding, group exposure and flexibility regulates protein amyloidogenicity.

Our data indicate that both amyloidogenic mutations induce protein destabilization in a region close to the mutated residue. The propagation of the destabilization to the N-terminal hot spots region, allowed by their proximity in the 3D structure, is a sine qua non condition for aggregation, as recently suggested by Das and coworkers [21]. The polymorphic behavior observed in our experimental system is not surprising, as polymorphism is a common feature of amyloid aggregation; in this case it could be also favored by the direct involvement of the N-terminal region alone in triggering aggregation, thus resulting in possible multiple arrangements of the rest of the protein.

Differently from the accepted pathway in which AApoA-I is cleaved prior to aggregation, Das and coworkers [21] suggested that AApoAI cleavage can occur only after aggregation of the full-length protein. Therefore, aggregation of the N-terminal region of the full-length protein would represent the first step in the fibrillogenic process. Following the specific cleavage of the full-length variant, the formation of mature fibrils could be observed. Our observation that L75P- and L174S-AApoA-I are able to aggregate as full-length proteins is consistent with this model, and the scantiness of mature fibrils can be explained by the lack of the proteolytic cleavage. Our findings highlight a potential key element in the evolution of the disease, i.e. the partial exposure of K96 and Y115 cleavage sites in L75P- and L174S-AApoAI, respectively. In fact, in this region, which is fully hindered in the native protein, the cleavage sites that allow the release of the fibrillogenic N-terminal polypeptide(s) are expected to be present. It is tempting to speculate that this region becomes fully exposed upon aggregation of the full-length variants.

In conclusion, our study adds knowledge, at a molecular level, to the general mechanism by which amyloidogenic mutations determine

ApoAI systemic amyloidosis, providing a new *tessera* in the puzzle of such a severe disease.

Supplementary data to this article can be found online at http://dx.doi.org/10.1016/j.bbagen.2015.10.019.

Author contribution

R.D.G and D.M.M. conceived the experiments; F.I. and R.D.G. constructed mutants; G.P. express and purified recombinant proteins; R.D.G. performed the biochemical experiments; M.M. and D.C. carried out proteolysis experiments; M.B. performed DLS experiments; A.M. performed the MD analyses; A.P. performed the AFM experiments; R.D.G., D.M.M., A.A., A.R., S.M.M., R.P. and P.P. analyzed the results; R.D.G., and D.M.M. wrote the paper with the contribution of all authors.

Funding

The authors thank the Italian MIUR (Ministero dell'Università e della Ricerca Scientifica, Progetti di Rilevante Interesse Nazionale) Project (PRIN 2009STNWX3) and the University of Genoa (Projects PRA2013 and PRA2014) for the financial support to the activities reported in the present study.

Transparency document

The Transparency document associated with this article can be found, in the online version.

References

[1] M. Eriksson, S. Schonland, S. Yumlu, U. Hegenbart, H. von Hutten, Z. Gioeva, P. Lohse, J. Büttner, H. Schmidt, C. Röcken, Hereditary apolipoprotein AI-associated amyloidosis in surgical pathology specimens: identification of three novel mutations in the APOA1 gene, J. Mol. Diagn. 11 (2009) 257–262.
[2] A. Relini, S. Torrassa, R. Rolandi, A. Gliozzi, C. Rosano, C. Canale, M. Bolognesi, G. Plakoutsi, M. Bucciantini, F. Chiti, M. Stefani, Monitoring the process of HypF fibrillization and liposome permeabilization by protofibrils, J. Mol. Biol. 338 (2004) 943–957.
[3] P. Westermark, M.D. Benson, J.N. Buxbaum, A.S. Cohen, B. Frangione, S. Ikeda, C.L. Masters, G. Merlini, M.J. Saraiva, J.D. Sipe, A primer of amyloid nomenclature, Amyloid 14 (2007) 179–183.
[4] S.T. Ferreira, F.G. De Felice, A. Chapeaurouge, Metastable, partially folded states in the productive folding and in the misfolding and amyloid aggregation of proteins, Cell Biochem. Biophys. 44 (2006) 539–548.
[5] S.T. Ferreira, M.N. Vieira, F.G. De Felice, Soluble protein oligomers as emerging toxins in Alzheimer's and other amyloid diseases, IUBMB Life 59 (2007) 332–345.
[6] K.A. Rye, P.J. Barter, Formation and metabolism of prebeta-migrating, lipid-poor apolipoprotein A-I, Arterioscler. Thromb. Vasc. Biol. 24 (2004) 421–428.
[7] G. Cavigiolio, E.G. Geier, B. Shao, J.W. Heinecke, M.N. Oda, Exchange of apolipoprotein A-I between lipid-associated and lipid-free states: a potential target for oxidative generation of dysfunctional high density lipoproteins, J. Biol. Chem. 285 (2010) 18847–18857.
[8] L. Obici, G. Franceschini, L. Calabresi, S. Giorgetti, M. Stoppini, G. Merlini, V. Bellotti, Structure, function and amyloidogenic propensity of apolipoprotein A-I, Amyloid 13 (2006) 1–15.
[9] D. Rowczenio, A. Dogan, J.D. Theis, J.A. Vrana, H.J. Lachmann, A.D. Wechalekar, J.A. Gilbertson, T. Hunt, S.D. Gibbs, P.T. Sattianayagam, et al., Amyloidogenicity and clinical phenotype associated with five novel mutations in apolipoprotein A-I, Am. J. Pathol. 179 (2011) 1978–1987.
[10] M. Gomaraschi, L. Obici, S. Simonelli, G. Gregorini, A. Negrinelli, G. Merlini, G. Franceschini, L. Calabresi, Effect of the amyloidogenic L75P apolipoprotein A-I variant on HDL subpopulations, Clin. Chim. Acta 412 (2011) 1262–1265.
[11] L. Obici, G. Palladini, S. Giorgetti, V. Bellotti, G. Gregorini, E. Arbustini, L. Verga, S. Marciano, S. Donadei, V. Perfetti, et al., Liver biopsy discloses a new apolipoprotein A-I hereditary amyloidosis in several unrelated Italian families, Gastroenterology 126 (2004) 1416–1422.
[12] P. Mangione, M. Sunde, S. Giorgetti, M. Stoppini, G. Esposito, L. Gianelli, L. Obici, L. Asti, A. Andreola, P. Viglino, et al., Amyloid fibrils derived from the apolipoprotein A1 Leu174Ser variant contain elements of ordered helical structure, Protein Sci. 10 (2001) 187–199.
[13] C.L. Murphy, S. Wang, K. Weaver, M.A. Gertz, D.T. Weiss, A. Solomon, Renal apolipoprotein A-I amyloidosis associated with a novel mutant Leu64Pro, Am. J. Kidney Dis. 44 (2004) 1103–1109.
[14] R. Del Giudice, D.M. Monti, C. Sarcinelli, A. Arciello, R. Piccoli, G.F. Hu, Amyloidogenic variant of apolipoprotein A-I elicits cellular stress by attenuating the protective activity of angiogenin, Cell Death Dis. 5 (2014), e1097.
[15] M. Marchesi, C. Parolini, C. Valetti, P. Mangione, L. Obici, S. Giorgetti, S. Raimondi, S. Donadei, G. Gregorini, G. Merlini, et al., The intracellular quality control system down-regulates the secretion of amyloidogenic apolipoprotein A-I variants: a possible impact on the natural history of the disease, Biochim. Biophys. Acta 1812 (2011) 87–93.
[16] A. Andreola, V. Bellotti, S. Giorgetti, P. Mangione, L. Obici, M. Stoppini, J. Torres, E. Monzani, G. Merlini, M. Sunde, Conformational switching and fibrillogenesis in the amyloidogenic fragment of apolipoprotein A-I, J. Biol. Chem. 278 (2003) 2444–2451.
[17] X. Mei, D. Atkinson, Crystal structure of C-terminal truncated apolipoprotein A-I reveals the assembly of HDL by dimerization, J. Biol. Chem. 286 (2011) 38570–38582.
[18] J. Petrlova, T. Duong, M.C. Cochran, A. Axelsson, M. Mörgelin, L.M. Roberts, J.O. Lagerstedt, The fibrillogenic L178H variant of apolipoprotein A-I forms helical fibrils, J. Lipid Res. 53 (2012) 390–398.
[19] J.O. Lagerstedt, G. Cavigiolio, L.M. Roberts, H.S. Hong, L.W. Jin, P.G. Fitzgerald, M.N. Oda, J.C. Voss, Mapping the structural transition in an amyloidogenic apolipoprotein A-I, Biochemistry 46 (2007) 9693–9699.
[20] S.A. Rosú, O.J. Rimoldi, E.D. Prieto, L.M. Curto, J.M. Delfino, N.A. Ramella, M.A. Tricerri, Amyloidogenic propensity of a natural variant of human apolipoprotein a-I: stability and interaction with ligands, PLoS ONE 10 (2015), e0124946.
[21] M. Das, X. Mei, S. Jayaraman, D. Atkinson, O. Gursky, Amyloidogenic mutations in human apolipoprotein A-I are not necessarily destabilizing- a common mechanism of apolipoprotein A-I misfolding in familial amyloidosis and atherosclerosis, FEBS J. 281 (2014) 2525–2542.
[22] O. Gursky, X. Mei, D. Atkinson, The crystal structure of the C-terminal truncated apolipoprotein A-I sheds new light on amyloid formation by the N-terminal fragment, Biochemistry 51 (2012) 10–18.
[23] L. Whitmore, B.A. Wallace, DICHROWEB: an online server for protein secondary structure analyses from circular dichroism spectroscopic data, Nucleic Acids Res. 32 (2004) 668–673.
[24] M. Koyama, M. Tanaka, P. Dhanasekaran, S. Lund-Katz, M.C. Phillips, H. Saito, Interaction between the N- and C-terminal domains modulates the stability and lipid binding of apolipoprotein A-I, Biochemistry 48 (2009) 2529–2537.
[25] B. Hess, C. Kutzner, D. van der Spoel, E. Lindahl, GROMACS 4: algorithms for highly efficient, load-balanced, and scalable molecular simulation, J. Chem. Theory Comput. 4 (2008) 435–447.
[26] S. Pronk, S. Pall, R. Schulz, P. Larsson, P. Bjelkmar, R. Apostolov, M.R. Shirts, J.C. Smith, P.M. Kasson, D. van der Spoel, et al., GROMACS 4.5: a high-throughput and highly parallel open source molecular simulation toolkit, Bioinformatics 29 (2013) 845–854.
[27] D. van der Spoel, R. van Druner, H.J.C. Berendsen, GROningenMAchine for chemical simulations, BIOSON Research Institute, Groningen, The Netherlands, 1994.
[28] H.J.C. Berendsen, J.P.M. Postma, W.F. van Gusteren, A. Di Nola, J.R. Haak, Molecular dynamics with coupling to an external bath, J. Chem. Phys. 81 (1984) 3684–3690.
[29] T. Darden, D. York, L. Pedersen, Particle mesh Ewald — an N·log(N) method for Ewald sums in large systems, J. Chem. Phys. 98 (1993) 10089–10092.
[30] G. Bussi, D. Donadio, M. Parrinello, Canonical sampling through velocity rescaling, J. Chem. Phys. 126 (2007) 014101.
[31] M. Parrinello, A. Rahman, Polymorphic transitions in single crystals: a new molecular dynamics method, J. Appl. Phys. 52 (1981) 7182–7190.
[32] B. Hess, H. Bekker, H.J.C. Berendsen, J.G.E.M. Frajie, LINCS: a linear constraint solver for molecular simulations, J. Comput. Chem. 18 (1997) 1463–1472.
[33] A. Merlino, L. Mazzarella, A. Carannante, A. Di Fiore, A. Di Donato, E. Notomista, F. Sica, The importance of dynamic effects on the enzyme activity: X-ray structure and molecular dynamics of onconase mutants, J. Biol. Chem. 280 (2005) 17953–17960.
[34] I. Di Lelio, S. Caccia, M. Coppola, M. Buonanno, G. Di Prisco, P. Varricchio, E. Franzetti, G. Corrado, S.M. Monti, R. Rao, et al., A virulence factor encoded by a polydnavirus confers tolerance to transgenic tobacco plants against lepidopteran larvae, by impairing nutrient absorption, PLoS ONE 9 (2014), e113988.
[35] H. Saito, P. Dhanasekaran, D. Nguyen, P. Holvoet, S. Lund-Katz, M.C. Phillips, Domain structure and lipid interaction in human apolipoproteins A-I and E, a general model, J. Biol. Chem. 278 (2003) 23227–23232.
[36] M. Tanaka, P. Dhanasekaran, D. Nguyen, S. Ohta, S. Lund-Katz, M.C. Phillips, H. Saito, Contributions of the N- and C-terminal helical segments to the lipid-free structure and lipid interaction of apolipoprotein A-I, Biochemistry 45 (2006) 10351–10358.
[37] J.A. Beckstead, B.L. Block, J.K. Bielicki, C.M. Kay, M.N. Oda, R.O. Ryan, Combined N- and C-terminal truncation of human apolipoprotein A-I yields a folded, functional central domain, Biochemistry 44 (2005) 4591–4599.
[38] D.P. Rogers, C.G. Brouillette, J.A. Engler, S.W. Tendian, L. Roberts, V.K. Mishra, G.M. Anantharamaiah, S. Lund-Katz, M.C. Phillips, M.J. Ray, Truncation of the amino terminus of human apolipoprotein A-I substantially alters only the lipid-free conformation, Biochemistry 36 (1997) 288–300.
[39] M. Tanaka, P. Dhanasekaran, D. Nguyen, M. Nickel, Y. Takechi, S. Lund-Katz, M.C. Phillips, H. Saito, Influence of N-terminal helix bundle stability on the lipid-binding properties of human apolipoprotein A-I, Biochim. Biophys. Acta 1811 (2011) 25–30.
[40] V. Granata, G. Graziano, A. Ruggiero, G. Raimo, M. Masullo, P. Arcari, L. Vitagliano, A. Zagari, Chemical denaturation of the elongation factor 1 alpha isolated from the hyperthermophilic archaeon *Sulfolobus solfataricus*, Biochemistry 45 (2006) 719–726.
[41] F. Dal Piaz, A. Casapullo, A. Randazzo, R. Riccio, P. Pucci, G. Marino, L. Gomez-Paloma, Molecular basis of phospholipase A2 inhibition by petrosaspongiolide M, Chembiochem 3 (2002) 664–671.
[42] G. Esposito, R. Michelutti, G. Verdone, P. Viglino, H. Hernàndez, C.V. Robinson, A. Amoresano, F. Dal Piaz, M. Monti, P. Pucci, et al., Removal of the N-terminal hexapeptide from human β2-microglobulin facilitates protein aggregation and fibril formation, Protein Sci. 9 (2000) 831–845.

[43] M. Monti, S. Principe, S. Giorgetti, P. Mangione, G. Merlini, A. Clark, V. Bellotti, A. Amoresano, P. Pucci, Topological investigation of amyloid fibrils obtained from β2-microglobulin, Protein Sci. 11 (2002) 2362–2369.
[44] H. Yagi, K. Hasegawa, Y. Yoshimura, Y. Goto, Acceleration of the depolymerization of amyloid β fibrils by ultrasonication, Biochim. Biophys. Acta 1834 (2013) 2480–2485.
[45] S. Grudzielanek, V. Smirnovas, R. Winter, Solvation-assisted pressure tuning of insulin fibrillation: from novel aggregation pathways to biotechnological applications, J. Mol. Biol. 356 (2006) 497–509.
[46] M. Lindgren, P. Hammarström, Amyloid oligomers: spectroscopic characterization of amyloidogenic protein states, FEBS J. 277 (2010) 1380–1388.

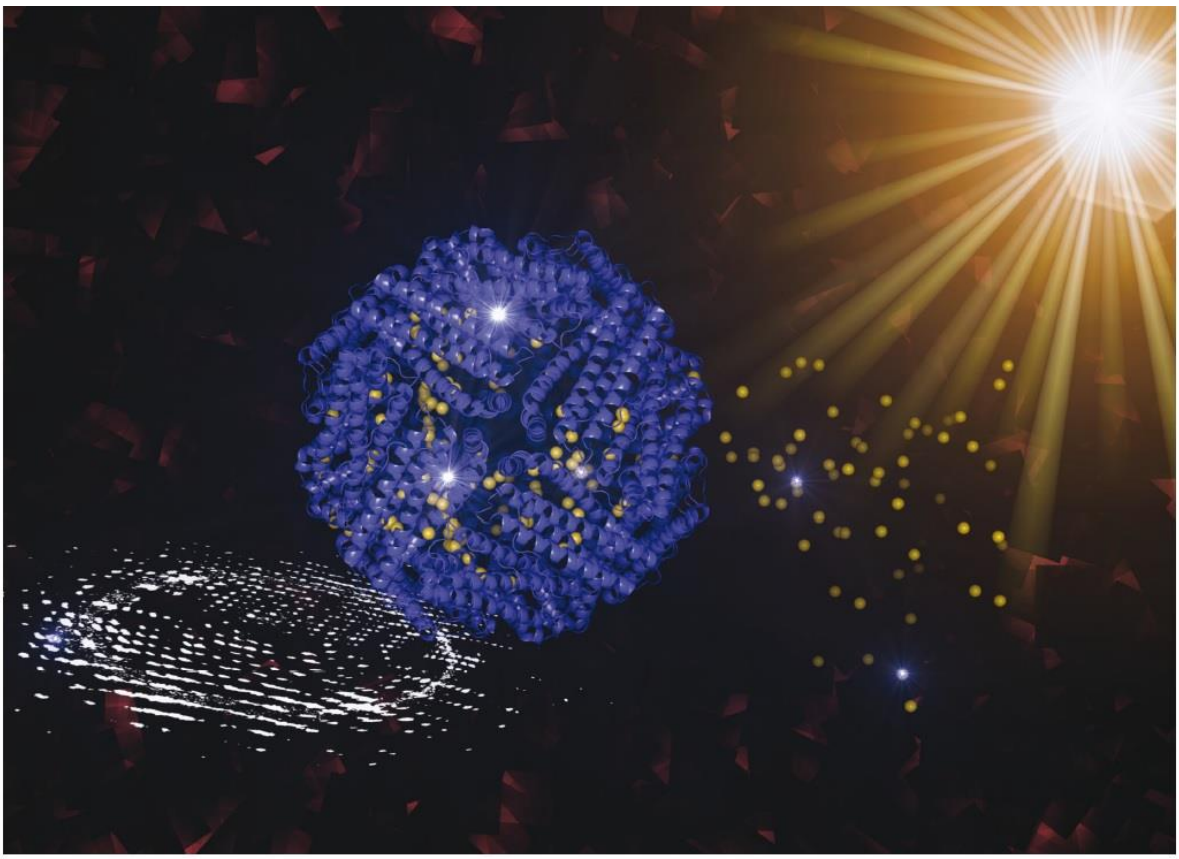

Showcasing research from Prof. Antonello Merlino's laboratory/ Department of Chemical Sciences, University of Naples Federico II, Napoli, Italy

Gold-based drug encapsulation within a ferritin nanocage: X-ray structure and biological evaluation as a potential anticancer agent of the Auoxo3-loaded protein

The authors have encapsulated a cytotoxic gold(III) compound within the ferritin nanocage. Gold binding sites have been identified by X-ray crystallography. The gold-encapsulated nanocarrier exhibits much higher cytotoxicity than free AFt, which is basically non-toxic. The adduct is much more cytotoxic on human cancer cells than on non-tumorigenic cells. These data indicate that encapsulation of gold-based drugs within Ft nanocages is a promising strategy to deliver gold-based drugs to their final targets.

As featured in:

See Antonello Merlino *et al.*, *Chem. Commun.*, 2016, 52, 9518.

ROYAL SOCIETY OF CHEMISTRY

www.rsc.org/chemcomm

Registered charity number: 207890

ChemComm

COMMUNICATION

View Article Online
View Journal | View Issue

CrossMark click for updates

Cite this: *Chem. Commun.*, 2016, 52, 9518

Received 23rd March 2016,
Accepted 10th June 2016

DOI: 10.1039/c6cc02516a

www.rsc.org/chemcomm

Gold-based drug encapsulation within a ferritin nanocage: X-ray structure and biological evaluation as a potential anticancer agent of the Auoxo3-loaded protein†

Giarita Ferraro,[a] Daria Maria Monti,[a] Angela Amoresano,[a] Nicola Pontillo,[a] Ganna Petruk,[a] Francesca Pane,[a] Maria Agostina Cinellu[bc] and Antonello Merlino*[ad]

Auoxo3, a cytotoxic gold(III) compound, was encapsulated within a ferritin nanocage. Inductively coupled plasma mass spectrometry, circular dichroism, UV-Vis absorption spectroscopy and X-ray crystallography confirm the potential-drug encapsulation. The structure shows that naked Au(I) ions bind to the side chains of Cys48, His49, His114, His114 and Cys126, Cys126, His132, His147. The gold-encapsulated nanocarrier has a cytotoxic effect on different aggressive human cancer cells, whereas it is significantly less cytotoxic for non-tumorigenic cells.

In recent years, gold-based compounds have emerged as promising alternatives to cisplatin and to other metal-based drugs by displaying specific activities against different cancer cells.[1–3] Yet, the clinical use of gold-based drugs has until now been hampered by a series of factors, including toxicity and low solubility of the compounds in aqueous media.[4] Encapsulation of cytotoxic gold compounds by microcapsules, gels, nanoparticles and micelles has been applied to overcome the limitations associated with poor aqueous solubility and to enhance the selectivity of these potential drugs for tumor cells, improving bioavailability, effectiveness and applicability of these molecules.[4,5]

Protein nanocages have attracted intense attention as drug delivery systems due to merits that include high biocompatibility, high solubility and ease of surface modification. Ferritin (Ft) nanocages have been used to encapsulate a variety of drugs and biologically active substances,[6] including gadolinium contrast agents,[7] desferrioxamine B,[8] doxorubicin,[9] inorganic and magnetite nanoparticles,[10,11] β-carotene,[12] a few photosensitizers,[13] cisplatin and carboplatin,[14,15] rhodium[16] and palladium compounds,[17] organometallic CO releasing systems containing Ru and Mn.[18,19] We have recently described the structure of a cisplatin encapsulated apoFt (Aft) nanocage,[20] whose cytotoxicity is well documented;[14,15] our structure has provided hints to explain the reasons why Ft can be efficiently used for the transport of drugs to malignant cells.

Although the use of AFt in the transport of metallodrugs[14,15,20] and in the fabrication of gold nanoparticles[21,22] is well documented, to our knowledge gold-based drugs have never been encapsulated within an AFt nanocage. Here, we have used Auoxo3, a potential gold(III) based drug, a member of a class of gold compounds of medicinal interest (Auoxos), already well characterized both in its cytotoxicity[23–25] and binding to proteins,[26–28] to prepare gold-based drug-encapsulated AFt.

The chemical structure of the *trans* isomer of the drug is reported in Fig. 1.

Previous data indicated that the probable biomolecular targets for Auoxos are histone deacetylase (HDAC), protein kinase C (PKc) or thioredoxin reductase.[23,29] According to mechanistic studies, the interactions between these compounds and the targets are likely dominated by redox transformations. Auoxos behave as prodrugs: they degrade and release gold(I) ions which eventually bind and inhibit the final target(s). It was found that the antiproliferative effects of the various Auoxos and the cytotoxicity profile of cisplatin are rather diverse, implying that their mechanisms of action are very different.

The potential antitumor drug-loaded nanostructure was prepared using the procedure previously described by Huang

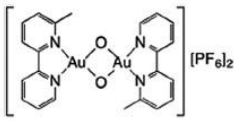

Auoxo3

Fig. 1 Chemical structure of the *trans* isomer of Auoxo3.

[a] *Department of Chemical Sciences, University of Naples Federico II, Complesso Universitario di Monte Sant'Angelo, Via Cintia, I-80126, Napoli, Italy. E-mail: antonello.merlino@unina.it; Fax: +39081674090; Tel: +39081674276*
[b] *Department of Chemistry and Pharmacy, University of Sassari, Via Vienna 2, 07100 Sassari, Italy*
[c] *CIRCC, Consorzio Interuniversitario Reattività Chimica e Catalisi, Università di Bari, Via Celso Ulpiani 27, 70126 Bari, Italy*
[d] *CNR Institute of Biostructures and Bioimages, Via Mezzocannone 16, I-80126, Napoli, Italy*

† Electronic supplementary information (ESI) available. See DOI: 10.1039/c6cc02516a

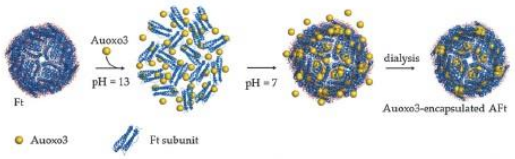

Fig. 2 Encapsulation of Auoxo3 within AFt. Horse spleen ferritin from Sigma (Ft, code F4503, mainly L-subunits) was dissociated at pH 13 using 0.1 M NaOH and reconstituted in the presence of the drugs using sodium phosphate buffer at pH 7.4. A ~ 75 : 1 Auoxo3 to protein molar ratio was used. The gold-compound was encapsulated within the Ft nanocage after its reconstitution.

and coworkers[15] and already used to encapsulate cisplatin and carboplatin.[14,15,20] A schematic picture representing the gold-based drug encapsulation with AFt is presented in Fig. 2.

The protein folding was verified by using far-UV circular dichroism (CD) spectroscopy (Fig. S1, ESI†). Data reveal that Ft can reassemble in the presence of the drug, retaining its native conformation. Inductively coupled plasma mass spectrometry (ICP-MS) was used to verify the potential drug encapsulation. A Ft nanocage can encapsulate about 420 gold atoms (from 350 to 500 atoms of gold depending on the preparation), much more than those found when gold ions from $AuCl_4^-$ were encapsulated in horse liver AFt (<185 gold atoms).[22] The size of Auoxo3-encapsulated AFt was measured in solution by dynamic light scattering (DLS). The average size (*Z*-average) of fresh solutions of Auoxo3-encapsulated AFt is 13.8 ± 0.9 nm, in good agreement with what is found for AFt.

The structure of Auoxo3-encapsulated AFt was refined at 1.85 Å resolution to an Rfactor of 0.180 (Rfree 0.226) (Fig. 3A). The X-ray structure confirms the proper assembly of the 24-mer Ft. The gold binding sites were unambiguously identified by using Fourier difference and anomalous electron density maps (Fig. 3B–E, see also the ESI† for further details and discussion).

As previously reported for the interaction of Auoxo3[28] and other members of the Auoxos series with the model proteins hen egg white lysozyme and bovine pancreatic ribonuclease,[27,28,30] upon encapsulation within AFt, the compound degrades extensively: gold atoms are found bound to the side chains of Cys48, His49, Cys48 and His49, His114 and Cys126, Cys126, His132 and His147 (Fig. 3C–F). The linear geometry close to gold atoms suggests that the metal is in the oxidation state +1 and thus that the original compound Auoxo3 undergoes degradation and reduction. Interestingly, His114 and Cys126 are conserved residues known to play a role in the iron transport to the Ft three-fold channel.[31] Gold ions were found close to the side chains of Cys48, His49, His114 and Cys126 also in the X-ray structure of horse liver apo-Ft with $AuCl_4^-$ (pdb code 3H7G),[22] although the details of the interactions between Au and protein residues are different when compared to those described here (see Fig. S2, ESI† for further details). In our structure, at the Cys48 binding site, a gold ion is located between the SG atom (unrestrained distance = 2.3 Å) and π electrons from the imidazole of His49 (distance from the centroid of imidazole = 3.0 Å), which in turn is also coordinated to another Au atom.

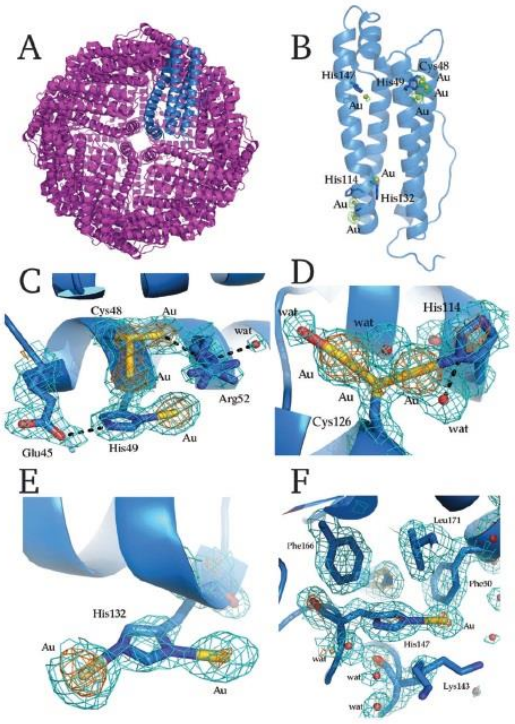

Fig. 3 The X-ray structure of Auoxo3-encapsulated AFt complex (A) expanded to show a single four-helix bundle subunit with Au binding sites evidenced and Bijvoet difference Fourier map calculated with anomalous data reported at 3σ (B). In panels C-F 2Fo-Fc electron density maps at 1σ (cyan) and 4σ (orange) of gold ions coordinated to Cys48, His49, Cys48 and His49 (C) His114 and Cys126, Cys126 (D), His132 (E) and His147 (F) are reported. The gold ions were refined with partial occupancy (0.30, 0.35, 0.45, 0.40, 0.45, 0.20 and 0.25); the average B-factors for gold ions are in the range 20.0–50.3 Å^2. The structure was deposited in the Protein Data Bank under accession code 5IX6.

The side chain of His49 is maintained in its position by the salt bridge that forms with the side chain of Glu45. At 3.1 Å from this Au ion, a second gold atom is bound to the SG of Cys48. This metal centre is in contact with the side chain atoms of Arg52 (Fig. 3C). A peculiar arrangement of Au ions is also found at the His114 and Cys126 binding sites. Here, the electron density map suggests the possibility that a water molecule could be accommodated in the cavity formed between the two gold centres that are at a distance of 3.7 Å. These atoms are bound to the SG atom of Cys126 (distance = 2.2 Å) and to a water molecule (distance = 2.5 Å), and to the SG atom of Cys126 (distance = 2.2 Å) and to the ND1 atom of His114 (distance = 2.2 Å), respectively (Fig. 3D). A detailed description of the interaction that Au atoms form with protein residues or solvent molecules is reported in Table S1 (ESI†).

With the exception of the Au ions bound to side chains of His114 and Cys126, which are buried at the interface between two AFt subunits, all of the Au binding sites identified in the

Auoxo3-encaspulated-AFt structure are located on the inner surface of the nanocage. This indicates that the structure and electrostatic potential of the outer surface of AFt are not affected by drug encapsulation. Thus, Auoxo3-encapsulated AFt retains the physico-chemical features that make this protein an ideal nanocarrier for drug delivery to target sites (*i.e.* biocompatibility, solubility and possibility to be recognized by specific receptors).

The effects of Auoxo3-encapsulated AFt were then tested on three human tumor cell lines (MCF-7, breast cancer cells, HeLa, cervical cancer cells and HepG2, hepatic carcinoma cells) and three non-tumorigenic cell lines (HRCE, human renal cortical epithelial cells, HaCaT, human keratinocyte cells and H9c2, rat cardiomyoblast cells) by using a cell viability assay.[32] Native Ft was used as control (Fig. 4 and Table 1). From the MTT assay, it was observed that native Ft had no effect on cancer cells (Fig. 4A), whereas the encapsulated nanocage showed a significant cytotoxic effect on all the analysed human cancer cell lines (Fig. 4B). Our data on free AFt are in agreement with previous studies, demonstrating that native Ft is non-toxic for Gastric Cancer (GCC) and HeLa cells.[14,15] Interestingly, Auoxo3-encapsulated AFt exerts lower effects on normal cells, as indicated by IC_{50} values reported in Table 1.

IC_{50} values were also derived for cisplatin and Auoxo3, used as positive controls, on the same cell lines (Table 2). Although a direct comparison between the IC_{50} values of these drugs and

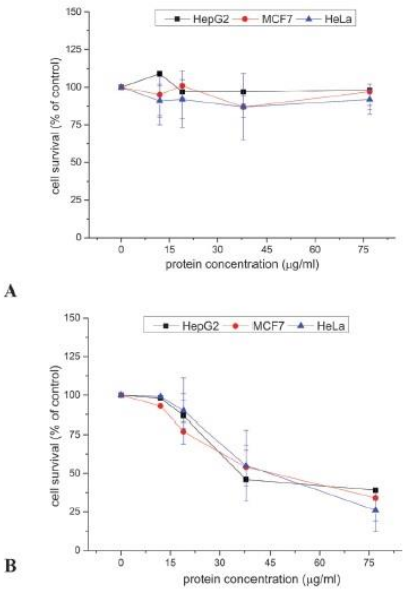

Fig. 4 Effects of free AFt (A) and Auoxo3-encapsulated AFt (B) on human cancer cells. HepG2, HeLa and MCF-7 were treated with increasing amounts of proteins for 72 hours. Cell viability was assessed by the MTT assay and expressed as described in the materials and methods section. All values are given as means ± SD ($n \geq 3$).

Table 1 Cytotoxic activity of Auoxo3-encapsulated AFt on different cancer (HepG2, HeLa and MCF-7) and normal cells (H9c2, HRCE and HaCaT). Cytotoxicity is expressed as IC_{50} values in μg mL^{-1}, *i.e.* the protein concentration inducing 50% cell death

	Auoxo3-encapsulated AFt	AFt
HepG2	35 ± 1	>1000
MCF-7	41 ± 9	>1000
Hela	42 ± 1	>1000
H9c2	59 ± 10	>1000
HRCE	61 ± 5	150 ± 55
HaCaT	69 ± 11	>1000

Table 2 Cytotoxic activity of Auoxo3 and cisplatin on the studied cell lines. Cytotoxicity is expressed as IC_{50} values in μg mL^{-1}, *i.e.* the compound concentration inducing 50% cell death

	Auoxo3	Cisplatin
HepG2	16 ± 6	2.8 ± 0.9
MCF-7	8 ± 2	21 ± 4
Hela	3 ± 1	2 ± 1
H9c2	4 ± 1	5 ± 2
HRCE	2.2 ± 0.4	2.0 ± 0.6
HaCaT	14.2 ± 0.7	2.1 ± 0.4

those obtained using Auoxo3-encapsulated AFt is not possible, since it is clear from previous experiments that drug-encapsulated Ft nanocages exert cytotoxicity by a mechanism of action different from free drugs,[15] it is interesting to note that Auoxo3 is rather toxic even on normal cells, contrary to Auoxo3-encapsulated AFt. The mechanism of Au release from Auoxo3-encapsulated AFt has not yet been studied in detail, but based on the literature data on other drug-encapsulated AFt adducts, it can be postulated that Auoxo3-encapsulated AFt can efficiently transport drugs to tumors through interactions with integrin or with specific receptors overexpressed on the surface of tumor cells.[15,33] Free Au(I) ions are probably released inside the cell upon protein degradation *via* a lysosome/proteasome pathway.[34] In order to obtain preliminary results on this issue, we quantified the gold uptake inside MCF-7 cells upon 24, 48 and 72 h of incubation with Auoxo3-encapuslated AFt using ICP-MS. The Au uptake ratio associated with Auoxo3-encapsulated AFt is 9.0, 11.9 and 21.6% after 24, 48 and 72 h, respectively (see the ESI† for further details). Furthermore, the apoptosis level in these tumor cell lines was examined by western blotting analyses using a specific antibody against Caspase 3, an effector Caspase. The results revealed that, after 24, 48 and 72 h incubation, no activation of Caspase 3 was observed in the presence of Auoxo3-encapsulated-Aft (Fig. S4, ESI†).

In conclusion, we have encapsulated a gold-based anticancer compound within a ferritin nanocage and have characterized the formed adduct from a structural viewpoint. The X-ray structure of Auoxo3-encapsulated AFt, refined at 1.85 Å resolution, reveals that naked gold(I) ions bind close to Cys or His side chains, mainly at the inner surface of the nanocage. The cytotoxicity of this adduct has been evaluated for three human cancer cells (HepG2, MCF-7, HeLa) and three non-tumorigenic cell lines (H9c2, HRCE and HaCaT). It exhibits much higher cytotoxicity than free AFt,

which is basically non-toxic. The adduct is much more toxic to tumor cells than to non-tumor cells.

Altogether these data indicate that encapsulation of gold-based drugs within Ft nanocages is a promising strategy to deliver these molecules to their final targets.

The authors thank G. Sorrentino and M. Amendola for technical assistance at CNR Institute of Biostructures and Bioimages. MAC gratefully acknowledges the Regione Autonoma della Sardegna for funds financed on L. R. 7/2007 bando 2013.

References

1 (*a*) T. Zou, C.-T. Lum, C.-N. Lok, J.-J. Zhang and C.-M. Che, *Chem. Soc. Rev.*, 2015, **44**, 8786–8801; (*b*) I. Ott, *Coord. Chem. Rev.*, 2009, **253**, 1670–1681.
2 (*a*) S. Nobili, E. Mini, I. Landini, C. Gabbiani, A. Casini and L. Messori, *Med. Res. Rev.*, 2010, **30**, 550–580; (*b*) L. Ronconi, L. Giovagnini, C. Marzano, F. Bettio, R. Graziani, G. Pilloni and D. Fregona, *Inorg. Chem.*, 2005, **44**, 1867–1881.
3 (*a*) B. Bertrand and A. Casini, *Dalton Trans.*, 2014, **43**, 4209–4219; (*b*) L. Messori and G. Marcon, *Met. Ions Biol. Syst.*, 2004, **42**, 385–424.
4 (*a*) J. J. Yan, R. W.-Y. Sun, P. Wu, M. C. M. Lin, A. S. C. Chan and C.-M. Che, *Dalton Trans.*, 2010, **39**, 7700–7705; (*b*) P. Lee, R. Zhang, V. Li, X. Liu, R. W.-Y. Sun, C.-M. Che and K. K. Y. Wong, *Int. J. Nanomed.*, 2012, **7**, 731–737.
5 (*a*) P. Ringhieri, R. Iannitti, C. Nardon, R. Palumbo, D. Fregona, G. Morelli and A. Accardo, *Int. J. Pharm.*, 2014, **473**, 194–202; (*b*) L. He, T. Chen, Y. You, H. Hu, W. Zheng, W.-L. Kwong, T. Zou and C.-M. Che, *Angew. Chem., Int. Ed.*, 2014, **53**, 12532–12536.
6 (*a*) B. Maity, K. Fujita and T. Ueno, *Curr. Opin. Chem. Biol.*, 2015, **25**, 88–97; (*b*) N. J. M. Sanghamitra and T. Ueno, *Chem. Commun.*, 2013, **49**, 4114–4126; (*c*) T. Ueno and Y. Watanabe, *Coordination Chemistry in Protein Cages-Principles, Design, Applications*, Wiley, Weinheim, 2013, ISBN 978-1-1180-7857-0.
7 (*a*) S. Aime, L. Frullano and S. G. Crich, *Angew. Chem., Int. Ed.*, 2002, **41**, 1017–1019; (*b*) J. C. Cutrin, S. G. Crich, D. Burghelea, W. Dastru' and S. Aime, *Mol. Pharmacol.*, 2013, **10**(5), 2079–2085.
8 J. M. Domınguez-Vera, *J. Inorg. Biochem.*, 2004, **98**, 469–472.
9 (*a*) M. Liang, K. Fan, M. Zhou, S. Duan, J. Zheng, D. Yang, J. Feng and X. Yan, *Proc. Natl. Acad. Sci. U. S. A.*, 2014, **111**, 14900–14905; (*b*) J. Polanams, A. D. Ray and R. K. Watt, *Inorg. Chem.*, 2005, **44**, 3203–3209; (*c*) M. A. Kilic, E. Ozlu and S. Callis, *J. Biomed. Nanotechnol.*, 2012, **8**, 508–514.
10 (*a*) T. Ueno, M. Suzuki, T. Goto, T. Matsumoto, K. Nagayama and Y. Watanabe, *Angew. Chem., Int. Ed.*, 2004, **43**, 2527–2530; (*b*) M. Li, C. Viravaidya and S. Mann, *Small*, 2007, **3**, 1477–1481; (*c*) K. Iwahori, K. Yoshizawa, M. Muraoka and I. Yamashita, *Inorg. Chem.*, 2005, **44**, 6393–6400; (*d*) K. W. Pulsipher and I. J. Dmochovski, *Methods Mol. Biol.*, 2015, **1252**, 27–37.
11 M. Uchida, M. L. Flenniken, M. Allen, D. A. Willits, B. E. Crowley, S. Brumfield, A. F. Willis, L. Jackiw, M. Jutila, M. J. Young and T. Douglas, *J. Am. Chem. Soc.*, 2006, **128**, 16626–16633.
12 L. Chen, G. Bai, R. Yang, J. Zang, T. Zhou and G. Zhao, *Food Chem.*, 2014, **149**, 307–312.
13 (*a*) Z. Zhen, W. Tang, W. Zhang and J. Xie, *Nanoscale*, 2015, **7**, 10330–10333; (*b*) Z. Zhen, W. Tang, C. Guo, H. Chen, X. Lin, G. Liu, B. Fei, X. Chen, B. Xu and J. Xie, *ACS Nano*, 2013, **7**, 6988–6996.
14 Z. Yang, X. Wang, H. Diao, J. Zhang, H. Li, H. Sun and Z. Guo, *Chem. Commun.*, 2007, 3453–3455.
15 X.-T. Ji, L. Huang and H.-Q. Huang, *J. Proteomics*, 2012, **75**, 3145–3157.
16 (*a*) S. Abe, K. Hirata, T. Ueno, K. Morino, N. Shimizu, M. Yamamoto, M. Takata, E. Yashima and Y. Watanabe, *J. Am. Chem. Soc.*, 2009, **131**, 6958–6960; (*b*) Z. Ke, S. Abe, T. Ueno and K. Morokuma, *J. Am. Chem. Soc.*, 2012, **134**, 15418–15429.
17 (*a*) S. Abe, T. Hikage, Y. Watanabe, S. Kitagawa and T. Ueno, *Inorg. Chem.*, 2010, **49**, 6967–6973; (*b*) Z. Wang, Y. Takezawa, H. Aoyagi, S. Abe, T. Hikage, Y. Watanabe, S. Kitagawa and T. Ueno, *Chem. Commun.*, 2011, **47**, 170–172.
18 (*a*) H. Fujita, Y. Tanaka, T. Sho, S. Ozeki, S. Abe, T. Hikage, T. Kuchimaru, S. Kizaka-Kondoh and T. Ueno, *J. Am. Chem. Soc.*, 2014, **136**, 16902–16908; (*b*) Y. Takezawa, P. Böckmann, N. Sugi, Z. Wang, S. Abe, T. Murakami, T. Hikage, G. Erker, Y. Watanabe, S. Kitagawa and T. Ueno, *Dalton Trans.*, 2011, **40**, 2190–2195.
19 H. Fujita, Y. Tanaka, S. Abe and T. Ueno, *Angew. Chem., Int. Ed.*, 2016, **55**, 1056–1060.
20 N. Pontillo, F. Pane, L. Messori, A. Amoresano and A. Merlino, *Chem. Commun.*, 2016, **52**, 4136–4139.
21 (*a*) R. Fan, S. W. Chen, V. V. Cheong and B. P. Orner, *Small*, 2010, **6**, 1483–1487; (*b*) J. D. Keyes, R. J. Hilton, J. Farrer and R. K. Watt, *J. Nanopart. Res.*, 2011, **13**(6), 2563–2575; (*c*) C. Sun, H. Yang, Y. Yuan, X. Tian, L. Wang, Y. Guo, L. Xu, J. Lei, N. Gao and G. J. Anderson, *J. Am. Chem. Soc.*, 2011, **133**, 8617–8624; (*d*) C. A. Butts, J. Swift, S. G. Kang, L. Di Costanzo, D. W. Christianson and J. G. Saven, *Biochemistry*, 2008, **47**, 12729–12739.
22 M. Suzuki, M. Abe, T. Ueno, S. Abe, T. Goto, Y. Toda, T. Akita, Y. Yamada and Y. Watanabe, *Chem. Commun.*, 2009, 4871–4873.
23 C. Gabbiani, A. Guerri, M. A. Cinellu and L. Messori, *Open Crystallogr. J.*, 2010, **3**, 29–40.
24 (*a*) F. Magherini, A. Modesti, L. Bini, M. Puglia, I. Landini, S. Nobili, E. Mini, M. A. Cinellu, C. Gabbiani and L. Messori, *J. Biol. Inorg. Chem.*, 2010, **15**, 573–582; (*b*) G. Ferraro, L. Massai, L. Messori, M. A. Cinellu and A. Merlino, *BioMetals*, 2015, **28**, 745–754.
25 (*a*) A. Casini, M. A. Cinellu, G. Minghetti, C. Gabbiani, M. Coronnello, E. Mini and L. Messori, *J. Med. Chem.*, 2006, **49**, 5524–5531; (*b*) M. A. Cinellu, L. Maiore, M. Manassero, A. Casini, M. Arca, H.-H. Fiebig, G. Kelter, E. Michelucci, G. Pieraccini, C. Gabbiani and L. Messori, *ACS Med. Chem. Lett.*, 2010, **1**, 336–339.
26 (*a*) C. Gabbiani, L. Massai, F. Scaletti, E. Michelucci, L. Maiore, M. A. Cinellu and L. Messori, *J. Biol. Inorg. Chem.*, 2012, **17**, 1293–1302; (*b*) C. Gabbiani, F. Scaletti, L. Massai, E. Michelucci, M. A. Cinellu and L. Messori, *Chem. Commun.*, 2012, **48**, 11623–11625; (*c*) L. Messori, M. A. Cinellu and A. Merlino, *ACS Med. Chem. Lett.*, 2014, **5**, 1110–1113.
27 L. Messori, F. Scaletti, L. Massai, M. A. Cinellu, I. Russo Krauss, G. di Martino, A. Vergara, L. Paduano and A. Merlino, *Metallomics*, 2014, **6**, 233–236.
28 I. Russo Krauss, L. Messori, M. A. Cinellu, D. Marasco, R. Sirignano and A. Merlino, *Dalton Trans.*, 2014, **43**, 17483–17488.
29 (*a*) F. Guidi, I. Landini, M. Puglia, F. Magherini, C. Gabbiani, M. A. Cinellu, S. Nobili, T. Fiaschi, L. Bini, E. Mini, L. Messori and A. Modesti, *Metallomics*, 2012, **4**, 307–314; (*b*) C. Gabbiani, A. Casini, L. Messori, A. Guerri, M. A. Cinellu, G. Minghetti, M. Corsini, C. Rosani, P. Zanello and M. Arca, *Inorg. Chem.*, 2008, **47**, 2368–2379.
30 L. Messori, F. Scaletti, L. Massai, M. A. Cinellu, C. Gabbiani, A. Vergara and A. Merlino, *Chem. Commun.*, 2013, **49**, 10100–10102.
31 S. Levi, P. Santambrogio, B. Corsi, A. Cozzi and P. Arosio, *Biochem. J.*, 1996, **317**, 467–473.
32 M. V. Berridge, P. M. Herst and A. S. Tan, *Biotechnol. Annu. Rev.*, 2005, **11**, 127–152.
33 (*a*) X. Lin, J. Xie, G. Niu, F. Zhang, H. Gao, M. Yang, Q. Quan, M. A. Aronova, G. Zhang, S. Lee, R. Leapman and X. Chen, *Nano Lett.*, 2011, **11**, 814–819; (*b*) Z. Zhen, W. Tang, C. Guo, H. Chen, X. Lin, G. Liu, B. Fei, X. Chen, B. Xu and J. Xie, *ACS Nano*, 2013, **7**, 6988–6996; (*c*) Z. Zhen, W. Tang, H. Chen, X. Lin, T. Todd, G. Wang, T. Cowger, X. Chen and J. Xie, *ACS Nano*, 2013, **7**(6), 4830–4837.
34 J. C. Kwok and D. R. Richardson, *Mol. Pharmacol.*, 2004, **65**, 181–195.

Electronic Supplementary Material (ESI) for ChemComm.

ARTICLE TYPE www.rsc.org/xxxxxx | XXXXXXXX

Supplementary information

Gold-based Drug Encapsulation within the Ferritin Nanocage: X-ray Structure and Biological Evaluation as Potential Anticancer Agent of the Auoxo3-loaded protein

Giarita Ferraro,[a] Daria Maria Monti,[a] Angela Amoresano,[a] Nicola Pontillo,[a] Ganna Petruk,[a] Francesca Pane,[a] Maria Agostina Cinellu,[b,c] and Antonello Merlino[a,d]*

[a]*Department of Chemical Sciences, University of Naples Federico II, Complesso Universitario di Monte Sant'Angelo, Via Cintia, I-80126, Napoli, Italy. Fax: +39081674090; Tel: +39081674276; E-mail: antonello.merlino@unina.it*
[b]*Department of Chemistry and Pharmacy, University of Sassari, via Vienna 2, 07100 Sassari, Italy*
[c]*CIRCC, Consorzio Interuniversitario Reattività Chimica e Catalisi, Università di Bari, Via Celso Ulpiani 27, 70126 Bari, Italy*
[d]*CNR Institute of Biostructures and Bioimages, Via Mezzocannone 16, I-80126, Napoli, Italy*
†*Electronic Supplementary Information (ESI) available: See DOI: 10.1039/b000000x*†

CREATED USING THE RSC COMMUNICATION TEMPLATE (VER. 3.1) - SEE WWW.RSC.ORG/ELECTRONICFILES FOR DETAILS
ARTICLE TYPE www.rsc.org/xxxxxx | XXXXXXXX

Supplementary information

Materials and Methods

Auoxo3 loading into the AFt nanocage

Horse spleen ferritin (Ft) was purchased from Sigma and used without further purification. Auoxo3 was prepared as previously described [1]; it is a *ca.* 1:1 mixture of the *cis* and *trans* isomers. Stock solution of Ft (code F4503) was the same used to prepare the CDDP-encapsulated AFt [2]. The solution was stored at 4 °C in 0.15 mM sodium chloride and contains iron in a protein subunit to metal ratio of 1:26.5, according to inductively coupled plasma mass spectrometry (ICP-MS) measurements.

The Auoxo3-encapsulated AFt was prepared following the procedure previously used to obtain CDDP-encapsulated AFt complex [2]. The loading was achieved by breaking down and then reassembling the Ft nanocage. Briefly, Ft (20 mg x mL^{-1}) was incubated at pH 13 in the presence of Auoxo3 (protein subunit to metal drug molar ratio 1:75); then this mixture was gently slowed down at neutral pH. In particular, the protein sample was slowly raised to pH 13 in the presence of Auoxo3 with 1 M NaOH (final concentration 0.1 M NaOH) and after 30 min, the pH of the resulting solution was adjusted to 7.4 using 1.0 M sodium phosphate buffer. After this process, the sample was extensively centrifuged at 5 000 rpm to remove the abundant precipitates (10 min); then it was recovered and ultra-filtrated (10 kDa cutoff) against 10 mM sodium phosphate buffer, pH 7.4. ICP-MS measurements indicate that Auoxo3-encapsulated Ft contained Au in a 1:8.8 Ft subunit:Auoxo3 ratio, i.e. 1:17.6 Ft subunit to metal ratio, and an undetectable amount of iron, thus the protein is in the Apo form (AFt).

The encapsulation of Auoxo3 in the AFt core was also assessed spectrophotometrically by comparing the UV-Vis spectra of Auoxo3-encapsulated AFt with those of the protein used as control (see below).

Control experiments indicate that Auoxo3 is stable at pH 13. In particular, to control the stability of Auoxo3 at pH 13, 53 mg (0.05 mmol) of the compound were treated with ca. 20 mL of NaOH 0.1 M (pH = 13) and the resulting suspension stirred for 45 min at room temperature, during which the color of the suspension turned from yellow to dark grey. Then the solid product was filtered under vacuum and extracted with MeCN and filtered through Celite to remove some metallic gold. The filtered yellow solution was concentrated to a small volume and diethyl ether added to give 34.6 mg (65 %) of the starting complex, as shown by its 1H NMR spectrum in CD_3CN (Figure S5).

Crystallization and X-ray diffraction data collection

Crystals of Auoxo3-encapsulated AFt with diamond-like morphology, suitable for X-ray diffraction data collection, were grown by hanging-drop vapor diffusion technique at 293 K mixing the protein (5-10 mg x mL^{-1}) with equal volumes of a reservoir solution consisting of 0.6-0.8 M $(NH_4)_2SO_4$, 0.1 M Tris pH 7.4-7.7, 50-60 mM $CdSO_4$.

X-ray diffraction data for Auoxo3-encapsulated AFt were collected from single crystals using a Saturn944 CCD detector equipped with CuKα X-ray radiation from a Rigaku Micromax 007 HF generator at the CNR Institute of Biostructures and Bioimages, Naples, Italy. Crystals were cryoprotected by adding glycerol to the mother liquor (final concentration= 25%) and flash cooled at 100 K. Data sets were indexed, integrated, reduced and scaled using HKL2000 [3] and the indications reported by Karplus and Diederichs [4]. Data collection statistics are reported in Table S2.

Structure resolution and refinement

The structure of Auoxo3-encapsulated AFt was solved by molecular replacement method, using the protein file 5ERK [2], without water molecules and other ligands, as a search probe and the program Phaser [5]. The crystals of this protein were obtained under the same experimental conditions, using a protein sample that was subjected to the same treatment used to encapsulate CDDP [2]. The structure was refined following the protocol used to refine the structure of CDDP-encapsulated AFt with Refmac5.7 [6]. Model building and map inspections were performed using Coot [7]. Gold ions were located if strong signals were observed in the 2Fo-Fc, Fo-Fc and anomalous electron density maps of Auoxo3-encapsulated AFt, but absent in the same positions in the corresponding maps of the starting model, which is a good control [2]. In the assignment of the metal centre, the nature and the arrangement (geometry) of the surrounding atoms were also considered.

To add confidence to out assignments, a detailed comparison of the binding specificity of gold ions versus cadmium ions to amino acids has been performed and the expected metal to ligand atom bond distances have been evaluated considering the standard uncertainties calculated using the 'Calc dpi' webserver [8].

According to statistical analysis carried out using a non-redundant dataset of 195 cadmium-bound proteins, Cd ions have a strong preference for glutamic acid and aspartic acid, although they can also bind the basic amino acid histidine and the polar amino acid cysteine [9]. The distance between Cd ions and atoms belonging to these side chains are on average = 2.3 Å for nitrogen, 2.4 Å for oxygen and 2.5 Å for sulfur [9].

Considering 1) the low affinity for Cd for sulfurs [9], 2) the high affinity of gold for Cys (formation of stable coordinative bonds to soft ligands) [10], 3) the distances between the electron density peaks and sulfur atoms of Cys residues in our structure (1.9 and 2.2 Å), it can be concluded that it is highly probable that Au atoms are bound to Cys48 and Cys126 side chains.

Regarding the binding to ND1 atom of His49 and His132 and NE2 atom His147, the distances between the electron density peaks and N atoms of His side chains are in the range 2.1-2.6 and thus these positions could be in principle occupied by Cd ions.

CREATED USING THE RSC COMMUNICATION TEMPLATE (VER. 3.1) - SEE WWW.RSC.ORG/ELECTRONICFILES FOR DETAILS
ARTICLE TYPE www.rsc.org/xxxxxx | XXXXXXXX

However, binding of Cd ions to ND1 atom of His49 and His132 and to NE2 atom of His147 is not observed in the crystals of the native protein used as control and in those of the cisplatin-encapsulated adduct grown under the same experimental conditions [2] and even in all the structures of horse spleen ferritin deposited in the protein data bank (see Table S2 in the SI of ref [2]). A comparison of the Cd binding site location in Auoxo3-encapsulated AFt and in previously determined structures of CCDP-encapsulated AFt and of the control, grown under the same experimental conditions used for Auoxo3-encapsulated AFt, are reported in Table S3. As an additional comment, it should be also recalled that gold ions were found close to the side chains of Cys48, His49, His114 and Cys126 also in the X-ray structure of horse liver apo-Ft with $AuCl_4^-$ by other authors (pdb code 3H7G) [11].

A detailed comparison of the native ferritin Cd binding sites and their own anomalous difference map peak heights with the binding sites in the Auoxo3-encapsulated AFt has been also performed. This comparison is reported in Table S4. Considering that gold f " at λ=1.5418 Å is about 1.5 times larger than that of Cd and also considering the analysis performed and discussed in previous paragraphs, we conclude that peaks that we have interpreted as due to Au ions are correctly assigned. We cannot exclude that other peaks, which we have assigned to Cd ions (for example Cd9) could be due to Au. However, since there are known structures of AFt where these positions are occupied by Cd ions (see for example PDB codes 2GYD, 2V2I, 2V2J, 2V2N, 2V2O, 2W0O, 1XZ3) and we cannot confirm Au/Cd replacement, we prefer to put Cd ions in these sites, according to recent guidelines suggested by Helliwell and co-workers: "If you are not sure, do not make an assignment".

The presence of Au ions bound to the protein unambiguously demonstrate that the Auoxo3 compound is broken down. However, to exclude the possibility that the full, starting gold compound could be bound to the protein, the distance between anomalous peaks of our structure was compared to the Au-Au distance observed in the X-ray structure of Auoxo3. Which is close to 3.0 Å [12]. There is only one site where there are two anomalous peaks at a distance comparable with those found in Auoxo3 (3.1 Å, Table S5): This site corresponds to the one where gold atoms are bound to Cys48 side chain. Here, there is not enough space to accommodate the whole Auoxo3 compound. In this respect, it should be also recalled that degradation of Auoxo3 and of other members of Auoxos series upon protein binding has been already observed in previous studies [13-16] and that it is rather well accepted the idea that Auoxos are sensible toward even very mildly reducing conditions, suggesting that they very likely undergo reduction to gold(I) or to colloidal gold upon protein binding.

Refinement statistics are reported in Table S2. Structure validations were carried out using Whatcheck [17]. In the final Fo-Fc difference electron density map, there are 17 peaks whose chemical interpretation is not possible and is commented in Table S6. Coordinates and structure factors of the Auoxo3-encapsulated AFt were deposited in the Protein Data Bank with PDB code 5IX6.

Spectrophotometric measurements

Auoxo3-encapsulated ferritin samples were analyzed by UV-vis absorption spectroscopy with a Cary UV−vis spectrophotometer with temperature controller using a quartz cuvette with 1 cm path length in the range of 240−700 nm. UV-Vis spectra were recorded in 10 mM sodium phosphate pH 7.4 and using the protein at concentration 0.25 mg x mL^{-1}. Data, reported in Figure S3, indicate that gold nanoparticles are probably formed within our sample over time, although in a small amount. Spectra also indicate that Auoxo3-encapsulated ferritin samples are stable for months.

Circular dichroism (CD) spectra were collected on a Jasco spectropolarimeter in the wavelength range 190−250 nm (far-UV) using protein concentration 0.1 mg x mL^{-1} in 10 mM sodium phosphate pH 7.4 (Figure S1).

Hydrodynamic radius (Z-average) of Auoxo3-encapsulated AFt was determined at 25 °C using a Zetasizer Nano ZSP (Malvern Instruments, Malvern, U.K). The average size (Z-average) of fresh solutions of Auoxo3-encapsulated AFt is 13.8 nm, in good agreement with what is found by other authors for cisplatin-encapsulated AFt [18]. Results are the average of three measurements. Aged samples of the Auoxo3-encapsulated AFt are not monodisperse, since they contain the protein and probably variable amounts of gold nanoparticles that can be formed inside the cage (for example a DLS peak centered at 6 nm is sometimes observed).

Inductively coupled plasma mass spectrometry

Protein samples were suspended in 600µl HNO_3 60% and 200µl HCl 37% overnight at 90 °C. Aliquots of acid solution from each sample were directly analyzed by ICP-MS. The solution was then transferred into polystyrene liners, and diluted 1:10 v/v with 5% HNO_3 and finally analyzed with an Agilent 7700 ICP-MS from Agilent Technologies, equipped with a frequency-matching RF generator and 3rd generation Octopole Reaction System (ORS3), operating with helium gas in ORF. The following parameters were used: radiofrequency power 1550 W, plasma gas flow 14 L/min; carrier gas flow 0.99 L/min; He gas flow 4.3 mL/min. 103Rh was used as an internal standard (50 µg x L^{-1} final concentration). Au calibration standards were prepared dissolving Auoxo3 in 5% HNO_3 at 4 different concentrations (1, 10, 50, and 100 µg x L^{-1}). Au concentration was measured. All the analyses were performed as triplicates.

Cytotoxicity, Au uptake and Western blotting analysis

Human breast cancer cells (MCF-7), cervical cancer cells (HeLa), hepatic carcinoma cells (HepG2), human keratinocyte cells (HaCaT), rat cardiomyoblasts cells (H9c2) were from ATCC and were cultured in Dulbecco's modified Eagle's medium (Sigma-Aldrich), supplemented with 10% fetal bovine serum (HyClone,

Logan, UT, USA), 2 mM L-glutamine and antibiotics. The growth medium of H9c2 cells was implemented with 2 mM L-glutamine and 2 mM sodium pyruvate. Human renal cortical epithelial cells HRCE (Innoprot, Biscay, Spain) were cultured in basal medium, supplemented with 2% fetal bovine serum, epithelial cell growth supplement, and antibiotics, all from Innoprot. All cells were grown in a 5% CO_2 humidified atmosphere at 37 °C.

Cells were seeded in 96-well plates at a density of 2.5×10^3/well. 24 h after seeding, cells were incubated with increasing amount of the protein under test (from 12 to 77 μg x mL^{-1}) for 72 h. At the end of incubation, cell viability was assessed by the MTT assay as previously described [19]. Cell survival was expressed as percentage of viable cells in the presence of the analysed protein, with respect to control cells. Control cells are represented by cells grown in the absence of protein and by cells supplemented with identical volumes of protein buffer (10 mM sodium phosphate buffer, pH 7.4).

To investigate Au uptake and to perform western blot analysis, the Auoxo3-encapsulated AFt amount able to induce 50% mortality (IC_{50}) was used. MCF-7 cells were incubated for 24, 48 and 72 h with the Auoxo3-encapsulated AFt and uptake was evaluated as previously reported [20]. Results are reported in Table S7.

To perform western blot analyses, cell lysates were analyzed as previously reported [20]. Results of these analyses are reported in Figure S4. Positive control was obtained by incubating cells in the presence of 50 μg/mL puromycin for 24 h.

References

1. M.A. Cinellu, G. Minghetti, M.V. Pinna, S. Stoccoro, A. Zucca, M. Manassero, M. Sansoni. *J. Chem. Soc., Dalton Trans*. 1998, 1735-1741.
2. N. Pontillo, F. Pane, L. Messori, A. Amoresano, L. Merlino. *Chem. Commun.* 2016, **52**, 4136-4139.
3. Z. Otwinowski, W. Minor, *Methods Enzymol*. 1997, **276**, 307-326.
4. P.A. Karplus, K. Diederichs. *Science* 2012, **336**(6084), 1030-1033; K. Diederichs, P.A. Karplus *Acta Crystallogr D Biol Crystallogr*. 2013, **69** (Pt 7), 1215-1222.
5. A. J. McCoy, R.W.Grosse-Kunstleve, P. D. Adams, M. D. Winn, L.C. Storoni, R.J. Read. *J. Appl. Crystallogr.* 2007, **40**, 658–674.
6. G. N. Murshudov, P. Skubak, A. A. Lebedev, N. S. Pannu, R. A. Steiner, R. A. Nicholls, M. D. Winn, F. Long, A. A. Vagin, *Acta Crystallogr., Sect. D: Biol. Crystallogr*. 2011, **67**, 355-367.
7. P. Emsley, B. Lohkamp, W. G. Scott, K. Cowtan. *Acta Crystallogr D Biol Crystallogr*. 2010, **66**, 486–501.
8. K. S. D. Kumar, M. Gurusaran, S. N. Satheesh, P. Radha, S. Pavithra, K. P. S. T. Tharshan, J. R. Helliwell, K. Sekar. *J. Appl. Cryst*. 2015, **48**, 939–942.
9. R. J. J. Sudan, C. Sudandiradoss. *Acta Crystallogr D Biol Crystallogr*. 2012, 68, 1346–1358.
10. F. Saccoccia, F. Angelucci, G. Boumis, M. Brunori, A. E. Miele, D. L. Williams, A. Bellelli. *J Inorg Biochem*. 2012, 108, 105–111.
11. M. Suzuki, M. Abe, T. Ueno, S. Abe, T. Goto, Y. Toda, T. Akita, Y. Yamada, Y. Watanabe. *Chem Commun*. 2009, 4871-4873.
12. C. Gabbiani A. Guerri, M. A. Cinellu, L. Messori. The Open Crystallography Journal, 2010, 3, 29-40.
13 A. Casini, C. Hartinger, C. Gabbiani. E. Mini, P. J. Dyson, B. K. Keppler, L. Messori. *J Inorg Biochem* 2008, 102, 564-575.
14. I. Russo Krauss, L. Messori, M. A. Cinellu, D. Marasco, R. Sirignano and A. Merlino, *Dalton Trans*., 2014, 43, 17483–17488.
15. L. Messori, F. Scaletti, L. Massai, M.A. Cinellu, C., Gabbiani, A. Vergara, A. Merlino. Chem Commun (Camb). 2013, 49, 86, 10100-10102.
16. L. Messori, M. A. Cinellu, A. Merlino. *ACS Med Chem Lett*. 2014, 5, 10, 1110-1113.
17. R.W.W. Hooft, G. Vriend, C. Sander, E. E. Abola, *Nature* 1996, **381**, 272.
18. (a) M. Uchida, M. L. Flenniken, M. Allen, D. A. Willits, B.E. Crowley,S. Brumfield, A. F. Willis, L. Jackiw, M. Jutila, M. J. Young, T. Douglas. J. Am. Chem Soc. 2006, 128, 16626-33; (b) E. Falvo, E. Tremante, R. Fraioli, C. Leonetti, C. Zamparelli, A. Boffi, V. Morea, P. Ceci, P. Giacomini. Nanoscale, 2013,5, 12278
19. R. Del Giudice, A. Raiola, G. C. Tenore, L. Frusciante, A. Barone, D.M. Monti, M.M. Rigano. *J. Funct. Foods*. 2015, **18**, 83-94.
20. E. Galano, A. Arciello, R. Piccoli, D. M. Monti, A. Amoresano. *Metallomics*, 2014, 6, 587--597

CREATED USING THE RSC COMMUNICATION TEMPLATE (VER. 3.1) - SEE WWW.RSC.ORG/ELECTRONICFILES FOR DETAILS

ARTICLE TYPE www.rsc.org/xxxxxx | XXXXXXXX

Table S1. Interactions between Au atoms and protein residues or solvent atoms in the structurte of Auoxo3-erncapsulated AFt.

Binding site	Distance (Å)	Angle (°)
Cys48 and His49		
Au2-SG Cys48	1.9	
Au6- centroid His49	3.2	
SG Cys48-Au6-centroid His49		152.5
Au6-SG Cys48	2.3	
Au2-Au6	3.1	
His49		
Au3-ND1 His49	2.1	
Cys126 and His114		
Au1-SG Cys126	2.2	
Au1-ND1 His114	2.2	
SG Cys126-Au1-ND1 His114		178.6
Au4-SG Cys126	2.2	
Au4-O Wat	2.5	
SG Cys126-Au4-O Wat		173.1
Au1-Au4	3.7	
His132		
Au7-ND1 His132	2.5	
His147		
Au5-NE2 His147	2.6	

Unrestrained selected bond distances and angles are in Å and °, respectively. Standard uncertainties on the coordinates 0.1 Å. Errors on distances<0.2 Å

Table S2. Data Collection and refinement statistics

Data reduction	
PDB code	5IX6
Space group	F432
Unit cell parameters	
a=b=c (Å)	180.645
Molecules per asymmetric unit	1
Observed reflections	151428
Unique reflections	22027
Resolution (Å)	104.30-1.85 (1.88-1.85)
Completeness (%)	99.5 (95.0)
Anomalous completeness (%)	99.2 (88.1)
Rpim in top intensity bin	0.032
Rpim	0.102 (0.659)
I/σ(I)	9.2 (0.8)
Multiplicity	6.9 (3.4)
$C_{1/2}$ last shell	0.284
CC*	0.666
Refinement	
Resolution (Å)	104.30-1.85
number of reflections in working set	20893
number of reflections in test set	1128
R-factor/Rfree/Rall (%)	18.0/18.2/22.6
Non-H atoms used in the refinement	1785
Mean B-value (Å^2)	19.7
Au atom occupancy	0.40, 0.30, 0.35, 0.45, 0.25, 0.45 and 0.20
Au atom B-factor (Å^2)	20.0, 34.8, 29.5, 20.6, 38.9, 38.7 and 50.5
Estimated overall coordinate errors	
Rmsd bonds (Å)	0.019
Rmsd angles (°)	1.77
Ramachandran values (%) from Coot	
Preferred region	96.32
Allowed	2.94
Disallowed	0.74 (1 residue:Ser157)

Parentheses indicate information for highest resolution shell.

CREATED USING THE RSC COMMUNICATION TEMPLATE (VER. 3.1) - SEE WWW.RSC.ORG/ELECTRONICFILES FOR DETAILS
ARTICLE TYPE www.rsc.org/xxxxxx | XXXXXXXX

Table S3. Interactions of Cd^{2+} ions in Auoxo3-encapsulated AFt, CCDP-encapsulated AFt and in the control

Auoxo3-encapsulated AFt	Auoxo3-encapsulated AFt	CDDP-encapsulated Aft and Control	CDDP-encapsulated AFt	Control	CDDP-encapsulated AFt (crystal 2)
Atom	Interactions at distance < 3.00 Å	Atom	Interactions at distance < 3.00 Å	Interactions at distance < 3.00 Å	Interactions at distance < 3.00 Å
CD1	Occupancy 0.40 B-factor 40.5 Å^2 OE1 Glu11 (2.6 Å) OE2 Glu11 (2.8 Å) WAT 129 (2.2 Å) WAT 384 (2.7 Å) WAT 399 (2.8 Å) WAT 447 (2.2 Å)	CD1	Occupancy 0.40 B-factor 22.9 Å^2 OE1 Glu11 (2.3 Å) OE2 Glu11 (2.6 Å) WAT 129 (2.2 Å) WAT 183 (2.3 Å) Cl 3 (2.60 Å)	Occupancy 0.40 B-factor 42.4 Å^2 OE1 Glu11 (2.7 Å) OE2 Glu11 (2.3 Å) WAT 129 (2.8 Å) WAT 319 (2.6 Å) Cl 3 (2.5 Å)	Occupancy 0.40 B-factor 41.4 Å^2 OE1 Glu11 (2.7 Å) OE2 Glu11 (2.5 Å) WAT 129 (2.0 Å) WAT 183 (2.6 Å) Cl 4 (2.6 Å)
CD2	Occupancy 0.45 B-factor 58.66 Å^2 OE1 Glu56 (2.5 Å)	CD2	Occupancy 0.40 B-factor 43.7 Å^2 OE1 Glu53 (2.9 Å) OE2 Glu53 (2.4 Å) OE1 Glu56 (2.5 Å) WAT 237 (2.5 Å)	Occupancy 0.30 B-factor 51.9 Å^2 OE1 Glu53 (2.5 Å) OE2 Glu53 (2.6 Å) OE1 Glu56 (2.5 Å) WAT 315 (2.3 Å)	Occupancy 0.40 B-factor 51.8 Å^2 OE1 Glu53 (2.9 Å) OE2 Glu53 (2.9 Å) OE1 Glu56 (2.4 Å) WAT 302 (2.9 Å)
CD8	Occupancy 0.40 B-factor 41.9 Å^2 OE1 Glu60 (2.8 Å) OE2 Glu60 (2.4 Å) OE1 Glu56 (2.7 Å) OE2 Glu57 (2.7 Å) WAT 471 (2.5 Å)	CD3	Occupancy 0.30 B-factor 44.0 Å^2 OE2 Glu56 (2.4 Å) OE1 Glu60 (2.8 Å) OE2 Glu60 (2.2 Å) Occupancy 0.20 B-factor 35.80 Å^2 OE1 Glu60 (2.4 Å) WAT 191 (2.2 Å)	Occupancy 0.30 B-factor 69.1 Å^2 OE1 Glu60 (2.5 Å) WAT 292 (2.8 Å)	Occupancy 0.30 B-factor 56.4 Å^2 OE2 Glu56 (2.9 Å) OE1 Glu60 (2.8 Å) OE2 Glu60 (2.7 Å) Occupancy 0.20 B-factor 60.5 Å^2 OE1 Glu60 (2.4 Å) WAT 191 (2.4 Å) Cl 6 (2.7 Å)
CD3	Occupancy 0.50 B-factor Å^2 OD1 Asp80 (2.4 Å) OD2 Asp80 (2.2 Å) OD1 Asp80* (2.4 Å) OD2 Asp80* (2.2 Å) WAT 386 (2.4 Å) WAT 386* (2.4 Å)	CD4 at the binary axis	Occupancy 0.40 B-factor 10.5 Å^2 OD1 Asp80 (2.3 Å) OD2 Asp80 (2.5 Å) OD1 Asp80* (2.3 Å) OD2 Asp80* (2.5 Å) Cl 1 (2.4Å) Cl 1* (2.5 Å) Occupancy 0.10 B-factor 19.5 Å^2 OD1 Asp80 (2.1 Å) OD2 Asp80 (1.9 Å) OD1 Asp80* (2.2 Å) OD2 Asp80* (2.1 Å) Cl 1 (2.9 Å)	Occupancy 0.50 B-factor 15.7 Å^2 OD1 Asp80 (2.4 Å) OD2 Asp80 (2.1 Å) OD1 Asp80* (2.5 Å) OD2 Asp80* (2.3 Å) Cl 2 (2.6 Å) Cl 2* (2.3 Å)	Occupancy 0.50 B-factor 16.4 Å^2 OD1 Asp80 (2.5 Å) OD2 Asp80 (2.2 Å) OD1 Asp80* (2.5 Å) OD2 Asp80* (2.4 Å) Cl 1 (2.5 Å) Cl 1* (2.7 Å)

CREATED USING THE RSC COMMUNICATION TEMPLATE (VER. 3.1) - SEE WWW.RSC.ORG/ELECTRONICFILES FOR DETAILS
ARTICLE TYPE www.rsc.org/xxxxxx | XXXXXXXX

			Cl 1* (3.0 Å)		
-	-	CD5	Occupancy 0.30 B-factor 44.4 Å^2 OE2 Glu88 (2.3 Å) WAT 81 (2.0 Å) WAT 181 (2.2 Å) WAT 187* (2.6 Å)	Occupancy 0.20 B-factor 61.0 Å^2 OE2 Glu 88 (2.3 Å) WAT 313 (2.5 Å) WAT187* (2.7 Å)	-
-	-	CD6	Occupancy 0.40 B-factor 45.3 Å^2 OG Ser131 (2.7 Å) OD1 Asp127 (3.0 Å) WAT 196 (2.5 Å) WAT 197 (2.5 Å) WAT 230 (2.0 Å)	Occupancy 0.40 B-factor 69.3 Å^2 OD1 Asp127 (2.9 Å) WAT 245 (2.5 Å) WAT 311 (2.2 Å)	Occupancy 0.40 B-factor 62.5 Å^2 OD1 Asp127 (2.4 Å) WAT 196 (2.8 Å)
CD4	Occupancy 0.50 B-factor 43.6 Å^2 NE2 His132 (2.2 Å) WAT335 (2.1 Å)	CD7	Occupancy 0.50 B-factor 42.1 Å^2 NE2 His132 (2.5 Å) OD2 Asp135* (2.9 Å) WAT 196 (2.4 Å) WAT 197 (2.5 Å) WAT 275 (1.7 Å)	Occupancy 0.40 B-factor 39.9 Å^2 NE2 His132 (2.7 Å) WAT 245 (2.2 Å) WAT 246 (2.2 Å) WAT 294 (2.1 Å) WAT 295 (2.4 Å)	Occupancy 0.50 B-factor 60.2 Å^2 NE2 His132 (2.7 Å) WAT196 (2.3 Å) WAT197 (2.5 Å) WAT275 (2.4 Å)
CD5	Occupancy 0.30 B-factor 28.2 Å^2 OE1 Glu130 (2.5 Å) OE2 Glu130 (2.5 Å) OE1 Glu130* (2.5 Å) OE2 Glu130* (2.5 Å) OE1 Glu130* (2.5 Å) OE2 Glu130* (2.5 Å)	CD8 at the ternary axis	Occupancy 0.20 B-factor 42.7 Å^2 OE1 Glu130 (2.4 Å) OE1 Glu130* (2.4 Å) OE1 Glu130* (2.4 Å) Cl 2 (1.9 Å) Cl 2* (1.9 Å) Cl 2* (1.9 Å)	Occupancy 0.20 B-factor 46.5 Å^2 OE1 Glu130 (2.5 Å) OE1 Glu130* (2.5 Å) OE1 Glu130* (2.4 Å) Cl 2 (2.3 Å) Cl 2* (2.3 Å) Cl 2* (2.3 Å)	Occupancy 0.30 B-factor 61.3 Å^2 OE1 Glu130 (2.3 Å) OE1 Glu130* (2.3 Å) OE1 Glu130* (2.3 Å) Cl 5 (2.9 Å) Cl 5* (2.9 Å) Cl 5* (2.9 Å)
-	-	CD9	Occupancy 0.40 B-factor 56.5 Å^2 NE2 His114 (2.7 Å) WAT 265* (2.9 Å)	Occupancy 0.20 B-factor 59.1 Å^2 WAT 252* (2.5 Å) Cl 1* (2.9 Å)	Occupancy 0.40 B-factor 72.6 Å^2 NE2 His114 (2.8 Å) WAT 265* (2.8 Å) Cl 5* (2.7 Å)
-	-	CD10	Occupancy 0.30 B-factor 42.1 Å^2 OE1 Glu63/A (2.7 Å) OE2 Glu63/A (2.3 Å) OE2 Glu63/B (2.3 Å) WAT 85 (1.7 Å) WAT 247 (2.5 Å)	Occupancy 0.20 B-factor 51.5 Å^2 OE1 Glu63 (2.6 Å)	Occupancy 0.30 B-factor 62.5 Å^2 OE1 Glu63 (2.9 Å) WAT 85 (2.4 Å) WAT 219 (2.8 Å)
-	-	CD11	Occupancy 0.30 B-factor 30.9 Å^2	Occupancy 0.30 B-factor 33.6 Å^2	Occupancy 0.30 B-factor 25.2 Å^2

CREATED USING THE RSC COMMUNICATION TEMPLATE (VER. 3.1) - SEE WWW.RSC.ORG/ELECTRONICFILES FOR DETAILS
ARTICLE TYPE www.rsc.org/xxxxxx | XXXXXXXX

			SG Cys48 (2.0 Å) WAT 231 (2.0 Å)	SG Cys48 (2.1 Å) WAT 310 (2.0 Å)	SG Cys48 (2.0 Å) WAT 231 (1.8 Å)
-	-	CD12	Occupancy 0.40 B-factor 56.8 Å^2 OE2 Glu45/B (2.4 Å) WAT 255 (2.2 Å) Cl 5 (2.7 Å)	Occupancy 0.30 B-factor 73.9 Å^2 OE1 Glu45 (2.5 Å) WAT 235 (2.2 Å)	Occupancy 0.40 B-factor 66.7 Å^2 OE2 Glu45 (2.6 Å) WAT 282 (2.9 Å)
CD6	Occupancy 0.35 B-factor 65.1 Å^2 OE1 Glu45/A (2.9 Å) WAT 364 (2.9 Å) WAT 387 (2.0 Å)	CD13	Occupancy 0.20 B-factor 44.1 Å^2 OE1 Glu45/A (2.2 Å) NE2 His49 (2.3 Å)	Occupancy 0.20 B-factor 44.1 Å^2 OE2 Glu45/A (2.5 Å) NE2 His49 (2.7 Å) WAT 236 (2.9 Å)	Occupancy 0.20 B-factor 57.4 Å^2 OE1 Glu45/A (2.2 Å) NE2 His49 (2.5 Å)
CD7	Occupancy 0.20 B-factor 37.4 Å^2 WAT 332 (2.3 Å) WAT 333 (2.4 Å) WAT 332 *(2.3 Å) WAT 333 *(2.4 Å) WAT 332 *(2.3 Å) WAT 333 *(2.4 Å)	-	-	-	-
CD9	Occupancy 0.15 B-factor 42.1 Å^2 OE1 Glu53 (1.9 Å)	-	-	-	-

* Symmetry related residue

CREATED USING THE RSC COMMUNICATION TEMPLATE (VER. 3.1) - SEE WWW.RSC.ORG/ELECTRONICFILES FOR DETAILS
ARTICLE TYPE www.rsc.org/xxxxxx | XXXXXXXX

Table S4. Anomalous map peak intensities in the structure reported in this work compared to those obtained using crystals of AFt, CDDP-encaspulated AFt and an additional internal control collected using X-ray from a CuKa generator.

Atom name in the Auoxo3-encapsulated AFt	Auoxo3-encapsulated AFt	Corresponding atoms in the structures of CDDP-encapsulated AFt and in the control	CDDP-encapsulated Aft Crystal 1	CDDP-encapsulated Aft Crystal 2	Control	Notes
	Resolution 1.85 Å		Resolution 2.06 Å	Resolution 1.45 Å	Resolution 1.82 Å	
	λ used for data collection 0.15418 nm		λ used for data collection 0.15418 nm	λ used for data collection 0.1065 nm	λ used for data collection 0.1065 nm	Notes
Atom	e/Å^3	***Atom***	e/Å^3	e/Å^3	e/Å^3	
CD1	0.22	***CD1***	0.24	0.28	0.14	
CD2	0.21	***CD2***	0.16	0.12	0.10	
CD8	0.20	***CD3***	0.31	0.10/0.08	0.12	
CD3	1.19	***CD4***	0.92	1.16	0.53	
-	-	***CD5***	-	0.09	0.09	
-	-	***CD6***	0.35	0.12	0.09	
CD4	0.25	***CD7***	0.28	0.17	0.09	
CD5	0.58	***CD8***	0.41	0.15	0.11	
-	-	***CD9***	0.25	0.15	0.10	
-	-	***CD10***	0.30	0.07	0.09	
-	-	***CD11***	0.25	0.06	0.10	
-	-	***CD12***	0.30	0.09	0.10	
CD6	0.22	***CD13***	0.21	0.09	0.16	
CD7	0.36	-	-	-	-	Not bound to protein residues, but to six water molecule (octahedral

						geometry)
CD9	0.19	-	-	-	-	Close to Glu53, as in other structures of AFt
Au1	0.76	-	-	-	-	Close to Cys126
Au2	0.37	-	-	-	-	Close to Cys48
Au3	0.52	-	-	-	-	Close to His49
Au4	1.00	-	-	-	-	Close to Cys126
Au5	3.14	-	-	-	-	Close to His147
Au6	0.50	-	-	-	-	Close to Cys48
Au7	0.16	***CPT***	0.21	0.24	-	Close to His132
-	-				-	

CREATED USING THE RSC COMMUNICATION TEMPLATE (VER. 3.1) - SEE WWW.RSC.ORG/ELECTRONICFILES FOR DETAILS
ARTICLE TYPE www.rsc.org/xxxxxx | XXXXXXXX

Table S5. Distances between main anomalous peaks in the structure of Auoxo3-encapsulated AFt

distance	*Assignment*
3.1 Å	Au2-Au6
3.7 Å	Au1-Au4
3.9 Å	Au3-Au6
5.0 Å	Cd5-Cd7
5.3 Å	Cd2-Cd8
5.3 Å	Au2-Au3
6.2 Å	Au7-Cd4
6.5 Å	Au3-Cd2
6.5 Å	Au3-Cd9
6.6 Å	Cd2-Cd9
7.6 Å	Au1-Cd5
7.7 Å	Au4-Cd5
8.4 Å	Au5-Cd9
9.1 Å	Au6-Cd9
9.5 Å	Au6-Cd6
9.8 Å	Cd4-Cd7

CREATED USING THE RSC COMMUNICATION TEMPLATE (VER. 3.1) - SEE WWW.RSC.ORG/ELECTRONICFILES FOR DETAILS
ARTICLE TYPE www.rsc.org/xxxxxx | XXXXXXXX

Table S6. Uninterpreted Fo-Fc electron density map peaks in the structure of Auoxo3-encapsulated AFt at level > 5σ

Peak number	e/Å^3	Rmsd (σ)	Note
1	1.08	9.15	Too close to Cd8 (1.9 Å)
2	0.96	8.06	Too close to CD atom of Arg153 (2.2 Å)
3	0.95	7.99	Too close to CE and NE atoms of His114 (0.7 and 0.8 Å, respectively)
4	0.90	7.63	Too close to CD2 atom of His114 (1.9 Å)
5	0.76	6.43	Too close to OD2 atom of Asp127 and to Wat311 (1.8 and 1.4 Å, respectively)
6	0.73	6.17	Too close to OE2 atom of Glu56 and to Cd8 (1.8 and 1.4 Å, respectively)
7	0.71	6.02	On symmetry axis
8	0.67	5.63	Too close to Wat248 (1.5 Å)
9	0.66	5.54	Too close to Wat334 and to OE2 atom of Glu130 (1.9 and 2.3 Å, respectively)
11	0.64	5.37	Too close to Wat382 (1.7 Å)
12	0.63	5.32	Too close to Wat386 (1.3 Å)
13	0.63	5.29	Too close to CE atom of Met96 (< 0.3 Å)
14	0.63	5.28	Too close to Au4 and to Wat 373 (1.5 and 1.8 Å, respectively)
15	0.61	5.14	Too close to CD and OE atoms of Glu63 (1.8 and 1.7 Å, respectively)
16	0.61	5.13	Too close to Wat 334 (1.7 Å)
17	0.60	5.05	Too close to OE1 atom of Glu57 and to Wat358 (2.1 and 1.3 Å, respectively)

CREATED USING THE RSC COMMUNICATION TEMPLATE (VER. 3.1) - SEE WWW.RSC.ORG/ELECTRONICFILES FOR DETAILS
ARTICLE TYPE www.rsc.org/xxxxxx | XXXXXXXX

Table S7. Cellular uptake of Au associated with Auoxo3-encaspulated AFt by MCF-7 cells during 24, 48 and 72 h normalized to 1x 10^6 cells.*

	24h	48h	72h
Sample			
	Au (%)	Au (%)	Au (%)
Total amount	100	100	100
Cell conditioned medium	87.5	71.4	68.4
Cell washing	3.1	1.2	3.6
Cell lysate	9.0	11.9	21.6

*Average of two different measurements. Errors about 10%.

CREATED USING THE RSC COMMUNICATION TEMPLATE (VER. 3.1) - SEE WWW.RSC.ORG/ELECTRONICFILES FOR DETAILS
ARTICLE TYPE www.rsc.org/xxxxxx | XXXXXXXX

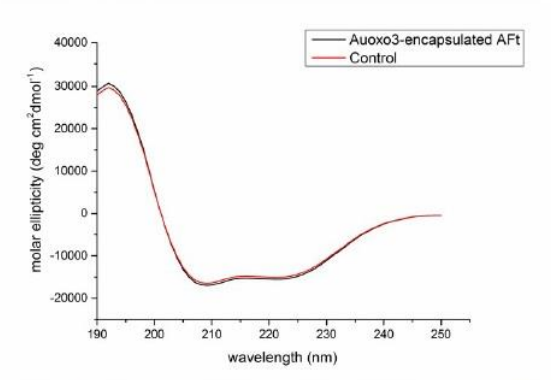

Figure S1. Far-UV CD spectra of Auoxo3-encapsulated AFt (black) compared to the control (red).

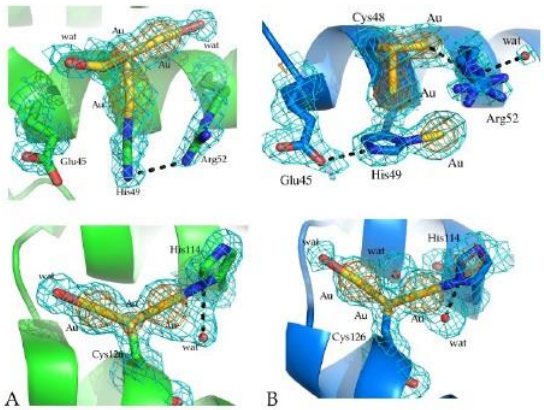

Figure S2. Comparison between Au binding sites observed in the structure of horse liver ferritin with $AuCl_4^-$ (A) and in Auoxo3-encapsulated AFt (B). 2Fo-Fc electron density maps are contoured at 1σ (cyan) and 4 σ (orange). The structure of horse liver ferritin with $AuCl_4^-$ is coloured in green; the structure of Auoxo3-encapulstaed Aft is coloured in cyan

CREATED USING THE RSC COMMUNICATION TEMPLATE (VER. 3.1) - SEE WWW.RSC.ORG/ELECTRONICFILES FOR DETAILS
ARTICLE TYPE www.rsc.org/xxxxxx | XXXXXXXX

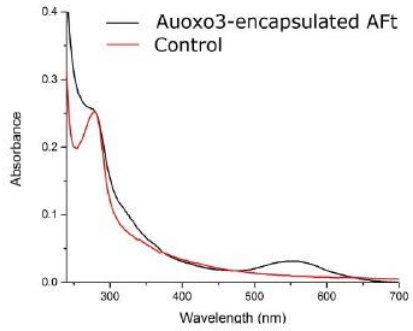

Figure S3. UV-vis absorption spectra of 0.25 mg x mL^{-1}Auoxo3-encapsulated AFt (black) compared to the control (red). The absorption differences between 250 and 280 nm and the appearance of a peak at 548 nm in aged samples confirm that Auoxo3 was successfully encapsulated in the AFt nanocage and suggest that a small amount gold nanoparticles could be formed in Auoxo3-encapsulated AFt sample.

CREATED USING THE RSC COMMUNICATION TEMPLATE (VER. 3.1) - SEE WWW.RSC.ORG/ELECTRONICFILES FOR DETAILS
ARTICLE TYPE www.rsc.org/xxxxxx | XXXXXXXX

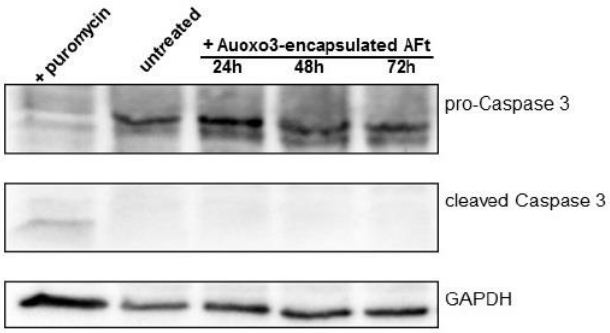

Figure S4. Detection of apoptosis in Auoxo3-encapsulated AFt-treated MCF-7 cells. MCF-7 cells were pre-incubated with 0.4 µg/mL Auoxo3-encapsulated AFt for 24, 48 and 72 h. Western blot was performed using anti-Caspase 3, which recognizes both pro-Caspase 3 and the activated form. GAPDH was used as loading control. A positive control was obtained by incubating cells in the presence of 50 µg/mL puromycin for 24 h.

CREATED USING THE RSC COMMUNICATION TEMPLATE (VER. 3.1) - SEE WWW.RSC.ORG/ELECTRONICFILES FOR DETAILS
ARTICLE TYPE www.rsc.org/xxxxxx | XXXXXXXX

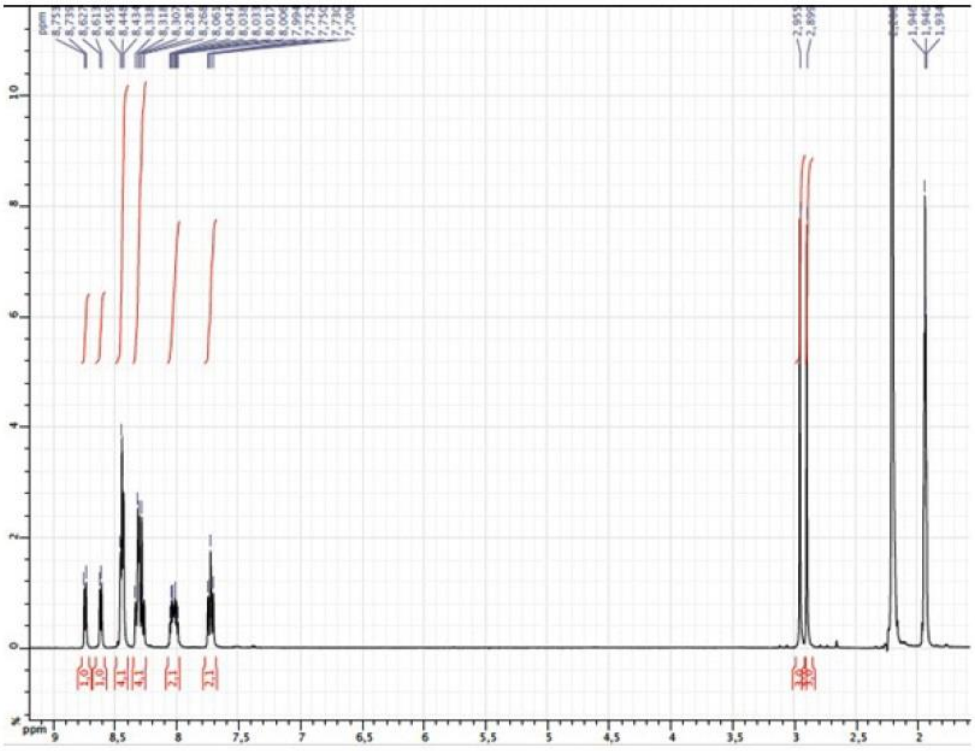

Figure S5. ^{1}H NMR (CD_3CN, 400 MHz) of Auoxo3 recovered from reaction with NaOH 0.1M

Dalton Transactions

Accepted Manuscript

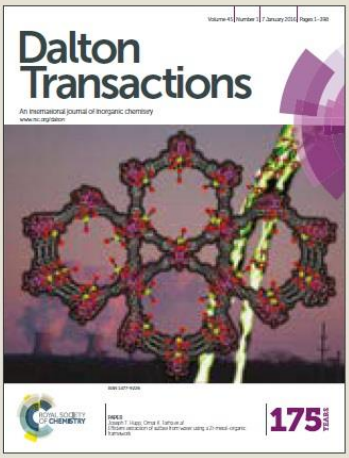

ROYAL SOCIETY OF CHEMISTRY

rsc.li/dalton

Page 1 of 9 Journal Name

Dalton Transactions

Dynamic Article Links ►
View Article Online
DOI: 10.1039/C7DT02370G

Cite this: DOI: 10.1039/coxx00000x

www.rsc.org/xxxxxx

ARTICLE TYPE

Ferritin nanocages loaded with gold ions induce oxidative stress and apoptosis in MCF-7 human breast cancer cells

Daria Maria Monti,[a] Giarita Ferraro,[a] Ganna Petruk,[a] Laura Maiore,[b] Francesca Pane,[a] Angela Amoresano,[a] Maria Agostina Cinellu,[b] and Antonello Merlino[a,c*]

Received (in XXX, XXX) Xth XXXXXXXXX 20XX, Accepted Xth XXXXXXXXX 20XX
DOI: 10.1039/b000000x

Two anticancer gold(III) compounds, Au_2phen and Auoxo4, were encapsulated within the ferritin nanocage. The gold-compound loaded proteins were characterized by UV-Vis spectroscopy, inductively plasma mass spectrometry and circular dichroism. X-ray crystallography shows that the compounds degrade upon encapsulation and gold(I) ions bind Ft within the cage, close to side chains of Cys126. The gold-encapsulated nanocarriers are cytotoxic to human cancer cells. Au(I)-loaded Ft, obtained upon encapsulation of Au_2phen within the cage, induces oxidative stress activation, which finally leads to apoptosis in MCF-7 cells.

Introduction

There is currently a great interest in the development of new biomaterials that can be used to selectively deliver drugs to their final targets. Nature offers a variety of protein scaffolds that self-assemble to form cages within nanometer scale and can be used to trap drugs in their interior cavity. Among these systems, a special position is occupied by the ferritin superfamily.[1] The mammalian iron-storage protein ferritin (Ft) is a heteropolymer consisting of two genetically distinct subunits, called H-chain (~21 kDa) and L-chain (~19 kDa). Ft is a four-helix bundle protein which forms a cage of 24 monomers (Ft nanocage), which is characterized by octahedral 432 symmetry, with internal and external diameters of ~80 and ~120 Å, respectively.[2] Ft is fundamental for life: its role is to protect cells from oxidative damage caused by the harmful products of the Fenton reaction and to store iron.

Ft cage is an attractive carrier for targeted drug delivery,[1, 3, 4] since it is not expensive, available in large amount, is easy to purify, biocompatible, stable, and monodisperse in the bloodstream. Ft is also characterized by a small size compared to other potential drug carriers; its structure allows chemical modifications, including conjugation of different chemical groups.[5] Most importantly, it is recognized and internalized by specific receptors which are over-expressed in a variety of malignant cells: the transferrin receptor 1 (TfR1) and Scara5.[6-8]

It was earlier shown that cisplatin[9] and the second generation Pt antitumor drug carboplatin[10] can be encapsulated in the cavity of apoferritin (AFt); the resulting drug-loaded proteins have well documented cytotoxic effects on tumor cells (pheochromocytoma, gastric, breast, cervix and melanoma cells),[11-14] demonstrating the efficiency of Ft as carrier of these drugs to malignant cells.

Gold-based compounds have emerged as a promising class of anticancer agents alternative to Pt-based drugs.[15-18] However, the clinical use of these potential drugs is up to now hampered by a series of factors, including their low solubility and stability in aqueous media.[15-18] Greater solubility and stability could be obtained by encapsulation of gold-based drugs within a protein nanocage. Ft-gold drug adducts could also have the advantage of enhanced selectivity for tumor cells.[19]

Recently, we have successfully encapsulated the gold-based drug $[Au_2(bipy^{Me})_2(\mu\text{-}O)_2][PF_6]_2$ ($bipy^{Me}$ = 6-methyl-2,2'-bipyridine), **Auoxo3**, with AFt nanocage.[19] The drug-loaded protein is cytotoxic towards different malignant cells (HeLa, MCF-7 and HepG2) and shows a lower toxicity for non-malignant cells (H9c2, HRCE and HaCaT).[19] Incorporation of **Auoxo3** inside the cage leads to the formation of gold(I) ions that bind AFt close to the side chains of Cys126, Cys48, His49, His132, His147. The UV-vis spectrum of **Auoxo3**-encaspulasted AFt suggests the formation also of a low amount of gold nanoparticles (Figure S3 in the Supporting information of reference 19), which absorb at 548 nm, in agreement with what recently observed for gold nanoparticles formed upon reduction with $NaBH_4$ of $AuCl_4^-$ encapsulated Ft variant.[20]

Here, we have encapsulated two other gold-based drugs of medicinal interest, namely $[Au_2(bipy^{nP})_2(\mu\text{-}O)_2][PF_6]_2$ ($bipy^{nP}$ = 6-*neo*-pentyl-2,2'-bipyridine), **Auoxo4**, and $[Au_2(Me_2phen)_2(\mu\text{-}O)_2][PF_6]_2$ (Me_2phen = 2,9-dimethyl-1,10-phenanthroline), **Au_2phen**, (Figure 1) in the AFt nanocage. **Auoxo4** and **Au_2phen** are both more cytotoxic than **Auoxo3**,[17, 21-24] and thus we expect an increased cytotoxicity of these Ft adducts when compared to the previously characterized **Auoxo3**-encapsulated AFt. X-ray structures of **Au_2phen-** and **Auoxo4**-encapsulated AFt were solved and the cytotoxicity of the two adducts assessed by MTT

CREATED USING THE RSC COMMUNICATION TEMPLATE (VER. 3.0) - SEE WWW.RSC.ORG/ELECTRONICFILES FOR DETAILS
Dalton Transactions
Page 2 of 9
ARTICLE TYPE
www.rsc.org/xxxxxx | XXXXXXXX
DOI: 10.1039/C7DT02370G

assay on human MCF-7 and HeLa cancer cell lines and on non-cancer cells, H9c2 and HaCaT. Data indicate that gold nanoparticles are not formed inside **Au$_2$phen**- and **Auoxo4**-encapsulated AFt cages. New adducts are much more cytotoxic than the **Auoxo3**-encapsulated AFt. The activation of oxidative stress and of apoptosis in MCF-7 cells treated with **Au$_2$phen**-loaded AFt is also reported.

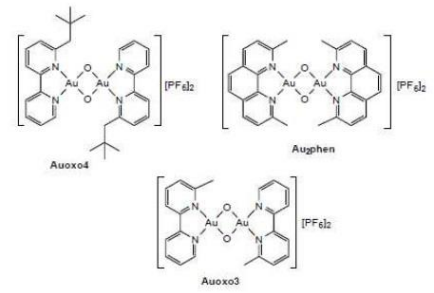

Figure 1. Structure of selected gold(III) compounds of interest for their antitumor action.

Results

Preparation and characterization of gold compound-encapsulated AFt

The potential antitumor drug-loaded nanostructure was prepared using the procedure previously described by Huang et al.[14] and already used to encapsulate cisplatin,[9] carboplatin[10] and the gold-based drug **Auoxo3**.[19] which belongs to the **Auoxos**, *i.e.* a series of dinuclear gold(III) oxo-bridged complexes supported by substituted 2,2'-bipyridine (*e.g.* 6-methyl-2,2'-bipyridine and 6-*neo*-pentyl-2,2'-bipyridine in **Auoxo3** and **Auoxo4**, respectively) or 1,10-phenanthroline (*e.g.* 2,9-dimethyl-1,10-phenanthroline in **Au$_2$phen**) ligands.[20-22,23, 24]

Ft cage can be disassembled at both acid and basic pHs. We have preferred the protocol using the basic pH, so that we can directly compare our new data with those previously obtained with **Auoxo3**.

Thus, in order to disassemble the Ft cage into subunits, horse spleen ferritin was incubated for 20 minutes at pH 13 adding NaOH up to a final concentration of 0.1 M. This solution was then mixed with powdered **Au$_2$phen** and **Auoxo4** and the two samples were incubated for 30 minutes at room temperature under stirring. Then, pH was decreased to 7.4 using 1.0 M sodium phosphate. The two gold-encapsulated samples were then dialysed through ultracentrifugation on centricon filters (10 kDa cutoff) to remove the excess of drugs. To confirm the encapsulation of gold compounds within the Ft shell and verify that upon encapsulation the protein re-assembles readopting its native conformation, UV-Vis absorption spectroscopy (Figure 2A), circular dichroism (Figure 2B) and inductively coupled plasma mass spectrometry (ICP-MS) data were collected.

UV-Vis spectra of **Au$_2$phen** and **Auoxo4**-encapsulated AFt were compared to those of AFt, used as control, and of **Auoxo3**-encapsulated AFt. Contrarily with what was found for **Auoxo3**-encapsulated AFt (see Figure 2A),[19] there is no absorption at 548 nm in UV-Vis spectra of the new encapsulated AFts, indicating that gold nanoparticles are not formed when these two compounds are within AFt. This indication was further supported by the inspection of the colour of the **Auoxo4**- and **Au$_2$phen**-encapsulated AFt solutions, which appear light yellow and remain of this colour for weeks, at variance with that of **Auoxo3**-encapsulated AFt which turns to violet with time (Figure S1). ICP-MS data indicate that Ft nanocage can encapsulate from 0.6 to 24 gold atoms per subunit, depending on the preparation. Data reported in this paper were collected on samples of **Auoxo4**- and **Au$_2$phen**-encapsulated AFt solutions containing 16 and 18 atoms of gold per Ft chain, i.e. 384 and 432 Au atoms per cage in the case of **Auoxo4** and **Au$_2$phen**, respectively. Interestingly aged-samples of **Au$_2$phen**-encapsulated AFt (10 months) retain the same amount of gold inside the cage when compared to freshly prepared samples.

Far-UV circular dichroism measurements reveal that the initial Ft secondary structure content was restored upon the encapsulation procedure (Figure 2B).

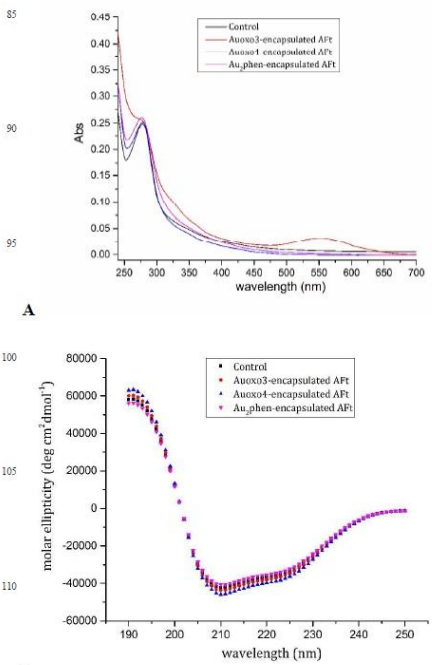

Figure 2. UV-Vis absorption spectra (A) and far-UV CD spectra (B) of gold-encapsulated Ft compared to the drug-free protein

DOI: 10.1039/C7DT02370G

(control). UV-vis spectra were acquired using a protein concentration of 0.25 mg mL^{-1} in 10 mM sodium phosphate at pH 7.4. Far-UV CD spectra were acquired using a protein concentration of 0.1 mg mL^{-1} in 10 mM sodium phosphate at pH 7.4. Superposition of the curves in the region between 250 nm and 280 nm confirms that the drugs are successfully encapsulated in the nanocage.

X-ray structure analysis of Auoxo4-encapsulated AFt and Au_2phen encapsulated AFt.

As indicated by Tosi and co-workers,[25] the effective clinical translation of drug-encapsulated Ft nanocages is probably limited also by the poor knowledge of the consequence of the protocols used to encapsulate the drugs on the overall architecture and structure of the nanocage. Circular dichroism is the technique that was most frequently used to evaluate the effects of the encapsulation protocols on the Ft structure. Although this technique provides reliable information on the secondary structure content of Ft, it does not show a real representation of the integrity of the cage after the disassembly/assembly process. X-ray crystallography is certainly the best choice to characterize the structure of the adducts. The X-ray structures of **Au_2phen**-encapsulated AFt and **Auoxo4**-encapsulated AFt were solved at 1.82 and 2.60 Å resolution, respectively (Figure 3A) and compared with those of ligand-free protein and of the adduct formed upon encapsulation of **Auoxo3**. The two structures were solved using the structure of the drug-free protein as a starting model and refined to Rfactor of 0.161 and 0.184 and Rfree of 0.187 and 0.236, respectively.

Positions of gold atoms in the structure were unambiguously identified by inspection of anomalous and 2Fo-Fc e.d. maps.

The structures are very similar to each other: they superimpose with a root mean square deviation between carbon alpha atoms of 0.38 Å. The structures of both **Au_2phen**-encapsulated AFt and **Auoxo4**-encapsulated AFt present two gold atoms bound to side chains of Cys126 (Figure 3B), whereas that of **Auoxo3**-encapsulated AFt shows gold atoms bound to the side chains of Cys126, Cys48, His49, His132, His147[19].

Geometry around the metal centres is linear, indicating that gold is probably in the oxidation state +1. The extensive degradation of the compounds and the reduction of the gold atom from +3 to +1 is not surprising since it was already observed in many other adducts of gold(III) based drugs with proteins, including members of **Auoxo** series [26-29].

We have searched for the origin of the different behaviour of **Auoxo3**, when compared to **Auoxo4** and **Au_2phen**, in the biophysical properties of the three compounds. **Auoxo3** and **Auoxo4** are structurally very similar and have similar redox potential (**Auoxo3**: E_p = -0.41 V vs SCE in DMSO, corresponding to E_p = -0.39 V vs NHE in aqueous solutions; **Auoxo4**: E_p = -0.40 V vs SCE in DMSO, corresponding to E_p = -0.38 V vs NHE in aqueous solutions). However, these two structurally related compounds show a different rate of hydrolysis reaction, which probably precedes the reduction process (half-life time at 70 °C ($t_{1/2}$) = about 1 h and 9 h for **Auoxo3** and **Auoxo4**, respectively). This difference, which we believe could be at the basis of the different behaviour of the two compounds, should be attributed to the presence of the large, hydrophobic, neopentyl group in the structure of **Auoxo4**, which protects the Au atom from the nucleophilic attack by water molecules (or by OH^- at alkaline pH) more effectively than the small methyl group.

Au_2phen behaves differently when compared to **Auoxo3** probably because of its highly negative redox potential (E_{pc1} = -0.946 V and E_{pc2} = -1.329 V *vs* F_c^+/F_c at a scan rate of 0.1 V s^{-1}),[23] which indicates high redox stability. Thus, both **Au_2phen** and **Auoxo4** have a lower tendency to reduction than **Auoxo3** and this could explain both the lower number of gold(I) binding sites observed in the structure of the encapsulated AFts here reported when compared to **Auoxo3**-encapsulated AFt and the higher tendency of **Auoxo3** to form gold nanoparticles inside the Ft cage when compared to **Au_2phen** and **Auoxo4**.

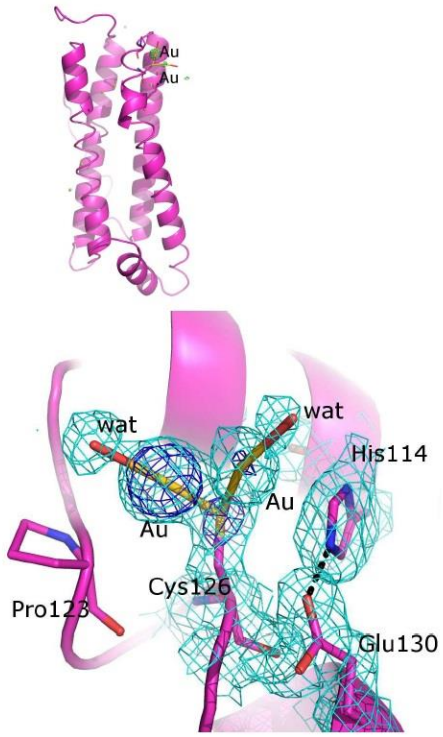

Figure 3. Overall structure of **Au_2phen**-encapsulated AFt subunit with Bijvoet difference Fourier map calculated with anomalous data and reported at 4 σ (A). An enlargement of the gold binding site region with the anomalous map is reported in Figure S2. In panel B, 2Fo-Fc electron density maps at 0.8 σ (cyan) and 4 σ (blue) of gold ions coordinated to Cys126 are reported. The gold ions were refined with partial occupancy (0.50 and 0.30); the average B-factors for gold ions are in the range 16.7–48.1 $Å^2$. Similar results were obtained for **Auoxo4**-encapsulated AFt

CREATED USING THE RSC COMMUNICATION TEMPLATE (VER. 3.0) - SEE WWW.RSC.ORG/ELECTRONICFILES FOR DETAILS
Dalton Transactions
Page 4 of 9
ARTICLE TYPE
www.rsc.org/xxxxxx | XXXXXXXX
DOI: 10.1039/C7DT02370C

(Figure S3 and S4). The structures were deposited in the Protein Data Bank under accession codes xxxx and yyyy.

Cytotoxicity

To assess the cytotoxic effect of **Auoxo4-** and **Au$_2$phen-**encapsulated AFt to inhibit cell growth, different cell lines were analysed. In particular, two cancer cell lines, human epithelial breast (MCF-7) and cervix carcinoma (HeLa) cells, and two normal cell lines, rat cardiomyoblasts (H9c2) and human keratinocytes (HaCaT) were used. Cells were incubated for 48 h with increasing concentrations of **Auoxo4-** and **Au$_2$phen-**encapsulated AFt, as well as with increasing concentrations of the free gold-based drugs. Then the ability of functional mitochondria to catalyse the reduction of MTT to form formazan salt by mitochondrial dehydrogenases was evaluated.[30] Drug-free Ft has been already used as control in a previous paper and it did not show significant toxicity on any of the analysed cell lines.[19] Results obtained after 48 h of incubation of cells with the new adducts are reported in Figure 4 and showed typical dose-response curves. The corresponding IC_{50} values, summarized in Table 1, indicate that, after 48 h incubation, encapsulated nanocages are more toxic towards cancer cell lines than towards normal cells. It is particularly interesting to underline that the presence of the cage significantly reduces the toxicity of the free gold drugs towards the non-cancer cell lines, enhancing the selectivity of the gold compounds towards tumour cells. Moreover, the new encapsulated AFts were more active than **Auoxo3-**encapsulated AFt, for which IC_{50} values were determined after 72h.[19]

In this respect, it is noteworthy that there are differences in the cytotoxicity profiles of the two gold-encapsulated AFts, that are probably due to the different amount of gold that is encapsulated within the Ft and thus, internalized by the cells. Moreover, it should be also recalled that since the structures of **Auoxo4-** and **Au$_2$phen** encapsulated AFt are similar, the differences should be due to the gold compounds that are within the cage, i.e. in the bulk. Interestingly, cytotoxicity experiments carried out on an aged-sample of **Au$_2$phen-**encapsulated AFt (10 months) lead to results that are very similar to those obtained by using freshly prepared samples, thus suggesting a high stability of the protein adduct.

Uptake data

To obtain a deeper insight into the amount of gold that is internalized by the cells, ICP-MS data on the uptake of **Au$_2$phen** and **Au$_2$phen-**encapsulated AFt, tested at the concentration needed to reach IC_{50} values, were collected. We found that the amount of gold uptake by MCF-7 cells is variable with **Au$_2$phen**, with values ranging from 2.2 μg up to 12.8 μg of gold per 1.5 x 10^6 cells, whereas it is constant in the case of **Au$_2$phen-**encapsulated AFt, with values close to 0.06 μg of gold per 1.5 x 10^6 cells. These data indicate that the use of Ft strongly reduces the gold uptake and that the amount of Au incorporated by cells and needed to kill 50% of them when the cells are treated with the free drug is 30-100 times higher than that needed when cells are treated with **Au$_2$phen-**encapsulated AFt. Moreover, it is found that the **Au$_2$phen-**encapsulated AFt is slightly more cytotoxic than the free gold complex. These findings indicate that the mode of action of the drug encapsulated within the cage is significantly different and more efficient when compared to that of the free drug, which enters the cells via passive diffusion. Further studies are needed to deeply analyse the reason of the greater cytotoxicity of **Au$_2$phen-**encapsulated AFt when compared to the free gold complex and the exact mechanism of action of these potential gold-based drugs.

Au$_2$phen-encapsulated AFt induces oxidative stress and apoptosis in MCF-7 human breast cancer cells

As it has been recently reported that ferrocenylated N-heterocyclic carbene supported gold(I) compounds are able to induce oxidative stress and subsequent cell death in cancer lung cells,[31] we analysed if **Au$_2$phen-**encapsulated AFt, which is endowed with the highest cytotoxic activity toward malignant cells, was able to alter the redox state of MCF-7 (the most sensitive cells to **Au$_2$phen-**encapsulated AFt). As shown in Figure 5A, we found an increase in ROS levels after 6 h of incubation with **Au$_2$phen-**encapsulated AFt and the drug alone, whereas no effect was observed for drug-free AFt. It is known that mitochondria are sensitive to changes in the cellular redox status and ROS activation is known to induce depolarization of mitochondrial membrane.[32] For this reason, we measured the mitochondrial potential of MCF-7 cells after **Au$_2$phen-**encapsulated AFt and **Au$_2$phen** treatment by TMRE (Mitochondrial Membrane Potential) assay[33] overtime (Figure 5B).

We observed that after 6 h of incubation, fluorescence intensity significantly decreases in cells treated with **Au$_2$phen** and **Au$_2$phen-**encapsulated AFt, when compared to untreated cells, thus suggesting that the treatment results in dissipation of mitochondrial membrane potential ($\Delta\psi$m). However, the lowest permeability threshold was found after 9 h of treatment and remained constant up to 24 h of incubation. This implies a mitochondrial damage during treatment with **Au$_2$phen-**encapsulated AFt and drug alone.

Furthermore, a decrease in intracellular GSH levels after 6 h of treatment (Figure 5C) and the increase in the phosphorylation level of p38, a protein involved in inflammation, cell cycle, development, differentiation and death, senescence and tumorgenesis,[34] confirmed the activation of the oxidative stress pathway (Figure 5D).

ARTICLE TYPE www.rsc.org/xxxxxx DOI: 10.1039/C7DT02370G

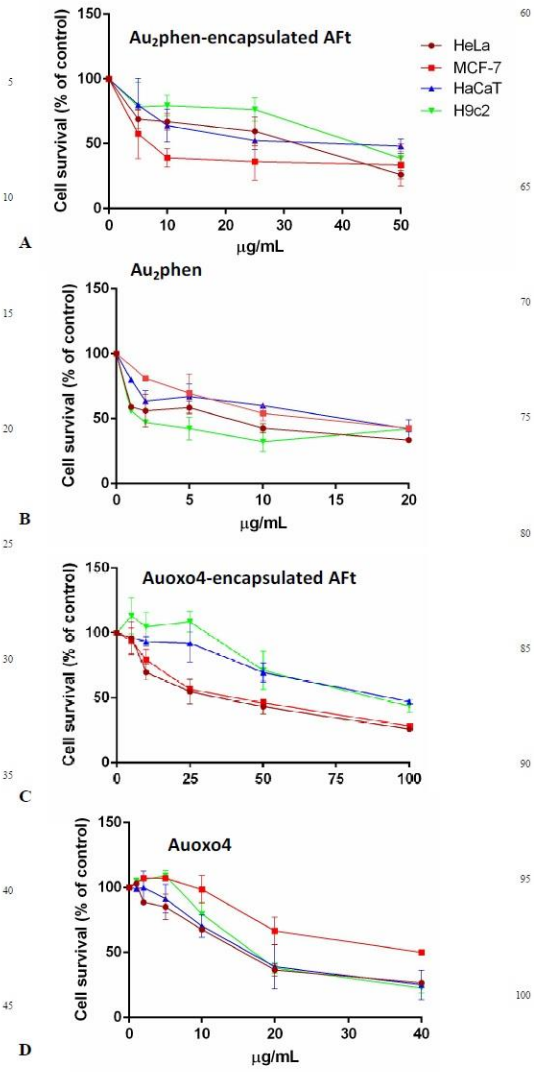

Figure 4. Effects of **Au_2phen**-encapsulated AFt (A), **Au_2phen** (B), **Auoxo4**-encapsulated AFt (C) and **Auoxo4** (D) on human cancer (HeLa and MCF-7) and normal cells (HaCaT and H9c2). Cells were treated with increasing amounts of the cage and of the free drug for 48 hours. Cell viability was assessed by the MTT assay and expressed as described in the materials and methods section. All values are given as means ±SD.

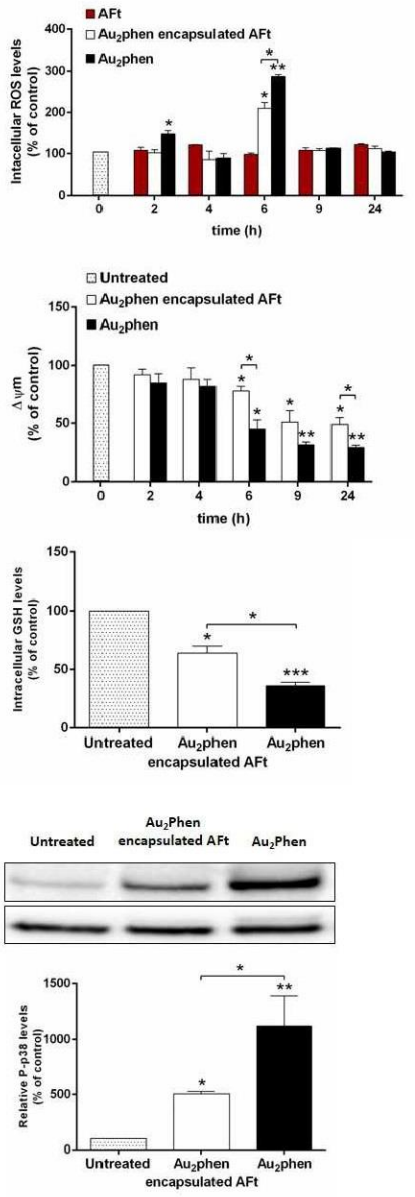

Figure 5: Activation of the oxidative stress pathway in MCF-7 cells after treatment with **Au_2phen**-encapsulated AFt and **Au_2phen**. MCF-7 were incubated in the presence of 7 μg mL^{-1} of **Au_2phen**-encapsulated AFt and 12 μg mL^{-1} of **Au_2phen** for different length of time (2 to 24 h) and markers of the

CREATED USING THE RSC COMMUNICATION TEMPLATE (VER. 3.0) - SEE WWW.RSC.ORG/ELECTRONICFILES FOR DETAILS
Dalton Transactions
Page 6 of 9
ARTICLE TYPE
www.rsc.org/xxxxxx | XXXXXXXX
DOI: 10.1039/C7DT02370C

oxidative stress were evaluated. Time-dependent changes in ROS levels were detected with a DCFDA probe and expressed as the fluorescence intensity percentage over control (%) (panel A). Time-dependent changes in mitochondrial membrane potential ($\Delta\psi m$) was determined using TMRE staining and expressed as the TMRE fluorescence intensity over control (%) (panel B). Intracellular GSH levels were determined by DTNB assay after 6 h of incubation. Values are expressed as fold increase with respect to control cells (panel C). Western blotting of the phosphorylation level of p38 (upper panel) after 24 h of incubation, with the relative densitometric analysis (panel D). GAPDH (lower panel) was used as internal standard. Data shown are the means ± S.D. of three independent experiments. * indicates $p<0.001$, ** indicates $p<0.0001$, *** indicates $p<0.00001$.

Table 1. IC_{50} values (μM) obtained for **Au_2phen**, **Auoxo4** and **Au_2phen-** and **Auoxo4**-encapsulated AFt in HeLa, MCF-7, H9c2 and HaCaT cell lines. Concentrations refer to gold amount.

IC_{50} μM 48h	**Au_2phen**-encapsulated AFt	**Au_2-phen**	**Auoxo4**-encapsulated AFt	**Auoxo4**
HeLa	32 ± 4	6.5 ± 1.0	23 ± 9	13.74 ± 0.96
MCF-7	6 ± 1	10.6 ± 2.5	30 ± 1	34.8 ± 4.3
H9c2	40 ± 1	1.28 ± 0.06	68 ± 6	14.6 ± 1.4
HaCaT	36 ± 9	14.3 ± 1.7	73 ± 6	12.4 ± 1.6

We finally analysed if apoptosis occurred in our experimental system, since it is known that cells are driven to apoptosis when ROS levels become too high [31, 35]. Cells were incubated for 48 h in the presence of **Au_2phen**-encapsulated AFt and **Au_2phen** and the activation of Caspase 8 and 3 was analysed. As shown in Figure 6, both Caspases were activated after 48 h incubation.

We hypothesized that apoptosis is triggered by the release of the drug inside the cell, in agreement with the data by Zhang et al. who have demonstrated that Ft can be internalized through TfR1 and can dissociate and release its cargo upon acidification of the endosomal compartment.[36]

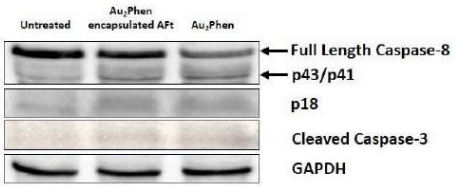

Figure 6: Apoptosis activation in MCF-7 incubated with **Au_2phen**-encapsulated AFt and **Au_2phen**. Cells were incubated for 48 h in the presence of 7 μg mL^{-1} of **Au_2phen**-encapsulated AFt and 12 μg mL^{-1} of **Au_2phen** and then cell extracts were prepared and subjected to Western blotting analysis. Western blot was performed using anti caspase-3, which recognizes the activated form of the protein and anti caspase-8, which recognizes pro-Caspase-8 and the activated forms (p43/41 and p18). GAPDH was used as loading control.

Materials and Methods

Sample preparation

Horse spleen ferritin was purchased from Sigma (code F4503, about 90% L chain) and used without further purification. Stock solution of Ft was stored at 4 °C in 0.15 mM sodium chloride. Gold based drugs **Auoxo4** and **Au_2phen** were synthetized as previously described.[20-22,23] **Au_2phen**-encapsulated AFt and **Auoxo4**-encapsulated AFt were prepared using the same procedure, i.e. following the protocols we have already used to encapsulate cisplatin, carboplatin and gold-based drug **Auoxo3**.[19] AFt protein nanocage is first dissociated into individual subunits at pH 13, using NaOH (final concentration 0.1 M), in the presence of the drug (protein to gold compound molar ratio 1:50), and then reassembled at pH 7.4 using 1.0 M sodium phosphate buffer. During the reassembly process, gold compounds were trapped within the inner cavity of the cage. Reaction solution was slowly stirred during all steps. The final solution was ultracentrifuged at 5000 rpm to remove the abundant precipitate and the surnatant recovered was then dialyzed using centricon filters (10 kDa cutoff) against 10 mM sodium phosphate buffer, pH 7.4 to remove the excess of the drug that is unbound.

Analytical and biophysical characterization of the samples

ICP-MS data were collected to confirm the encapsulation of gold compounds inside the cages, to quantitatively evaluate the efficiency of the gold compound encapsulation and estimate the amount of gold inside the cells. Gold standard solutions were prepared in 5 % HNO_3 at 4 different concentrations (1, 10, 50, and 100 μg L^{-1}). Au concentration was measured. All the analyses were performed in triplicates.

ARTICLE TYPE www.rsc.org/xxxxxx DOI: 10.1039/C7DT02370G

To determine the amount of gold inside the cells, treated and untreated cells were extensively washed with PBS and aliquots of the medium of treated and untreated cells and their cell pellets were incubated with 200 µl 65 % HNO_3 (Sigma Aldrich) and 600 µl 35 % HCl (Sigma Aldrich) overnight at 90 °C. The solution was then transferred into polystyrene liners, and diluted 1:10 v/v with 5 % HNO_3 and finally analysed with an Agilent 7700 ICP-MS from Agilent Technologies, equipped with a frequency-matching RF generator and 3rd generation Octopole Reaction System (ORS3), operating with helium gas in ORF. The following parameters were used: radiofrequency power 1550 W, plasma gas flow 14 L min^{-1}; carrier gas flow 0.99 L min^{-1}; He gas flow 4.3 mL min^{-1}. ^{103}Rh was used as an internal standard (final concentration: 50 µg L^{-1}). The error in the determination of the gold amount within the cells is within 10%.

Data indicate that **Auoxo4**-encapsulated AFt and **Au$_2$phen**-encapsulated AFt contained Ft subunit to Au ratio in a variable amount, depending on the preparation, and an undetectable amount of iron, confirming that the protein is in the Apo form (AFt) in the final adduct.

The gold compound-encapsulated AFts were also characterized by collecting UV-Vis absorption and circular dichroism spectra.

UV−Vis absorption spectra were recorded on a Jasco V650 UV-visible spectrophotometer in 10 mM sodium phosphate pH 7.4 and using the protein at concentration 0.25 mg mL^{-1}. Experimental conditions: 240-700 nm wavelength range, 200 nm/min scanning speed, 1 nm data pitch.
CD spectra were recorded on a Jasco V815 spectropolarimeter in the 190−250 nm range using protein concentration of 0.1 mg mL^{-1} in 10 mM sodium phosphate pH 7.4. Experimental conditions: 2 nm band width, 50 nm/min scanning speed, 1 nm data pitch, 4 s response time.

Crystallization and X-ray diffraction data collection

Auoxo4 and **Au$_2$phen**-encapsulated AFt were crystallized by hanging-drop vapor diffusion method at 298 K: 1 µL drops of 5 to 10 mg mL^{-1} protein adduct were mixed with equal volumes of 0.6-0.8 M $(NH_4)_2SO_4$, 0.1 M Tris HCl pH 7.4-7.7, 50-60 mM $CdSO_4$.

X-ray diffraction data were collected from single crystals at 100 K at CNR Institute of Biostructure and Bioimages, Naples, Italy, as previously done for **Auoxo3**-encapsulated AFt [19]. Data sets were processed with HKL2000.[37] The results are summarized in Table S1.

Structure resolution and refinement

Phases have been obtained by molecular replacement using the program Phaser [38] and the coordinates of the protein extracted from the PDB file 5ERK[9] as starting model. Refinement of atomic positions and individual B-factor were carried out using Refmac5.7.[39] Inspection of the structure and analysis of the electron density maps were performed using Wincoot.[40] Gold atoms were identified as previously described, i.e. considering anomalous, 2Fo-.Fc and Fo-Fc electron density maps. Details of the assignment of Au versus Cd ions are reported in Table S2. The structures final models refine at 1.82 and 2.60 Å resolution to a Rfactor of 0.161 and 0.184 and Rfree of 0.187 and 0.236, respectively. Refinement statistics are reported in Table S1. Coordinates and structure factors were provided to reviewers and Editor for review process and deposited in the Protein Data Bank under the accession codes xxxx and yyyy, respectively. Unintepreted peaks of electron density in the Fo-Fc electron density maps are discussed in Table S3.

Cell culture and MTT assay

Human breast cancer cells (MCF-7), cervical cancer cells (HeLa) and rat cardiomyoblasts cells (H9c2) were from ATCC. Human keratinocyte cells (HaCaT) were from Innoprot. All cells lines were cultured in Dulbecco's Modified Eagle's Medium (Sigma-Aldrich, St Louis, Mo, USA), supplemented with 10% foetal bovine serum (HyClone), 2 mM L-glutamine and antibiotics, all from Sigma-Aldrich, in a 5% CO_2 humidified atmosphere at 37 °C. The growth medium of H9c2 cells was implemented with 2 mM L-glutamine and 2 mM sodium pyruvate. For dose-response and time-course experiments, cells were seeded in 96-well plates at a density of 2 x 10^3/well. 24 h after seeding, increasing concentrations of compounds were added to the cells. Cell viability was assessed by the MTT (3-(4,5-dimethylthiazol-2-yl)-2,5-diphenyltetrazolium bromide) assay, as described in Monti et al.[41] Cell survival was expressed as the percentage of viable cells in the presence of the drug compared to controls. Two groups of cells were used as control, i.e. cells untreated with the drug and cells supplemented with identical volumes of buffer. Each sample was tested in three independent analyses, each carried out in triplicates.

Oxidative stress analyses

To estimate ROS production, the protocol described by Petruk [42] was followed, with some modifications. Briefly, MCF-7 cells were incubated with 7 µg mL^{-1} of **Au$_2$phen**-encapsulated AFt and 12 µg mL^{-1} of **Au$_2$phen** alone, for different length of time (0-24 h) and then incubated with 2',7'-dichlorodihydrofluorescein diacetate (H_2-DCFDA, Sigma-Aldrich). Fluorescence intensity was measured by a Perkin-Elmer LS50 spectrofluorimeter (525 nm emission wavelength, 488 nm excitation wavelength, 300 nm min^{-1} scanning speed, 5 nm slit width for both excitation and emission). ROS production was expressed as percentage of DCF fluorescence intensity of the sample under test, with respect to the untreated sample. Each value was assessed by three independent experiments, each with three determinations. Significance was determined by Student's t-test.
To analyse mitochondrial membrane potential ($\Delta\psi m$) the cells were pleated at density of $2x10^4$ cells/well and after 24 h were treated as described above. At the end of treatment, the cells were incubated with 200 nM of cationic lipophilic dye tetramethylrhodamine ethyl ester (TMRE) for 20 min at 37 °C. Then, cells were gently washed with 0.2% BSA in PBS for three

DOI: 10.1039/C7DT02370C

times and the fluorescence was measured in a microplate reader with peak Ex/Em =549/575 nm. Each value is the mean of three independent experiments, each with three determinations. Significance was determined by Student's t-test.

To estimate intracellular glutathione levels, cells were pleated and treated as described above and then incubated at 37 °C for 6 h. At the end of the incubation, DTNB assay was performed as described by Petruk et al. [42] Briefly, the cells were detached by trypsin, lysed and protein concentration was determined by the Bradford assay. Then, 50 µg of proteins were incubated with 3 mM EDTA, 144 µM 5,5′-dithiobis-2-nitrobenzoic acid (DTNB) in 30 mM Tris-HCl pH 8.2, centrifuged and the absorbance of the supernatant was measured at 412 nm by using a multiplate reader (Biorad). GSH levels were expressed as the percentage of TNB absorbance in the sample under test with respect to the untreated sample. Values are the mean of three independent experiments, each with triplicate determinations. Significance was determined by Student's t-test.

For western blotting analyses, cells were plated at a density of 2 x 10^4 cells/cm^2 in complete medium for 24 h and then treated as described above. After 48 h of incubation, cell lysates were analysed by Western blotting performed as reported in Galano et al [43]. Antibodies for phospho-p38, activated CASP-3 and CASP-8 were purchased from Cell Signal Technology (Danvers, MA, USA). To normalize protein intensity levels, specific antibodies against internal standards were used, i.e. anti-GAPDH (Thermo Fisher, Rockford, IL, USA). The chemiluminescence detection system (SuperSignal® West Pico) was from Thermo Fisher.

Conclusions

Ferritin has been used as scaffold for the fabrication of gold nanoparticles and for encapsulation of a variety of molecules, including metallodrugs. Here, taking advantages of the reversible dissociation of Ft at alkaline pH, we have encapsulated two different gold-based anticancer compounds (**Au$_2$phen** and **Auoxo4**), belonging to **Auoxos** series, within the ferritin nanocage and have characterized the adducts formed by X-ray crystallography. The cytotoxicity of these adducts has been evaluated on different cell lines. Data have been compared with those obtained for **Auoxo3**-encapsulated AFt. As expected, **Auoxo4** and **Au$_2$phen**-encapsulated AFt exhibit higher cytotoxicity than **Auoxo3**-encapsulated AFt, showing high cytotoxicity to MCF-7 and HeLa cell lines in a dose-dependent manner. The adducts show moderate selectivity, since they kill tumour cell lines at lower concentration than that needed to kill normal cell lines. The structures of the two adducts do not reveal significant differences, indicating that the differences in the cytotoxicity of the gold-encapsulated AFt depend mainly on the intrinsic properties of the encapsulated compounds rather than on the structure of the ferritin adduct obtained upon encapsulation. On the contrary, both structural and biological features of the new encapsulated AFts are different when compared to those previously reported for **Auoxo3**-encapsulated AFt. Differences are attributed to the diverse propensity of these gold drugs to undergo hydrolysis and successive reduction.

Surprisingly, uptake data indicate that the amount of gold internalized by MCF-7 cells is higher when cells are treated with the free drug than in the case of **Au$_2$phen**-encapsulated AFt. This suggests that internalization of **Au$_2$phen**-encapsulated AFt into cancer cells, which probably occurs via receptor-mediated endocytosis, is less efficient when compared to the passive diffusion of the free drug. However, the drug-loaded AFt nanocages are more selective than free drugs in killing cancer cells; selectivity may reside in the different mechanism of endocytosis of the two molecules. At present, the origin of the specificity of the ferritin nanocages and of its higher cytotoxicity when compared to the free drug is still unknown and will be the subject of further investigations. It is also unknown if horse spleen apoferritin (composed by 85% L chains and 15% H chains) enters the cell by TfR1 and/or Scara5 receptors. Geninatti Crich et al. reported that the chimeric nanocage enters the cell by Scara5[44], whereas Zhang and coworkers reported that internalization of H/L-chimeric Ft nanocage was due to TfR1[36]. The higher expression of both receptors on cancer cell surface, with respect to normal cells, could give specificity to the treatment, as supported by the different IC_{50} obtained for cancer and normal cells.

Finally, we have demonstrated that **Au$_2$phen**-encapsulated AFt is able to alter MCF-7 cell redox homeostasis, thus inducing apoptosis activation. We hypothesize that the lower sensitivity of normal cells to **Au$_2$phen**-encapsulated AFt can be due to the higher ability of adaptation of normal cells to counteract the negative effects of oxidative stress and, in turn, to cell death.

The authors thank G. Sorrentino and M. Amendola for technical assistance at CNR Institute of Biostructures and Biomages and N. Pontillo for his help in the preliminary characterization of the encapsulated AFts. MAC kindly acknowledges Regione Autonoma della Sardegna (RAS) for the financial support coming from L.R. 7, CRP-78365; A. M. acknowledges University of Naples Federico II for financial support (000005–ALTRI_DR_409_2017_Rec_Ateneo).

Notes and references

[a]*Department of Chemical Sciences, University of Naples Federico II, Complesso Universitario di Monte Sant'Angelo, Via Cintia, I-80126, Napoli, Italy. Fax: +39081674000; Tel: +39081674276; E-mail: antonello.merlino@unina.it*

[b]*Department of Chemistry and Pharmacy, University of Sassari, Italy*

[c]*CNR Institute of Biostructures and Bioimages, Via Mezzocannone 16, I-80126, Napoli, Italy*

†*Electronic Supplementary Information (ESI) available: See DOI: 10.1039/b000000x†*

References

1. M. Uchida, S. Kang, C. Reichhardt, K. Harlen and T. Douglas, *Bba-Gen Subjects*, 2010, **1800**, 834-845.
2. S. C. Andrews, P. Arosio, W. Bottke, J. F. Briat, M. Vondarl, P. M. Harrison, J. P. Laulhere, S. Levi, S. Lobreaux and S. J. Yewdall, *J Inorg Biochem*, 1992, **47**, 161-174.
3. M. Uchida, M. L. Flenniken, M. Allen, D. A. Willits, B. E. Crowley, S. Brumfield, A. F. Willis, L. Jackiw, M. Jutila, M. J. Young and T. Douglas, *J Am Chem Soc*, 2006, **128**, 16626-16633.
4. J. Xie, Z. P. Zhen and W. Tang, *Cancer Res*, 2013, **73**.

5. T. Kitagawa, H. Kosuge, M. Uchida, M. M. Dua, Y. Iida, R. L. Dalman, T. Douglas and M. V. McConnell, *Mol Imaging Biol*, 2012, **14**, 315-324.
6. D. Hogemann-Savellano, E. Bos, C. Blondet, F. Sato, T. Abe, L. Josephson, R. Weissleder, J. Gaudet, D. Sgroi, P. J. Peters and J. P. Basilion, *Neoplasia*, 2003, **5**, 495-506.
7. L. Mendes-Jorge, D. Ramos, A. Valenca, M. Lopez-Luppo, V. M. R. Pires, J. Catita, V. Nacher, M. Navarro, A. Carretero, A. Rodriguez-Baeza and J. Ruberte, *Plos One*, 2014, **9**.
8. J. Y. Li, N. Paragas, R. M. Ned, A. D. Qiu, M. Viltard, T. Leete, I. R. Drexler, X. Chen, S. Sanna-Cherchi, F. Mohammed, D. Williams, C. S. Lin, K. M. Schmidt-Ott, N. C. Andrews and J. Barasch, *Dev Cell*, 2009, **16**, 35-46.
9. N. Pontillo, F. Pane, L. Messori, A. Amoresano and A. Merlino, *Chem Commun*, 2016, **52**, 4136-4139.
10. N. Pontillo, G. Ferraro, H. H. R. Helliwell, A. Amoresano and A. Merlino, *Acs Med Chem Lett*, 2017, **8**, 433-437.
11. Z. P. Zhen, W. Tang, C. L. Guo, H. M. Chen, X. Lin, G. Liu, B. W. Fei, X. Y. Chen, B. Q. Xu and J. Xie, *Acs Nano*, 2013, **7**, 6988-6996.
12. Z. P. Zhen, W. Tang, W. Z. Zhang and J. Xie, *Nanoscale*, 2015, **7**, 10330-10333.
13. Z. P. Zhen, W. Tang, H. M. Chen, X. Lin, T. Todd, G. Wang, T. Cowger, X. Y. Chen and J. Xie, *Acs Nano*, 2013, **7**, 4830-4837.
14. X. T. Ji, L. Huang and H. Q. Huang, *J Proteomics*, 2012, **75**, 3145-3157.
15. T. Zou, C. T. Lum, C. N. Lok, J. J. Zhang and C. M. Che, *Chemical Society reviews*, 2015, **44**, 8786-8801.
16. C. Nardon, G. Boscutti and D. Fregona, *Anticancer research*, 2014, **34**, 487-492.
17. C. Gabbiani, A. Casini and L. Messori, *Gold Bull*, 2007, **40**, 73-81.
18. B. Bertrand and A. Casini, *Dalton T*, 2014, **43**, 4209-4219.
19. G. Ferraro, D. M. Monti, A. Amoresano, N. Pontillo, G. Petruk, F. Pane, M. A. Cinellu and A. Merlino, *Chem Commun*, 2016, **52**, 9518-9521.
20. B. Maity, A. Abe and T. Ueno, *Nature Commun*, 2017, 8:14820.
21. A. Casini, M. A. Cinellu, G. Minghetti, C. Gabbiani, M. Coronnello, E. Mini and L. Messori, *J Med Chem*, 2006, **49**, 5524-5531.
22. C. Gabbiani, A. Guerri, M. A. Cinellu and L. Messori, *The Open Crystallography Journal*, 2010, **3**, 29-40.
23. M. A. Cinellu, L. Maiore, M. Manassero, A. Casini, M. Arca, H. H. Fiebig, G. Kelter, E. Michelucci, G. Pieraccini, C. Gabbiani and L. Messori, *Acs Med Chem Lett*, 2010, **1**, 336-339.
24. C. Gabbiani, A. Casini, L. Messori, A. Guerri, M. A. Cinellu, G. Minghetti, M. Corsini, C. Rosani, P. Zanello and M. Arca, *Inorg Chem*, 2008, **47**, 2368-2379.
25. G. Tosi, D. Belletti, F. Pederzoli and B. Ruozi, *Expert Opin Drug Del*, 2016, **13**, 1341-1343.
26. I. Russo Krauss, L. Messori, M. A. Cinellu, D. Marasco, R. Sirignano and A. Merlino, *Dalton Trans*, 2014, **43**, 17483-17488.
27. L. Messori, F. Scaletti, L. Massai, M. A. Cinellu, I. Russo Krauss, G. di Martino, A. Vergara, L. Paduano and A. Merlino, *Metallomics*, 2014, **6**, 233-236.
28. L. Messori, M. A. Cinellu and A. Merlino, *Acs Med Chem Lett*, 2014, **5**, 1110-1113.
29. L. Messori, F. Scaletti, L. Massai, M. A. Cinellu, C. Gabbiani, A. Vergara and A. Merlino, *Chem Commun (Camb)*, 2013, **49**, 10100-10102.
30. J. C. Stockert, A. Blazquez-Castro, M. Canete, R. W. Horobin and A. Villanueva, *Acta Histochem*, 2012, **114**, 785-796.
31. J. F. Arambula, R. McCall, K. J. Sidoran, D. Magda, N. A. Mitchell, C. W. Bielawski, V. M. Lynch, J. L. Sessler and K. Arumugam, *Chem Sci*, 2016, **7**, 1245-1256.
32. G. Petrosillo, F. M. Ruggiero and G. Paradies, *Faseb J*, 2003, **17**, 2202-2208.
33. Y. Piao, H. G. Kim, M. S. Oh and Y. K. Pak, *Biochimica et biophysica acta*, 2012, **1820**, 577-585.
34. D. Munoz-Espin and M. Serrano, *Nat Rev Mol Cell Bio*, 2014, **15**, 482-+.
35. Y. Zhao, E. B. Butler and M. Tan, *Cell Death Dis*, 2013, **4**.
36. L. Zhang, L. Li, A. Di Penta, U. Carmona, F. Yang, R. Schops, M. Brandsch, J. L. Zugaza and M. Knez, *Advanced healthcare materials*, 2015, **4**, 1305-1310.
37. Z. Otwinowski and W. Minor, *Method Enzymol*, 1997, **276**, 307-326.
38. A. J. McCoy, R. W. Grosse-Kunstleve, P. D. Adams, M. D. Winn, L. C. Storoni and R. J. Read, *J Appl Crystallogr*, 2007, **40**, 658-674.
39. G. N. Murshudov, P. Skubak, A. A. Lebedev, N. S. Pannu, R. A. Steiner, R. A. Nicholls, M. D. Winn, F. Long and A. A. Vagin, *Acta Crystallographica Section D-Biological Crystallography*, 2011, **67**, 355-367.
40. P. Emsley, B. Lohkamp, W. G. Scott and K. Cowtan, *Acta Crystallographica Section D-Biological Crystallography*, 2010, **66**, 486-501.
41. D. M. Monti, D. Guarnieri, G. Napolitano, R. Piccoli, P. Netti, S. Fusco and A. Arciello, *J Biotechnol*, 2015, **193**, 3-10.
42. G. Petruk, A. Raiola, R. Del Giudice, A. Barone, L. Frusciante, M. M. Rigano and D. M. Monti, *J Photoch Photobio B*, 2016, **163**, 284-289.
43. E. Galano, A. Arciello, R. Piccoli, D. M. Monti and A. Amoresano, *Metallomics*, 2014, **6**, 587-597.
44. S. Geninatti Crich, M. Cadenazzi, S. Lanzardo, L. Conti, R. Ruiu, D. Alberti, F. Cavallo, J. C. Cutrin, S. Aime, *Nanoscale*, 2015, **7**, 6527-6533.

Electronic Supplementary Material (ESI) for Dalton Transactions.

Journal Name

Dynamic Article Links ►

Cite this: DOI: 10.1039/coxxoooooox

www.rsc.org/xxxxxx

ARTICLE TYPE

Supporting information

Ferritin nanocages loaded with gold ions induce oxidative stress and apoptosis in MCF-7 human breast cancer cells

Daria Maria Monti,[a] Giarita Ferraro,[a] Ganna Petruk,[a] Laura Maiore,[b] Francesca Pane,[a] Angela Amoresano,[a] Maria Agostina Cinellu,[b] and Antonello Merlino[a,c*]

Received (in XXX, XXX) Xth XXXXXXXXX 20XX, Accepted Xth XXXXXXXXX 20XX
DOI: 10.1039/b000000x

CREATED USING THE RSC COMMUNICATION TEMPLATE (VER. 3.1) - SEE WWW.RSC.ORG/ELECTRONICFILES FOR DETAILS

ARTICLE TYPE www.rsc.org/xxxxxx | XXXXXXXX

5 **Figure S1**. Photo of the solutions of **Au_2phen** -encapsulated AFt, **Auoxo4**-encapsulated AFt and of **Auoxo3**-encapsulated AFt.

10

CREATED USING THE RSC COMMUNICATION TEMPLATE (VER. 3.1) - SEE WWW.RSC.ORG/ELECTRONICFILES FOR DETAILS

ARTICLE TYPE www.rsc.org/xxxxxx | XXXXXXXX

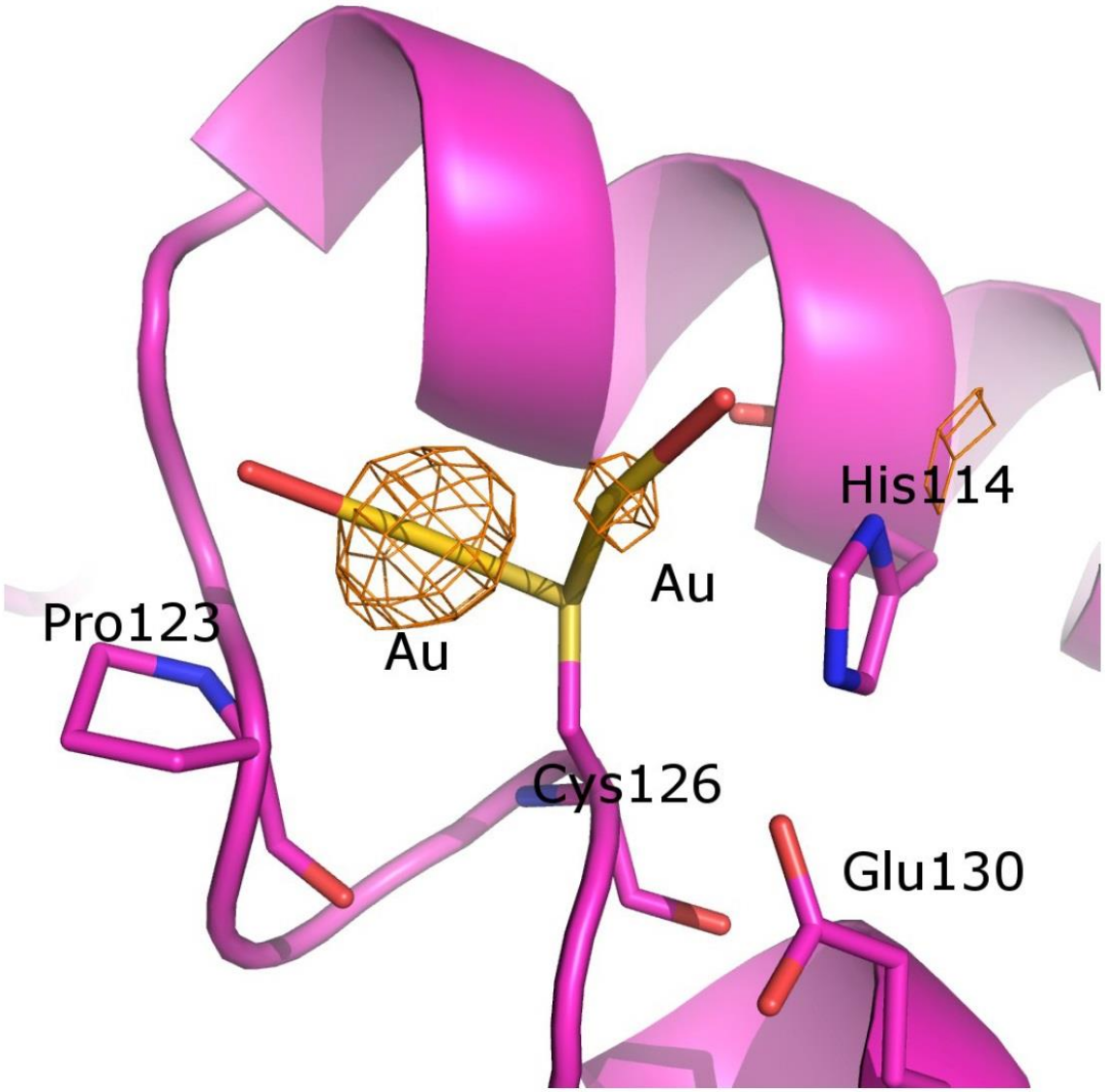

Figure S2. Gold binding site region in **Au_2phen**-encapsulated AFt. Bijvoet difference Fourier map calculated with anomalous data and reported at 4 σ.

CREATED USING THE RSC COMMUNICATION TEMPLATE (VER. 3.1) - SEE WWW.RSC.ORG/ELECTRONICFILES FOR DETAILS

ARTICLE TYPE www.rsc.org/xxxxxx | XXXXXXXX

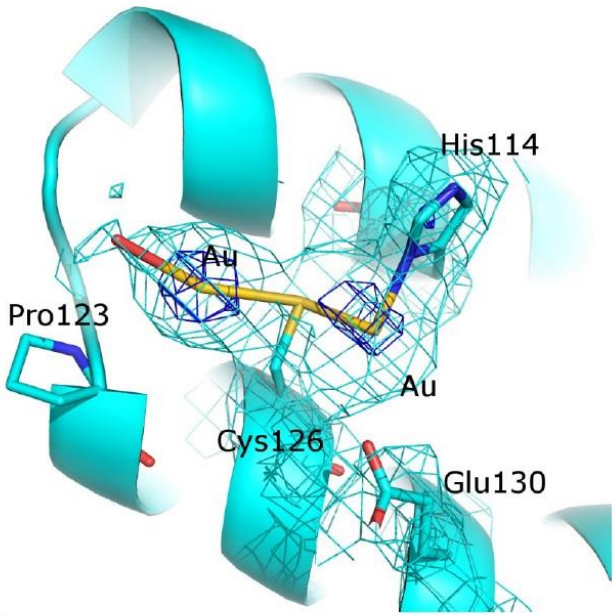

A

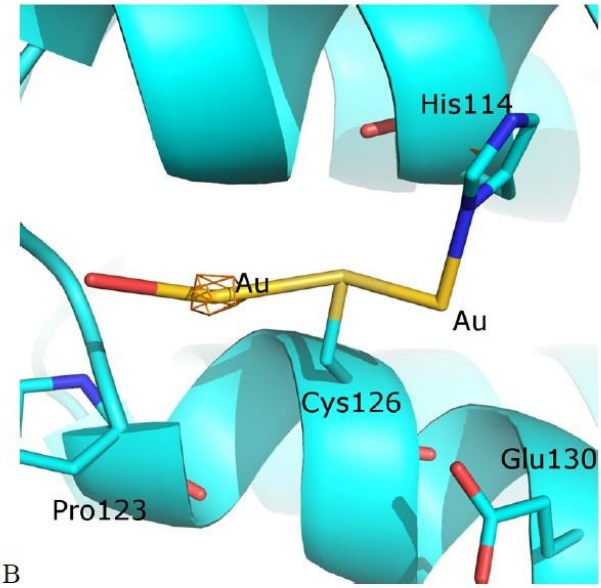

B

CREATED USING THE RSC COMMUNICATION TEMPLATE (VER. 3.1) - SEE WWW.RSC.ORG/ELECTRONICFILES FOR DETAILS

ARTICLE TYPE www.rsc.org/xxxxxx | XXXXXXXX

Figure S3. Gold binding site region in **Auoxo4**-encapsulated AFt. 2Fo-Fc electron density maps are reported at 0.8 σ (cyan) and 4 σ (blue). Bijvoet difference Fourier map calculated with anomalous data and reported at 3 σ is in orange in panel B.

5

Table S1. Data collection and refinement statistics

	Au_2phen-encapsulated AFt	**Auoxo4**-encapsulated AFt
Data Collection statistics		
X-ray source	Rotating anode	Rotating anode
Wavelength	λ=1.5418Å	λ=1.5418Å
Space group	F432	F432
Unit-cell parameters a=b= c (Å), α,β,γ (°)	 180.97 90	 180.88 90
Ft Monomers per a. u.	1	1
Resolution (Å)	104.5-1.82 (1.85-1.82)	104.4-2.60 (2.64-2.60)
Observed reflections	287733	32931
Unique reflections	23324	8209
Completeness (%)	99.9 (100)	99.0 (99.7)
Rmerge	0.121 (0.680)	0.187 (0.414)
Rpim	0.126 (0.269)	0.145 (0.401)
I/σ(I)	11.9 (3.2)	5.4 (2.9)
Multiplicity	12.3 (7.2)	4.0 (4.1)
CC1/2	0.857	
Refinement		
Resolution (Å)	104.5-1.82	104.4-2.60
n. of reflections in working set	22173	7881
n. of reflections in test set	1138	391
R factor/Rfree (%)	14.3/17.2	18.4/23.6
n of non-H atoms in the refinement	1822	1605
Occupancy of Au ions	0.50, 0.30	0.50, 0.35
B-factor of Au ions (Å^2)	16.9, 48.1	41.5, 47.1
Overall B-factor	18.6	23.6
Deviations from ideality values R.m.s.d. bonds (Å)	0.022	0.013

R.m.s.d. angles (Å)	1.86	1.47

CREATED USING THE RSC COMMUNICATION TEMPLATE (VER. 3.1) - SEE WWW.RSC.ORG/ELECTRONICFILES FOR DETAILS

ARTICLE TYPE www.rsc.org/xxxxxx | XXXXXXXX

Table S2. Comparison of anomalous peak intensity of the most representative Cd ions, i.e. those conserved in the structures of AFts, in **Au2phen-**, **Auoxo4- Auoxo3-**encapsulated AFts and in the structure of CDDP- and CBDCA-encapsulated AFts, used as control. Only data collected using CuKα are compared.

	Auoxo4-encapsulated AFt	Au2phen-encapsulated AFt	Auoxo3-encapsulated AFt	CDDP-encapsulated AFt	CBDCA-encapsulated AFt
Source Resolution PDB code	CuKα λ=1.5418 Å 2.6 Å	CuKα λ=1.5418 Å 1.82 Å	CuKα λ=1.5418 Å 1.96 Å 5IX6	CuKα λ=1.5418 Å 2.06 Å	CuKα λ=1.5418 Å 1.96 Å 5MIK
Atom in 5ERK					e/Å^3
CD 1. Close to Glu11	<0.10	0.23	0.22 (CD8)	0.24	0.22
CD 2. Close to Glu53/Glu56	<0.10	0.16	0.21(CD9)	0.16	0.22
CD 3. Close to Glu60	<0.10	0.28	0.20 (CD15)	0.31	0.25
CD 4. At the binary axis. Close to Asp80	<0.10	1.80	1.19 (CD10)	0.92	1.08
CD 5. Close to Glu88	Absent	0.10	<0.10	<0.10	0.12
CD 6. Close to Asp127		0.10	<0.10	0.35	<0.10
CD 7. Close to His132	0.13	0.23	0.25(CD11)	0.28	< 0.10 (0.17 using λ=0.97Å) **Interpreted as Pt**
CD 8. At the ternary axis. Close to Glu130	0.30	0.51	0.58 (CD12)	0.41	0.39
CD 9. Close to His114 and at 3.7 from Cys126	<0.10	<0.10	0.19	0.25	0.08/0.09
Atoms in 5IX6					
Au1 close to SG Cys126 and His114	Absent	Absent	0.76 **Interpreted as Au**	<0.10	
Au2 close to Cys48 (and Close to Arg52)	E.d. absent <0.1	E.d. absent <0.1	0.37 **Interpreted as Au**	<0.10	0.16 **Interpreted as Cd**
Au3 close to His49	<0.10	< 0.10 Interpreted as water	0.52 **Interpreted as Au**	<0.10	0.04/0.13 (0.17 using λ=0.97Å) **Interpreted as Pt**
Au4 close to SG Cys126	0.22 **Interpreted as Au**	1.06 **Interpreted as Au**	1.00 **Interpreted as Au**	<0.10	-
Au5 close to His147	-	< 0.1 Interpreted as water	**Interpreted as Au** 3.14	<0.10	-
CD 11. Close to Cys48	<0.10	0.16 Interpreted as Cd	0.50 **Interpreted as Au6** close to Cys48 (and close to His49	0.25 Interpreted as Cd	0.16 Interpreted as Cd

Au7 close to His132	E.d. absent <0.10	E.d absent <0.1	**Interpreted as Au** 0.16	0.21 **Interpreted as Pt**	
Au close to Cys126	**Interpreted as Au** 0.13	**Interpreted as Au** 0.23	Interpreted as water. Close to Au1	<0.10	
CD16	<0.10	Interpreted as water <0.10	0.21	Absent Close to Asp53	

CREATED USING THE RSC COMMUNICATION TEMPLATE (VER. 3.1) - SEE WWW.RSC.ORG/ELECTRONICFILES FOR DETAILS

ARTICLE TYPE www.rsc.org/xxxxxx | XXXXXXXX

Table S3.Uninterpreted peaks of electron density in the Fo-Fc map:

Auoxo4-encapsulated AFt

	e/Å^3	Reason
Peak 1	0.81	Too close to SG atom of Cys126, CL and Au atoms
Peak 2	0.80	In the middle oft he nanocage. Not bound tot he protein
Peak 3	0.68	Too close to side chain of His149
Peak 4	0.60	Too close to CD20 and wat 266
Peak 5	0.59	Too close to side chain of Arg153
Peak 6	0.56	Too close to side chain of His149
Peak 7	0.51	Too close to CD1

.

Au_2phen-encapsulated AFt

	e/Å^3	Reason

Peak 1	0.81	Too close to gold atom and SG atom of Cys126
Peak 2	0.80	Too close to a water molecule
Peak 3	0.68	Too close to side chain of Gln79
Peak 4	0.60	Too close to side chain of Glu163
Peak 5	0.59	
Peak 6	0.56	
Peak 7	0.51	

molecules

MDPI

Review

Bioactive Compounds in *Brassicaceae* Vegetables with a Role in the Prevention of Chronic Diseases

Assunta Raiola [1], Angela Errico [1], Ganna Petruk [2], Daria Maria Monti [2], Amalia Barone [1,*] and Maria Manuela Rigano [1,*]

1 Department of Agricultural Sciences, University of Naples Federico II, Via Università 100, 80055 Naples, Italy; assuntaraiola@hotmail.com (A.R.); angela.errico@unina.it (A.E.)

2 Department of Chemical Sciences, University of Naples Federico II, Complesso Universitario di Monte Sant'Angelo, 80055 Naples, Italy; ganna.petruk@unina.it (G.P.); mdmonti@unina.it (D.M.M.)

* Correspondence: ambarone@unina.it (A.B.); mrigano@unina.it (M.M.R.); Tel.: +39-081-2539486 (A.B.); +39-081-2532125 (M.M.R.); Fax: +39-081-2531718 (A.B. & M.M.R.)

Received: 11 December 2017; Accepted: 20 December 2017; Published: 23 December 2017

Abstract: The beneficial role of the Mediterranean diet in the prevention of chronic diseases, including cardiovascular diseases, diabetes, and obesity, is well-recognized. In this context, *Brassicaceae* are considered important vegetables due to several evidences of their health promoting effects that are associated to bioactive compounds present in the edible parts of the plants. In this review, the mechanisms of action and the factors regulating the levels of the bioactive compounds in *Brassicaceae* have been discussed. In addition, the impact of industrial and domestic processing on the amount of these compounds have been considered, in order to identify the best conditions that are able to preserve the functional properties of the *Brassicaceae* products before consumption. Finally, the main strategies used to increase the content of health-promoting metabolites in *Brassica* plants through biofortification have been analyzed.

Keywords: chronic diseases; glucosinolates; phenolic compounds; ascorbic acid; carotenoids; biofortification

1. Introduction

The *Brassicaceae* family consists of about 3500 species, and includes 350 genera, such as *Brassica*, *Camelina*, *Crambe*, *Sinapis*, and *Thlaspi*. In particular, the genus *Brassica* includes some species of worldwide economic importance, such as *Brassica oleracea*, *Brassica rapa* L., and *Brassica napus* [1].

Several species, which belong to the *Brassicaceae* family, represent an important part of the human diet worldwide; indeed, when regularly consumed, they have been found to exert health-promoting effects, such as a reduction in the risk of chronic diseases, particularly cardio-vascular diseases and several types of cancer [2,3]. These effects have been linked to the presence in these plants of phenolics, glucosinolates, carotenoids, tocopherols, and ascorbic acid, well-known antioxidants [4]. In particular, broccoli, white cabbage, and cauliflower are rich in glucosinolates, and, more in detail, in glucoraphanin, a molecule that is transformed by myrosinase into sulforaphane, that is a compound endowed with anticarcinogenic properties [5].

In this review, we describe how a reduced risk of chronic diseases development may be a consequence of *Brassicaceae* consumption. Furthermore, we analyze the specific mechanisms of action of the most important bioactive compounds that are present in the genus *Brassica*. Finally, we debate on the biotechnological approaches that can be used to enrich the content of antioxidant compounds in the edible parts of *Brassica* plants.

Brassicaceae are usually consumed after cooking; therefore, it is necessary to use appropriate agronomic techniques combined with proper processing techniques to manage and/or improve the general quality of the final *Brassica* product used for consumption [6]. Therefore, here, the impact of different practices used both pre- and post-harvest and their effects on the amount of bioactive compounds in *Brassicaceae* products are also discussed.

2. Bioactive Compounds in *Brassicaceae* and Their Effects on Chronic Diseases

The Mediterranean diet, which is characterized by a high consumption of plant-based foods, has been associated with a lower risk of cardiovascular diseases and mortality in different epidemiological studies. In the last few years, several studies, both in vitro and in vivo, have focused on the effects of *Brassicaceae* on chronic diseases and on the bioactive compounds of these plants that may be responsible for the observed effects [7,8] (Figure 1). It has been discussed that the known healthy effects of *Brassicaceae* may be related to the presence of several bioactive compounds in the edible parts, such as ascorbic acid (AsA), phenolics, carotenoids, and glucosinolates, as summarized in Table 1 [9,10].

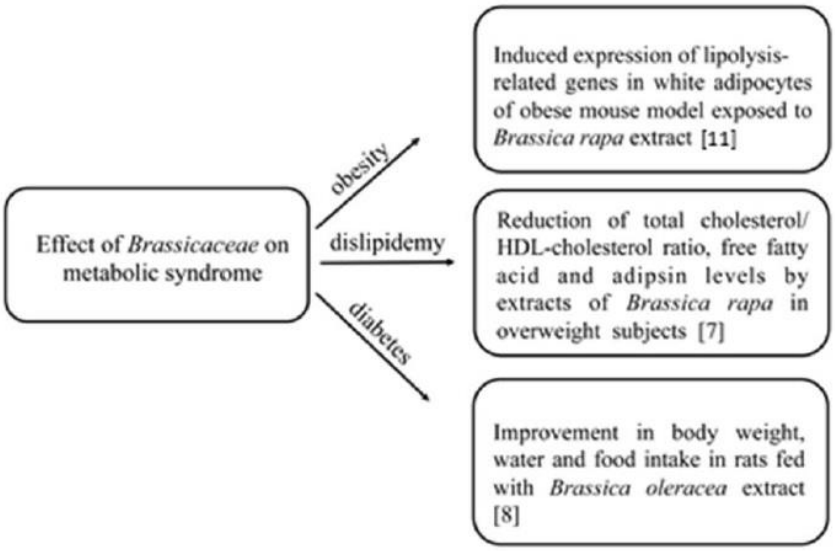

Figure 1. Main effects of *Brassicaceae* consumption on metabolic syndromes.

Table 1. Mechanisms of action of bioactive compounds in *Brassicaceae*.

Compound	Mechanism	Reference
Ascorbic acid	ROS reduction and neutralization	[12]
	Protection against LDL oxidation	[13]
	Prevention of oxLDL-induced overexpression of Vascular Endothelial Growth Factor	
Phenolics	ROS neutralization	[14]
	Chelation of redox-active metal ions and inhibition of LDL-cholesterol oxidation	
Carotenoids	Radical scavengers and quenches of singlet oxygen	[15]
Glucosinolates	Inhibition of the invasive potential of human cancer cell line in vitro	[16]
	Regulation of the phase I and/or phase II detoxification enzymes activity	[17]

AsA and dehydroascorbic acid are known to reduce and neutralize reactive oxygen species (ROS) [12]. Moreover, AsA is able to protect the myocardium when associated to ferulic acid [18], and, in association with vitamin E, it can prevent oxLDL-induced overexpression of vascular endothelial growth factor (VEGF), responsible for atherosclerotic plaque formation [13]. Cultivated broccoli normally contain high amount of Vitamin C, ranging between 70 and 120 mg/100 g fresh weight (FW) [19].

However, the content of AsA in *Brassica* depends on the investigated cultivar, sulfur fertilization, and on post-harvest handling conditions [20–23]. For example, the microorganism *Trichoderma harzianum*, a known biocontrol agent, and its metabolites (harzianum acid and 6-pentyl-a-pyrone) were able to increase AsA content when used on plants of the ecotype "Friariello" from the Campania region [14].

Phenolic compounds have been studied for their ability to chelate redox-active metal ions, to inhibit LDL cholesterol oxidation, and to neutralize other processes involving ROS, since they are efficient free radical scavengers [14]. Moreover, dietary polyphenols may inhibit the growth of adipose tissue by modulating adipocyte metabolism [24]. It is reported that polyphenols are able to enhance glucose uptake in adipocytes and muscle cells by GLUT4, a glucose transporter that exerts its action through the AMP-activated protein kinase pathway [25]. It has also been demonstrated that flavonoids can normalize blood glucose levels and promote β-cell regeneration in islets of alloxan-treated rats [26], while epicatechin and quercetin can improve insulin production in isolated rat islets [27]. Turnip leaf (*Brassica rapa*) extracts, which are rich in flavonoids and tannins, showed an anti-hyperglycemic activity in alloxan-induced diabetic rats [28]. In general, different varieties of broccoli may have different total phenolics content, ranging from 5 up to 8 mg/g dry weight (DW) [19,21]. The amount of total phenolics in *Brassica* may be further increased by using specific agronomic techniques, such as sulphur fertilization and/or light-treatment [4,29].

Carotenoids are pigments precursors of vitamin A (i.e., β-carotene, γ-carotene, and β-cryptoxanthin), which are characterized by the presence of conjugated double bonds responsible for the radical scavengers and quenchers of singlet oxygen. It has been reported that carotenoids level in *Brussels sprouts* is 6 mg/100 g FW, about 2 mg/100 g FW in broccoli, 0.5 mg/100 g FW in red cabbage, and 0.26 mg/100 g FW in white cabbage [15]. Higher β-carotene serum levels have been linked to lower rates of cancer and cardiovascular diseases, as well as to decreased risks of myocardial infarction. Moreover, serum β-cryptoxanthin and β-carotene amount have been negatively correlated with metabolic syndrome factors [30].

Glucosinolates represent a group of phytochemicals found in 15 botanical families of the order of *Capparales* and are very abundant in *Brassicaceae* [31]. A very different profile of glucosinolates may be found in different broccoli extracts [32]. In a recent paper, the most abundant glucosinolates found in different broccoli samples were glucobrassicin and neoglucobrassicin, followed by glucoraphanin. Interestingly, glucoraphanin, which is one of the most representative glucosinolates in broccoli, was completely absent in the ecotype "Friariello" from the Campania region [31]. Also, the content of glucosinolates may be deeply different in different broccoli varieties. For example, analyses conducted on a collection of 113 varieties of turnip greens (*Brassica rapa* L.), cultivated in two different sites in Spain, showed glucosinolates contents ranging from 12 to 70 μmol/g DW at one site, and from 7 to 60 μmol/g DW at the other site [32].

Intact glucosinolates are biologically inactive, whereas after the disruption of plant cells, they are hydrolysed by a β-thioglucosidase enzyme called myrosinase. Among the breakdown products, the isothiocyanates are associated to important protecting effects [33]. In addition to the prevention of chronic disease, it is largely reported a strong correlation between the consumption of cruciferous vegetables and the decreased risk for different types of cancer. Indeed, it has been demonstrated that extracts of broccoli and watercress inhibit the invasive potential of human breast cancer cell lines in vitro [31]. This effect may be explained by the ability of glucosinolates-hydrolysis products to regulate the phase I and/or phase II detoxification enzymes activity [17]. Therefore, isothiocyanates could be considered as a new class of invasion inhibitors.

In the last few years, several studies both in vitro and in vivo have been carried out on the effects of *Brassicaceae* on chronic diseases [7,8]. By using an obese mouse model, a study demonstrated that the exposure of mice to ethanolic extracts from *Brassica rapa* resulted in the expression of lipolysis-related genes in white adipocytes, in the activation of cyclic AMP-dependent protein kinase, and in the induction of extracellular signal-regulated kinase, suggesting that *Brassicaceae* extracts may be used as safe and effective anti-obesity agents [11].

In another in vivo study, extracts from *Brassica rapa* were used for 10 weeks as a part of the diet of overweight human subjects. At the end of the experiment, a significant increase in the high-density lipoprotein cholesterol (HLDL-cholesterol) concentration and a significant reduction in the total cholesterol/HDL-cholesterol ratio, free fatty acid, and adipsin levels were measured [7]. Also, Shah et al. [8] used extracts from *Brassica oleracea* leaves to analyze its anti-diabetic effect on rats. After having induced diabetes in rats, animals were fed for 28 days with *Brassica oleracea*, and then, a significant improvement in body weight and in water and food intake was observed [8]. In rats fed with an atherogenic diet, the assumption of red cabbage, highly rich in anthocyanins, was able to increase faecal lipid excretion, with a reduced risk of tissue lipids, hepatic, and cardiac peroxidation [34]. Moreover, it has been demonstrated that *Brassica oleracea* kale leaves extracts can inhibit lipid peroxidation in LDL isolated from human volunteers [35], while extracts from *Brassica rapa* L. *oleifera* can suppress postprandial hypertriglyceridemia in mice due to the presence of gluconapin and sinigrin [36]. Finally, it has been proved that the combination of *Brassica olearaceae* L. and hydrosoluble chitosan was able to reduce triglycerides, serum total cholesterol, and LDL-cholesterol in rats, and that this combination was much more effective than that obtained by combining chitosan and Aloe vera extract [37,38]. A further protective effect of *Brassicaceae* is represented by the inhibition of mechanisms regulating the development of cancer. Indeed, a 2-pyrrolidinone rich extract from *Brassica oleracea* showed in vitro cytotoxicity on HeLa and PC-3 human cancer cell lines, and it also exhibited antioxidant activity in a cell-free system [39]. Adverse effects of compounds that are present in *Brassicaceae* towards metabolic syndromes are also possible. For example, the potential additive and synergistic effects of flavonoids from *Brassicaceae* with other molecules could interfere with the bioavailability of specific drugs with a narrow therapeutic index [9].

3. Biofortification to Optimize the Content of Bioactive Compounds in *Brassicaceae*

Biofortification is a sustainable approach that is based on the fortification of crops through the utilization of nutrient-rich fertilizers, breeding or plant engineering strategies in order to produce and/or accumulate nutritionally important molecules [40]. Among these techniques, conventional breeding could show some disadvantages since it requires long time to introduce traits of interest into local varieties, whereas, through genetic engineering, novel genes can be directly introduced into the genome of transgenic plants. Furthermore, genetic engineering allows for combining several traits in the same plants and nutritional traits can be targeted to specific plant organs [41,42].

Brassicaceae represent an ideal system for studying the genetic factors that are controlling the accumulation of bioactive compounds. Indeed, up to date, in the *Brassicaceae* family, the genomes of ten species have been partially or completely sequenced and the conserved sequence homology to *Arabidopsis thaliana* allows for the development of specific genomic resources [43]. Several molecular markers have been introduced for genetic studies in *Brassica* plants, such as restriction fragment length polymorphisms (RFLP), amplified fragment length polymorphisms (AFLP), sequence-related amplified polymorphisms (SRAP), random amplified polymorphic DNA (RAPD), and simple sequence repeats (SSR) [44]. Molecular maps and mapping populations have also been developed by using several varietal groups and subspecies as parents. Quantitative trait loci (QTLs) controlling the accumulation of bioactive compounds, including carotenoids and glucosinolates, have also been identified in *Brassicaceae* [44]. Several studies have been conducted on the structural and regulatory genes involved in the biosynthesis of bioactive compounds of broccoli. For example, a recent study [45] reported that the protein phosphatase 2A regulatory subunit B′γ (PP2A-B′γ) physically interacts with indole glucosinolate methyltransferases. In this way, both the methoxylation of indole glucosinolates and the synthesis of 4-methoxy-indol-3-yl-methyl glucosinolate in *Arabidopsis thaliana* leaves are controlled. These evidences provide a new perspective for metabolic engineering of glucosinolate metabolism in cruciferous plants.

Obtaining transgenic plants could be a valid alternative strategy to improve the content of specific molecules by either inactivating or overexpressing genes, or cloning the regulatory factors [46]. In this

regard, many studies have been conducted in order to increase the content of glucosinolates. In one study, transgenic Chinese cabbage (*Brassica rapa*) was obtained by overexpressing the *Arabidopsis* genes *MAM1*, *CYP79F1*, and *CYP83A1*. Only in the MAM1 transgenic line, increased levels of aliphatic glucosinolates, gluconapin, and glucobrassicanapin were observed [47]. Overexpression of three paralogous *BrMYB28* genes in transgenic Chinese cabbage increased the total content of glucosinolates in homozygous T_1 and T_2 generation plants [48]. Finally, overexpressing a *rolB* gene in *Arabidopsis thaliana* calli, a 3-folds increase in the levels of indol-3-ylmethyl glucosinolate and 4-methoxy indol-3-ylmethyl glucosinolate was found. This effect was probably due to the ability of the *rolB* gene to induce the expression of the transcription factors MYB34, MYB51 and MYB122 [49].

A high level of vitamin E was also achieved in transgenic *Brassica napus* plant seeds by overexpressing *Arabidopsis* genes encoding hydroxyl phenyl pyruvate dioxygenases, alone or in combination with genes encoding chimeric homogentisate phytyl transferase and tocopherol cyclase [50]. To enhance the amount of carotenoids in *Brassica napus* plants, seven key enzyme genes that are involved in ketocarotenoid synthesis, isolated from the soil bacterium *Pantoea ananatis*, and from the marine bacteria *Brevundimonas* and *Paracoccus strain*, were expressed in transgenic plants [51]. In another paper, the *Arabidopsis* regulatory gene *Production of Anthocyanin Pigment 1* (*AtPAP1*) was expressed in *Brassica napus*, thus obtaining a significant increase in the levels of the phenolic compounds cyanidin, pelargonidin, and quercetin [52].

A further possible strategy for the production of healthy compounds, such as glucosinolates and phenolic compounds in turnip, could be represented by infection with *Agrobacterium rhizogenes* to obtain transgenic hairy root cultures [53]. For example, metabolic engineering of indolic glucosinolates in Chinese cabbage hairy roots was obtained by the overexpression of the *Arabidopsis* genes *CYP79B2*, *CYP79B3*, and *CYP83B1* [54,55].

Finally, another approach to increase the content of bioactive compounds has been recently considered and is represented by plant cell cultures in vitro. This method offers several advantages when compared with whole plants. For example, using sterilized containers, pathogens are avoided, as well as an undesirable distribution of pollen and cross-fertilization. In addition, cultured plant cells need simple nutrients to grow. Moreover, the purification of the bioactive compound is facilitated since complex plant fibers are not present with the consequent reduction of production costs [56]. These factors can allow for further optimizing the culture conditions, and, thus, increase the bioproduction of glucosinolates [57].

4. Effect of Food Processing Techniques on Bioactive Compounds Content

It has been demonstrated that food processing may significantly affect the concentration and biological activity of the compounds that are present in vegetables. This is an important point, as the majority of vegetables are consumed after thermal treatment, which can have several effects, some of which are reported in Table 2.

During cooking, qualitative changes, antioxidant degradation, and release into surrounding water may affect the antioxidant activity of vegetables. As for *Brassicaceae*, it has been reported that boiling determined losses of 97, 74, and 87% in flavonoids, sinapic acid derivatives, and caffeoylquinic acid derivatives, respectively [58]. Losses were reduced to 20–30% by steaming cooking, revealing that this is the optimal method to safeguard secondary metabolites in *Brassica* crops [59].

After boiling and steaming, a loss in AsA content of 34% and 22% was reported for broccoli, while microwaving and pressure-cooking, caused more than 90% retention [60] and conversion of AsA to dehydroascorbic acid (DHAA) was observed after the thermal treatments for 15 min of crushed broccoli at 30 °C up to 60 °C [61]. Thermal treatment, such as steaming, is associated to the inactivation of myrosinases enzymes, resulting in low loss of glucosinolates. When compared to steaming, a higher reduction of glucosinolates was observed during boiling and microwave cooking since glucosinolates leach into the boiling water due to their highwater solubility, while around 90% of glucosinolates is lost in cooking water [62]. Glucosinolates were reduced by 55%, 54%, 60%, and 41%, in stir-fried,

stir-fried/boiled, microwaved, and boiled broccoli, respectively [63]. The majority of domestic cooking causes myrosinase denaturation, while glucosinolates remain intact. Blanching cruciferous vegetables prior to freezing may denature myrosinase, thus whole glucosinolates are consumed [64]. Also, storage at a low temperature has an effect on the antioxidant activity, as chilling at 6 °C for 35 days determined sulforaphane loss of 29%, while storage at −18 °C for 60 days resulted in loss mainly attributed to the blanching step [61].

Modified atmosphere packaging (MAP) also may exert an effect on the content of glucosinolates of broccoli florets. MAP treatment reduced the decreasing levels rates of individual, indole glucosinolates and total aliphatic in broccoli florets when compared to those in the control, during 23 days of storage at 4 °C or five days of storage at 20 °C [65].

On the other side, cooking of vegetables can enhance the bioavailability of some bioactive molecules. A study investigated the extractability of carotenoids, flavonoids, phenolic compounds, and chlorophylls in cooked broccoli and cauliflower, and found that cooking can, in some cases, improve the extractability of bioactive compounds in vegetables [66].

Table 2. Summary of impact of domestic and industrial processing on the nutritional quality of *Brassicaceae*.

Treatment	Effect on Nutritional Quality	Reference
High pressure boiling	Degradation of hydroxycinnamic acids and flavonoids Glucosinolates hydrolysis causing the formation of isothiocyanates	[60] [62]
Steaming cooking	Reduction of phenolic degradation Inactivation of myrosinase and low loss of glucosinolates	[59] [62]
Microwaving- pressure cooking	Low loss of AsA and carotenoids	[60]
MAP treatment	Good preservation of glucosinolates	[65]

5. Conclusions

A variety of vegetables belong to the family of *Brassicaceae* that are considered among the most important weeds in the world. These vegetables provide dietary fiber, vitamins, anti-cancer glucosinolates, dietary flavonols, and anthocyanins. The content of these compounds in *Brassica* food is affected by genetic background, climatic conditions, crop management strategies, time, and other conditions of storage, characterizing the time from harvest to initial processing in the industry or retailer, as well as the methods that are adopted for cooking and consumption at home [67].

Bioavailability of antioxidants and glucosinolates are also related to the association with other food constituents. The bioavailability of glucosinolates and their breakdown products depends also by the inactivation or not of myrosinases. Further investigations are desirable in order to deeply analyze the impact of each agronomic parameter on the accumulation and synthesis of these compounds in the different crops belonging to *Brassicaceae*. In addition, further genetic studies are needed to identify the genetic determinants that control the accumulation of bioactive compounds in these vegetables. These studies will help to obtain novel plant lines that will be able to accumulate higher levels of bioactive compounds, through conventional breeding programs, or, in alternative, through more efficient metabolic engineering approaches.

Acknowledgments: The authors would like to thank BenTen Project (POR Campania 2007/2013) for the financial support to their activities.

Author Contributions: A.R., G.P., D.M.M. and M.M.R wrote the manuscript with the contribution of other authors; A.B. and A.E. revised the manuscript.

Conflicts of Interest: The authors declare no conflict of interest.

References

1. Sasaki, K.; Takahashi, T. A flavonoid from *Brassica rapa* flower as UV-absorbing nectar guide. *Phytochemistry* **2002**, *61*, 339–343. [CrossRef]
2. Jahangir, M.; Kim, H.K.; Choi, Y.H.; Verpoorte, R. Health-affecting compounds in *Brassicaceae*. *Compr. Rev. Food Sci. Food Saf.* **2009**, *8*, 31–43. [CrossRef]
3. Comhaire, F. Nutriceutical approach to the metabolic syndrome. *Endocrinol. Metab. Syndr.* **2014**, *3*, 134. [CrossRef]
4. De Pascale, S.; Maggio, A.; Pernice, R.; Fogliano, V.; Barbieri, G. Sulphur fertilization may improve the nutritional value of *Brassica rapa* L. subsp. *sylvestris*. *Eur. J. Agron.* **2007**, *26*, 418–424. [CrossRef]
5. Lippmann, D.; Lehmann, C.; Florian, S.; Barknowitz, G.; Haack, M.; Mewis, I.; Wiesner, M.; Schreiner, M.; Glatt, H.; Brigelius-Flohé, R. Glucosinolates from pakchoi and broccoli induce enzymes and inhibit inflammation and colon cancer differently. *Food Funct.* **2014**, *5*, 1073–1081. [CrossRef] [PubMed]
6. Wilson, R.A.; Sangha, M.H.; Banga, S.S.; Atwal, A.K.; Gupta, S. Heat stress tolerance in relation to oxidative stress and antioxidants in *Brassica juncea*. *J. Environ. Biol.* **2014**, *35*, 383–387. [PubMed]
7. Jeon, S.M.; Kim, J.E.; Shin, S.K.; Kwon, E.Y.; Jung, U.J.; Baek, N.I.; Lee, K.T.; Jeong, T.S.; Chung, H.G.; Choi, M.S. Randomized double-blind placebo-controlled trial of powdered *Brassica rapa* ethanol extract on alteration of body composition and plasma lipid and adipocytokine profiles in overweight subjects. *J. Med. Food* **2013**, *16*, 133–138. [CrossRef] [PubMed]
8. Shah, M.A.; Sarker, M.M.R.; Gousuddin, M. Antidiabetic potential of *Brassica oleracea* var. *Italica* in Type 2 diabetic Sprague dawley (sd) rats. *Int. J. Phar. Phytochem. Res.* **2016**, *8*, 462–469.
9. Peluso, I.; Palmery, M. Is a flavonoid-rich diet with steamer cooking safe during calcineurin inhibitors therapy? *J. Clin. Pharm. Therap.* **2014**, *39*, 471–474. [CrossRef] [PubMed]
10. Cohen, J.H.; Kristal, A.R.; Stanford, J.L. Fruit and vegetable intakes and prostate cancer risk. *J. Nat. Cancer Inst.* **2000**, *92*, 61–68. [CrossRef] [PubMed]
11. An, S.; Han, J.I.; Kim, M.J.; Park, J.S.; Han, J.M.; Baek, N.I.; Chung, H.G.; Choi, M.S.; Lee, K.T.; Jeong, T.S. Ethanolic extracts of *Brassica campestris* spp. *rapa* roots prevent high-fat diet-induced obesity via beta(3)-adrenergic regulation of white adipocyte lipolytic activity. *J. Med. Food.* **2010**, *13*, 406–414. [CrossRef] [PubMed]
12. Padayatty, S.J.; Katz, A.; Wang, Y.; Eck, P.; Kwon, O.; Lee, J.H.; Chen, S.; Corpe, C.; Dutta, A.; Dutta, S.K.; et al. Vitamin C as an antioxidant: Evaluation of its role in disease prevention. *J. Am. Coll. Nutr.* **2003**, *22*, 18–35. [CrossRef] [PubMed]
13. Rodríguez, J.A.; Nespereira, B.; Pérez-Ilzarbe, M.; Eguinoa, E.; Páramo, J.A. Vitamins C and E prevent endothelial VEGF and VEGFR-2 overexpression induced by porcine hypercholesterolemic LDL. *Cardiovasc. Res.* **2005**, *65*, 665–673. [CrossRef] [PubMed]
14. Gallo, M.; Esposito, G.; Ferracane, R.; Vinale, F.; Naviglio, D. Beneficial effects of Trichoderma genus microbes on qualitative parameters of *Brassica rapa* L. subsp. *sylvestris* L. Janch. var. esculenta Hort. *Eur. Food Res. Technol.* **2013**, *236*, 1063–1071. [CrossRef]
15. Podsędek, A. Natural antioxidants and antioxidant capacity of *Brassica* vegetables: A review. *LWT Food Sci. Technol.* **2007**, *40*, 1–11. [CrossRef]
16. Rose, P.; Huang, Q.; Ong, C.N.; Whiteman, M. Broccoli and watercress suppress matrix metalloproteinase-9 activity and invasiveness of human MDA-MB-231 breast cancer cells. *Toxicol. Appl. Pharmacol.* **2005**, *209*, 105–113. [CrossRef] [PubMed]
17. Das, S.; Tyagi, A.K.; Kaur, H. Cancer modulation by glucosinolates: A review. *Current Sci.* **2000**, *79*, 1665–1671.
18. Yogeeta, S.K.; Hanumantra, R.B.R.; Gnanapragasam, A.; Senthilkumar, S.; Subhashini, R.; Devaki, T. Attenuation of abnormalities in the lipid metabolism during experimental myocardial infarction induced by isoproterenol in rats: beneficial effect of ferulic acid and ascorbic acid. *Basic Clin. Pharmacol. Toxicol.* **2006**, *98*, 467–472. [CrossRef] [PubMed]
19. Vallejo, F.; Tomas-Barberan, F.A.; Garcia-Viguera, C. Effect of climatic and sulphur fertilisation conditions, on phenolic compounds and vitamin C, in the inflorescences of eight broccoli cultivars. *Eur. Food Res. Technol.* **2003**, *216*, 395–401. [CrossRef]

20. Kaur, C.; Kumar, K.; Anil, D.; Kapoor, H.C. Variations in antioxidant activity in broccoli (*Brassica oleracea* L.) cultivars. *J. Food Biochem.* **2007**, *31*, 621–638. [CrossRef]
21. Borowski, J.; Szajdek, A.; Borowska, E.J.; Ciska, E.; Zieliński, H. Content of selected bioactive components and antioxidant properties of broccoli (*Brassica oleracea* L.). *Eur. Food Res. Technol.* **2008**, *226*, 459–465. [CrossRef]
22. Koh, E.; Wimalasiri, K.M.S.; Chassy, A.W.; Mitchell, A.E. Content of ascorbic acid, quercetin, kaempferol and total phenolics in commercial broccoli. *J. Food Compos. Anal.* **2009**, *22*, 637–643. [CrossRef]
23. Domínguez-Perles, R.; Mena, P.; García-Viguera, C.; Moreno, D.A. Brassica foods as a dietary source of vitamin C: A review. *Crit. Rev. Food Sci. Nutr.* **2014**, *54*, 1076–1091. [CrossRef] [PubMed]
24. Herranz-López, M.; Fernández-Arroyo, S.; Pérez-Sanchez, A.; Barrajón-Catalána, E.; Beltrán-Debónc, R.; Menéndez, J.A.; Alonso-Villaverdee, C.; Segura-Carretero, A.; Jovenc, J.; Micol, V. Synergism of plant-derived polyphenols in adipogenesis. *Perspimpl. Phyt.* **2012**, *19*, 253–261. [CrossRef] [PubMed]
25. Zhang, B.; Kang, M.; Xie, Q.; Xu, B.; Sun, C.; Chen, K.; Wu, Y. Anthocyanins from Chinese bayberry extract protect beta cells from oxidative stress-mediated injury via HO-1 upregulation. *J. Agric. Food Chem.* **2011**, *59*, 537–545. [CrossRef] [PubMed]
26. Vessal, M.; Hemmati, M.; Vasei, M. Antidiabetic effects of quercetin in streptozocin-induced diabetic rats. *Comp. Biochem. Physiol. Toxicol. Pharmacol.* **2003**, *135*, 357–364. [CrossRef]
27. Tabatabaei-Malazy, O.; Larijani, B.; Abdollahi, M.A. Novel management of diabetes by means of strong antioxidants′ combination. *J. Med. Hypotheses Ideas* **2013**, *7*, 25–30. [CrossRef]
28. Fard, M.H.; Naseh, G.; Lotfi, N.; Hosseini, S.M.; Hosseini, M. Effects of aqueous extract of turnip leaf (*Brassica rapa*) in alloxan-induced diabetic rats. *Avicenna J. Phytomed.* **2015**, *5*, 148–156.
29. Büchert, A.M.; Lobato, M.E.G.; Villarreal, N.M.; Civello, P.M.; Martínez, G.A. Effect of visible light treatments on postharvest senescence of broccoli (*Brassica oleracea* L.). *J. Sci. Food Agric.* **2011**, *91*, 355–361. [CrossRef] [PubMed]
30. Suzuki, K.; Ito, Y.; Inoue, T.; Hamajima, N. Inverse association of serum carotenoids with prevalence of metabolic syndrome among Japanese. *Clin. Nutr.* **2011**, *30*, 369–375. [CrossRef] [PubMed]
31. Barbieri, G.; Bottino, A.; Orsini, F.; De Pascale, S. Sulfur fertilization and light exposure during storage are critical determinants of the nutritional value of ready-to-eat friariello campano (*Brassica rapa* L. subsp. *sylvestris*). *J. Agric. Food Chem.* **2009**, *89*, 2261–2266. [CrossRef]
32. Padilla, G.; Cartea, M.E.; Velasco, P.; de Haro, A.; Ordás, A. Variation of glucosinolates in vegetable crops of *Brassica rapa*. *Phytochemistry* **2007**, *68*, 536–545. [CrossRef] [PubMed]
33. Mukherjee, S.; Gangopadhyay, H.; Das, D. Broccoli: A unique vegetable that protects mammalian hearts through the redox cycling of the thioredoxin superfamily. *J. Agric. Food Chem.* **2008**, *56*, 609–617. [CrossRef] [PubMed]
34. Sankhari, J.M.; Thounaojam, M.C.; Jadeja, R.N.; Devkar, R.V.; Ramachandran, A.V. Anthocyanin-rich red cabbage (*Brassica oleracea* L.) extract attenuates cardiac and hepatic oxidative stress in rats fed an atherogenic diet. *J. Sci. Food Agric.* **2012**, *92*, 1688–1693. [CrossRef] [PubMed]
35. Kural, B.V.; Küçük, N.; Yücesan, F.B.; Örem, A. Effects of kale (*Brassica oleracea* L. var. *acephala* DC) leaves extracts on the susceptibility of very low and low density lipoproteins to oxidation. *Ind. J. Biochem. Biophys.* **2011**, *48*, 361–364.
36. Washida, K.; Miyata, M.; Koyama, T.; Yazawa, K.; Nomoto, K. Suppressive effect of yamato-mana (*Brassica rapa* L. *oleifera* group) constituent 3-Butenyl glucosinolate (gluconapin) on postprandial hypertriglyceridemia in mice. *Biosci. Biotechnol. Biochem.* **2010**, *74*, 1286–1289. [CrossRef] [PubMed]
37. Geremias, R.; Pedrosa, R.C.; Locatelli, C.; De Favere, V.T.; CouryPedrosa, R.; Laranjeira, M.C.M. Lipid lowering activity of hydrosoluble chitosan and association with *Aloe vera* L. and *Brassica olearaceae* L. *Phytother. Res.* **2006**, *20*, 288–293. [CrossRef] [PubMed]
38. Mohamed, S. Functional foods against metabolic syndrome (obesity, diabetes, hypertension and dyslipidemia) and cardiovasular disease. *Trends Food Sci. Technol.* **2014**, *35*, 114–128. [CrossRef]
39. Thangam, R.; Suresh, V.; Rajkumar, M.; Vincent, J.D.; Gunasekaran, P.; Anbazhagan, C.; Kaver, K.; Kannan, S. Antioxidant and in vitro anticancer effect of 2-pyrrolidinone rich fraction of *Brassica oleracea* var. capitata through induction of apoptosis in human cancer cells. *Phytother. Res.* **2013**, *27*, 1664–1670. [CrossRef] [PubMed]

40. Gómez-Galera, S.; Rojas, E.; Sudhakar, D.; Zhu, C.; Pelacho, A.M.; Capell, T.; Christou, P. Critical evaluation of strategies for mineral fortification of staple food crops. *Transgenic Res.* **2010**, *19*, 165–180. [CrossRef] [PubMed]
41. Naqvi, S.; Farré, G.; Sanahuja, G.; Capell, T.; Zhu, C.; Christou, P. When more is better: Multigene engineering in plants. *Trends Plant Sci.* **2010**, *15*, 49–56. [CrossRef] [PubMed]
42. Zhu, C.; Sanahuja, G.; Yuan, D.; Farré, G.; Arjó, G.; Berman, J.; Zorrilla-López, U.; Banakar, R.; Bai, C.; Pérez-Massot, E.; et al. Biofortification of plants with altered antioxidant content and composition: Genetic engineering strategies. *Plant Biotechnol. J.* **2013**, *11*, 129–141. [CrossRef] [PubMed]
43. Brown, A.F.; Yousef, G.G.; Chebrolu, K.K.; Byrd, R.W.; Everhart, K.W.; Thomas, A.; Reid, R.W.; Parkin, I.A.; Sharpe, A.G.; Oliver, R.; et al. High-density single nucleotide polymorphism (SNP) array mapping in *Brassica oleracea*: Identification of QTL associated with carotenoid variation in broccoli florets. *Theor. Appl. Genet.* **2014**, *127*, 2051–2064. [CrossRef] [PubMed]
44. Sotelo, T.; Soengas, P.; Velasco, P.; Rodríguez, V.M.; Cartea, M.E. Identification of metabolic QTLs and candidate genes for glucosinolate synthesis in *Brassica oleracea* leaves, seeds and flower buds. *PLoS ONE* **2014**, *9*, e91428. [CrossRef] [PubMed]
45. Rahikainen, M.; Trotta, A.; Alegre, S.; Pascual, J.; Vuorinen, K.; Overmyer, K.; Moffatt, B.; Ravanel, S.; Glawischnig, E.; Kangasjärvi, S. PP2A-B′γ modulates foliar trans-methylation capacity and the formation of 4-methoxy-indol-3-yl-methyl glucosinolate in Arabidopsis leaves. *Plant J.* **2017**, *89*, 112–127. [CrossRef] [PubMed]
46. Velasco, P.; Rodríguez, V.M.; Francisco, M.; Cartea, M.E.; Soengas, P. Genetics and breeding of *Brassica* crops. In *Glucosinolates*; Mérillon, J.M., Ramawat, K.G., Eds.; Springer: Cham, Switzerland, 2016; pp. 1–26.
47. Zang, Y.X.; Kim, J.H.; Park, Y.D.; Kim, D.H.; Hong, S.B. Metabolic engineering of aliphatic glucosinolates in Chinese cabbage plants expressing Arabidopsis MAM1, CYP79F1, and CYP83A1. *BMB Rep.* **2008**, *41*, 472–478. [CrossRef] [PubMed]
48. Seo, M.S.; Jin, M.; Chun, J.H.; Kim, S.J.; Park, B.S.; Shon, S.H.; Kim, J.S. Functional analysis of three BrMYB28 transcription factors controlling the biosynthesis of glucosinolates in *Brassica rapa*. *Plant Mol. Biol.* **2016**, *90*, 503–516. [CrossRef] [PubMed]
49. Bulgakov, V.P.; Veremeichik, G.N.; Grigorchuk, V.P.; Rybin, V.G.; Shkryl, Y.N. The rolB gene activates secondary metabolism in *Arabidopsis calli* via selective activation of genes encoding MYB and bHLH transcription factors. *Plant Physiol. Biochem.* **2016**, *102*, 70–79. [CrossRef] [PubMed]
50. Raclaru, M.; Gruber, J.; Kumar, R.; Sadre, R.; Lühs, W.; Zarhloul, M.K.; Friedt, W.; Frentzen, M.; Weier, D. Increase of the tocochromanol content in transgenic *Brassica napus* seeds by overexpression of key enzymes involved in prenylquinone biosynthesis. *Mol. Breed.* **2006**, *18*, 93–107. [CrossRef]
51. Fujisawa, M.; Takita, E.; Harada, H.; Sakurai, N.; Suzuki, H.; Ohyama, K.; Shibata, D.; Misawa, N. Pathway engineering of *Brassica napus* seeds using multiple key enzyme genes involved in ketocarotenoid formation. *J. Exp. Bot.* **2009**, *60*, 1319–1332. [CrossRef] [PubMed]
52. Li, X.; Gao, M.J.; Pan, H.Y.; Cui, D.J.; Gruber, M.Y. Purple canola: *Arabidopsis PAP1* increases antioxidants and phenolics in *Brassica napus* leaves. *J. Agric. Food Chem.* **2010**, *58*, 1639–1645. [CrossRef] [PubMed]
53. Chung, I.M.; Rekha, K.; Rajakumar, G.; Thiruvengadam, M. Production of glucosinolates, phenolic compounds and associated gene expression profiles of hairy root cultures in turnip (*Brassica rapa* ssp. *rapa*). *3 Biotech* **2016**, *6*, 175. [CrossRef] [PubMed]
54. Zang, Y.X.; Lim, M.H.; Park, B.S.; Hong, S.B.; Kim, D.H. Metabolic engineering of indole glucosinolates in Chinese cabbage plants by expression of Arabidopsis CYP79B2, CYP79B3, and CYP83B1. *Mol. Cells* **2008**, *30*, 231–241.
55. Zang, Y.X.; Kim, H.U.; Kim, J.A.; Lim, M.H.; Jin, M.; Lee, S.C.; Kwon, S.J.; Lee, S.I.; Hong, J.K.; Park, T.H.; et al. Genome-wide identification of glucosinolate synthesis genes in *Brassica rapa*. *FEBS J.* **2009**, *276*, 3559–3574. [CrossRef] [PubMed]
56. Ramirez-Estrada, K.; Vidal-Limon, H.; Hidalgo, D.; Moyano, E.; Golenioswki, M.; Cusidó, R.M.; Palazon, J. Elicitation, an effective strategy for the biotechnological production of bioactive high-added value compounds in plant cell factories. *Molecules* **2016**, *21*, 182. [CrossRef] [PubMed]
57. Sánchez-Pujante, P.J.; Borja-Martínez, M.; Pedreño, M.Á.; Almagro, L. Biosynthesis and bioactivity of glucosinolates and their production in plant in vitro cultures. *Planta* **2017**, *246*, 19–32. [CrossRef] [PubMed]

58. Vallejo, F.; Tomás-Barberán, F.A.; García-Viguera, C. Phenolic compound contents in edible parts of broccoli inflorescences after domestic cooking. *J. Sci. Food Agric.* **2003**, *83*, 1511–1516. [CrossRef]
59. Francisco, M.; Moreno, D.A.; Cartea, M.E.; Ferreres, F.; Garcia-Viguera, C.; Velasco, P. Simultaneous identification of glucosinolates and phenolic compounds in a representative collection of vegetable *Brassica rapa*. *J. Chromatogr. A* **2009**, *1216*, 6611–6619. [CrossRef] [PubMed]
60. Galgano, F.; Favati, F.; Caruso, M.; Pietrafesa, A.; Natella, S. The Influence of processing and preservation on the retention of health-promoting compounds in broccoli. *J. Food Sci.* **2007**, *72*, S130–S135. [CrossRef] [PubMed]
61. Munkaya, A.W.; Mankule, E.E.; Oey, I.; Loey, A.V.; Hendrikx, M. Thermal stability of L-Ascorbic Acid and ascorbic acid oxidase in broccoli (*Brassica oleracea* var. *italica*). *J. Food Sci.* **2010**, *75*, 336–340. [CrossRef] [PubMed]
62. Song, L.; Thornalley, P.J. Effect of storage, processing and cooking on glucosinolate content of *Brassica* vegetables. *Food Chem. Toxicol.* **2007**, *45*, 216–224. [CrossRef] [PubMed]
63. Yuan, G.; Sun, B.; Yuan, J.; Wang, Q. Effects of different cooking methods on health-promoting compounds of broccoli. *J. Zhejiang Univ. Sci. B.* **2009**, *10*, 580–588. [CrossRef] [PubMed]
64. Traka, M.; Mithen, R. Glucosinolates, isothiocyanates and human health. *Phytochem. Rev.* **2009**, *8*, 269–282. [CrossRef]
65. Jia, C.G.; Xu, C.J.; Wei, J.; Yuan, J.; Yuan, G.F.; Wang, B.L.; Wang, Q.M. Effect of modified atmosphere packaging on visual quality and glucosinolates of broccoli florets. *Food Chem.* **2009**, *114*, 28–37. [CrossRef]
66. Dos Reis, L.C.R.; de Oliveira, V.R.; Hagen, M.E.K.; Jablonski, A.; Flores, S.H.; de Oliveira Rios, A. Carotenoids, flavonoids, chlorophylls, phenolic compounds and antioxidant activity in fresh and cooked broccoli (*Brassica oleracea* var. *Avenger*) and cauliflower (*Brassica oleracea* var. *Alphina* F1). *LWT Food Sci. Technol.* **2015**, *63*, 177–183. [CrossRef]
67. Francisco, M.; Tortosa, M.; del Carmen Martínez-Ballesta, M.; Velasco, P.; García-Viguera, C.; Moreno, D.A. Nutritional and phytochemical value of *Brassica* crops from the agri-food perspective. *Ann. Appl. Biol.* **2017**, *170*, 273–285. [CrossRef]

50. Raclaru, M.; Gruber, J.; Kumar, R.; Sadre, R.; Lühs, W.; Zarhloul, M.K.; Friedt, W.; Frentzen, M.; Weier, D. Increase of the tocochromanol content in transgenic *Brassica napus* seeds by overexpression of key enzymes involved in prenylquinone biosynthesis. *Mol. Breed.* **2006**, *18*, 93–107. [CrossRef]
51. Fujisawa, M.; Takita, E.; Harada, H.; Sakurai, N.; Suzuki, H.; Ohyama, K.; Shibata, D.; Misawa, N. Pathway engineering of *Brassica napus* seeds using multiple key enzyme genes involved in ketocarotenoid formation. *J. Exp. Bot.* **2009**, *60*, 1319–1332. [CrossRef] [PubMed]
52. Li, X.; Gao, M.J.; Pan, H.Y.; Cui, D.J.; Gruber, M.Y. Purple canola: *Arabidopsis PAP1* increases antioxidants and phenolics in *Brassica napus* leaves. *J. Agric. Food Chem.* **2010**, *58*, 1639–1645. [CrossRef] [PubMed]
53. Chung, I.M.; Rekha, K.; Rajakumar, G.; Thiruvengadam, M. Production of glucosinolates, phenolic compounds and associated gene expression profiles of hairy root cultures in turnip (*Brassica rapa* ssp. *rapa*). *3 Biotech* **2016**, *6*, 175. [CrossRef] [PubMed]
54. Zang, Y.X.; Lim, M.H.; Park, B.S.; Hong, S.B.; Kim, D.H. Metabolic engineering of indole glucosinolates in Chinese cabbage plants by expression of Arabidopsis CYP79B2, CYP79B3, and CYP83B1. *Mol. Cells* **2008**, *30*, 231–241.
55. Zang, Y.X.; Kim, H.U.; Kim, J.A.; Lim, M.H.; Jin, M.; Lee, S.C.; Kwon, S.J.; Lee, S.I.; Hong, J.K.; Park, T.H.; et al. Genome-wide identification of glucosinolate synthesis genes in *Brassica rapa*. *FEBS J.* **2009**, *276*, 3559–3574. [CrossRef] [PubMed]
56. Ramirez-Estrada, K.; Vidal-Limon, H.; Hidalgo, D.; Moyano, E.; Golenioswki, M.; Cusidó, R.M.; Palazon, J. Elicitation, an effective strategy for the biotechnological production of bioactive high-added value compounds in plant cell factories. *Molecules* **2016**, *21*, 182. [CrossRef] [PubMed]
57. Sánchez-Pujante, P.J.; Borja-Martínez, M.; Pedreño, M.Á.; Almagro, L. Biosynthesis and bioactivity of glucosinolates and their production in plant in vitro cultures. *Planta* **2017**, *246*, 19–32. [CrossRef] [PubMed]

Journal of Functional Foods 41 (2018) 223–231

Contents lists available at ScienceDirect

Journal of Functional Foods

journal homepage: www.elsevier.com/locate/jff

Phenolic compounds from *Syzygium jambos* (Myrtaceae) exhibit distinct antioxidant and hepatoprotective activities *in vivo*

Mansour Sobeh[a,*], Ahmed Esmat[b], Ganna Petruk[c], Mohamed A.O. Abdelfattah[d], Malak Dmirieh[a], Daria Maria Monti[c], Ashraf B. Abdel-Naim[e], Michael Wink[a,*]

[a] Institute of Pharmacy and Molecular Biotechnology, Heidelberg University, Heidelberg, Germany
[b] Department of Pharmacology and Toxicology, Faculty of Pharmacy, Ain Shams University, Cairo 11566, Egypt
[c] Department of Chemical Sciences, University of Naples Federico II, Complesso Universitario Monte Sant'Angelo, via Cinthia 4, 80126 Naples, Italy
[d] Department of Chemistry, American University of the Middle East, Eqaila 54200, Kuwait
[e] Department of Pharmacology and Toxicology, Faculty of Pharmacy, King Abdulaziz University, Jeddah, Saudi Arabia

ARTICLE INFO

Keywords:
Syzygium jambos
HPLC-PDA-ESI-MS/MS
Antioxidant
Hepatoprotective
In vivo
Caenorhabditis elegans

ABSTRACT

HPLC-PDA-MS/MS analysis of *Syzygium jambos* leaf extract allowed the identification of 17 secondary metabolites, including flavonol glycosides, flavonol di-glycosides, and flavones as well as ellagitannins and phenolic acids. The extract showed promising antioxidant activities in different experimental models. In *Caenorhabditis elegans*, the extract mediated a dose dependent survival rate and decreased the intracellular ROS level and HSP-16.2 expression. In a rat model against acute CCl_4 intoxication, the extract reduced the levels of all tested liver markers ALT, AST, TB, TC, TG, and MDA and increased GSH and SOD; effects were similar to those of silymarin. In hepatocytes, pre-treatment with the extract inhibited ROS production, against the deleterious effects of sodium arsenite, and increased GSH levels, without alteration in the phosphorylation levels of p38 and of its direct target, MAPKAPK-2. These results demonstrate the high efficacy of *S. jambos* extract in free radical-scavenging, and inhibition of reactive oxygen species.

1. Introduction

Liver plays a central role in filtering and clearing blood received from digestive tract prior to pass it to other body tissues and organs. Moreover, it is involved in detoxifying the body from xenobiotics, toxins, and in mediating drug transformations and metabolism. However, despite its physiological role, the liver is highly susceptible to damage from different toxins, viruses and reactive oxygen and nitrogen species (ROS and RNS, respectively) (De Abajo, Montero, Madurga, & Garcia Rodriguez, 2004; Hoek & Pastorino, 2002). Such damage is often associated with metabolic and synthetic dysfunctions which can lead to fatal complications (Orhan, Orhan, Ergun, & Ergun, 2007).

Reactive oxygen and nitrogen species are produced as an inevitable outcome of cell metabolism and as a result of environmental stress as well. Even if ROS and RNS show some beneficial effects, such as cytotoxicity against bacteria and other pathogens, a high concentration of these reactive free radical species can cause oxidative damage of cellular macromolecules, such as lipids, proteins, and DNA, thus, in turn, leading to DNA mutations and disrupting cellular functionality that enhances the pathogenesis of various disorders affecting liver and other organs and systems (Valko et al., 2007).

Keeping the levels of ROS under control is achieved through some enzymatic cellular mechanisms, such as superoxide dismutase (SOD) which catalyses the transformation of super oxide radicals into either molecular oxygen, or the less reactive hydrogen peroxide which can be then destroyed by catalase (CAT) (Fridovich, 1993). The endogenous glutathione (GSH) is crucial for cells as it is able to scavenge many free radicals, peroxides, lipid peroxides, electrophiles, physiological metabolites, and xenobiotics forming soluble mercapturates (Rees & Sinha, 1960).

In case of enhanced ROS levels, the ingestion of dietary antioxidants. i.e. carotenoids, vitamin C, anthocyanins, vitamin E and several other plant secondary metabolites, such as polyphenolics, can support the organism in the defence pathway (Sies & Stahl, 1995). In this context, hepatic diseases, often associated with increased intracellular ROS levels are of special concern, as they can evolve into fatal complications. Some plants and their secondary metabolites can provide safe, efficacious, antioxidant multi-mechanistic agents that may be useful as hepatoprotective drugs (Abbas & Wink, 2014; Youssef et al., 2016).

* Corresponding authors.
E-mail addresses: sobeh@uni-heidelberg.de (M. Sobeh), wink@uni-heidelberg.de (M. Wink).

https://doi.org/10.1016/j.jff.2017.12.055
Received 2 June 2017; Received in revised form 20 December 2017; Accepted 21 December 2017

The genus *Syzygium* comprises 1200 species occurring in Africa and the Pacific region. *Syzygium* is one of 131 genera belonging to the complex, well-studied myrtle family, Myrtaceae (with 5500 species). This genus, along with the other strongly aromatic genera (i.e. *Myrtus, Eugenia, Melaleuca, and Eucalyptus*), are rich in essential oils, flavonoids, flavonols, anthocyanins, ellagitannins, and phenolic acids (Haron, Moore, & Harborne, 1992; Kuo, Yang, & Lin, 2004; Nawwar et al., 2016; Sobeh et al., 2016).

The phytochemistry and pharmacology of several members of this genus (including *S. cumini*, *S. aqueum, S. samarangense*, *S. aromaticum*, and *S. jambolanum*) have been extensively investigated. In traditional medicine, some of them have been used to treat several disorders, such as hemorrhage, dysentery and gastrointestinal disorders, as well as diabetes and inflammation as these extracts possess antifungal, antimicrobial, antihypertensive, analgesic and antiviral (against herpes virus) properties (Kuiate, Mouokeu, Wabo, & Tane, 2007; Kuo et al., 2004; Raga et al., 2011; Sharma, Kishore, Hussein, & Lall, 2013).

The rose apple, *Syzygium jambos* (syn. *Eugenia jambos* L.), is a large shrub or small to medium in size tree, known to grow originally in Southeast Asia, but now widely distributed in the tropics. The plant has been traditionally used for its antipyretic and anti-inflammatory properties and to treat hemorrhages, syphilis, leprosy, wounds, ulcers, and lung diseases. In Indo-China, all plant parts are employed to treat digestive tract and tooth disorders. The leaves decoction is used as antirheumatic, diuretic, and to relieve sore eye conditions (Kuiate et al., 2007; Nawwar et al., 2016).

Generally, leaf extracts of *S. jambos* and isolated flavonoid glycosides have shown substantial anti-inflammatory activity (Slowing, Carretero, & Villar, 1994). A study from Venezuela has reported promising anti-inflammatory and analgesic activities for the leaf extract when compared to the positive controls diclofenac and morphine, respectively (Avila-Peña, Peña, Quintero, & Suárez-Roca, 2007). In another study, leaf extracts from plants grown in Pretoria, South Africa, have been subjected to bioassay guided fractionation resulting in the isolation of ursolic acid and the anacardic acid analogue, squalene (Sharma et al., 2013). Kuiate et al. (2007) have reported antidermatophytic activity of the ethyl acetate extract of the stem bark and its isolated compounds against three dermatophyte species.

The phytochemical investigation of the plant parts revealed several secondary metabolites. For instance, a recent study from plants cultivated in Egypt has reported three unknown compounds from the aqueous ethanol extract of the whole plant along with 8 known compounds including myricetin 3-*O*-xylosyl-(1 → 2) rhamnoside, quercetin 3-*O*-xylosyl-(1 → 2) rhamnoside and ellagic acid (Nawwar et al., 2016). In Taiwan, two hydrolyzable tannins, 1-*O*-galloylcastalagin and casuarinin, were isolated from the leaf extract; they turned out to exhibit potent anticancer activity *in vitro* (Yang, Lee, & Yen, 2000).

From plants coming from Sri Lanka, the phytochemical profiling of the methylene chloride extract of the leaves revealed three dihydrochalcones, myrigalone G, myrigalone B, and phloretin 4 -*O*-methyl with appreciable radical scavenging properties (Jayasinghe, Ratnayake, Medawala, & Fujimoto, 2007). The phytochemical investigation of the fruits from Chinese plants revealed seven new phloroglucinol derivatives (jambone A, B to G) along with four known triterpenoids and two known flavones, some of which showed promising cytotoxic activities against melanoma cells (Li et al., 2015).

In the current study, the polyphenols of *S. jambos* were investigated using HPLC-PDA-MS/MS. The potential antioxidant activity of a methanol extract was evaluated both *in vitro* using DPPH and FRAP assays, on hepatocytes, and *in vivo* using the well-established nematode *Caenorhabditis elegans* model. Moreover, the potential hepatoprotective activity of a methanol extract was demonstrated in stressed hepatic cells and in an acute CCl_4-induced hepatic injury rat model.

2. Materials and methods

2.1. Chemicals

Carbon tetrachloride (CCl_4) was purchased from Sigma Aldrich, St Louis, MO, USA. All colorimetric kits for biochemical parameters were obtained from Biodiagnostic Co, Cairo, Egypt. All other chemicals and kits were of the highest analytical grade.

2.2. Plant material and extraction

During the spring season (April-May 2015), fresh mature plant leaves were collected from trees grown in a private garden in El Obour city (Egypt). A voucher specimen is kept under accession number P8617 at IPMB, Heidelberg, Germany. Air dried leaves (50 g) were ground and exhaustively extracted with 100% methanol at room temperature during an overall extraction period of 3 d. The combined extracts were evaporated under vacuum at 40 °C until dryness. The residues were further dissolved in methanol, centrifuged, and then only the methanol soluble extract was evaporated under vacuum at 40 °C until dryness. After freezing at −70 °C, the extract was lyophilized yielding fine dried powder (8 g).

2.3. High performance liquid chromatography (HPLC-PDA-MS/MS)

HPLC-PDA-MS/MS system was Thermofinnigan (Thermo electron Corporation, USA) coupled with an LCQ–Duo ion trap mass spectrometer with an ESI source (ThermoQuest). The separation was achieved by using a C18 reversed-phase column (Zorbax Eclipse XDB-C18, Rapid resolution, 4.6 × 150 mm, 3.5 µm, Agilent, USA). A gradient of water and acetonitrile (ACN) (0.1% formic acid each) was applied from 5% to 30% ACN in 60 min in flow rate of 1 mL/min with a 1:1 split before the ESI source. The sample was injected automatically using autosampler surveyor ThermoQuest. The instrument was controlled by Xcalibur software (Xcalibur™ 2.0.7, Thermo Scientific). The MS conditions were set as described before (Sobeh et al., 2017). The ions were detected in the negative mode, a full scan mode and mass range of 50–2000 *m/z*. In brief, to quantify the concentration of phenolic compounds, gallic acid was used as a standard and expressed as its equivalents, whereas the diglucoside flavonoid rutin was used for flavonoids.

2.4. Biological activity experiments

2.4.1. Antioxidant activities in vitro

Determination of total phenolic contents was investigated using the Folin-Ciocalteu method (Ghareeb et al., 2017). The antioxidant activities were investigated by DPPH radical scavenging activity and FRAP assay as previously described (Ghareeb et al., 2017).

2.4.2. Biocompatibility of SJE extracts on HepG2 cells

Human hepatic carcinoma cells (HepG2) were from ATCC and were cultured in Dulbecco's Modified Eagle's Medium (EuroClone), supplemented with 10% foetal bovine serum (HyClone), 2 mM L-glutamine and antibiotics (EuroClone) in a 5% CO_2 humidified atmosphere at 37 °C. Every 48–72 h the culture medium was removed and cells were rinsed with PBS (EuroClone), detached with trypsin-EDTA (EuroClone) and diluted in fresh complete growth medium.

The influence of SJE on proliferation of HepG2 cells was assessed by MTT assay. In this set of experiments, cells were seeded in 96-well plates at a density of 2 x 10^3/well, and 24 h after seeding, increasing concentrations of the methanolic extract (from 25 to 200 µg/mL) were added to the cells for 24 and 48 h. Cell viability was assessed by the MTT (3-(4,5-dimethylthiazol-2-yl)-2,5-diphenyltetrazolium bromide) assay, as described in Guglielmi et al. (2009). Cell survival was expressed as the percentage of viable cells in the presence of the extract compared to controls. Two groups of cells were used as control, i.e. cells

untreated with the extract and cells supplemented with identical volumes of methanol. Each sample was tested in three independent analyses, each carried out in triplicates.

2.4.3. Oxidative stress

To study the antioxidant effect of SJE, cells were plated at a density of 5 x 10^4 cells/cm^2. After 24 h, cells were incubated for 2 h in the presence or absence of 50 μg/mL of the extract and then exposed to 300 μM sodium arsenite (SA) for 2 h.

2.4.4. Intracellular reactive oxygen species measurement

The 2′,7′-dichlorofluorescein diacetate (H_2-DCFDA, Sigma-Aldrich) method was used to measure the intracellular levels of ROS by using the protocol described by Del Giudice et al. (2017). Briefly, at the end of incubation, cells were incubated with the DCFDA probe (20 μM). Fluorescence intensity was measured by a Perkin-Elmer LS50 spectrofluorimeter (525 nm emission wavelength, 488 nm excitation wavelength, 300 nm/min scanning speed, 5 slit width for both excitation and emission). ROS production was expressed as percentage of DCF fluorescence intensity of the sample under test, with respect to the untreated sample. Each value was assessed by three independent experiments, each with three determinations.

2.4.5. Intracellular GSH levels measurement

DTNB assay was performed as described by Petruk et al. (2016) and it was used to analyze total GSH levels. Briefly, at the end of the experiment, cells were detached by trypsin, centrifuged at 1000*g* for 10 min and resuspended in lysis buffer (0.1 M Tris HCl, pH 7.4 containing 0.3 M NaCl, 0.5% NP-40 and protease inhibitors (Roche). Upon 30 min incubation on ice, lysates were centrifuged at 14,000*g* for 30 min at 4 °C. Protein concentration was determined by the Bradford assay and 50 μg of proteins were incubated with 3 mM EDTA, 144 μM 5,5′-dithiobis-2-nitrobenzoic acid (DTNB) in 30 mM Tris HCl pH 8.2, centrifuged at 14,000*g* for 5 min at 4 °C and the absorbance of the supernatant was measured at 412 nm by using a multiplate reader (Biorad). Total GSH content in the lysate was expressed as the percentage of TNB, as its production is directly related to the rate of this recycling reaction, which, in turn, is directly related to the concentration of GSH in the sample. Values are the mean of three independent experiments, each with triplicate determinations.

2.4.6. Western blot analyses

To investigate the activation of MAPK cascade, cells were plated at a density of 5 x 10^4 cells/cm^2 in complete medium for 24 h and then treated as described above. After treatment, cells were lysed and then analyzed by Western blotting by using protocol described by Galano, Arciello, Piccoli, Monti, and Amoresano (2014). Phosphorylation levels of p38 and MAPKAPK-2 were detected by using specific antibodies purchased from Cell Signal Technology (Danvers, MA, USA). To normalize protein intensity levels, specific antibodies against internal standards were used, i.e. anti-GAPDH (Thermo Fisher, Rockford, IL, USA). The chemiluminescence detection system (SuperSignal® West Pico) was from Thermo Fisher.

2.4.7. Antioxidant activity in vivo

2.4.7.1. Caenorhabditis elegans strains and maintenance. Nematodes were maintained under the following conditions: 20 °C, on nematode growth medium (NGM), fed with living *E. coli* OP50. Age synchronized cultures were obtained by treating gravid adults with sodium hypochlorite. The eggs were kept in M9 buffer for hatching and the larvae were transferred to S-media seeded with living *E. coli* OP50 ($O.D._{600nm}$ = 1.0). The *C. elegans* strains such as Wild type (N2), TJ375 [*hsp-16.2: GFP (gpls1)*] and TJ356 were obtained from the *Caenorhabditis* Genetic Center (CGC). The *in vivo* assays, including survival rate and ROS concentration, were done according to our previous description (Sobeh et al., 2018).

2.5. Hepatoprotective activity in vivo

2.5.1. Animals

The study was conducted with male Sprague-Dawley rats, weighing 200–250 g, obtained from the animal facility, King Abdulaziz University, Geddah (KSA). Rats were kept under air-conditioned environment at 22 ± 2 °C, with a 12 h light–dark cycle. They were supplied with rodent chow and water *ad libitum*. Animal care and experiments were conducted in accordance with the protocols approved by the Unit of Biomedical Ethics Research Committee, Faculty of Medicine, King Abdulaziz University, following the Institutional Animal Care and Use Committee guidelines.

2.5.2. Experimental design

Rats were divided into 4 groups of 6 rats each. The first group served as a control and took water orally followed by intraperitoneal (IP) injection of corn oil after 4 h. The second group was injected once with 1 mL/kg of CCl_4-corn oil 50% mixture. Group 3 was pretreated with the known hepatoprotective lignan silymarin (200 mg/kg orally) as a positive control. Group 4 was pretreated with *S. jambos* extract (200 mg/kg orally). Four hours after the pretreatment, groups 3 and 4 have received an IP injection of CCl_4-corn oil 50% mixture.

After 24 h, blood samples were collected by cardiac puncture and allowed to clot. The sera were obtained by centrifugation for 10 min at 3000 rpm, and then kept at −80 °C till analysis. The sera were used to measure hepatotoxicity parameters: alanine aminotransferase (ALT), aspartate aminotransferase (AST), total bilirubin (TB), total cholesterol (TC), and triglycerides (TG). Rats were then sacrificed and liver tissues were dissected. Representative tissue from each lobe was cut and fixed in 10% formalin/saline and then embedded in paraffin for histopathological examination. The remaining liver tissues were re-weighed, washed, and homogenized in ice-cold PBS to yield 10% w/v homogenates and then stored at −80 °C till analyses.

2.5.3. Biochemical analyses

Activities of serum ALT and AST, serum levels of TB, TC, and TG were determined colourimetrically using Mindray BS-120 clinical chemistry auto-analyzer (Shenzhen Mindray Bio-medical Electronics Co. Ldt., Shenzhen, China). Levels of glutathione (GSH), lipid peroxidation marker malondialdehyde (MDA) and the activity of the antioxidant enzyme superoxide dismutase (SOD) were determined using the commercially available kits (Biodiagnostics, Cairo, Egypt).

2.5.4. Histopathological examination

Storage of tissue samples was done in 10% buffered neutral formalin for 24 h and tap water was used for washing. For dehydration, serial dilutions of methyl, ethyl and absolute ethyl alcohols were used. Specimens were embedded in xylene for clarification, immersed in paraffin, and kept for 24 h at 56 °C inside hot air oven. Slide microtome was used to prepare paraffin bee wax tissue sections at 4 μm thickness that were placed on glass slides, had the paraffin cleared, and stained either with eosin and hematoxylin for histopathology. Glass slides were examined through the light electric microscope (Olympus BX-50 Olympus Corporation, Tokyo, Japan) (Banchroft, Stevens, & Turner, 1996).

2.6. Statistical analysis

Statistical analyses for biological data were carried out three times unless otherwise mentioned in the procedure. Data are presented as mean and S.D. One way analysis of variance (ANOVA) was used to carry out the comparisons that were followed by post hoc analysis using Tukey's test. A level of $p < .05$ was taken as cut off to accept statistical significance. GraphPad Prism software, version 5.00 (GraphPad Software, Inc. La Jolla, CA, USA) and (SigmaPlot® 11.0) were used to perform all the required statistical analyses.

Table 1
Chemical composition of a methanol extract of *S. jambos* leaves using LC-MS/MS.

Peak No	Proposed compounds	t_R (min.)	$[M-H]^-$ (*m/z*)	MS/MS fragments	μg gallic equivalent	References
1	Malic acid	1.61	133	–	13.56	Sobeh et al. (2017)
2	Citric acid	1.64	191	111, 173	14.55	Mena et al. (2012)
3	Hexahydroxydiphenoyl-hexoside	1.96	481	257, 301	62.31	Mena et al. (2012)
4	Castalagin/vescalagin isomer	2.85	933	301, 569, 613, 871	31.60	Nonaka, Aiko, Aritake, and Nishioka (1992)
5	Galloyl-HHDP-DHHDP-hexoside*	3.32	951	301, 569, 613, 915	8.47	
6	bis-HHDP-hexoside*	3.43	783	229, 257, 301, 481	59.91	Bresciani et al. (2015)
7	Castalagin/Vescalagin isomer	3.86	933	301, 569, 631, 915	44.38	Nonaka et al. (1992)
8	Galloyl-HHDP-DHHDP-hexoside*	4.86	951	301, 783	11.36	
9	bis-HHDP-hexoside*	5.39	783	229, 257, 301, 481	23.57	Bresciani et al. (2015)
10	Galloyl-bis-HHDP-hexoside (casuarinin)*	8.73	935	301, 481, 571, 633	42.75	Yang et al. (2000)
11	Ellagic acid pentoside	18.52	433	257, 301	55.40	Mena et al. (2012)
12	Ellagic acid rhamnoside	19.64	447	257, 301	105.04	Mena et al. (2012)
13	Ellagic acid	20.58	301	229, 257, 301	35.29	Nawwar et al. (2016)
14	Myricetin rhamnoside[1]	20.89	463	151, 179, 317	5.38	Celli, Pereira-Netto, and Beta (2011)
15	Myricetin 3-*O*-xylosyl-(1 → 2) rhamnoside[§,1]	21.96	595	179, 317, 463	68.07	Nawwar et al. (2016)
16	Rosmarinic acid rhamnoside	23.99	505	359	3.21	
17	Quercetin 3-*O*-xylosyl-(1 → 2) rhamnoside[§,1]	27.74	579	179, 300, 301, 447	121.60	Nawwar et al. (2016)

* HHDP = hexahydroxydiphenoyl.
§ Previously isolated from the plant.
[1] μg rutin equivalent.

3. Results and discussion

3.1. Identification of constituents by HPLC-PDA-MS/MS

The polyphenol content of a methanol extract of *S. jambos* leaves has been of interest from both phytochemical and biological points of view. HPLC-PDA-ESI-MS/MS analyses (full scan and product ion scan mode) have provided comprehensive structural information that successfully led to the identification and characterization of 17 secondary metabolites representing different classes of compounds including phenolic acids, flavonol glycosides, flavonol di-glycosides, flavones, and ellagitannins.

Compounds detected in the current work were identified by means of their MS data, together with the structural information of both the daughter MS ions and the spectral data from the PDA detector. These data were compared to those of formerly identified compounds from plants of the same family or described in the reported online data. Table 1 shows the proposed chemical composition of a methanol extract of *S. jambos* based on LC-MS analysis; the corresponding total ion chromatogram is documented in Fig. 1.

A molecular ion peak of $[M-H]^-$ (*m/z*) 595 with daughter ions at 463 [M − 132], 317 [M − 132 − 146] was identified as myricetin 3-*O*-xylosyl-(1 → 2) rhamnoside as previously described (Nawwar et al., 2016). Another peak exhibiting $[M-H]^-$ (*m/z*) 579 with MS^2 fragments of 447 [M-132], 301 [M − 132 − 146] was assigned to quercetin 3-*O*-xylosyl-(1 → 2) rhamnoside (Nawwar et al., 2016).

Two compounds showed molecular ion peaks at $[M-H]^-$ (*m/z*) 433, 447 and daughter ion at *m/z*301 and two characteristic fragment ions at 257 and 229; they were assigned to ellagic acid pentoside and ellagic acid rhamnoside, respectively (Mena et al., 2012) along with ellagic acid aglycone at $[M-H]^-$ (*m/z*) 301 (Nawwar et al., 2016). Compound 10 was identified as casuarinin with $[M-H]^-$ (*m/z*) 935 as previously reported (Yang et al., 2000). Malic and citric acids were identified also along with several ellagitannins (Table 1).

3.2. Biological activities

3.2.1. In vitro antioxidant activity

Polyphenols are known to exhibit a wide range of biological activities. In addition to scavenging free radicals and ROS, they have been shown to cure or slow the progress of various diseases and health conditions (Abbas & Wink, 2014). Flavonoids represent an important subclass of polyphenols and are widely distributed among many plant families at varying levels. Several studies have highlighted the potent health benefits of flavonoids, substantially, the antioxidant, anticancer, anti-inflammatory effects, and the hepatoprotective activities as well (Cheng, Yi, Wang, Huang, & He, 2017; Lesjak et al., 2018).

Our leaf extract (SJE) contained a high total phenolic content of 466 mg gallic acid equivalents (GAE)/g extract. The extract showed a strong antioxidant activity, as evaluated *in vitro* by using DPPH and FRAP assays. In particular, DPPH indicated an EC_{50} of 5.7 ± 0.45 μg/mL and FRAP exhibited an EC_{50} of 19.77 ± 0.79 mM $FeSO_4$ equivalent/mg sample when compared to the reference compounds ascorbic acid (EC_{50} of 2.92 ± 0.29) and quercetin (24.04 ± 1.23 mM $FeSO_4$ equivalent/mg sample), respectively. Such high free radical-scavenging properties of the crude extracts have been reported only for few other plants as well (Abbas & Wink, 2014; Nawwar et al., 2016).

3.2.2. Antioxidant activity in vivo in C. elegans

3.2.2.1. Survival assay and intracellular ROS content under juglone induced oxidative stress. The extract was able to decrease the intracellular ROS level of wild-type nematodes in a dose dependent manner; ROS levels were reduced in the SJE groups by 59.22% (at 200 μg/mL extract) when compared to control group. Data are shown in Fig. 2(a).

In the current study, the natural pro-oxidant juglone (5-hydroxy-1,4-naphthoquinone) (80 μM) was used to induce fatal oxidative stress in *C. elegans*. Worms which were pre-treated with antioxidant compounds or extracts are often able to survive juglone toxicity. In our experiments, worms, pre-treated with SJE showed a dose-dependent survival activity when compared to the control group that was treated with juglone only (survival rate as low as 18%). Data are shown in Fig. 2(b) indicating that the polyphenols are absorbed and exhibit antioxidant activity inside the nematodes.

3.2.2.2. Quantification of Phsp-16.2::GFP expression and subcellular DAF-16::GFP localization. To get an insight in the corresponding antioxidant mechanisms, we have used a transgenic worm strain in which the stress-responding heat shock protein HSP-16.2 is fused with GFP. Worms were incubated with 20 μM juglone for 24 h to induce oxidative stress followed by measuring the expression of P*hsp*-16.2::GFP by fluorescence microscopy. As shown in Fig. 2(c), SJE was able to significantly decrease the HSP-16.2 expression in a dose dependent manner. These findings indicate that the studied extract is not only scavenging reactive radicals but also it modulates the expression of stress-response genes.

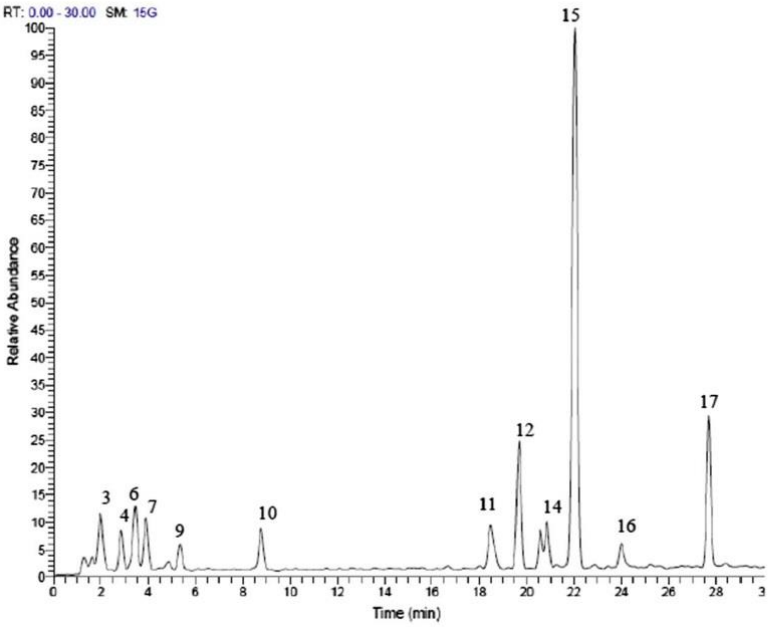

Fig. 1. Total ion chromatogram of the methanol extract from *S. jambos* leaves (LC-MS base peak in the negative ionization mode ESI).

The DAF-16/insulin pathway is often associated with antioxidant response in *C. elegans*. A critical element is the transcription factor DAF-16/FOXO which regulates the expression of heat shock and other stress-related genes. When inactive, DAF-16 is located in the cytoplasm; only when translocated in the nucleus, DAF-16 can regulate stress genes. The extract induced a nuclear translocation of DAF-16::GFP at low concentrations (Fig. 2d), indicating that the *in vivo* antioxidant effect could involve DAF-16/FOXO signaling pathway.

It is worth to mention that this appreciable antioxidant potential of *S. jambos* extract is comparable to that of some polyphenols such as aspalathin in Rooibos tea extracts, EGCG in green tea, and anthocyanins in purple wheat (Abbas & Wink, 2014; Chen, Rezaizadehnajafi, & Wink, 2013; Chen, Sudji, et al., 2013).

3.2.3. Hepatotoxicity markers

Carbon tetrachloride is one of the chemicals associated with severe hepatic toxicity, as it is known that a single exposure is enough to cause serious necrosis and steatosis of liver tissues. It thus represents an optimum choice to induce liver injury in the models required to screen for the hepatoprotective potential of new drugs (Al-Sayed, Abdel-Daim, Kilany, Karonen, & Sinkkonen, 2015). The pathogenesis of the damage is multivariate, involving propagation of free radicals such as trichloromethyl radical ($CCl_3^{\cdot}$) and trichloromethyl peroxy radical ($CCl_3O_2^{\cdot}$), leading to lipid peroxidation, cell membrane destruction and DNA damage, followed by triggering an inflammatory response by the body (Fahmy, Al-Sayed, Abdel-Daim, Karonen, & Singab, 2016).

In this study, a one day CCl_4-induced liver injury model was implemented, as CCl_4 deleterious toxic effects have a peak 24 h following injection, and then slowly normalize. Drugs able to reverse CCl_4 damage during its peak period represent promising candidates for treating liver diseases and intoxication (Al-Sayed & Abdel-Daim, 2014).

Table 2 shows the effects of SJE on the hepatotoxicity markers. Following the CCl_4 administration, there was a marked leakage of the liver enzymes into the blood, manifested as significant elevation of ALT and AST serum activities. In addition, acute CCl_4 intoxication caused a significant increase in TB, TC and TG serum levels compared to the control group. These effects could be attributed to hepatocellular damage (Al-Sayed & Abdel-Daim, 2014). Pretreatment with the known liver-protecting silymarin reduced the levels of all tested markers comparable to normal values that were shown to be statistically different from the CCl_4-challenged group while being not from the control group. Pretreatment of animals with SJE significantly reduced the levels of the hepatic markers relative to the CCl_4-challenged group; effects are similar to those of silymarin (Table 2). Similar activities were reported for other plant crude extracts (Abbas & Wink, 2014; Youssef et al., 2016).

3.2.3.1. Oxidative stress markers. The pathogenesis and progression of liver diseases is often associated with oxidative stress, which is also pivotally involved in promoting drug-induced hepatotoxicity (Al-Sayed, El-Lakkany, Seif el-Din, Sabra, & Hammam, 2014). Toxicity of CCl_4 is, to a wide extent, a matter of free radical mediated damage where the formed reactive species covalently bind cell macromolecules leading to formation of protein, nucleic acid, and/or lipid adducts (Azab, Abdel-Daim, & Eldahshan, 2013). This in turn results in disturbed cellular functionality and protein synthesis that finally ends up in apoptosis and/or necrosis (Williams & Burk, 1990).

The determination of intracellular GSH and lipid peroxidation levels are among the most common techniques used to detect liver injuries owing to oxidative stress (Lykkesfeldt, 2007; Matés, Pérez-Gómez, & De Castro, 1999). As shown in Fig. 3, CCl_4 intoxication induced a significant depletion in GSH level and caused about 3-fold increase in MDA level compared to the control group. Alterations in GSH content (Fig. 3a) and MDA level (Fig. 3b) were inhibited by pretreatment with silymarin or SJE.

While GSH represents the non-enzymatic side of the host antioxidant defense mechanism, superoxide dismutase (SOD) and others constitute the major enzymatic part. Accordingly, SOD activity was significantly decreased by the CCl_4 challenge and restored to almost normal levels by silymarin and *S. jambos* extract (200 mg/kg) pretreatments, (Fig. 3c). These findings further confirm a substantial free radical scavenging and antioxidant potential for *S. jambos*.

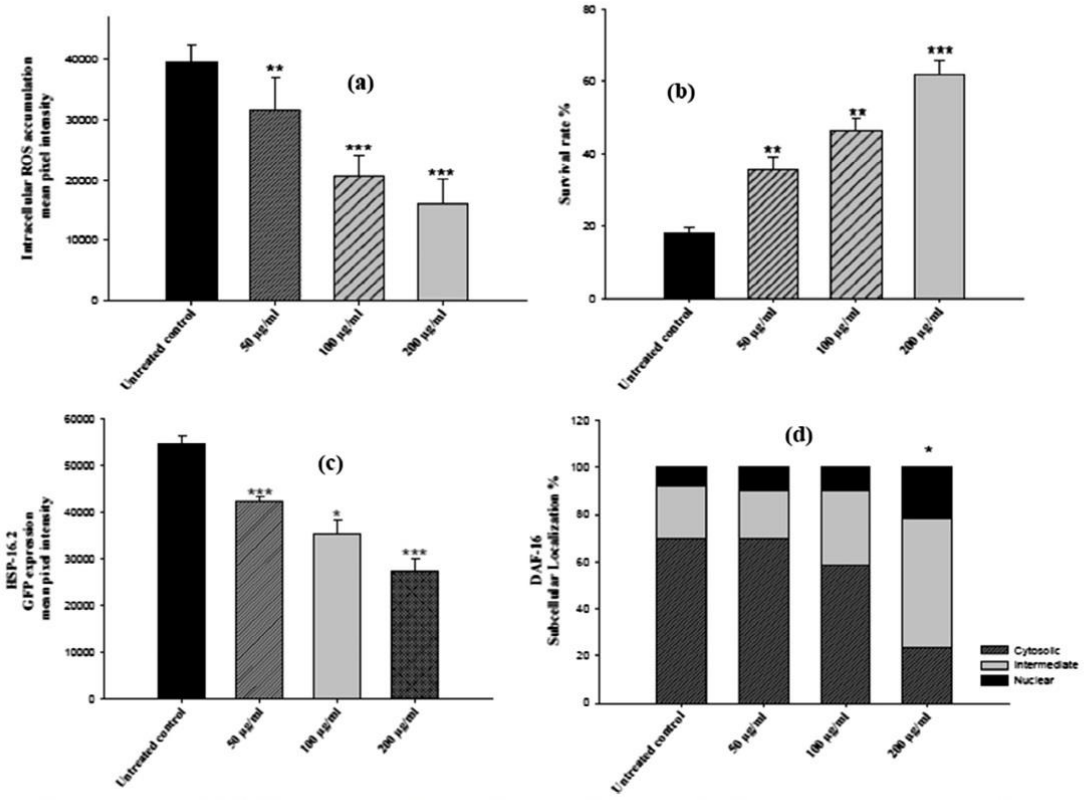

Fig. 2. (a) Intracellular ROS content in N2 wild-type nematodes treated with the fluorescent ROS indicator dye H2DCF-DA. Data are presented as the percentage of fluorescent pixel related to control. ROS content were significantly decreased after pre-treatment of the nematodes with SJE in a concentration dependent manner. (b) SJE effect on stress resistance under juglone treatment (80 µM). Survival rates of the worms (N2, wild-type) were significantly increased after pre-treatment with SJE in a dose dependent manner. (c) P*hsp*-16.2::GFP expression in mutant TJ375 worms. Data are presented as the intensity of fluorescent pixels. P*hsp-16.2*::GFP was significantly decreased after pre-treatment of the nematodes withSJE in a dose dependent manner. (d) Translocation of DAF-16::GFP in mutant TJ356 worms. Data are presented as the percentage of worms exhibiting a DAF-16 subcellular localization pattern, namely, cytosolic, intermediate, and nuclear translocation of DAF-16::GFP in mutant TJ356 worms. Data are presented as percentage of survival (mean ± SEM, n = 3). $^{***}p < .001$, $^{**}p < .01$, $^{*}p < .05$, related to control was analyzed by one-way ANOVA. Survival of untreated nematodes was set 100%.

3.2.3.2. Histopathological examination. The antioxidant properties of SJE were further confirmed by histopathological examination of representative liver tissues, as shown in Fig. 4D. Sections taken from a liver of control rats showed normal hepatic architecture, hepatocytes structure and central veins (Fig. 4A), while CCl_4-intoxicated rat liver was characterized by dilated central vein and centrilobular necrosis (Fig. 4B). Pretreatments with silymarin and/or SJE were able to preserve hepatic architecture with only scattered cytoplasmic vacuolization (Fig. 4C and D). Similar protective activities were determined in plants containing flavonoids, tannins, and ellagitannins (Al-Sayed et al., 2014; Azab et al., 2013; Fahmy et al., 2016).

3.2.4. Antioxidant activity in a hepatic cell model

Human hepatic cells (HepG2) were incubated in the presence of increasing concentrations of the extract (from 25 to 200 µg/mL) for 24 and 48 h. At the end of the incubation, cell survival was analyzed (Fig. 5A) and no significant toxicity was observed up to 50 µg/mL up to 48 h. Thus, this concentration value was selected to analyze the

Table 2
Effect of pretreatment of methanol extract of *S. jambos* on hepatotoxicity markers in the rat model of acute CCl_4 intoxication (number of rats = 6).

Group	ALT (U/L)	AST	TB (mg/dL)	TC	TG
Control	15.4[b] ± 4.07	13.4[b] ± 0.9	0.24[b] ± 0.06	56.7[b] ± 2.9	73.6[b] ± 3.06
CCl_4	137.5[a] ± 6.77	95.2[a] ± 4.49	1.27[a] ± 0.12	135.0[a] ± 7.05	174.2[a] ± 6.45
CCl_4 + silymarin (200 mg/kg)	27.6[b] ± 2.12	24.4[b] ± 1.77	0.28[b] ± 0.03	65.2[b] ± 3.29	80.3[b] ± 3.38
CCl_4 + SJE(200 mg/kg)	29.6[a,b] ± 2.26	31.4[a,b] ± 0.86	0.37[b] ± 0.092	70.1[b] ± 3.15	84.8[b] ± 2.03

Statistical analysis was carried out by one-way ANOVA followed by Tukey post hoc test.
[a] Statistically significant from the corresponding control at $p < .05$
[b] Statistically significant from CCl_4-treated group at $p < .05$

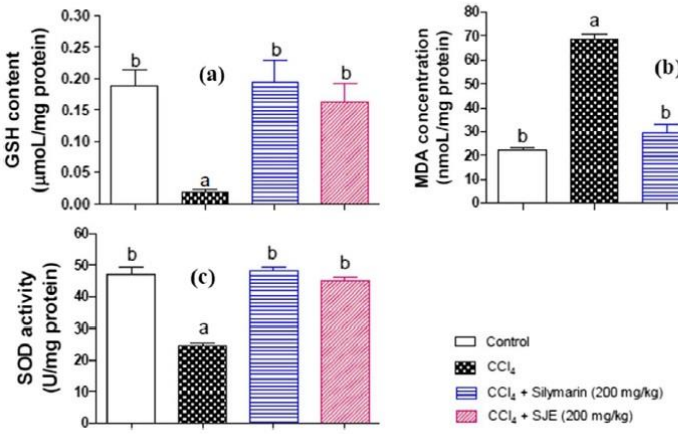

Fig. 3. Effect of pretreatment with SJE on oxidative stress markers in rats with acute CCl_4 intoxication on (a) GSH content; (b) MDA level; (c) SOD activity, (n = 6). Statistical analysis was carried out by one-way ANOVA followed by Tukey post hoc test. [a]Statistically significant from the corresponding control at $p < .05$. [b]Statistically significant from CCl_4-treated group at $p < .05$.

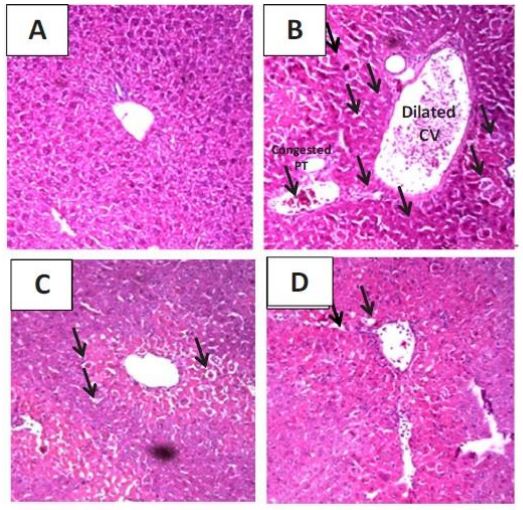

Fig. 4. Representative photomicrographs of liver sections stained by hematoxylin and eosin (×100); (A) Section taken from a liver of control rat showing normal hepatic architecture, hepatocyte structure and central vein; (B) Section taken from a liver of CCl_4 intoxicated rat showing dilated central vein with central hepatocellular necrosis (arrows) and congested portal triad; (C) Section taken from a rat liver pretreated with silymarin with preserved hepatic architecture and only scattered cytoplasmic vacuolization (arrows); (D) Section taken from a rat liver pretreated with SJE showing scattered cytoplasmic vacuolization (arrows).

antioxidant activity in cells in which oxidative stress was induced by sodium arsenite (SA). Trivalent inorganic arsenic (iAs^{3+}) is a toxic and carcinogenic environmental contaminant that humans are inadvertently exposed to every day through drinking water, food and air. It exerts its toxic effect through ROS generation that, in turn, causes loss of GSH homeostasis and oxidations of different molecules (such as formation or lipid peroxides, DNA strand breaks, and chromosome breakages), and leads to cell death.

Cells were incubated with SJE for 120 min prior to induce oxidative stress by 300 µM SA for 120 min. At the end of incubation, intracellular ROS levels were determined (Fig. 5B). No alteration in ROS levels was observed when cells were incubated in the presence of SJE, whereas, as expected, a 70% increase in ROS levels was observed in the presence of oxidative stress. Interestingly, pre-incubation of hepatic cells with SJE prior to exposure to SA resulted in an inhibition of ROS production. The protective effect was confirmed by the analysis of intracellular GSH levels, whose homeostasis plays a crucial role in counteracting iAs^{3+}-induced oxidative stress. As shown in Fig. 5C, a significant decrease (about 40%) was observed after SA-treatment, but no oxidation in GSH was observed when cells were protected by SJE extract. The antioxidant activity of SJE was finally confirmed by Western blotting analyses, in which the phosphorylation levels of p38 and of its direct target, MAPKAPK-2, were analyzed. These two proteins belong to a MAPK family, which are evolutionarily highly conserved enzymes that manage the response to growth stimulatory signals, such as insulin or EGF, as well as adverse signals, such as cytotoxic and genotoxic substances or radiations (Klotz et al., 1999). During oxidative stress, the phosphorylation level of these two proteins increases. Fig. 5D clearly shows that SA induces high phosphorylation levels of these two markers, whereas, in the presence of SJE, the phosphorylation levels of p38 and MAPKAPK-2 are similar to those observed in untreated cells. Therefore, SJE is able to prevent SA activated signaling cascade.

4. Conclusions

In the current study, the chemical profiling of *S. jambos* leaf extract by HPLC-PDA-ESI-MS/MS revealed 17 compounds including flavonol glycosides, flavonol di-glycosides and flavones as well as ellagitannins and phenolic acids. The antioxidative and hepatoprotective activities of SJE were investigated *in vitro*, on human hepatic cells and *in vivo*. As expected, from the phytochemical data SJE showed promising antioxidant activities in two reliable and commonly used assays (DPPH and FRAP), as well as high total phenolic contents. *S. jambos* leaves extract exerted substantial antioxidant activity *in vivo* in *C. elegans* organism. Moreover, potent hepatoprotective activities in human hepatic cells in which oxidative stress was induced using sodium arsenite, and in an acute CCl_4-induced hepatic injury rat model were observed. This protective effect may be ascribed to antioxidant molecules present in the leaf extract.

In conclusion, our results suggest that *S. jambos* leaf extract may provide an interesting candidate in pharmaceutical formulations for the treatment of diseases resulting from elevated reactive oxygen species. However, further experiments are still needed to investigate the pharmacodynamics and pharmacokinetics of the extract.

Funding

This research did not receive any specific grant from funding agencies in the public, commercial, or not-for-profit sectors.

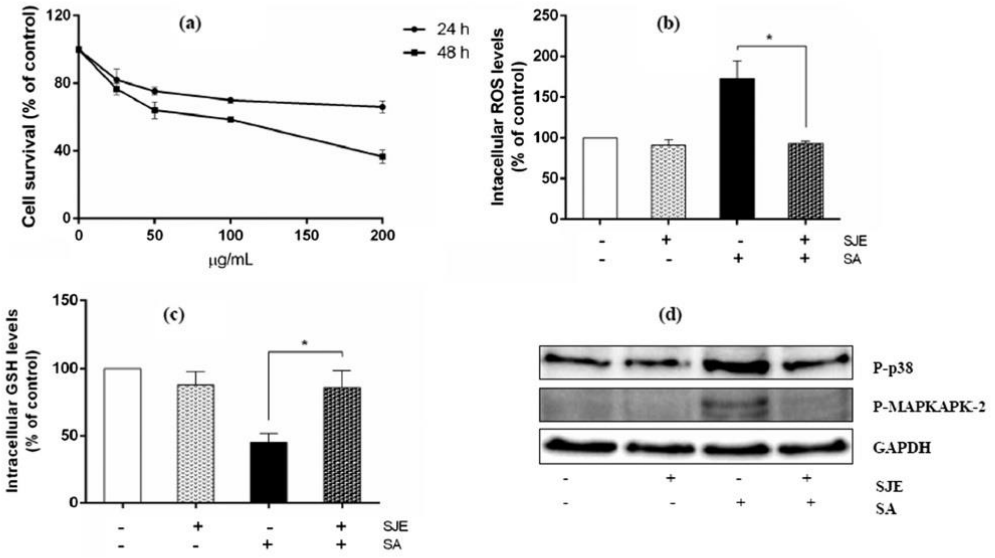

Fig. 5. Effects of SJE on human hepatic cells. (a) MTT analysis: cells were treated with increasing concentrations of extract (25–200 µg/mL) for 24–48 h. Cell viability was assessed by the MTT assay and values are given as means ± SEM (n ≥ 3). (b) and (c), DCFDA and DTNB assays: cells were pre-incubated in the presence of 50 µg/mL of the extract for 120 min and exposed to 300 µM SA for 120 min. White bars refer to control cells, black bars to stressed cells, dotted bars to cells incubated with SJE, and black dotted bars to cells pretreated with SJE and then stressed by SA. Asterisks (*) indicate values that are significantly different from SA treated cells ($p < .05$) as determined by Student's *t*-test. (d) Western blotting analysis: cells were pre-incubated as described and western blot was performed using specific antibodies against phospho-p38 and phospho-MAPKAPK-2. GAPDH was used as loading control.

Conflict of interest

The authors declare no conflict of interest.

Acknowledgements

We thank Dr. Roberta Giampà for the work done during her master thesis and Dr. B. Wetterauer (IPMB) for his help in collecting LC-MS data.

References

Abbas, S., & Wink, M. (2014). Green tea extract induces the resistance of *Caenorhabditis elegans* against oxidative stress. *Antioxidants, 3*, 129–143.
Al-Sayed, E., & Abdel-Daim, M. M. (2014). Protective role of Cupressuflavone from *Cupressus macrocarpa* against carbon tetrachloride-induced hepato-and nephrotoxicity in mice. *Planta Medica, 80*, 1665–1671.
Al-Sayed, E., Abdel-Daim, M. M., Kilany, O. E., Karonen, M., & Sinkkonen, J. (2015). Protective role of polyphenols from *Bauhinia hookeri* against carbon tetrachloride-induced hepato-and nephrotoxicity in mice. *Renal Failure, 37*, 1198–1207.
Al-Sayed, E., El-Lakkany, N. M., Seif el-Din, S. H., Sabra, A.-N. A., & Hammam, O. A. (2014). Hepatoprotective and antioxidant activity of Melaleuca styphelioides on carbon tetrachloride-induced hepatotoxicity in mice. *Pharmaceutical Biology, 52*, 1581–1590.
Avila-Peña, D., Peña, N., Quintero, L., & Suárez-Roca, H. (2007). Antinociceptive activity of *Syzygium jambos* leaves extract on rats. *Journal of Ethnopharmacology, 112*, 380–385.
Azab, S. S., Abdel-Daim, M., & Eldahshan, O. A. (2013). Phytochemical, cytotoxic, hepatoprotective and antioxidant properties of *Delonix regia* leaves extract. *Medicinal Chemistry Research, 22*, 4269–4277.
Banchroft, J., Stevens, A., & Turner, D. (1996). *Theory and practice of histological techniques.* New York, London, San Francisco, Tokyo: Churchil Livingstone.
Bresciani, L., Calani, L., Cossu, M., Mena, P., Sayegh, M., Ray, S., & Del Rio, D. (2015). (Poly)phenolic characterization of three food supplements containing 36 different fruits, vegetables and berries. *PharmaNutrition, 3*, 11–19.
Celli, G. B., Pereira-Netto, A. B., & Beta, T. (2011). Comparative analysis of total phenolic content, antioxidant activity, and flavonoids profile of fruits from two varieties of Brazilian cherry (*Eugenia uniflora* L.) throughout the fruit developmental stages. *Food Research International, 44*, 2442–2451.
Chen, W., Rezaizadehnajafi, L., & Wink, M. (2013). Influence of resveratrol on oxidative stress resistance and life span in Caenorhabditis elegans. *Journal of Pharmacy and Pharmacology, 65*, 682–688.
Chen, W., Sudji, I. R., Wang, E., Joubert, E., van Wyk, B.-E., & Wink, M. (2013). Ameliorative effect of aspalathin from rooibos (*Aspalathus linearis*) on acute oxidative stress in *Caenorhabditis elegans*. *Phytomedicine, 20*, 380–386.
Cheng, J., Yi, X., Wang, Y., Huang, X., & He, X. (2017). Phenolics from the roots of hairy fig (*Ficus hirta* Vahl.) exert prominent anti-inflammatory activity. *Journal of Functional Foods, 31*, 79–88.
De Abajo, F. J., Montero, D., Madurga, M., & Garcia Rodriguez, L. A. (2004). Acute and clinically relevant drug-induced liver injury: A population based case-control study. *British Journal of Clinical Pharmacology, 58*, 71–80.
Del Giudice, R., Petruk, G., Raiola, A., Barone, A., Monti, D. M., & Rigano, M. M. (2017). Carotenoids in fresh and processed tomato (*Solanum lycopersicum*) fruits protectcells from oxidative stress injury. *Journal of the Science of Food and Agriculture, 97*, 1616–1623.
Fahmy, N. M., Al-Sayed, E., Abdel-Daim, M. M., Karonen, M., & Singab, A. N. (2016). Protective effect of *Terminalia muelleri* against carbon tetrachloride-induced hepato and nephro-toxicity in mice and characterization of its bioactive constituents. *Pharmaceutical Biology, 54*, 303–313.
Fridovich, I. (1993). Superoxide and superoxide dismutases. *Free Radical Biology and Medicine, 15*, 472.
Galano, E., Arciello, A., Piccoli, R., Monti, D. M., & Amoresano, A. (2014). A proteomicapproach to investigate the effects of cadmium and lead onhuman primary renal cells. *Metallomics, 6*, 587–597.
Ghareeb, M. A., Mohamed, T., Saad, A. M., Refahy, L. A.-G., Sobeh, M., & Wink, M. (2017). HPLC-DAD-ESI-MS/MS analysis of fruits from *Firmiana simplex* (L.) and evaluation of their antioxidant and antigenotoxic properties. *Journal of Pharmacy and Pharmacology*. http://dx.doi.org/10.1111/jphp.12843.
Guglielmi, F., Monti, D. M., Arciello, A., Torrassa, S., Cozzolino, F., Pucci, P., ... Piccoli, R. (2009). Enzymatically active fibrils generated by the self-assembly of the ApoA-I fibrillogenic domain functionalized with a catalytic moiety. *Biomaterials, 30*, 829–835.
Haron, N. W., Moore, D. M., & Harborne, J. B. (1992). Distribution and taxonomic significance of flavonoids in the genus *Eugenia* (Myrtaceae). *Biochemical Systematics and Ecology, 20*, 266–268.
Hoek, J. B., & Pastorino, J. G. (2002). Ethanol, oxidative stress, and cytokine-induced liver cell injury. *Alcohol, 27*, 63–68.
Jayasinghe, U., Ratnayake, R., Medawala, M., & Fujimoto, Y. (2007). Dihydrochalcones with radical scavenging properties from the leaves of *Syzygium jambos*. *Natural Product Research, 21*, 551–554.
Klotz, L. O., Pellieux, C., Briviba, K., Pierlot, C., Aubry, J. M., & Sies, H. (1999). Mitogen-activated protein kinase (p38-, JNK-, ERK-) activation pattern induced by extracellular and intracellular singlet oxygen and UVA. *The FEBS Journal, 260*, 917–922.
Kuiate, J. R., Mouokeu, S., Wabo, H. K., & Tane, P. (2007). Antidermatophytic triterpenoids from Syzygium jambos (L.) Alston (Myrtaceae). *Phytotherapy Research, 21*, 149–152.
Kuo, Y.-C., Yang, L.-M., & Lin, L.-C. (2004). Isolation and immunomodulatory effect of flavonoids from *Syzygium samarangense*. *Planta Medica, 70*, 1237–1239.
Lesjak, M., Beara, I., Simin, N., Pintać, D., Majkić, T., Bekvalac, K., ... Mimica-Dukić, N.

(2018). Antioxidant and anti-inflammatory activities of quercetin and its derivatives. *Journal of Functional Foods, 40*, 68–75.
Li, G.-Q., Zhang, Y.-B., Wu, P., Chen, N.-H., Wu, Z.-N., Yang, L., ... Li, Y.-L. (2015). New phloroglucinol derivatives from the fruit tree *Syzygium jambos* and their cytotoxic and antioxidant activities. *Journal of Agricultural and Food Chemistry, 63*, 10257–10262.
Lykkesfeldt, J. (2007). Malondialdehyde as biomarker of oxidative damage to lipids caused by smoking. *Clinica Chimica Acta, 380*, 50–58.
Matés, J. M., Pérez-Gómez, C., & De Castro, I. N. (1999). Antioxidant enzymes and human diseases. *Clinical Biochemistry, 32*, 595–603.
Mena, P., Calani, L., Dall'Asta, C., Galaverna, G., García-Viguera, C., Bruni, R., ... Del Rio, D. (2012). Rapid and comprehensive evaluation of (poly) phenolic compounds in pomegranate (*Punica granatum* L.) juice by UHPLC-MSn. *Molecules, 17*, 14821–14840.
Nawwar, M., Hashem, A., Hussein, S., Swilam, N., Becker, A., Haertel, B., ... Linscheid, M. (2016). Phenolic profiling of an extract from Eugenia jambos L. (Alston)-the structure of three flavonoid glycosides–antioxidant and cytotoxic activities. *Die Pharmazie-An International Journal of Pharmaceutical Sciences, 71*, 162–168.
Nonaka, G.-I., Aiko, Y., Aritake, K., & Nishioka, I. (1992). Tannins and related compounds. CXIX. Samarangenins a and b, novel proanthocyanidins with doubly bonded structures, from *Syzygium samarangens* and *S. aqueum*. *Chemical and Pharmaceutical Bulletin, 40*, 2671–2673.
Orhan, D. D., Orhan, N., Ergun, E., & Ergun, F. (2007). Hepatoprotective effect of *Vitis vinifera* L. leaves on carbon tetrachloride-induced acute liver damage in rats. *Journal of Ethnopharmacology, 112*, 145–151.
Petruk, G., Raiola, A., Del Giudice, R., Barone, A., Frusciante, L., Rigano, M. M., & Monti, D. M. (2016). An ascorbic acid-enriched tomato genotype to fight UV-A-inducedoxidative stress in normal human keratinocytes. *Journal of Photochemistry and Photobiology B, 163*, 284–289.
Raga, D. D., Cheng, C. L. C., Lee, K. C. I. C., Olaziman, W. Z. P., Guzman, V. J. A. D., & Shen, C.-C. (2011). Bioactivities of triterpenes and a sterol from *Syzygium samarangense*. *Zeitschrift für Naturforschung C, 66*, 235–244.
Rees, K., & Sinha, K. (1960). Blood enzymes in liver injury. *The Journal of Pathology and Bacteriology, 80*, 297–307.
Sharma, R., Kishore, N., Hussein, A., & Lall, N. (2013). Antibacterial and anti-inflammatory effects of *Syzygium jambos* L. (Alston) and isolated compounds on acne vulgaris. *BMC Complementary and Alternative Medicine, 13*, 292.
Sies, H., & Stahl, W. (1995). Vitamins E and C, beta-carotene, and other carotenoids as antioxidants. *The American Journal of Clinical Nutrition, 62*, 1315S–1321S.
Slowing, K., Carretero, E., & Villar, A. (1994). Anti-inflammatory activity of leaf extracts of *Eugenia jambos* in rats. *Journal of Ethnopharmacology, 43*, 9–11.
Sobeh, M., Braun, M. S., Krstin, S., Youssef, F. S., Ashour, M. L., & Wink, M. (2016). Chemical profiling of the essential oils of *Syzygium aqueum*, *Syzygium samarangense* and *Eugenia uniflora* and their discrimination using chemometric analysis. *Chemistry and Biodiversity, 13*, 1537–1550.
Sobeh, M., Mahmoud, M. F., Abdelfattah, M. A., Cheng, H., El-Shazly, A. M., & Wink, M. (2018). A proanthocyanidin-rich extract from *Cassia abbreviata* exhibits antioxidant and hepatoprotective activities in vivo. *Journal of Ethnopharmacology, 213*, 38–47.
Sobeh, M., Mahmoud, M. F., Abdelfattah, M. A., El-Beshbishy, H. A., El-Shazly, A. M., & Wink, M. (2017). *Albizia harveyi*: Phytochemical profiling, antioxidant, antidiabetic and hepatoprotective activities of the bark extract. *Medicinal Chemistry Research, 26*, 3091–3105.
Valko, M., Leibfritz, D., Moncol, J., Cronin, M. T., Mazur, M., & Telser, J. (2007). Free radicals and antioxidants in normal physiological functions and human disease. *The International Journal of Biochemistry and Cell Biology, 39*, 44–84.
Williams, A. T., & Burk, R. F. (1990). Carbon tetrachloride hepatotoxicity: An example of free radical-mediated injury. *Semin Liver Disease, 10*, 279–284.
Yang, L.-L., Lee, C.-Y., & Yen, K.-Y. (2000). Induction of apoptosis by hydrolyzable tannins from *Eugeniajambos* L. on human leukemia cells. *Cancer Letters, 157*, 65–75.
Youssef, F. S., Ashour, M. L., Sobeh, M., El-Beshbishy, H. A., Singab, A. N., & Wink, M. (2016). *Eremophila maculata* – Isolation of a rare naturally-occurring lignan glycoside and the hepatoprotective activity of the leaf extract. *Phytomedicine, 23*, 1484–1493.

Acknowledgments

This is the hardest page to write… Because a lot of people have taken part in this "training journey" and I am afraid to forget to THANK someone…

My first thank goes to Prof. Renata Piccoli. She welcome me in her team when I was really young, during an exchange between University and High School. Then, at second year of University, she passed to me her love for Biochemistry, I will be always grateful to her for this.

I would also like to thank Prof. Giovanni Sannia, the scientific coordinator of the doctoral programme. He was an excellent guide throughout these years of professional growth.

I am absolutely grateful to my supervisor, Dr. Daria Maria Monti. I started to work with her since my Bachelor thesis. She believed in me and gave me the possibility to work with her, also, during my Master thesis and then during three years of the PhD project. I am so grateful to her for giving me continuous scientific and moral support all over these years. I will never forget her determination and ability to involve me in several projects by stimulating my curiosity and increasing my passion for research. The most part of my achieved goals is the result of her hard work.

I am very grateful to Prof. Michael Wink for giving me the opportunity to work in his lab. I have really appreciated his comments and suggestion to make my work more complete and productive.

I wish to express my gratitude to Dr. Angela Arciello for her precious help and her friendly presence.

I am grateful to Prof. Antonello Merlino, Dr. Manuela Rigano and Dr. Mansour Sobeh, co-authors of my publications, for giving me the possibility to take part of their stimulant projects.

A very special thank to all the people with whom I shared these years in the lab, in particularly those who strictly worked with me:

- *Rita, she was my strict teacher. Nevertheless, thanks to her I achieved a lot of my results. Now she is also my Friend and I am proud to have been her student. I will never forget her work ethic as well as her trying always to be better. She will be always an example for me;*
- *Francesco and Rosa, for being good friends besides colleagues, sharing with me funny moments inside the lab, even in the hardest times. Rosa thank you for all the times that you encouraged me during difficult times and invited me to think first and act then;*
- *Paola and Eliana, for all the best moments during our coffee breaks, in particular Paola for funny readings and her gallows humor;*
- *Roberta and Alessia, for being my best Master Students;*
- *Luca Tartaglione, for being my favourite "Slave" Student as well as the best bartender;*
- *Angelica and Mariano, for our amusing lunch breaks.*

I am really thankful to my colleague, collaborator as well as best friend, Imma (Bionda). She shared with me all the learning process. I will never forget our moments of madness spent together and I hope I sent to her a bit of my optimism.

I would also to thank my "German" colleagues with whom I shared only three months during my staying in Heidelberg. This period was short but very intense and full of parties:

- Herbenya, for her publication about antioxidant activity of açai extract in C. elegans. In fact, thanks to this publication I decided where to spend my period abroad;

- Mariana and Felix for teaching me to work with C. elegans. In particular to Mariana for helping me with analysis of data with GraphPad. Of course, I will never forget the "Silent Party";

- Carina, for being the best friend as well as the best person it is possible to meet in another country. My home will be always open for you;

- Gabi, Sonja, Nessa and Erjia, for all fun moments spent together;

- Quian, Hanmei and Malak for allowing me to try Chinese and Arabic restaurant, respectively. Also, I will never forget our times spent for lunch at 12 o'clock.

- Liviu, for being the best photographer; Nami, for being the best parties organizer; and Roberto, for being the best cook. They are amazing person as well as real jokers.

How can I forget to thank the people from Car-pooling.

- For first, I would like to thank two creators of this very useful service, Alfredo Maria Gravagnuolo and Alfredo Ronca. Thanks to their idea, my trip to Naples was enjoyable and less stressful. Gravagnuolo's carelessness and Ronca's irritability will be always in my memory.

-I would also like to thank Ilario, Alfredo Senatore (Pollastro), Alfonso Sessa, Massimiliano Fasano, Dalila, Luchino, Fedup, Aurelio, Marialuisa and Rita for all funny moments shared during back trips at the beginning of my PhD.

-Instead, Veronica, Sharon, Benedetta and Salvatore, I thank specially for "Petruk's day". I hope that we will go to eat something together more often in the future.

-The last two years of my PhD I shared the trip to Naples with Roberto and Carlo, therefore, I am really grateful for all hours spent together, in particular during my crazy moods on. It is difficult for me to image them without any secretary and me without sweet Roberto's voice.

To conclude, an extraordinary thanks to my family. I would like to thank them because they strongly supported me during all my years of study, continuously giving love to me, even if sometimes I forget how to express mine to them. Thank you for sharing with me all the positive and negative moments on my way, all the successes and failures.

- Thanks to my Mammina, the strongest woman of the world and the sweetest mom.

- A huge thanks to my Papì, to my brothers, Andrea and Roman, to my little niece, Anastasia, and to my sister in law, Vlada. I cannot image my life without all of you.

- I am truly grateful to Carla and Antonio, my parents in law, they had welcome me at their home as daughter. You will be always in my heart.

- I would like to thank also all Venosi's Family, because to be part of so close-knit family has no words.

- A big thanks to my uncle, Ivan, and my aunt, Olga, for their continuous support.

- At the end, but not the less important, an infinite thank to Simone, my boyfriend as well as my other half. He always believed in me and never stopped helping me to be a better person. He will be always the apple of my eye.

Anna

*"**Everybody** is a genius,*
*but if you judge a **fish** by its ability to **climb** a tree,*
*it will live its whole life **believing** that it is **stupid**"*

-Albert Einstein